Universal state conversion in discrete and slowly varying non-Hermitian cyclic systems: An analytic proof and exactly solvable examples

Nicholas S. Nye*

School of Electrical and Computer Engineering, Aristotle University of Thessaloniki, Thessaloniki GR-54124, Greece

(Received 18 December 2022; accepted 10 July 2023; published 26 July 2023)

In this paper, we formally prove how, by cyclically varying the parameters of a generalized two-level discrete and non-Hermitian Hamiltonian, the respective state vector converts to the instantaneous eigenstate of the system in the adiabatic limit, irrespective of how the state was initially prepared or of the form of the cyclic trajectory followed within the parameter space ($\mathcal{R}$) or of whether a singularity/exceptional point is encircled or not. Our proof also applies to continuous configurations in the limit of infinitesimally small discrete time steps. The observed mode switching behavior, which is a clear signature of the irreversible nature of non-Hermitian arrangements, can be either of *symmetric* (clockwise [CW] and counterclockwise [CCW] encirclements in $\mathcal{R}$ space lead to state conversion to the same instantaneous eigenstate) or *asymmetric* (CW and CCW encirclements in $\mathcal{R}$ space lead to state conversion to different instantaneous eigenstates). As a specific example, we investigate the case of rhombic parametric trajectories for a discrete parity-time ($\mathcal{PT}$)-symmetric-like setting. Exact analytical solutions are retrieved in terms of *Weber/parabolic cylinder* (large rhombic loops) and *Airy functions* (small rhombic loops), with their asymptotic behavior dictated by the *Stokes phenomenon*. Both analytical derivations and numerical computations indicate that the observed mode conversion is primarily an artifact of the adiabatic character of the state vector evolution, while the encirclement or not of a singularity/exceptional point affects only the magnitude of the required adiabaticity rate for mode switching to take place. Overall, our results provide a deeper theoretical insight on slowly varying discrete non-Hermitian Hamiltonian systems, and pave the way towards exploring the dynamics underpinning the traversal of higher-dimensional cyclic parametric trajectories in the vicinity (or not) of higher-order spectral singularities for both continuous and discrete settings under linear or nonlinear conditions.

DOI: 10.1103/PhysRevResearch.5.033053

I. INTRODUCTION

The adiabatic theorem, as originally developed by Born and Fock [1–3], constitutes one of the fundamental principles of Hermitian quantum systems. It guarantees that a physical setting will remain in its instantaneous eigenstate, if the system parameters vary slowly enough—adiabatically—with time (a finite energy gap must also exist—for all points along the evolution—between the associated eigenvalue and the rest of the Hamiltonian spectrum). In the same time, the derivation of the aforementioned theorem gave rise to two important phase term contributions, when a cyclic and adiabatic quantum state evolution is considered: the dynamical phase (integral of eigenenergies with respect to time, typically linear with respect to the period of evolution T), and the gauge-invariant geometric/Berry phase (defined as the integral of the Berry connection/potential within the parameter space and thus independent of T) [4–6]. The essence of Berry's phase has been identified in various fields of physics, including quantum mechanics (Aharonov-Bohm effect, topologically quenched tunnel splitting [7–10]), solid-state physics (Jahn-Teller effect, quantum Hall and spin Hall effects, topological insulators [11–16]), and topological photonics [17–25], to mention a few.

The extension of such concepts in the non-Hermitian domain has attracted a lot of attention in the last few years [26–28]. In stark contrast to closed/conservative quantum systems, non-Hermitian structures exhibit a number of gain/lossy modes, each of which is characterized by a different rate of growth. In this case, it is expected to see drastic changes in the mode occupancy levels, along with eigenstate "flips", which in turn lead to the breakdown of the conventional adiabatic theorem [29,30]. Such a mode switching behavior has been closely associated with the encirclement of spectral singularity points in parameter space (the so-called exceptional points or in short EPs [31–45]) and has been observed in appropriately modulated microwave and optomechanical structures, semiconductor optical platforms, and single-spin quantum setups [46–50]. Along these lines, the notion of Berry phase (and curvature) has been properly redefined for nonconservative physical settings, and subsequently utilized in order to explain a rich variety of unique transport effects and topological phenomena occurring in such systems [51–57].

*nnai@ece.auth.gr

While the topic of adiabatic and cyclic state evolution has been intensively studied in continuous time configurations, its implications have not yet been recognized in their full extent within discrete physical arrangements. Especially in the context of open quantum systems, there is a lack of analytical and experimental frameworks to describe the properties of discrete and cyclic non-Hermitian Hamiltonians. In the Hermitian regime, analytic proofs of the adiabatic theorem for discrete time evolution have been provided in the works of Dranov *et al.* [58] and Tanaka [59], with applications in the fields of quantum maps and chaos [60], quantum information theory/computation [61,62], and quantum circuits/logic gates [63,64]. To the best of our knowledge, an analogous proof does not exist in the case of open and discrete quantum settings.

On the other hand, the recent emergence of active fiber photonic platforms (discrete networks of fiber loops) endowed with $\mathcal{PT}$-symmetric characteristics have opened up the possibility of observing novel phenomena, otherwise unattained in conventional continuous optical arrangements [65–67]. A precise tailoring of the temporal phase and gain/loss experienced by a propagating mode can be achieved in such photonic structures, which in turn offers the unique advantage of experimentally studying the discrete evolution of light in the adiabatic limit. The lack of rigorous analytical treatments along with the recent experimental demonstration by Nasari *et al.* [67] of omnipolarizer action in active fiber loop systems, deems as necessary the development of an appropriate theoretical framework to analyze the underlying non-Hermitian adiabatic light transport dynamics in the discrete domain.

In this paper, we methodically investigate the implications of slow non-Hermitian cycling within discrete quantum (and photonic) settings. More specifically, by appropriately factorizing the time evolution operator/propagator at each time step, it is proven—in the most general manner—that when a discrete and non-Hermitian system evolves around an arbitrary closed trajectory within the parameter space, then the state vector is transformed to an instantaneous eigenvector at the end of the cycle assuming that no spectrum singularities are crossed. This is shown to be true independently of whether an exceptional point is encircled or not, as long as the cyclic process is performed adiabatically enough. Moreover, such mode switching effect might have a symmetric or an asymmetric character, depending on whether the clockwise (CW) and counterclockwise (CCW) encircling directions lead to a state conversion to the same or different instantaneous eigenstates (by *instantaneous*, we will always refer to the attributes of the time-dependent Hamiltonian at a specific instant, which in this case is at the end of the parameter cycle). In this vein, special emphasis is given to the behavior of the eigenspectra as time progresses, while the notation of $\mathcal{P}, \mathcal{N}$ modes is also introduced in order to track the identity of the dominant and weaker modes. (This will become especially useful, when a mode might stop being dominant at some point during the cyclic parameter variation.) As a specific example, exact analytical solutions (Weber and Airy functions) are retrieved, when a $\mathcal{PT}$-symmetric-like system traverses a rhombic loop within a two-dimensional (2D) parameter space (gain g_n and detuning σ_n are the time-dependent factors and T is period of revolution). The dynamics of the individual state vector components a_n and b_n (along with their ratio $r_n = b_n/a_n$) are examined, while a formal mathematical analogy is also drawn with the model of the discrete harmonic oscillator characterized by a complex and time-dependent damping profile [68–73]. Finally, by exploiting the asymptotics of the respective analytical solutions, we theoretically show in the case of small square loops that the ensued state conversion indeed takes place in the adiabatic limit as a direct consequence of the Stokes phenomenon [74,75]. Of course, in the last section this statement is generalized in an analytical manner to arbitrarily shaped parameter-space loops.

II. DISCRETE NON-HERMITIAN MODEL DEFINITION AND UNDERLYING DYNAMICS

A. Generalized two-level Hamiltonian system

The discrete evolution dynamics of the state vector $|u_n\rangle$ are dictated by

$$\begin{bmatrix} a_{n+1} \\ b_{n+1} \end{bmatrix} = \begin{bmatrix} 1+\Delta m_n^{11} & \Delta m_n^{12} \\ \Delta m_n^{21} & 1+\Delta m_n^{22} \end{bmatrix} \begin{bmatrix} a_n \\ b_n \end{bmatrix}, \tag{1}$$

where $n \in \mathbb{N}$, a_n, b_n are the individual components of $|u_n\rangle$, m_n^{jk} are the elements of matrix M_n (j, $k = 1, 2$), Δ represents the discrete time step (typically considered small), and $q_n = q(t = t_n = n\Delta)$ stands for a discrete and time-dependent quantity ($q = a$, b). The above equation is nothing but the discrete equivalent of Schrödinger's equation for a two-level time-dependent Hamiltonian $H_n = [h_n^{jk}]$, with $h_n^{jk} = im_n^{jk}$ and $i = \sqrt{-1}$ representing the imaginary unit (see Appendix A). In this respect, we define $\Xi_n = [\xi_n^{jk}]$ as the propagator (or evolution) matrix, which in turn describes the evolution of state vector $|u_n\rangle$ according to Eq. (1) (i.e., $|u_{n+1}\rangle = \Xi_n|u_n\rangle$, $\Xi_n = I + \Delta M_n$ and I is the 2×2 identity matrix). In Appendix B 1, additional details are provided regarding the conditions for (non-)Hermitian evolution, along with an in-depth discussion on the effect of different physical symmetries and conservation laws on the dynamical properties of discrete quantum Hamiltonian systems [in Sec. IV of Supplemental Material (SM) [76], an analogous analysis is performed in terms of Jones calculus for classical photonic polarization systems obeying equations similar to Eq. (1)].

The instantaneous eigenvalues of matrix M_n can be found to be

$$\lambda_n^{\pm} = \mu_n^s \pm \sqrt{m_n^{12}m_n^{21}}\cos\theta_n, \tag{2}$$

where $\sin\theta_n = -i\mu_n^d/\sqrt{m_n^{12}m_n^{21}}$, $\mu_n^s = (m_n^{22} + m_n^{11})/2$, $\mu_n^d = (m_n^{22} - m_n^{11})/2$, and $\cos\theta_n = \sqrt{1-\sin^2\theta_n}$ (see calculations in Appendix B 2). The respective instantaneous eigenvectors $|v_n^{\pm}\rangle = [v_{n,x}^{\pm}\ v_{n,y}^{\pm}]^{\mathcal{T}}$ ($\mathcal{T}$ represents the matrix transposition operator) will satisfy the ratio relation

$$\frac{v_{n,y}^{\pm}}{v_{n,x}^{\pm}} = \pm\sqrt{\frac{m_n^{21}}{m_n^{12}}}\, e^{\pm i\theta_n}. \tag{3}$$

Since the evolution (Ξ_n) and Hamiltonian (H_n) matrices are linearly related to M_n, it should be true that $\lambda_{\Xi_n}^{\pm} = 1 - i\Delta\lambda_{H_n}^{\pm} = 1 + \Delta\lambda_n^{\pm}$ and $|v_{\Xi_n}^{\pm}\rangle = |v_{H_n}^{\pm}\rangle = |v_n^{\pm}\rangle$ [in the notation used in the present paper, λ_{Q_n} and $|v_{Q_n}\rangle$ will stand for the

eigenvalues and eigenvectors, accordingly, of matrix Q_n (in this regard, λ_{H_n} will represent the eigenenergies of the Hamiltonian system)]. Exceptional point degeneracies occur when both eigenvalues and eigenvectors coalesce. This can happen for some $n = n_{EP}$ iff $\theta_{n_{EP}} = \pm\pi/2$, which in turn implies that $\lambda^{\pm}_{n_{EP}} = \lambda_{n_{EP}} = \mu^{s}_{n_{EP}}$ and $|v^{\pm}_{n_{EP}}\rangle = |v_{n_{EP}}\rangle$ with $v_{n_{EP},y}/v_{n_{EP},x} = \pm i\sqrt{m^{21}_{n_{EP}}/m^{12}_{n_{EP}}}$.

The difference equations that a_n, b_n satisfy can be directly retrieved based on Eq. (1) as (see Appendix A)

$$a_{n+2} + p^{a}_{n,1}a_{n+1} + p^{a}_{n,0}a_n = 0, \tag{4}$$

with $p^{a}_{n,1} = -(\xi^{12}_n\xi^{11}_{n+1} + \xi^{12}_{n+1}\xi^{22}_n)/\xi^{12}_n$ and $p^{a}_{n,0} = (\xi^{11}_n\xi^{22}_n - \xi^{12}_n\xi^{21}_n)\xi^{12}_{n+1}/\xi^{12}_n$. In an analogous manner, it can be found that the dynamics of component b_n will be described by

$$b_{n+2} + p^{b}_{n,1}b_{n+1} + p^{b}_{n,0}b_n = 0, \tag{5}$$

with $p^{b}_{n,1} = -(\xi^{21}_n\xi^{22}_{n+1} + \xi^{21}_{n+1}\xi^{11}_n)/\xi^{21}_n$ and $p^{b}_{n,0} = (\xi^{11}_n\xi^{22}_n - \xi^{12}_n\xi^{21}_n)\xi^{21}_{n+1}/\xi^{21}_n$. Equations (4) and (5) will each accept two linearly independent solutions $a_{n,1}$, $a_{n,2}$ and $b_{n,1}$, $b_{n,2}$ with nonzero respective Casoratians $C(a_{n,1}, a_{n,2}) \neq 0$ and $C(b_{n,1}, b_{n,2}) \neq 0$ (see Appendix A and [77,78] for further details on the properties of Casoratians). The initial conditions a_0, b_0 along with Eqs. (4) and (5) can now fully determine the evolution of a_n, b_n.

In the present study, we are particularly interested in examining the adiabatic behavior of the ratio of the state vector components ($r_n = b_n/a_n$). In this respect, the evolution of r_n has been found to be dictated by the following recursive relation (see Appendix A):

$$r_{n+1} = \mathcal{G}_{\Xi_n}(r_n) = \frac{\xi^{21}_n + \xi^{22}_n r_n}{\xi^{11}_n + \xi^{12}_n r_n}. \tag{6}$$

In the above formula, $\mathcal{G}_{\Xi_n}$ is a function that maps r_n to r_{n+1}, based on the elements of the evolution matrix Ξ_n (see Appendix C for the general definition of the $\mathcal{G}$ transform, along with a discussion regarding its associated properties). If coefficients ξ^{jk}_n are all constant and independent from parameter n (time-independent Hamiltonian), then Eq. (6) would simply represent a *Möbius transformation*. In the general case of a time-dependent Hamiltonian model, Eq. (6) corresponds to a nonlinear difference equation of the *general Riccati type* [78].

Overall, Eqs. (1)–(6) provide a full description of the evolution dynamics for a generalized two-level discrete Hamiltonian system. In Appendix A, we analytically show the direct correspondence between the discrete evolution equations developed in this section and their continuous counterparts as the discrete time step goes to zero ($\Delta \to 0$). This leads to the generalization of our derivation in Sec. III regarding the state conversion property of cyclic and discrete non-Hermitian systems, to the case of continuous time settings.

B. Traceless and symmetric non-Hermitian Hamiltonian model

Here, we shall assume a traceless and symmetric Hamiltonian with matrix components of the form $h^{11}_n = -h^{22}_n = if_n = ig_n + \sigma_n$ and $h^{12}_n = h^{21}_n = -\kappa$ ($m^{11}_n = -m^{22}_n = f_n = g_n - i\sigma_n$, $m^{12}_n = m^{21}_n = i\kappa$), where g_n, σ_n, κ are real-valued parameters [in a discrete optical setup, g_n and σ_n will represent the time-dependent gain/loss and detuning factors, respectively, while κ will stand for the constant and (without loss of generality) positive coupling strength between the state vector components a_n, b_n]. The resulting matrix equation describing the underlying dynamics will be given by

$$\begin{bmatrix} a_{n+1} \\ b_{n+1} \end{bmatrix} = \begin{bmatrix} 1 + \Delta f_n & i\Delta\kappa \\ i\Delta\kappa & 1 - \Delta f_n \end{bmatrix} \begin{bmatrix} a_n \\ b_n \end{bmatrix}, \tag{7}$$

which in essence corresponds to an almost parity-time-symmetric arrangement {for an extensive discussion on the topics of parity, time, and parity-time reversal symmetries, along with their implications in discrete Hamiltonian systems, refer to both Appendix B 1 (quantum mechanical setups) and Sec. IV within SM [76] (optical setups)} . The instantaneous eigenvalues of matrix M_n can be expressed as ($\mu^{s}_n = 0$, $\mu^{d}_n = -f_n$, $\sin\theta_n = f_n/\kappa$)

$$\lambda^{\pm}_n = \pm i\kappa\cos\theta_n = \pm i\sqrt{\kappa^2 - f^2_n}, \tag{8}$$

while the respective eigenvectors will satisfy the ratio relation

$$\frac{v^{\pm}_{n,y}}{v^{\pm}_{n,x}} = \pm e^{\pm i\theta_n} = \pm\sqrt{1 - \frac{f^2_n}{\kappa^2}} + i\frac{f_n}{\kappa}. \tag{9}$$

Exceptional point degeneracies will occur iff $f_n/\kappa = 1$ or -1 (or equivalently when $g_n = \kappa$ or $-\kappa$ and $\sigma_n = 0$) for some $n = n_{EP}$, with the resulting coalescent eigenvectors taking the form $|v_{n_{EP}}\rangle = [1 \;\; i]^{\mathcal{T}}$ ($\lambda_{n_{EP}} = 0$, $f_{n_{EP}}/\kappa = 1$) or $|v_{n_{EP}}\rangle = [1 \;\; -i]^{\mathcal{T}}$ ($\lambda_{n_{EP}} = 0$, $f_{n_{EP}}/\kappa = -1$).

The discrete dynamics of the state vector components and their ratio will now be dictated by the following difference equations:

$$\begin{aligned} a_{n+2} &+ (-2 + \Delta f_n - \Delta f_{n+1})a_{n+1} \\ &+ \left(1 + \Delta^2\kappa^2 - \Delta^2 f^2_n\right)a_n = 0, \end{aligned} \tag{10a}$$

$$\begin{aligned} b_{n+2} &+ (-2 - \Delta f_n + \Delta f_{n+1})\, b_{n+1} \\ &+ \left(1 + \Delta^2\kappa^2 - \Delta^2 f^2_n\right) b_n = 0, \end{aligned} \tag{10b}$$

$$r_{n+1} = \frac{i\Delta\kappa + (1 - \Delta f_n)r_n}{1 + \Delta f_n + i\Delta\kappa r_n}. \tag{10c}$$

An experimental implementation of such a $\mathcal{PT}$-symmetric-like Hamiltonian model is shown in [67], in the context of a fiber-based omnipolarizer. In such a discrete optical setting, a_n, b_n describe the electric field components along the x and y directions, while parameter n stands for the successive round trips along an appropriately designed fiber loop. Precise tailoring of the gain/loss and detuning (or birefringence) factors is achieved via electro-optic amplitude and phase modulators, while an electrically driven polarization controller produces the constant coupling factor between the two polarization components. Omnipolarizer action is demonstrated by monitoring the polarization state of light $|u_n\rangle$ in terms of the evolution of the respective Stokes parameters on the Poincaré sphere under both Hermitian and non-Hermitian conditions. In Sec. IV within SM [76], additional details are provided as to why the dynamics of such a discrete fiber network can be equivalently described by Eq. (7) or Eqs. (10).

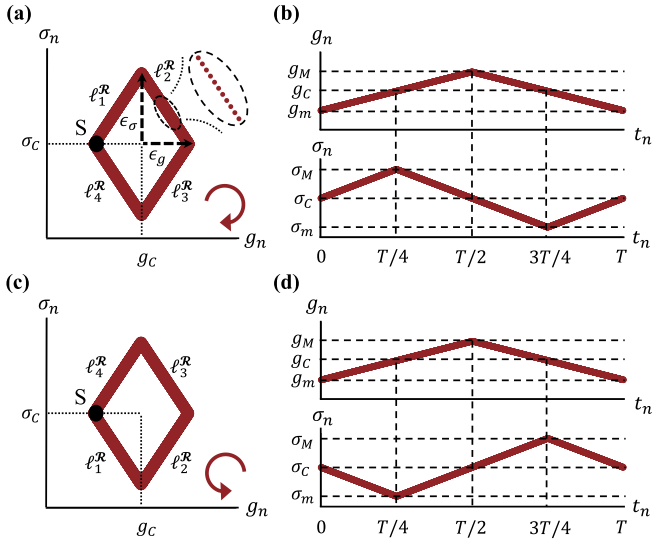

FIG. 1. Schematic of rhombic trajectory $\mathcal{C}^{\mathcal{R}}_{\mathcal{R}\hbar}$ (first column), along with the respective parametric temporal dependencies of the gain (g_n) and detuning (σ_n) coefficients (second column) for CW [(a), (b)] and CCW [(c), (d)] encircling directions. In both cases, the starting point S of evolution was considered to be at the leftmost point of the rhombic loop (in Sec. I within SM [76] analogous plots are provided when S is located at the topmost point of the loop). The magnified image in (a) shows the discrete nature of evolution.

C. Rhombic parametric paths: Exact solutions and adiabatic dynamics

Having derived the discrete evolution equations governing the dynamics of time-dependent non-Hermitian arrangements, here we shall emphasize on the special (and analytically solvable) case of a traceless and symmetric Hamiltonian system moving along rhombic trajectories (see Fig. 1) within the parameter space $\boldsymbol{\mathcal{R}} = (g_n, \sigma_n)$. Such a family of closed paths will be assigned as $\mathcal{C}^{\mathcal{R}}_{\mathcal{R}\hbar} = \cup_{j=1}^{4} \ell_j^{\mathcal{R}}$ ($\ell_j^{\mathcal{R}}$ denotes each of the linear segments comprising the overall rhombic loop and according to our convention they will always be traversed in the order $\ell_1^{\mathcal{R}} \to \ell_2^{\mathcal{R}} \to \ell_3^{\mathcal{R}} \to \ell_4^{\mathcal{R}}$), and can be defined uniquely by the following parameters: (g_C, σ_C) represents the location of the center of the loop ($f_C = g_C - i\sigma_C$, with $g_C, \sigma_C \in \mathbb{R}$), ϵ_g and ϵ_σ denote the modulation ranges of the gain and detuning coefficients, respectively ($\epsilon_g, \epsilon_\sigma \in \mathbb{R}^+$), while $T = N\Delta$ corresponds to the cycling period with $N \in \mathbb{N}$ [this implies for the evolution matrix that $\Xi(t = T) = \Xi(t = 0)$ or equivalently $\Xi_{n=N} = \Xi_{n=0}$]. The magnitudes of ϵ_g and ϵ_σ will eventually determine the family of solutions describing the associated dynamics. The distinct roles of variables N and Δ should also be highlighted at this point: the former dictates the degree of adiabaticity (the greater the number of points along $\mathcal{C}^{\mathcal{R}}_{\mathcal{R}\hbar}$, the more adiabatic the evolution), while the latter indicates how close we are to the continuous time limit. (See also our detailed discussion in Sec. I within SM [76] with respect to rhombic and generalized parametric trajectories.)

In Fig. 1, we graphically show the geometry of path $\mathcal{C}^{\mathcal{R}}_{\mathcal{R}\hbar}$ along with the respective time dependencies of both gain and detuning factors, when the starting point of evolution is located at $(g_C - \epsilon_g, \sigma_C)$. In this case, the CW and CCW evolution equations will become equivalent after substituting $\epsilon_\sigma \to -\epsilon_\sigma$. Analogous graphs and relations are also provided in Sec. I within SM [76], when the starting point lies at the topmost point of $\mathcal{C}^{\mathcal{R}}_{\mathcal{R}\hbar}$. In all scenarios (irrespective of encircling direction or starting conditions), subpaths $\ell_j^{\mathcal{R}}$ are defined in a way such that they are traversed in the order $\ell_1^{\mathcal{R}} \to \ell_2^{\mathcal{R}} \to \ell_3^{\mathcal{R}} \to \ell_4^{\mathcal{R}}$ (see Fig. 1 and Fig. S1 within SM [76]). Moreover, as shown in Figs. 1(b) and 1(d), model parameters g_n, σ_n exhibit a linear discrete time dependence, which in turn implies that the complex factor f_n ($= g_n - i\sigma_n$) will display an analogous behavior: $f_n = \eta_{f,1} t_n + \eta_{f,0}$. Complex coefficients $\eta_{f,1}$ and $\eta_{f,0}$ will depend solely on $\ell_j^{\mathcal{R}}$, i.e., $\eta_{f,1} \to \eta_{f,1}^{(j)}$, $\eta_{f,0} \to \eta_{f,0}^{(j)}$ (in Sec. I within SM [76], such terms have been evaluated for all segments $\ell_j^{\mathcal{R}}$). Here, we can omit superscripts (j) and emphasize on the dynamics along a specific linear subpath. Based on Eq. (10a), the discrete time evolution of component a_n will be described by

$$a_{n+2} - (2 + \Delta^2 \eta_{f,1}) a_{n+1} + \big(1 + \Delta^2 \kappa^2 - \Delta^2 \eta_{f,0}^2 - \Delta^2 \eta_{f,1}^2 t_n^2 - 2\Delta^2 \eta_{f,1} \eta_{f,0} t_n\big) a_n = 0. \tag{11}$$

The general solution to the aforementioned difference equation can be expressed as $a_n = c_1^a a_{n,1} + c_2^a a_{n,2}$, where $a_{n,1}$, $a_{n,2}$ denote two linearly independent solutions [$C(a_{n,1}, a_{n,2}) \neq 0$] and c_1^a, c_2^a represent constants to be determined from the initial conditions a_{n_o}, b_{n_o} [$n, n_o \in \mathbb{N}$ with $n \geqslant n_o$ and $n_o = (j-1)N/4$, i.e., n_o signifies the starting point of linear section $\ell_j^{\mathcal{R}}$]. Substituting the Newton series expansions of a_{n+1} and a_{n+2} [see Eq. (D12) in Appendix D] in Eq. (11) will yield for small values of Δ that

$$\frac{\delta^2 a_n}{\delta t_n^2} + \big(-\eta_{f,1}^2 t_n^2 - 2\eta_{f,1}\eta_{f,0} t_n - \eta_{f,0}^2 + \kappa^2 - \eta_{f,1}\big) a_n = 0 \tag{12}$$

with δ standing for the forward difference operator ($\delta a_n = a_{n+1} - a_n$, $\delta t_n = t_{n+1} - t_n = \Delta$). After applying an appropriate complex coordinate transformation, the above dynamical equation can be classified to be of the *Weber/parabolic type* (see Sec. II within SM [76]). As such, the respective solutions take the form of *discrete Weber/parabolic cylinder functions* and can be expressed as $a_{n,1} = D_{s^+}(\psi_n^+)$, $a_{n,2} = D_{s^-}(\psi_n^-)$, where orders s^+, s^- and arguments ψ_n^+, ψ_n^- of the associated functions depend on the model parameters in a manner indicated in Sec. II within SM [76]. The linear independence of $D_{s^+}(\psi_n^+)$ and $D_{s^-}(\psi_n^-)$ is guaranteed by the nonzero value of the corresponding Casoratian (see SM [76]).

An alternative family of solutions arises when the modulating parameters $\epsilon_g, \epsilon_\sigma$ attain considerably small values, such that a first-order analysis can be performed. [Using dimensionless variables $\breve{\epsilon}_g = \epsilon_g/\kappa$, $\breve{\epsilon}_\sigma = \epsilon_\sigma/\kappa$, this implies that $\breve{\epsilon}_g \gg \breve{\epsilon}_g^2$, $\breve{\epsilon}_\sigma \gg \breve{\epsilon}_\sigma^2$ or practically $\breve{\epsilon}_g \lesssim 0.1$, $\breve{\epsilon}_\sigma \lesssim 0.1$, i.e., $\breve{\epsilon}_g$, $\breve{\epsilon}_\sigma$ have the same or smaller order of magnitude than 0.1; see also Sec. II within SM [76] for the scaled versions of Eqs. (11) and (12).] In this case, terms of the order ϵ_g^2, ϵ_σ^2, $\epsilon_g\epsilon_\sigma$, and higher, can be neglected in the respective evolution equations. For times t_n comparable to the cycling period T, it will be true that $\eta_{f,1}^2 t_n^2 = (\eta_{f,1} T)^2 \propto \epsilon_g^2 - \epsilon_\sigma^2 \pm 2\epsilon_g\epsilon_\sigma$ ($\eta_{f,1} = 4(\pm\epsilon_g \pm i\epsilon_\sigma)/T$ according to Sec. I within SM [76]). Such a second-order term can be now omitted from

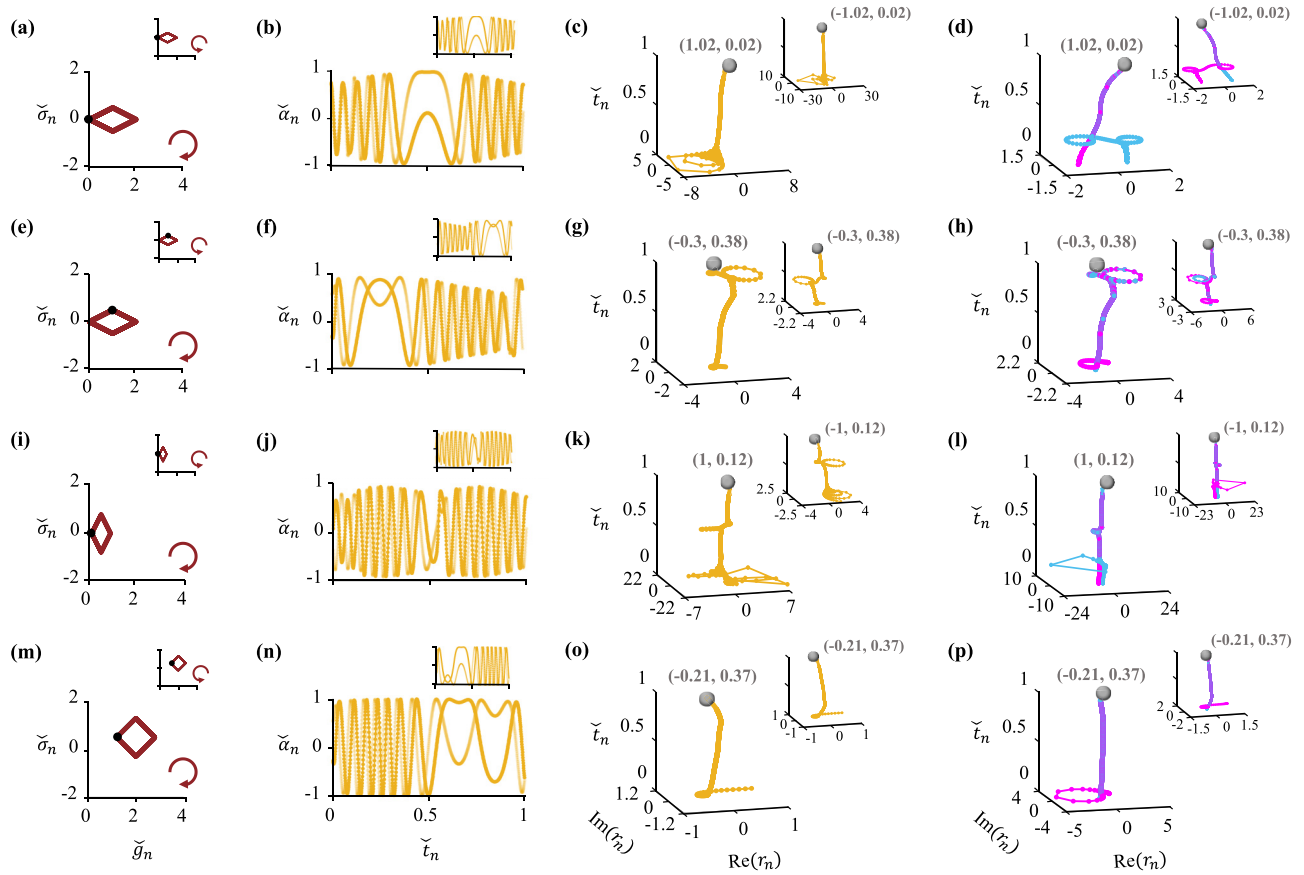

FIG. 2. State vector dynamics (here, the first component of the normalized state vector $|\breve{u}_n\rangle = [\breve{a}_n \ \breve{b}_n]^\mathcal{T} = |u_n\rangle/\sqrt{\langle u_n||u_n\rangle}$ is depicted, along with the ratio factor $r_n = \breve{b}_n/\breve{a}_n = b_n/a_n$) for different rhombic trajectories $\mathcal{C}^{\mathcal{R}}_{\mathcal{R}\hbar}$ and for both CW (main figures) and CCW (inset figures) directions of encirclement ($\breve{t}_n = t_n/T = n/N$ and $\breve{q}_n = q_n/\kappa$, $\breve{\epsilon}_q = \epsilon_q/\kappa$, where q represents the gain or detuning parameter). The dynamical behaviors are indicated when $\breve{\epsilon}_g \sim 1$ or $\breve{\epsilon}_\sigma \sim 1$ (i.e., either of the modulating parameters becomes comparable to unity) and as a result *Weber solutions* apply ($\breve{g}_C = 1, 1, 0.5, 2$, $\breve{\sigma}_C = 0, 0, 0, 0.5$, $\breve{\epsilon}_g = 1, 1, 0.4, 0.8$, $\breve{\epsilon}_\sigma = 0.5, 0.5, 0.8, 0.8$, for each of the four rows in the above figure, accordingly, while $N = 1000$, $\Delta\kappa = 0.1$ in all cases). As starting point S of evolution (signified with a filled black circle) we considered the leftmost point of curve $\mathcal{C}^{\mathcal{R}}_{\mathcal{R}\hbar}$, except in row two where S was located at the topmost point of $\mathcal{C}^{\mathcal{R}}_{\mathcal{R}\hbar}$ (the exceptional point degeneracy is also indicated with a green asterisk). For each closed parametric path, the real (solid curves) and imaginary (faded curves) parts of $\breve{a}_n$ are plotted with time, along with the respective behavior of r_n, for random initial excitation conditions [see orange curves in second ($\breve{a}_n$) and third (r_n) columns]. In the rightmost column, the temporal dynamics of r_n is illustrated when either of the instantaneous eigenmodes of the Hamiltonian is excited at time instant zero (magenta and light blue curves). In all scenarios, symmetric (rows two and four) or asymmetric (rows one and three) state conversion was observed [the exact value of r_N is indicated by the grey coordinates (w, q): $r_N = w + iq$]. Insets typically have the same axis margins with the corresponding main figures, unless otherwise noted. The interested reader can also refer to Fig. S4 within SM [76], where the state vector evolution is demonstrated when $\breve{\epsilon}_g \sim 0.1$ and $\breve{\epsilon}_\sigma \sim 0.1$ (Airy dynamics).

Eqs. (11) and (12) (remaining factors need to be considered since they contain first-order terms with respect to $\epsilon_g, \epsilon_\sigma$) and consequently the resulting dynamics will follow a *discrete Airy-like evolution pattern*. The solutions can be expressed in terms of the *Airy functions of the first and second kind* as $a_{n,1} = \mathrm{Ai}(\chi_n)$ and $a_{n,2} = \mathrm{Bi}(\chi_n)$, where the formula for χ_n and the respective Casoratian computation have been both provided in Sec. II within SM [76].

In Fig. 2, the state vector dynamics is illustrated for both CW (main set of figures) and CCW (inset figures) encirclements and for different rhombic paths in $\mathcal{R}$ space. Only numerical results are presented [in this case, a_n, b_n were determined recursively based on Eq. (7), given the values of f_n, κ and the excitation conditions a_0, b_0 (r_n then becomes equal to b_n/a_n)], as they are in complete accordance with the corresponding analytical calculations. [See our previous discussion pertaining to Eqs. (11) and (12) along with Appendix E, where it is shown how an analytical expression for a_n, b_n can be attained along the entire trajectory $\mathcal{C}^{\mathcal{R}}_{\mathcal{R}\hbar}$ given the form of $a_{n,1}$, $a_{n,2}$ and the initial values a_0, b_0.] Moreover, we emphasize only on the simulation scenario $\breve{\epsilon}_g \sim 1$ or $\breve{\epsilon}_\sigma \sim 1$ (Weber dynamics), while the case $\breve{\epsilon}_g \sim 0.1$ and $\breve{\epsilon}_\sigma \sim 0.1$ (Airy dynamics) has been also covered in Fig. S4 within SM [76] (relation $w \sim q$ implies that quantities w, q have a magnitude of the same order).

For all parameter sets (i.e., each distinct row) of Fig. 2, it is clearly shown that given the encircling direction in parameter space [either clockwise (see main panels) or counterclockwise (see insets)], the value of the ratio factor r_N ($n = N$, $t_N = T$ for a full adiabatic cycle) is the same independent of the

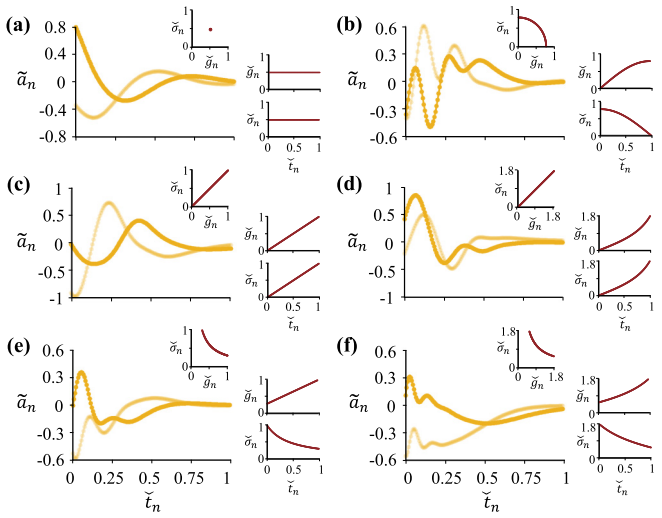

FIG. 3. Evolution of the transformed state vector component $\widetilde{a}_n$ (real and imaginary parts are depicted with solid and faded orange lines, respectively) with time ($\breve{t}_n = t_n/T = n/N$) for different open trajectories in parameter space ($\Delta\kappa = 0.1, N = 150$) and for random initial excitation conditions: (a) $\breve{g}_n = \breve{\sigma}_n = 0.5$, (b) $\breve{g}_n = 0.8\sin(\pi\breve{t}_n/2)$, $\breve{\sigma}_n = 0.8\cos(\pi\breve{t}_n/2)$, (c) $\breve{g}_n = \breve{\sigma}_n = \breve{t}_n$, (d) $\breve{g}_n = \breve{\sigma}_n = \tan(0.34\pi\breve{t}_n)$, (e) $\breve{g}_n = 0.7\breve{t}_n + 0.3$, $\breve{\sigma}_n = 0.3/\breve{g}_n$, and (f) $\breve{g}_n = \tan(0.18\pi\breve{t}_n + 0.16\pi)$, $\breve{\sigma}_n = 1/\breve{g}_n$. Insets show the actual paths followed in $\boldsymbol{\mathcal{R}}$ space (top right inset), along with the explicit time dependencies (center right and bottom right insets) of the gain ($\breve{g}_n = g_n/\kappa$) and detuning parameters ($\breve{\sigma}_n = \sigma_n/\kappa$). Such parametric trajectories lead to exactly solvable models, whose dynamics are described by a class of discrete generalized hypergeometric functions (see Sec. III within SM [76]).

excitation conditions. [Here, we have considered: (i) random initial conditions (orange curves in second and third columns of Fig. 2), (ii) excitation of either of the instantaneous eigenstates at time instant $t_0 = 0$ (magenta and light blue curves in last column of Fig. 2).] What is of even greater interest is that in all cases such value happens to also describe one of the instantaneous eigenmodes $|v_n^{\pm}\rangle$ at time instant $t_N = T$, i.e., $r_N = v_{N,y}^{\pm}/v_{N,x}^{\pm}$. [The exact value of $v_{N,y}^{\pm}/v_{N,x}^{\pm}$ is provided by Eq. (9) for the traceless and symmetric Hamiltonian arrangement under study.] This in turn is a signature of *conversion (or switching) to either eigenstate* (+) *or* (−) ($|u_N\rangle = [a_N\ b_N]^{\mathcal{T}}$ and $|v_N^{\pm}\rangle = [v_{N,x}^{\pm}\ v_{N,y}^{\pm}]^{\mathcal{T}}$ will of course correspond to the same state here, since $r_N = b_N/a_N = v_{N,y}^{\pm}/v_{N,x}^{\pm}$) and is a signifying characteristic of non-Hermitian and time-dependent Hamiltonians under the assumption of adiabatic and cyclic evolution.

Given now that state conversion to eigenvectors $|v_N^{\pm}\rangle$ indeed takes place, then such an effect can be characterized as either symmetric or asymmetric if at the end of the CW and CCW parametric encirclements switching to the same (see second and fourth rows) or different (see first and third rows) eigenmodes has been observed, accordingly. For instance, in the first row of Fig. 2, it is shown that $r_N = 1.02 + i0.02$ and $-1.02 + i0.02$ for clockwise (main panels) and counterclockwise (insets) evolutions, respectively [see Figs. 2(c) and 2(d)]—this is referred to as *asymmetric state conversion*. On the other hand, in the second row of Fig. 2, it is shown that $r_N = -0.3 + i0.38$ under both CW and CCW conditions [see Figs. 2(g) and 2(h)]—this is called *symmetric state conversion*. As evident from Fig. 2, the type (symmetric/asymmetric) of the observed mode switching behavior will highly depend not only on the location of the cyclic path within the parameter space, but also on the initial values of the gain (g_0) and detuning (σ_0) coefficients. In Sec. V within SM [76], an analytic proof of such an effect is illustrated for the special case of traceless and symmetric non-Hermitian Hamiltonian structures evolving adiabatically along square trajectories ($\epsilon_g = \epsilon_\sigma$) of small dimensions (in Sec. III C, this is extended to arbitrary closed paths in $\boldsymbol{\mathcal{R}}$ space and for generalized non-Hermitian configurations). Elements of such derivation are also provided in Appendix E, where our goal is to shed light on the mode switching mechanism but through a more brief and intuitive mathematical description.

While in the present section emphasis is given on non-Hermitian Hamiltonians of a specific form following closed trajectories of a specific geometric shape in parameter space, in Sec. III we will expand our analytical treatments to the general class of two-level open quantum structures. In this vein, the basic premises of the adiabatic theorem, as originally developed for Hermitian arrangements [1–6], shall be revisited and the notions of Berry and dynamical phase factors will be appropriately extended (see Secs. III A and III B). A generalized approach based on the eigendecomposition of the propagator matrices Ξ_n will be employed (Sec. III C), in order to analytically show that the ensued (symmetric/asymmetric) mode switching behavior takes place for cyclic parametric paths $\mathcal{C}^{\boldsymbol{\mathcal{R}}}$ of arbitrary form (under the assumption that no spectral degeneracy points are crossed). By tracking (and studying the topological features of) the trajectories that the eigenvalues of matrices M_n follow within the complex domain [Re(λ_n), Im(λ_n)], we will show how the resulting state vector $|u_n\rangle$ can be uniquely determined irrespective of the initial excitation conditions $|u_0\rangle$ [Re(.) and Im(.) represent the real and imaginary parts of the associated complex arguments].

D. Emulating discrete harmonic oscillator systems with complex and time-dependent damping profiles

Before proceeding to the analysis of generalized non-Hermitian Hamiltonian systems, here we will attempt to provide an alternative but mathematically equivalent description of the discrete $\mathcal{PT}$-symmetric-like configuration introduced in Sec. II B. For that purpose, a transformation of the following form

$$a_n = \prod_{j=0}^{n-1} \xi_j^{11} \widetilde{a}_n,\ b_n = \prod_{j=0}^{n-1} \xi_j^{22} \widetilde{b}_n, \tag{13}$$

shall be applied to Eq. (1) (the choice of the lower bound in the above product implies that $a_0 = \widetilde{a}_0$ and $b_0 = \widetilde{b}_0$, but we can choose any lower bound that facilitates our analysis). After employing the forward difference operator δ, Eq. (1) can be reexpressed with respect to $\widetilde{a}_n$ and $\widetilde{b}_n$ as

$$\begin{bmatrix} \delta\widetilde{a}_n \\ \delta\widetilde{b}_n \end{bmatrix} = \begin{bmatrix} 0 & \Omega_n^{12} \\ \Omega_n^{21} & 0 \end{bmatrix} \begin{bmatrix} \widetilde{a}_n \\ \widetilde{b}_n \end{bmatrix}, \tag{14}$$

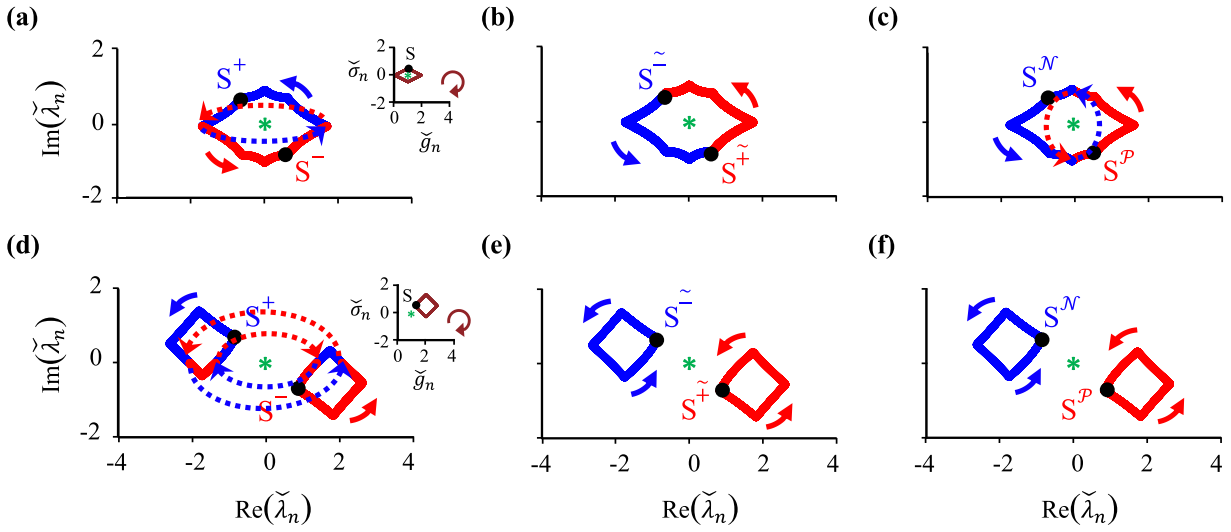

FIG. 4. Eigenspectra evolution in complex domain [Re($\breve{\lambda}_n$), Im($\breve{\lambda}_n$)] corresponding to (±) [(a),(d)], ($\tilde{\pm}$) [(b),(e)], and $\mathcal{P}, \mathcal{N}$ [(c),(f)] mode representations ($\breve{\lambda}_n = \lambda_n/\kappa$, $\breve{g}_n = g_n/\kappa$, $\breve{\sigma}_n = \sigma_n/\kappa$, and λ_n represent the eigenvalues of matrix M_n defined in Sec. II A). Notation ($\tilde{\pm}$) refers to an appropriate reordering of modes (±) ($\lambda_n^{\pm} = \pm i\sqrt{\kappa^2 - f_n^2}$, as found in Sec. II B for the traceless and symmetric Hamiltonian model), so as to achieve a smooth spectra evolution [as shown in (b),(e), ($\tilde{+}$) is assigned to the mode branch, which at least originally becomes dominant] and avoid any discontinuities {such abrupt "jumps" appear in (a) and (d) owing to the evaluation of the principal square root in the formula for $\lambda_n^{\pm}$—see definition of principal roots in Sec. II within SM [76]—and are generally denoted in our graphs with dotted lines} . This becomes necessary when studying the behavior of the arrangement in the continuous time limit ($\Delta \to 0$), so as to ensure the continuity of the involved time-dependent functions and consequently the well definedness of the respective time derivatives and integrals. On the other hand, $\mathcal{P}, \mathcal{N}$ mode notation emphasizes on the classification of modes (±) into dominant ($\mathcal{P}$) and nondominant ($\mathcal{N}$) ones, at each time instant [i.e., $\mathrm{Re}(\Delta\lambda_n^{\mathcal{P}}) \geqslant \mathrm{Re}(\Delta\lambda_n^{\mathcal{N}}) \overset{\Delta\geqslant 0}{\Rightarrow} \mathrm{Re}(\lambda_n^{\mathcal{P}}) \geqslant \mathrm{Re}(\lambda_n^{\mathcal{N}})$ for all values of n, with the equality not holding simultaneously for all operation points in $\boldsymbol{\mathcal{R}}$ space so as the distinction into $\mathcal{P}$ and $\mathcal{N}$ modes holds ground; see also respective analysis in Sec. III C]. The numerical study was based on the $\mathcal{PT}$-symmetric-like model of Sec. II B [in this case, it can be shown that $\mathrm{Re}(\lambda_n^{\mathcal{P}}) \geqslant 0$ and $\mathrm{Re}(\lambda_n^{\mathcal{N}}) \leqslant 0$ as also indicated in (c) and (f)] evolving in a clockwise manner along rhombic parametric loops $\mathcal{C}_{\mathcal{R}\hbar}^{\boldsymbol{\mathcal{R}}}$ (see inset schematics). The following parameter scenarios were considered: (i) $\breve{g}_C = 1$, $\breve{\sigma}_C = 0$, $\breve{\epsilon}_g = 1$, $\breve{\epsilon}_\sigma = 0.5$ (top row results) and (ii) $\breve{g}_C = 2$, $\breve{\sigma}_C = 0.5$, $\breve{\epsilon}_g = 0.8$, $\breve{\epsilon}_\sigma = 0.8$ (bottom row results). In all cases, the starting point S of evolution along path $\mathcal{C}_{\mathcal{R}\hbar}^{\boldsymbol{\mathcal{R}}}$ is illustrated with a filled black circle in the inset schematics ($S^{\pm}$, $S^{\tilde{\pm}}$, $S^{\mathcal{P},\mathcal{N}}$ denote the respective points in the eigenspectra complex domain), while the exceptional point degeneracy is signified with a green asterisk. Finally, the interested reader can also resort to Sec. VI within SM [76], where the distinctions among the various mode formalisms are described in even more detail with respect to the top row graphs in the above figure.

where $\Omega_n^{12} = \xi_n^{12}(\prod_{j=0}^{n}\xi_j^{11})^{-1}\prod_{j=0}^{n-1}\xi_j^{22}$ and $\Omega_n^{21} = \xi_n^{21}(\prod_{j=0}^{n}\xi_j^{22})^{-1}\prod_{j=0}^{n-1}\xi_j^{11}$. The new and equivalent set of evolution equations is now described by a hollow matrix, which in turn allows to more clearly identify the cross-modulation effect between the transformed state vector components ($\delta\widetilde{a}_n = \Omega_n^{12}\widetilde{b}_n$, $\delta\widetilde{b}_n = \Omega_n^{21}\widetilde{a}_n$). As shown in Appendix A, the following difference relations can be attained from Eq. (14),

$$\delta^2\widetilde{a}_n + p_{n,1}^{\delta\widetilde{a}}\delta\widetilde{a}_n + p_{n,0}^{\delta\widetilde{a}}\widetilde{a}_n = 0, \quad (15a)$$

$$\widetilde{a}_{n+2} + \left(-2 + p_{n,1}^{\delta\widetilde{a}}\right)\widetilde{a}_{n+1} + \left(1 - p_{n,1}^{\delta\widetilde{a}} + p_{n,0}^{\delta\widetilde{a}}\right)\widetilde{a}_n = 0, \quad (15b)$$

where $p_{n,1}^{\delta\widetilde{a}} = (\xi_n^{12}\xi_{n+1}^{11} - \xi_{n+1}^{12}\xi_n^{22})/(\xi_n^{12}\xi_{n+1}^{11})$ and $p_{n,0}^{\delta\widetilde{a}} = -\xi_{n+1}^{12}\xi_n^{21}/(\xi_n^{11}\xi_{n+1}^{11})$. The respective evolution equations that $\widetilde{b}_n$ satisfies can be retrieved by a simple exchange of superscripts $1 \leftrightarrow 2$ in the expressions for $p_{n,1}^{\delta\widetilde{a}}$ and $p_{n,0}^{\delta\widetilde{a}}$.

For the special case of the $\mathcal{PT}$-symmetric-like arrangement of Sec. II B, Eqs. (15) will assume the subsequent form

($\delta t_n = \Delta$, $\delta t_n^2 = \Delta^2$)

$$\frac{\delta^2\widetilde{a}_n}{\delta t_n^2} + \frac{f_{n+1} + f_n}{1 + \Delta f_{n+1}}\frac{\delta\widetilde{a}_n}{\delta t_n} + \frac{\kappa^2}{(1 + \Delta f_{n+1})(1 + \Delta f_n)}\widetilde{a}_n = 0, \quad (16a)$$

$$\widetilde{a}_{n+2} + \frac{-2 + \Delta(f_n - f_{n+1})}{1 + \Delta f_{n+1}}\widetilde{a}_{n+1} + \frac{1 + \Delta^2(\kappa^2 - f_n^2)}{(1 + \Delta f_{n+1})(1 + \Delta f_n)}\widetilde{a}_n = 0. \quad (16b)$$

.

In the continuous time limit ($\Delta \to 0$), the difference operator δ can be replaced by the differential operator d and consequently Eq. (16a) will read as [$t_n \to t$, f_{n+1} & $f_n \to f(t)$, $\widetilde{a}_n \to \widetilde{a}(t)$; see also Appendix A]

$$\frac{d^2\widetilde{a}(t)}{dt^2} + 2f(t)\frac{d\widetilde{a}(t)}{dt} + \kappa^2\widetilde{a}(t) = 0. \quad (17)$$

Such an equation clearly corresponds to a harmonic oscillator exhibiting a complex and time-dependent damping coefficient [$2f(t)$] with a positive or negative real profile, depending on the sign of $g(t)$[=Re($f(t)$)] or g_n[= Re(f_n)].

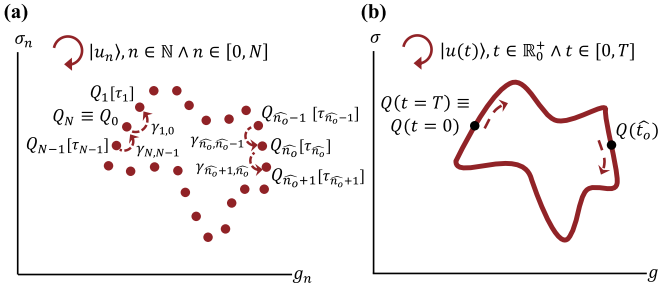

FIG. 5. (a) Evolution of state vector $|u_n\rangle$ in N discrete steps along closed path $\mathcal{C}^{\boldsymbol{\mathcal{R}}}$ residing within a 2D parameter space $\boldsymbol{\mathcal{R}} = (g_n, \sigma_n)$ and defined by points Q_n ($n \in \mathbb{N} \wedge n \in [0, N]$, $\widehat{n_o}$ is an arbitrary value that n might take). Terms $\gamma_{n+1,n} = -i \ln\langle v_{n+1}^L || v_n^R\rangle$ and $\tau_n = -i \ln\lambda_{\Xi_n} = -i \ln(1 + \Delta\lambda_n)$ designate the discrete contributions to the complex Berry ($\gamma = \sum_{n=0}^{N-1} \gamma_{n+1,n}$) and dynamical phases ($\tau = \sum_{n=0}^{N-1} \tau_n$). In the previous formulas, $\langle v_n^L|$ and $|v_n^R\rangle$ denote the instantaneous left and right eigenvectors related to eigenvalue level λ_n (or equivalently λ_{Ξ_n}). (b) Continuum limit, in which gain and detuning parameters become continuous functions of time [$g = g(t), \sigma = \sigma(t)$] with $t \in \mathbb{R}_0^+ \wedge t \in [0, T]$ ($\widehat{t_o}$ is an arbitrary value that t might assume). The continuous time complex Berry and dynamical phases after a full cycle will be given by $\gamma = \int_0^T \langle v^L(t) || i\, d v^R(t)/dt\rangle dt = \oint_{\mathcal{C}^{\boldsymbol{\mathcal{R}}}} \langle v^L(\boldsymbol{\mathcal{R}}) || i \nabla_{\boldsymbol{\mathcal{R}}} v^R(\boldsymbol{\mathcal{R}})\rangle d\boldsymbol{\mathcal{R}}$ and $\tau = \int_0^T \lambda(t) dt = -i \int_0^T \lambda_H(t) dt$, where $\langle v^L(t)|$ and $|v^R(t)\rangle$ are the instantaneous left and right eigenvectors corresponding to eigenvalue level $\lambda(t) = -i\lambda_H(t)$ (see Appendix F).

After setting $f(t) \to -f(t)$ in Eq. (17), we can directly obtain the differential equation that coefficient $\widetilde{b}(t)$ satisfies [in this case, if one of the quantities $\widetilde{a}(t)$, $\widetilde{b}(t)$ experiences gain, the other will experience loss]. In other words, the components of the transformed state vector $[\widetilde{a}_n \;\; \widetilde{b}_n]^{\mathcal{T}}$ can faithfully describe the dynamics underpinning the generalized damped harmonic oscillator in its discrete manifestation (see Eqs. (16) and [68–73]). From an experimental perspective, the complex and discrete factor $f_n = g_n - i\sigma_n$ can be precisely tuned within an active fiber loop network after exploiting appropriate electro-optic and phase modulators (see [65–67], along with discussions in Sec. II B and Sec. IV within SM [76]). In this regard, an arbitrary complex damping profile can be synthesized and as a result, access to the rich dynamics of Eqs. (16) and (17) can be guaranteed. Specific examples, which lead to analytically solvable models, are depicted in Fig. 3 (the exact forms of the associated solutions are illustrated in Sec. III within SM [76]). The case of a constant damping profile, which corresponds to a *Caldirola-Kanai Hamiltonian system* [79–81], is also shown Fig. 3(a) for comparison purposes.

In general, the essence of the broad class of *time-dependent parametric oscillators* (characterized by a time-dependent damping factor and natural frequency of oscillation) is twofold: (i) they can describe a diverse variety of physical settings, and (ii) they can lead to exactly solvable models (e.g., oscillator systems satisfying equations of the *Mathieu-Hill, Laguerre, Meijer G function,* or *generalized hypergeometric type*, to mention a few; see also Sec. III within SM [76]). For instance, it has been shown that the equations of motion for charged particles moving nonrelativistically within a time-varying magnetic field of the form $\boldsymbol{B} = h(t)\boldsymbol{B_o}$ [vector $\boldsymbol{B_o}$ is constant and the scalar potential is assumed to be zero; bold quantities refer here to vectors] can be reduced to those of a classical time-dependent parametric oscillator with complex phase space parameters [82–85]. More exotic examples exist within the quantum field theory of external fields, i.e., in the particle production in an expanding cosmological background or in a strong time-dependent electric field—*Schwinger effect* [86]. Similar canonical oscillator schemes appear frequently in the fields of physiology and behavioral/perception analysis. Two prominent examples are the attempts to describe (a) the excellent tuning properties along with the extreme auditory sensitivity exhibited within the mammalian cochlea [87,88], and (b) the erratic behavior (cycles of alternating hypomanic and depressive episodes) displayed by patients exhibiting acute bipolar type-II disorder [89]. Overall, it becomes evident how essential the role of parametric oscillator models is in investigating a variety of phenomena arising from the field of modern physics. As such, the alternative Hamiltonian framework introduced in the present section to describe the $\mathcal{PT}$-symmetric-like dimer model of Sec. II B, opens up the unique possibility of emulating the aforementioned (or dynamically equivalent) effects within discrete photonic platforms and in that manner derive useful qualitative and quantitative conclusions based on ordinary optical benchtop experiments.

III. ADIABATIC DYNAMICS OF GENERALIZED AND DISCRETE NON-HERMITIAN SYSTEMS

A. Discrete time complex dynamical and Berry phase factors

In Sec. II C, it was numerically illustrated that a traceless and symmetric non-Hermitian Hamiltonian system evolving along rhombic parametric trajectories $\mathcal{C}^{\boldsymbol{\mathcal{R}}}_{\mathcal{R}\hbar}$ will exhibit either a symmetric or an asymmetric mode switching behavior for sufficiently large cycling periods (a heuristic analytical derivation was also provided in Appendix E). Of course, this is not solely a property of paths $\mathcal{C}^{\boldsymbol{\mathcal{R}}}_{\mathcal{R}\hbar}$ and naturally should generalize to trajectories of arbitrary geometric forms. Our emphasis in Sec. III will be to develop the necessary machinery to accurately describe the adiabatic dynamics of discrete Hamiltonian arrangements moving along arbitrary closed paths $\mathcal{C}^{\boldsymbol{\mathcal{R}}}$ in parameter space $\boldsymbol{\mathcal{R}}$. In this regard, alternative mode representations [generically assigned as $(\widehat{\pm})$] were used throughout our subsequent theoretical and numerical calculations in order to (i) highlight different dynamical aspects of generalized non-Hermitian settings, and (ii) allow for the presence of abrupt transitions (or discontinuities) in the eigenspectra evolution (see Fig. 4 for a description of the $(\pm)$, $(\widetilde{\pm})$, and $\mathcal{P}, \mathcal{N}$ mode designations, along with the detailed investigation provided in Sec. VI within SM [76]).

As a first step in the analysis, the key concepts of both dynamical and geometric Berry phase factors will be revisited and appropriately redefined for discrete non-Hermitian environments. In this vein, the requirement for smooth eigenspectra evolution (see for instance studies [1–6,51–55]) shall be relaxed and notation $(\widehat{\pm})$ will be employed (this will prove

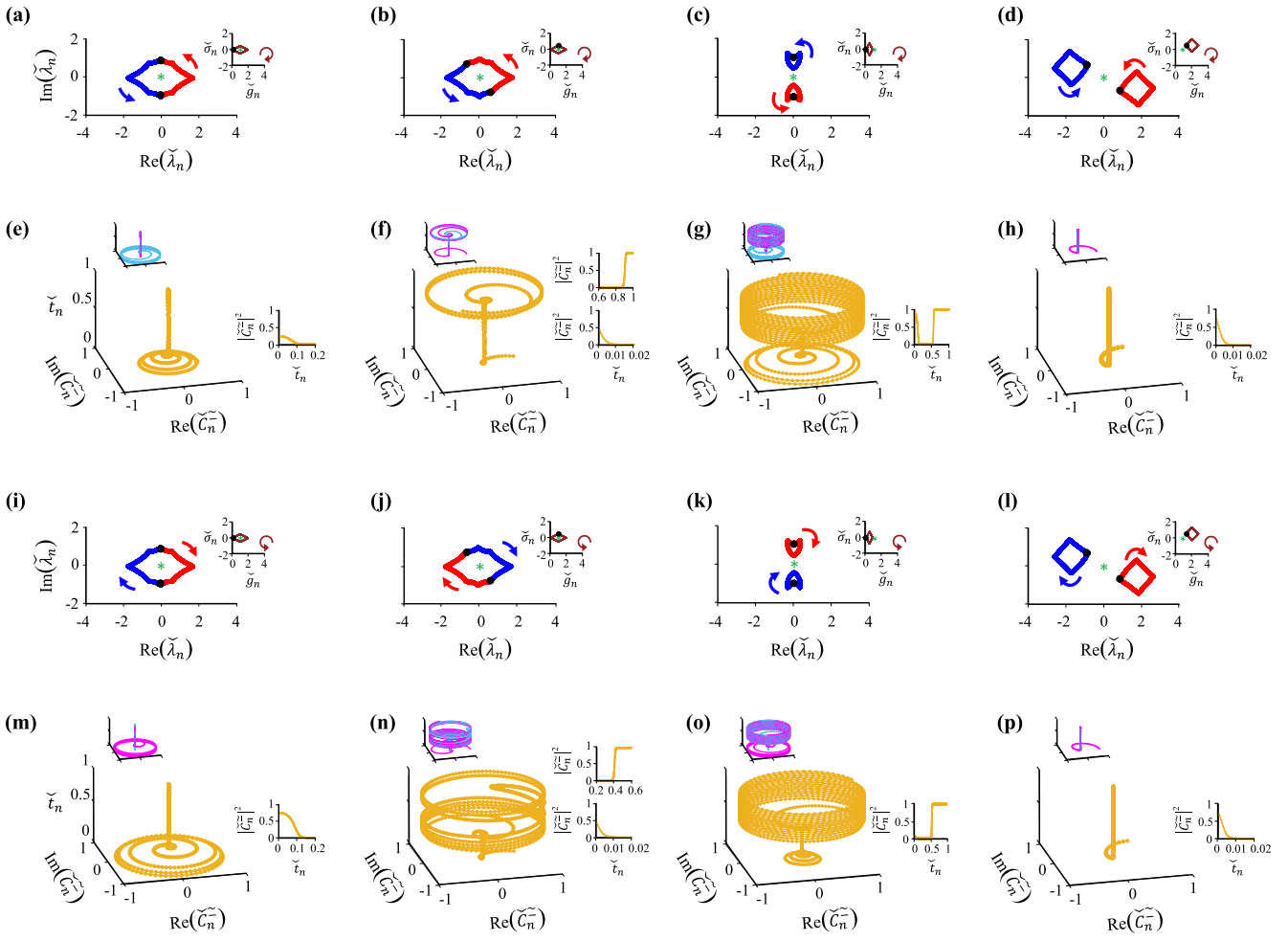

FIG. 6. Discrete evolution dynamics of modes ($\tilde{\pm}$) associated with standard quantum adiabatic theory (see Sec. III B). For comparison purposes, model parameters are kept to the same values as in the four rows of Fig. 2 (first/second/third/fourth column in the above figure corresponds to the first/second/third/fourth row in Fig. 2), except from doubling the number of points along curve $\mathcal{C}_{\mathcal{R}\mathfrak{f}}^{\mathcal{R}}$ in order to examine the effect of variable N on the observed mode switching behavior. The first and third rows depict the eigenspectra evolution [red and blue branches correspond to the ($\tilde{+}$) and ($\tilde{-}$) modes, respectively] for CW and CCW encircling directions in parameter space, accordingly (insets refer to the paths followed in $\boldsymbol{\mathcal{R}}$ space, filled black circles indicate the starting points within both parameter space and eigenspectrum domain, green asterisk shows the exceptional point). The second (CW) and last (CCW) rows depict the dynamics associated with mode ($\tilde{-}$) ($\breve{C}_n^{\tilde{-}} = C_n^{\tilde{-}}/\sqrt{|C_n^{\tilde{+}}|^2 + |C_n^{\tilde{-}}|^2}$, $C_n^{\tilde{\pm}} = \langle v_n^{\tilde{\pm},L} || u_n \rangle$) for random excitation conditions (see main figures) and for excitation of eigenmodes ($\tilde{\pm}$) (see magenta and light blue curves at insets; axis margins were kept the same to the main figures). Additional insets are provided to show the behavior of $|\breve{C}_n^{\tilde{-}}|^2$ in various time intervals of interest. The failure of adiabatic theory becomes evident from (f), (g), (n), (o), as mode ($\tilde{-}$) (originally identified as the nondominant eigenstate) attains a more prominent role at the end of the cyclic evolution [this comes in stark contrast to (e), (h), (m), (p), where $\breve{C}_N^{\tilde{-}} \simeq 0$]. The interested reader can also refer to Fig. S5 within SM [76] regarding the discrete evolution results corresponding to mode ($\tilde{+}$).

especially useful in Sec. III C, when deriving the asymptotic state conversion property of cyclic and slowly varying non-Hermitian Hamiltonian structures). Following such a consideration, we can return to Eq. (1), which describes the dynamics of state vector $|u_n\rangle$ under the most general conditions ($|u_{n+1}\rangle = \Xi_n |u_n\rangle$). By expressing $|u_n\rangle$ as a linear superposition of the instantaneous right eigenvectors $|\hat{v}_n^{\tilde{\pm},R}\rangle$ of the propagator matrix Ξ_n, we can pursue solutions to Eq. (1) of the form [77,78]

$$|u_n\rangle = c_n^{\hat{+}} \prod_{j=0}^{n-1} \lambda_{\Xi_j}^{\hat{+}} |v_n^{\hat{+},R}\rangle + c_n^{\hat{-}} \prod_{j=0}^{n-1} \lambda_{\Xi_j}^{\hat{-}} |v_n^{\hat{-},R}\rangle$$
$$= c_n^{\hat{+}} \prod_{j=0}^{n-1} \left(1 + \Delta\lambda_j^{\hat{+}}\right) |v_n^{\hat{+},R}\rangle + c_n^{\hat{-}} \prod_{j=0}^{n-1} \left(1 + \Delta\lambda_j^{\hat{-}}\right) |v_n^{\hat{-},R}\rangle, \tag{18}$$

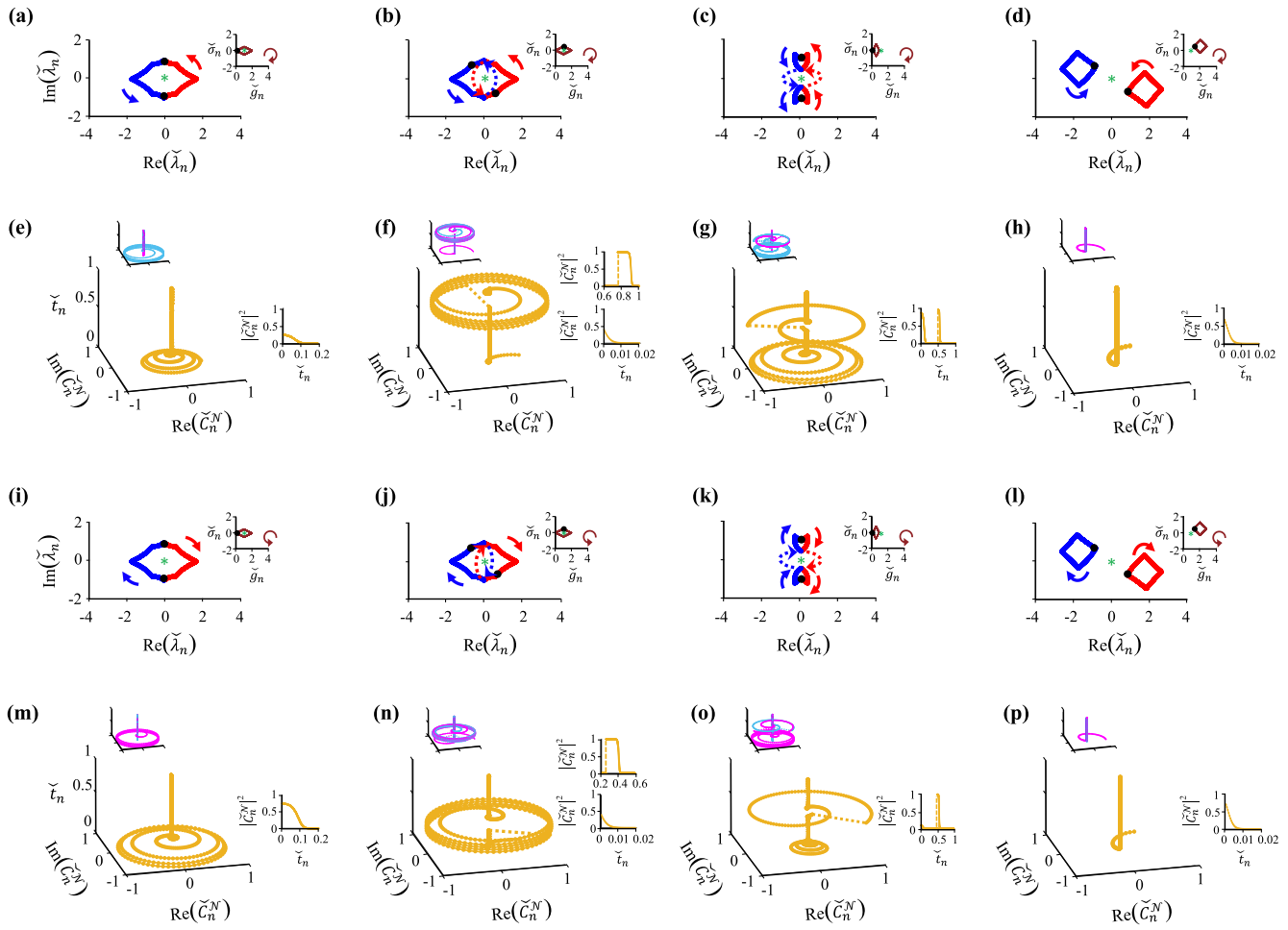

FIG. 7. Discrete evolution dynamics of the instantaneous (non)dominant $(\mathcal{P},\mathcal{N})$ eigenstates (see Sec. III C). Model parameters for each of the four columns in the above figure are kept the same to the values used in the corresponding four columns of Fig. 6. Overall, the structure of the present figure is analogous to that of Fig. 6, with the difference being that here we refer to the $\mathcal{P},\mathcal{N}$ modes of the traceless and symmetric non-Hermitian Hamiltonian arrangement of Sec. II B (the red and blue branches appearing in the eigenspectra evolution graphs of rows one and three are associated now with the $\mathcal{P}$ and $\mathcal{N}$ modes, respectively). Moreover, in all cases conversion to the $\mathcal{P}$ mode is noticed as expected from the analysis of Sec. III C, irrespective of the encircling direction in $\boldsymbol{\mathcal{R}}$ space ($\check{C}_N^{\mathcal{N}} \simeq 0$ as shown in (e)–(h) and (m)–(p), with $\check{C}_n^{\mathcal{N}} = C_n^{\mathcal{N}}/\sqrt{|C_n^{\mathcal{P}}|^2+|C_n^{\mathcal{N}}|^2}$ and $C_n^{\mathcal{P}} = \langle v_n^{\mathcal{P},L}||u_n\rangle$, $C_n^{\mathcal{N}} = \langle v_n^{\mathcal{N},L}||u_n\rangle$; the dynamics of the $\mathcal{P}$ mode is complementary to that of the $\mathcal{N}$ mode and has been included in Fig. S6 within SM [76]). Both symmetric (columns two and four) and asymmetric (columns one and three) mode switching can occur depending on whether the ending points of the $\mathcal{P}$ mode branch coincide [compare (b) with (j), and (d) with (l)] or not [compare (a) with (i), and (c) with (k)] at the end of the CW and CCW parametric evolutions. The discontinuities, appearing as dotted/dashed lines in columns two and three, can be attributed to the relation $\mathrm{Re}(\Delta\lambda_n^{\mathcal{P}}) \geqslant \mathrm{Re}(\Delta\lambda_n^{\mathcal{N}})$ that the $\mathcal{P},\mathcal{N}$ modes need to satisfy (see also Fig. 4 or Sec. III C). This in turn implies that the results demonstrated in the aforementioned columns will be different as compared to the corresponding graphs in Fig. 6 [relation $\mathrm{Re}(\Delta\lambda_n^{\tilde{+}}) \geqslant \mathrm{Re}(\Delta\lambda_n^{\tilde{-}})$ will not be satisfied in these numerical scenarios]. On the other hand, the schematics appearing in the first and last columns of Fig. 7 are in accordance with the respective diagrams shown in Fig. 6 [relation $\mathrm{Re}(\Delta\lambda_n^{\tilde{+}}) \geqslant \mathrm{Re}(\Delta\lambda_n^{\tilde{-}})$ is now satisfied and thus mode $(\tilde{+})$ remains dominant along the entire parametric loop],

where $\lambda_j^{\hat{\pm}}$ ($\lambda_{\Xi_j}^{\hat{\pm}} = 1 + \Delta\lambda_j^{\hat{\pm}}$) describe the eigenvalues of matrix M_n ($\Xi_n = I + \Delta M_n$) as defined in Sec. II A and $c_n^{\hat{\pm}}$ denote the complex amplitudes (phasors) associated with modes $(\hat{+})$ and $(\hat{-})$. It should be highlighted that in the analytical study of Sec. III, we shall mostly focus on the behavior of the eigenvalues λ_n of matrix M_n (as opposed to the more conventional Hamiltonian formalism, where emphasis is given on the eigenenergies λ_{H_n} of the Hamiltonian H_n), along with their effect on the dynamics of state vector $|u_n\rangle$. If we now consider the continuous time limit of Eq. (18), coefficients $\prod_{j=0}^{n-1}(1+\Delta\lambda_j^{\hat{\pm}})$ can become clearly related to the dynamical phase factor. Indeed, after replacing mode notation $(\hat{\pm})$ with $(\tilde{\pm})$ to signify the absence of any ill-defined derivatives or integrals arising from spectral discontinuities [see Figs. 4(b) and 4(e) and compare with Figs. 4(a), 4(d), and 4(c), 4(f)], it will be true as $\Delta \to 0$ based also on the standard definition of

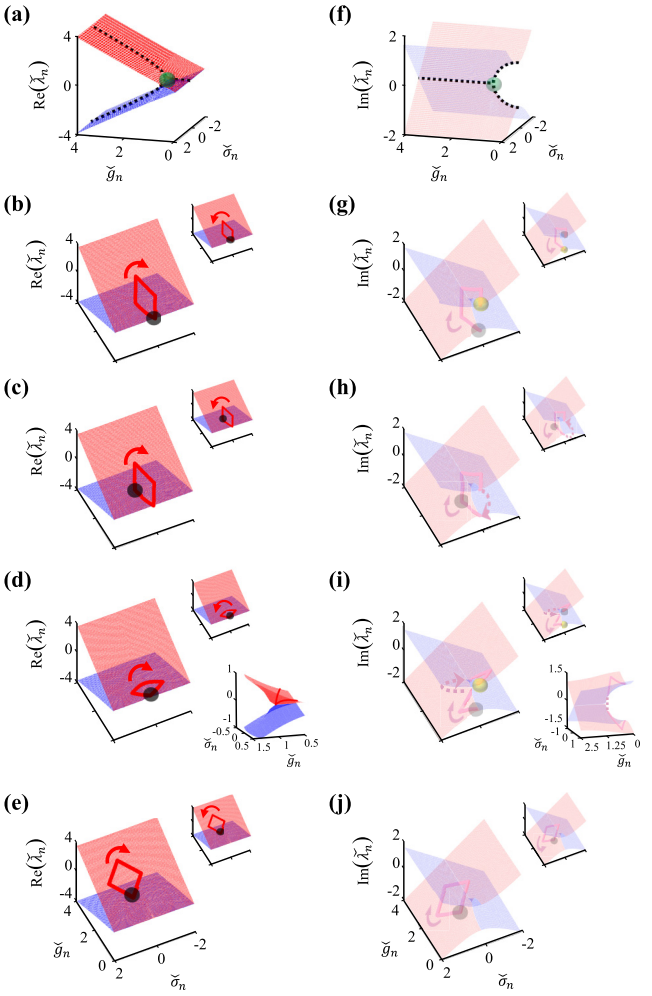

FIG. 8. Riemann surfaces related to the $\mathcal{PT}$-symmetric-like Hamiltonian model of Sec. II B (the red and blue sheets indicate the $\mathcal{P}$ and $\mathcal{N}$ modes, respectively, while the left and right columns represent the real and imaginary parts of eigenvalues $\breve{\lambda}_n^{\mathcal{P},\mathcal{N}} = \lambda_n^{\mathcal{P},\mathcal{N}}/\kappa$, correspondingly). The trajectories that the instantaneous dominant eigenvalue $\breve{\lambda}_n^{\mathcal{P}}$ follows for each of the four parametric paths associated with the four columns of Fig. 7, are illustrated in rows two through five [(b)–(e) and (g)–(j) depict the real and imaginary spectra for the numerical case scenarios shown in columns one through four of Fig. 7, accordingly; main and inset figures depict simulation results for CW and CCW evolution in parameter space $\boldsymbol{\mathcal{R}}$, respectively]. Black and yellow spheres denote the starting and ending points of evolution in the eigenspectra domain (see rows two through five—if the ending and starting points coincide, then the yellow spheres are omitted), while the position of the exceptional point at $(\breve{g}_{n_{EP}}, \breve{\sigma}_{n_{EP}}, \breve{\lambda}_{n_{EP}}) = (1, 0, 0)$ is denoted with a green sphere (see top row). Abrupt transitions in the evolution of $\breve{\lambda}_n^{\mathcal{P}}$ appear in the imaginary spectra shown in rows three and four (light red dotted lines), as also expected from Figs. 7(b), 7(c), 7(j), and 7(k). In all cases, insets have the same axis margins with the main graphs, except in the extra insets provided in row four depicting a magnification of the underlying geometry near the EP.

Riemann sums that $\prod_{j=0}^{n-1}(1+\Delta\tilde{\lambda}_j^{\tilde{\pm}}) \simeq e^{\Delta\sum_{j=0}^{n}\tilde{\lambda}_j^{\tilde{\pm}}} \simeq e^{\int_0^t \tilde{\lambda}^{\tilde{\pm}}(t')dt'} = e^{-i\int_0^t \tilde{\lambda}_H^{\tilde{\pm}}(t')dt'}$ [$\lambda(t) = -i\lambda_H(t)$ according to Sec. II A]. It should be noted that while for continuous time systems mode designation $(\tilde{\pm})$ is more appropriate in order to ensure the continuity of the involved time-dependent functions, discrete time arrangements do not show analogous limitations and as a result the alternative mode representations presented in Fig. 4 can become also applicable (for a more in-depth discussion on the topic of [eigen]state continuity, the reader can refer to Sec. VI within SM [76]).

In all the analysis so far, we have assumed right eigenvectors of the respective matrices/operators. At this point, we need to to also introduce the left eigenvectors $\langle \hat{v}_n^{\hat{\pm},L}|$ of matrices Ξ_n, which form a complete biorthogonal basis with $|\hat{v}_n^{\hat{\pm},R}\rangle$ [90]. This in turn implies that $\langle \hat{v}_n^{\hat{\pm},L}||\hat{v}_n^{\hat{\mp},R}\rangle = 0$, while we also demand the convention $\langle \hat{v}_n^{\hat{\pm},L}||\hat{v}_n^{\hat{\pm},R}\rangle = 1$ (this can be easily satisfied after appropriately normalizing the left and right eigenvectors as demonstrated in Appendix F). Such biorthonormality conditions preclude that the Hamiltonian system cannot operate at an exceptional point during its evolution in parameter space, since at such a point it must apply that $\langle v_{n_{EP}}^L||v_{n_{EP}}^R\rangle = 0$ as shown in Appendix F ($\langle \hat{v}_{n_{EP}}^{\hat{\pm},L}| = \langle v_{n_{EP}}^L|$, $|\hat{v}_{n_{EP}}^{\hat{\pm},R}\rangle = |v_{n_{EP}}^R\rangle$). After substituting the expression of Eq. (18) to Eq. (1), we can obtain the difference equations that $\hat{c}_n^{\hat{\pm}}$ satisfy

$$\hat{c}_{n+1}^{\hat{+}}\prod_{j=0}^{n}\left(1+\Delta\hat{\lambda}_j^{\hat{+}}\right)\left|\hat{v}_{n+1}^{\hat{+},R}\right\rangle + \hat{c}_{n+1}^{\hat{-}}\prod_{j=0}^{n}\left(1+\Delta\hat{\lambda}_j^{\hat{-}}\right)\left|\hat{v}_{n+1}^{\hat{-},R}\right\rangle = \hat{c}_n^{\hat{+}}\prod_{j=0}^{n}\left(1+\Delta\hat{\lambda}_j^{\hat{+}}\right)\left|\hat{v}_n^{\hat{+},R}\right\rangle + \hat{c}_n^{\hat{-}}\prod_{j=0}^{n}\left(1+\Delta\hat{\lambda}_j^{\hat{-}}\right)\left|\hat{v}_n^{\hat{-},R}\right\rangle, \tag{19}$$

where we have used that $\Xi_n|\hat{v}_n^{\hat{\pm},R}\rangle = (1+\Delta\hat{\lambda}_n^{\hat{\pm}})|\hat{v}_n^{\hat{\pm},R}\rangle$. Subsequently, Eq. (19) can be further simplified after multiplying both its left- and right-hand sides with $\prod_{j=0}^{n}(1+\Delta\hat{\lambda}_j^{\hat{\pm}})^{-1}\langle\hat{v}_{n+1}^{\hat{\pm},L}|$. By taking advantage of the biorthonormality conditions between the left and right eigenvectors, the population dynamics of eigenmodes $(\hat{\pm})$ can now be described by

$$\hat{c}_{n+1}^{\hat{\pm}} = \hat{c}_n^{\hat{\pm}}\langle\hat{v}_{n+1}^{\hat{\pm},L}||\hat{v}_n^{\hat{\pm},R}\rangle + \hat{c}_n^{\hat{\mp}}\prod_{j=0}^{n}\frac{1+\Delta\hat{\lambda}_j^{\hat{\mp}}}{1+\Delta\hat{\lambda}_j^{\hat{\pm}}}\langle\hat{v}_{n+1}^{\hat{\pm},L}||\hat{v}_n^{\hat{\mp},R}\rangle. \tag{20}$$

In the above formula, the first and second terms in the right-hand side are referred to as the *adiabatic (or "self-modulation") and nonadiabatic (or "cross-modulation") factors*, respectively. Equation (20) can be also reexpressed as follows after subtracting element $\hat{c}_n^{\hat{\pm}} = \hat{c}_n^{\hat{\pm}}\langle\hat{v}_{n+1}^{\hat{\pm},L}||\hat{v}_{n+1}^{\hat{\pm},R}\rangle$ ($\delta\hat{c}_n^{\hat{\pm}} = \hat{c}_{n+1}^{\hat{\pm}} - \hat{c}_n^{\hat{\pm}}$, $\delta t_n = \Delta$),

$$i\frac{\delta\hat{c}_n^{\hat{\pm}}}{\delta t_n} = -\hat{c}_n^{\hat{\pm}}\left\langle\hat{v}_{n+1}^{\hat{\pm},L}\middle|i\frac{\delta\hat{v}_n^{\hat{\pm},R}}{\delta t_n}\right\rangle - \hat{c}_n^{\hat{\mp}}\prod_{j=0}^{n}\frac{1+\Delta\hat{\lambda}_j^{\hat{\mp}}}{1+\Delta\hat{\lambda}_j^{\hat{\pm}}}\left\langle\hat{v}_{n+1}^{\hat{\pm},L}\middle|i\frac{\delta\hat{v}_n^{\hat{\mp},R}}{\delta t_n}\right\rangle. \tag{21}$$

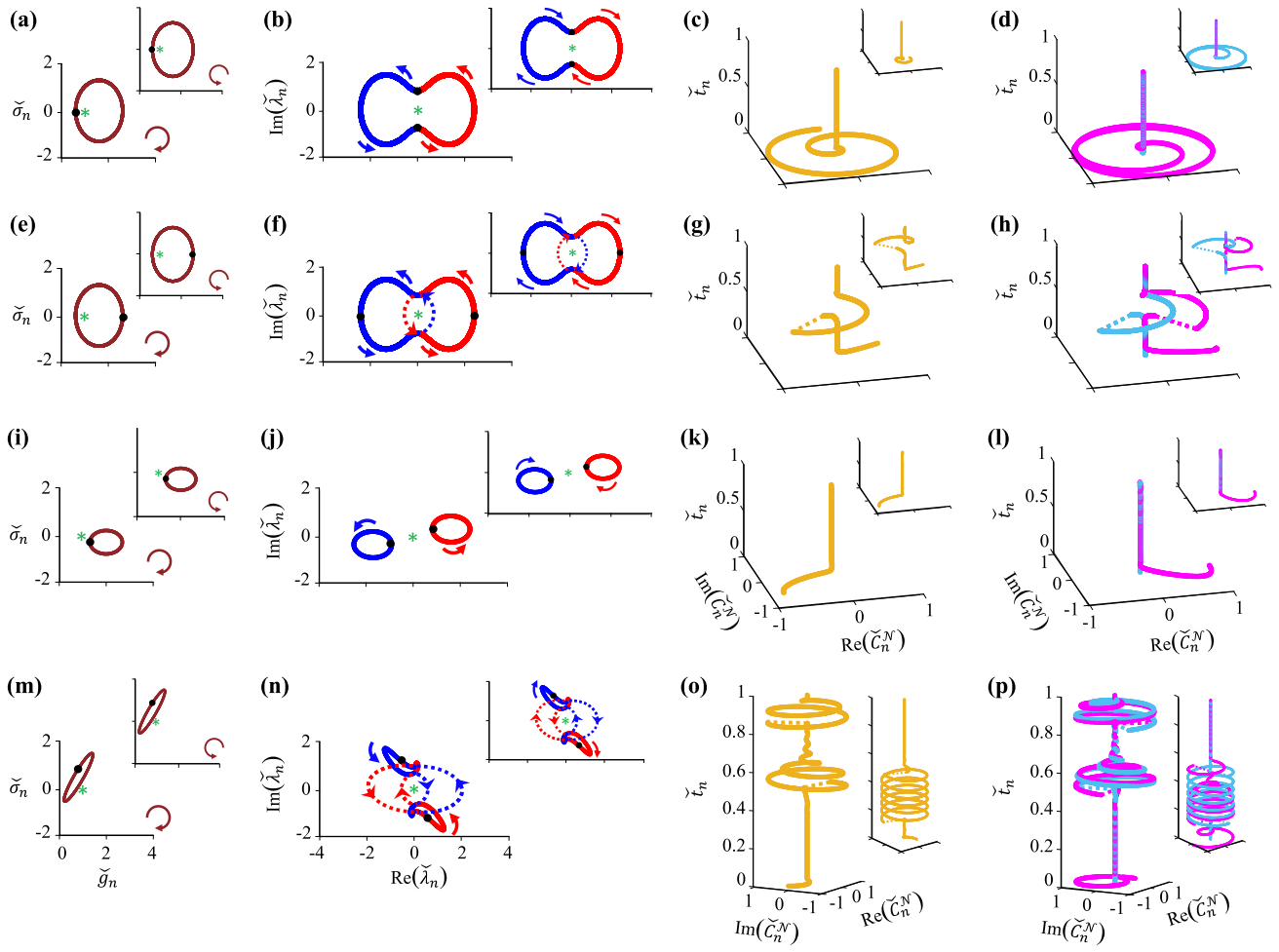

FIG. 9. Discrete evolution dynamics of the instantaneous $\mathcal{P},\mathcal{N}$ eigenstates associated with the traceless and symmetric non-Hermitian Hamiltonian system (see Sec. II B) moving along elliptical trajectories $\mathcal{C}^{\boldsymbol{\mathcal{R}}}$ (see first column) described parametrically by equations $\breve{g}_n = \breve{g}_C + \breve{R}_g\cos\phi_n\cos\theta - \breve{R}_\sigma\sin\phi_n\sin\theta$, $\breve{\sigma}_n = \breve{\sigma}_C + \breve{R}_g\cos\phi_n\sin\theta + \breve{R}_\sigma\sin\phi_n\cos\theta$, where $\phi_n = \phi_o \mp 2\pi\breve{t}_n = \phi_o \mp 2\pi n/N$ ($-$ and $+$ signs refer to CW and CCW encirclements along $\mathcal{C}^{\boldsymbol{\mathcal{R}}}$, accordingly) and θ defines the rotation angle of the ellipse (symbol $\vee$ denotes here normalization with respect to κ, except when used for time where $\breve{t}_n = t_n/T = n/N$; see also captions of Figs. 2 and 4). Each row corresponds to a different simulation scenario (main graphs and insets correspond to CW and CCW evolution in parameter space, respectively): (a)–(h) $\breve{g}_C = 1.6$, $\breve{\sigma}_C = 0$, $\breve{R}_g = 1$, $\breve{R}_\sigma = 1.3$, $\theta = 0$ and $\phi_o = \pi$, $N = 30000$ [(a)–(d)] or $\phi_o = 0$, $N = 2000$ [(e)–(h)], [(i)–(l)] $\breve{g}_C = 2$, $\breve{\sigma}_C = -0.3$, $\breve{R}_g = 0.7$, $\breve{R}_\sigma = 0.5$, $\theta = 0$, $\phi_o = \pi$, $N = 6000$, [(m)–(p)] $\breve{g}_C = 0.8$, $\breve{\sigma}_C = 0.5$, $\breve{R}_g = 0.2$, $\breve{R}_\sigma = 1.2$, $\theta = -\pi/6$, $\phi_o = 8\pi/9$, $N = 11000$. A smaller value for the coupling strength was used here ($\Delta\kappa = 0.01$) as compared to all previously simulated examples ($\Delta\kappa = 0.1$—see captions of Figs. 2, 6, and 7), which in turn resulted in an overall increased period of encirclement T (or equivalently a larger value for N as Δ was kept fixed in all cases) for state conversion to take place. The dynamical behavior of the instantaneous eigenvalues $\lambda_n^{\mathcal{P},\mathcal{N}}$ is depicted in the second column (red and blue branches are associated with the $\mathcal{P}$ and $\mathcal{N}$ modes, accordingly), while in the last two columns the population dynamics of the $\mathcal{N}$ mode ($\breve{C}_n^{\mathcal{N}} = C_n^{\mathcal{N}}/\sqrt{|C_n^{\mathcal{P}}|^2 + |C_n^{\mathcal{N}}|^2}$, $C_n^{\mathcal{P}} = \langle v_n^{\mathcal{P},L}||u_n\rangle$, $C_n^{\mathcal{N}} = \langle v_n^{\mathcal{N},L}||u_n\rangle$) is demonstrated for random initial excitation conditions (orange curves in third column) and for excitation of either of the instantaneous eigenmodes of the traceless non-Hermitian system (magenta and light blue curves in last column). In all scenarios, state conversion to the $\mathcal{P}$ mode is noticed ($\breve{C}_N^{\mathcal{N}} \simeq 0$ after a full adiabatic cycle) irrespective of the number of abrupt "jumps" (discontinuities) during the evolution of $\lambda_n^{\mathcal{P},\mathcal{N}}$ [see dotted lines in (e)–(h) (single "jump") and (m)–(p) (double "jump")]. Both symmetric (rows two through four) and asymmetric (first row) mode switching is observed and this can be directly deduced from the eigenspectra schematics in the second column [in all cases, the $\mathcal{P}$ mode branch will end at the same point after a full cycle irrespective of the encircling direction (CW or CCW) in $\boldsymbol{\mathcal{R}}$ space, except for the first row]. In the first two columns, filled black circles denote the starting points of evolution, while the green asterisk shows the position of the EP $(\breve{g}_{n_{EP}}, \breve{\sigma}_{n_{EP}}, \breve{\lambda}_{n_{EP}}) = (1, 0, 0)$. All insets have the same axis margins with the corresponding main panels.

A clear resemblance between the aforementioned expression and its continuous time counterpart, as retrieved in Appendix F, can be noticed. In that manner, the first term in Eq. (21) can be directly associated with the Berry phase factor. Based now on Eqs. (18), (20), and (21), we can define the *overall complex Berry* ($\hat{\gamma}^{\pm}$) *and dynamical* ($\hat{\tau}^{\pm}$) *phase factors along a discretely defined cyclic trajectory* $\mathcal{C}^{\boldsymbol{\mathcal{R}}}$ [comprised of N discrete points Q_n, with $T = N\Delta$, $Q_N \equiv Q_0$, n , $N \in \mathbb{N}$ and

$0 \leqslant n \leqslant N$ - see Fig. 5(a)] as follows:

$$e^{i\hat{\gamma}^{\hat{\pm}}} = \prod_{n=0}^{N-1} e^{i\hat{\gamma}^{\hat{\pm}}_{n+1,n}} = \prod_{n=0}^{N-1} \langle \hat{v}^{\hat{\pm},L}_{n+1} || \hat{v}^{\hat{\pm},R}_{n} \rangle, \tag{22a}$$

$$e^{i\hat{\tau}^{\hat{\pm}}} = \prod_{n=0}^{N-1} e^{i\hat{\tau}^{\hat{\pm}}_{n}} = \prod_{n=0}^{N-1} \hat{\lambda}^{\hat{\pm}}_{\Xi_n} = \prod_{n=0}^{N-1} (1 + \Delta\hat{\lambda}^{\hat{\pm}}_{n}), \tag{22b}$$

where $\hat{\gamma}^{\hat{\pm}}_{n+1,n}$ ($e^{i\hat{\gamma}^{\hat{\pm}}_{n+1,n}} = \langle \hat{v}^{\hat{\pm},L}_{n+1} || \hat{v}^{\hat{\pm},R}_{n} \rangle$) and $\hat{\tau}^{\hat{\pm}}_{n}$ ($e^{i\hat{\tau}^{\hat{\pm}}_{n}} = \hat{\lambda}^{\hat{\pm}}_{\Xi_n} = 1 + \Delta\hat{\lambda}^{\hat{\pm}}_{n}$) are the discrete contributions to $\hat{\gamma}^{\hat{\pm}} (= \sum_{n=0}^{N-1} \hat{\gamma}^{\hat{\pm}}_{n+1,n})$ and $\hat{\tau}^{\hat{\pm}} (= \sum_{n=0}^{N-1} \hat{\tau}^{\hat{\pm}}_{n})$, correspondingly. An important feature of the discrete complex Berry phase can be now distinguished based on Eq. (22a), i.e., its modulo 2π invariance with respect to gauge transformations of the form $|v'^{\hat{\pm},R}_{n}\rangle = |\hat{v}^{\hat{\pm},R}_{n}\rangle e^{i\phi_n}$ and $\langle v'^{\hat{\pm},L}_{n}| = \langle \hat{v}^{\hat{\pm},L}_{n}| e^{-i\phi_n}$ with ϕ_n denoting a single-valued discrete function modulo 2π ($\phi_{n+N} = \phi_n \bmod 2\pi$). The geometric nature of Berry's phase is also illustrated in Appendix F, along with the continuous time limit behavior of Eqs. (20), (21), and (22). (This is found to be consistent with the respective formulas in continuous quantum systems under Hermitian [1–6] or non-Hermitian [51–55] conditions.)

In the following section, we shall focus on the behavior of Eqs. (20) and (21) in the adiabatic limit. In this regard, the state vector dynamics will be described in terms of the discrete complex Berry and dynamical phase factors, while the shortcomings of conventional quantum adiabatic theory pertaining to non-Hermitian settings will be also discussed. To overcome such limitations, an alternative approach will be presented in the last section based on the decomposition of the Hamiltonian system into its instantaneous dominant and nondominant modes ($\mathcal{P}, \mathcal{N}$ mode notation). Along these lines, emphasis will be given on the eigenspectra evolution in this new mode representation.

B. Adiabatic approximation in discrete Hamiltonian environments

It is interesting to note that Eq. (20) or equivalently Eq. (21) can become greatly simplified, if we assume that the quantum response is largely dominated by the adiabatic term. Under such an *adiabatic approximation*, a closed-form analytical expression can be found for state vector $|u_n\rangle$. In the present section, we shall use notation $\tilde{(\pm)}$ and in that manner imply a smooth evolution of the complex modal amplitudes c_n. In this respect, Eq. (20) yields that $c^{\tilde{+}}_{n} = c^{\tilde{+}}_{0} \prod_{j=0}^{n-1} \langle \tilde{v}^{\tilde{+},L}_{j+1} || \tilde{v}^{\tilde{+},R}_{j} \rangle$, assuming also that only eigenmode $\tilde{(+)}$ becomes initially excited ($c^{\tilde{-}}_{0} = 0$). The final state—after a complete evolution around cyclic path $\mathcal{C}^{\mathcal{R}}$—will attain the following form [after also employing Eqs. (18) and (22)]

$$\begin{aligned} |u_N\rangle &= c^{\tilde{+}}_{0} \left\{ \prod_{n=0}^{N-1} \langle \tilde{v}^{\tilde{+},L}_{n+1} || \tilde{v}^{\tilde{+},R}_{n} \rangle (1 + \Delta\tilde{\lambda}^{\tilde{+}}_{n}) \right\} |\tilde{v}^{\tilde{+},R}_{N}\rangle \\ &= c^{\tilde{+}}_{0} e^{i\tilde{\gamma}^{\tilde{+}}} e^{i\tilde{\tau}^{\tilde{+}}} |\tilde{v}^{\tilde{+},R}_{N}\rangle. \end{aligned} \tag{23}$$

Analogous conclusions will apply, if mode $\tilde{(-)}$ gets initially excited ($c^{\tilde{+}}_{0} = 0$) and only the associated adiabatic term is considered. Consequently, the system is expected to remain in its instantaneous eigenstate [either $\tilde{(+)}$ or $\tilde{(-)}$], while also acquiring a dynamical and a Berry phase factor. In Appendix G, an extensive analysis is provided as to the criteria under which Eq. (23) becomes applicable, by studying the behavior of the nonadiabatic/cross-modulation term appearing in Eq. (20). In this vein, it was found that *the condition for adiabatic evolution* can be summarized as follows for a generalized quantum Hamiltonian system (Hermitian or non-Hermitian):

$$\begin{aligned} |\tilde{\lambda}^{\tilde{\mp}}_{n} - \tilde{\lambda}^{\tilde{\pm}}_{n}| \gg \left| \frac{\langle \tilde{v}^{\tilde{\pm},L}_{n+1} || \tilde{v}^{\tilde{\mp},R}_{n} \rangle}{\delta t_n} \right| &= \left| \langle \tilde{v}^{\tilde{\pm},L}_{n+1} || i\frac{\delta \tilde{v}^{\tilde{\mp},R}_{n}}{\delta t_n} \rangle \right| \\ &\simeq \left| \frac{\langle \tilde{v}^{\tilde{\pm},L}_{n+1} | i\frac{\delta M_n}{\delta t_n} | \tilde{v}^{\tilde{\mp},R}_{n+1} \rangle}{\tilde{\lambda}^{\tilde{\mp}}_{n} - \tilde{\lambda}^{\tilde{\pm}}_{n}} \right|. \end{aligned} \tag{24}$$

The above expression essentially suggests that the system parameters must vary very slowly in time with respect to the magnitude of the separation of the eigenvalues $\tilde{\lambda}^{\tilde{\pm}}_{n}$. Overall, Eqs. (23) and (24) lie at the heart of the quantum adiabatic theorem (in its discrete manifestation), and indicate that a quantum arrangement is expected to remain in its instantaneous eigenstate [Eq. (23)] under the slow driving limit [Eq. (24)]. Of course, as becomes apparent from Eq. (24), the adiabatic condition/approximation cannot apply if $\tilde{\lambda}^{\tilde{+}}_{n} = \tilde{\lambda}^{\tilde{-}}_{n}$, i.e., when eigenspectrum degeneracy points (known as diabolical/exceptional points for Hermitian/non-Hermitian configurations) are crossed. Practically, for operation sufficiently close to such degeneracies, the Hamiltonian system can never behave adiabatically [51–55,91,92].

On the other hand, within non-Hermitian settings the adiabatic approximation holds true for the dominant/prevalent mode (see discussion in Appendix G), but will fail for the remaining nondominant eigenstates as nonadiabatic terms will be developed with magnitude comparable to the adiabatic ones. It is naturally expected then that the resulting dynamics will be described by the dominant mode, even if the other eigenstates become initially excited (see first and last columns in Fig. 6). Even this statement though utterly breaks down, if a different mode becomes prevalent somewhere along the loop (see second and third columns in Fig. 6). Such a behavior has already been reported in continuous nonconservative systems, in the presence (or not) of higher-order exceptional points or of resonances in the vicinity of EPs [29,30,33–37,43]. Yet, here our interest lies particularly in the discrete non-Hermitian case and whether it is possible then to systematically predict the mode population dynamics for arbitrary initial excitation conditions and temporal dependencies of the Hamiltonian model parameters (by answering to such a question, essentially we also address the continuous time version of the same problem when $\Delta \to 0$ is considered). Along these lines, an alternative mode representation has been employed in the last section, which emphasizes on the instantaneous dominant ($\mathcal{P}$)

and nondominant ($\mathcal{N}$) eigenstates of a generalized and slowly varying non-Hermitian arrangement. The topological features of the trajectories that the eigenvalues $\lambda_n^{\mathcal{P}}$, $\lambda_n^{\mathcal{N}}$ follow within the complex domain will be analyzed, along with their effect on the evolution of state vector $|u_n\rangle$.

C. Universal state conversion under the action of cyclic and slowly varying non-Hermitian Hamiltonians

In order to study the dynamics of $|u_n\rangle$ for arbitrary closed paths $\mathcal{C}^{\boldsymbol{\mathcal{R}}}$, as a first step, the evolution matrix ($\Xi_n = I + \Delta M_n$) becomes factorized in terms of its eigenvalues and eigenvectors (in our analysis here, Ξ_n describes a generalized non-Hermitian setting). In this regard, we obtain that $\Xi_n = V_n^R D_{\Xi_n} (V_n^L)^\dagger$ (symbol $\dagger$ refers to the conjugate transpose/adjoint of a matrix), with matrices V_n^R, D_{Ξ_n}, V_n^L defined as

$$V_n^R = \begin{bmatrix} v_{n,x}^{\mathcal{P},R} & v_{n,x}^{\mathcal{N},R} \\ v_{n,y}^{\mathcal{P},R} & v_{n,y}^{\mathcal{N},R} \end{bmatrix}, \quad D_{\Xi_n} = \begin{bmatrix} \lambda_{\Xi_n}^{\mathcal{P}} & 0 \\ 0 & \lambda_{\Xi_n}^{\mathcal{N}} \end{bmatrix},$$
$$V_n^L = \begin{bmatrix} v_{n,x}^{\mathcal{P},L} & v_{n,x}^{\mathcal{N},L} \\ v_{n,y}^{\mathcal{P},L} & v_{n,y}^{\mathcal{N},L} \end{bmatrix} \tag{25}$$

and $\lambda_{\Xi_n}^{\mathcal{P},\mathcal{N}} = 1 + \Delta\lambda_n^{\mathcal{P},\mathcal{N}} \simeq e^{\Delta\lambda_n^{\mathcal{P},\mathcal{N}}}$ for small time steps (such a matrix decomposition applies only in the absence of any eigenspectrum degeneracy points, as then the Jordan canonical form must be employed). Indices $\mathcal{P}$ and $\mathcal{N}$ refer to the instantaneous dominant and nondominant eigenmodes of the non-Hermitian structure and satisfy the property that $\mathrm{Re}(\Delta\lambda_n^{\mathcal{P}}) \geqslant \mathrm{Re}(\Delta\lambda_n^{\mathcal{N}}) \overset{\Delta>0}{\Rightarrow} \mathrm{Re}(\lambda_n^{\mathcal{P}}) \geqslant \mathrm{Re}(\lambda_n^{\mathcal{N}})$ for every point along $\mathcal{C}^{\boldsymbol{\mathcal{R}}}$ [typically $\mathrm{Re}(\lambda_n^{\mathcal{P}}) > \mathrm{Re}(\lambda_n^{\mathcal{N}})$, except maybe at a limited number of points where the equality might apply; see also Fig. 4 for more details regarding the adopted mode terminology]. Left ($\langle v_n^{\mathcal{P},L}| = [v_{n,x}^{\mathcal{P},L}\ v_{n,y}^{\mathcal{P},L}]^*$, $\langle v_n^{\mathcal{N},L}| = [v_{n,x}^{\mathcal{N},L}\ v_{n,y}^{\mathcal{N},L}]^*$) and right ($|v_n^{\mathcal{P},R}\rangle = [v_{n,x}^{\mathcal{P},R}\ v_{n,y}^{\mathcal{N},R}]^\mathcal{T}$, $|v_n^{\mathcal{N},R}\rangle = [v_{n,x}^{\mathcal{N},R}\ v_{n,y}^{\mathcal{N},R}]^\mathcal{T}$) eigenvectors will form a biorthonormal basis: $\langle v_n^{\mathcal{P},L}|v_n^{\mathcal{P},R}\rangle = \langle v_n^{\mathcal{N},L}|v_n^{\mathcal{N},R}\rangle = 1$, $\langle v_n^{\mathcal{P},L}|v_n^{\mathcal{N},R}\rangle = \langle v_n^{\mathcal{N},L}|v_n^{\mathcal{P},R}\rangle = 0$ (symbol $*$ represents the complex conjugate of the respective quantity). This equivalently implies that $(V_n^L)^\dagger V_n^R = (V_n^R)^\dagger V_n^L = I$ (I: 2×2 identity matrix). It should be noted that for regular Hermitian systems [$\mathrm{Re}(\lambda_n^{\mathcal{P}}) = \mathrm{Re}(\lambda_n^{\mathcal{N}}) = 0$], $\mathcal{P}, \mathcal{N}$, and $(\tilde{\pm})$ mode formalisms become identical and standard quantum adiabatic theory will apply for all modes assuming Eq. (24) is satisfied (see also analysis of Sec. III B). An analogous situation arises in the special case when $\mathrm{Re}(\lambda_n^{\mathcal{P}}) = \mathrm{Re}(\lambda_n^{\mathcal{N}}) \neq 0$ along the entire loop $\mathcal{C}^{\boldsymbol{\mathcal{R}}}$ [this becomes equivalent to a Hamiltonian H_n' with shifted energy levels such that $\mathrm{Re}(\lambda_n^{\mathcal{P}'}) = \mathrm{Re}(\lambda_n^{\mathcal{N}'}) = 0$], then again there is no discrimination between dominant and nondominant eigenmodes and thus the quantum adiabatic theorem would still apply for all modes given Eq. (24). In the present analysis, we are particularly concerned with non-Hermitian systems exhibiting an imbalance between $\mathrm{Re}(\lambda_n^{\mathcal{P}})$ and $\mathrm{Re}(\lambda_n^{\mathcal{N}})$ along the parametric trajectory $\mathcal{C}^{\boldsymbol{\mathcal{R}}}$.

The total transfer matrix (for a single loop encirclement) will now be given by $Z = \Xi_{N-1}\Xi_{N-2}\cdots\Xi_0 = \prod_{n=0}^{N-1}\Xi_n = \prod_{n=0}^{N-1} V_n^R D_{\Xi_n}(V_n^L)^\dagger$ (an ordered matrix product is used here), which can be alternatively expressed as

$$Z = V_{N-1}^R \left[D_{\Xi_{N-1}} \prod_{n=0}^{N-2} \left(V_{n+1}^L\right)^\dagger V_n^R D_{\Xi_n} \right] \left(V_0^L\right)^\dagger$$
$$= V_{N-1}^R\, \mathcal{F}\, \left(V_0^L\right)^\dagger. \tag{26}$$

In the above formula, N indicates the total number of points along the discrete trajectory $\mathcal{C}^{\boldsymbol{\mathcal{R}}}$ [$|u_N\rangle = Z|u_0\rangle$, see also Fig. 5(a)] and $\mathcal{F} = [\mathcal{F}^{jk}] = D_{\Xi_{N-1}} \prod_{n=0}^{N-2} (V_{n+1}^L)^\dagger V_n^R D_{\Xi_n}$ ($j,k = 1,2$). Of interest is to study the behavior of matrices $\mathcal{F}$ and Z for the different geometric forms of $\mathcal{C}^{\boldsymbol{\mathcal{R}}}$ as N grows large (adiabatic limit). Even though not immediately apparent, Eqs. (25) and (26) are simply a reformulation of Eqs. (18)–(21), on which the analysis of Secs. III A and III B was based on (see Appendix H). Yet, the former set of equations shall be employed in the forthcoming asymptotic study, as it will allow us to access the dynamics underpinning the evolution of slowly varying non-Hermitian systems in a mathematically more neat and elegant manner. In order to validate our theoretical conclusions, specific numerical results will be provided in terms of the time-dependent $\mathcal{PT}$-symmetric-like model described in Eq. (7), assuming evolution along rhombic (see Figs. 7 and 8) and elliptical trajectories (see Fig. 9) in parameter space $\boldsymbol{\mathcal{R}}$. Moreover, direct comparisons will be performed between Figs. 6 (Sec. III B) and 7–9 (Sec. III C) to illustrate the differences between the $(\tilde{\pm})$ (Fig. 6) and $\mathcal{P}, \mathcal{N}$ (Figs. 7–9) mode representations, which in turn will enable us to also reveal the limitations of the standard adiabatic theory results summarized in Sec. III B.

1. Absence of abrupt transitions/discontinuities during the evolution of $\lambda_n^{\mathcal{P}}$ and $\lambda_n^{\mathcal{N}}$ in the complex domain

Characteristic parametric trajectories of this form are shown in the insets of Figs. 7(a) [or 7(i)] and 7(d) [or 7(l)] (first and last columns of Fig. 7). The respective main figure panels clearly show the absence of any discontinuities in the evolution of eigenvalues $\lambda_n^{\mathcal{P}}$ and $\lambda_n^{\mathcal{N}}$ within the complex space. Based now on Figs. 6(a), 6(d), 6(i), and 6(l), it can be seen that mode $(\tilde{+})$ remains dominant along the entire parametric loop [$\mathrm{Re}(\Delta\lambda_n^{\tilde{+}}) \geqslant \mathrm{Re}(\Delta\lambda_n^{\tilde{-}})$] and as such it coincides with the instantaneous dominant eigenmode $\mathcal{P}$ [$(\tilde{+}) \equiv \mathcal{P}$ and $(\tilde{-}) \equiv \mathcal{N}$]. In other words, mode designations $(\tilde{\pm})$ (used in the conventional adiabatic theory treatments of Sec. III B) and $\mathcal{P}, \mathcal{N}$ (used in the present section) become equivalent [$\lambda_n^{\mathcal{P}} \equiv \lambda_n^{\tilde{+}}$ and $\lambda_n^{\mathcal{N}} \equiv \lambda_n^{\tilde{-}}$], which reflects in the fact that the numerical results of the first and last columns of Fig. 6 are identical with the respective results of Fig. 7 (see also Sec. VII within SM [76] for a more detailed discussion).

For small discrete time steps Δ, it becomes now true that $(V_{n+1}^L)^\dagger V_n^R \simeq (V_n^L)^\dagger V_n^R = I$ and consequently matrix $\mathcal{F}$ takes the form

$$\mathcal{F} = D_{\Xi_{N-1}} \prod_{n=0}^{N-2} \left(V_{n+1}^L\right)^\dagger V_n^R D_{\Xi_n} \simeq \prod_{n=0}^{N-1} D_{\Xi_n} = \begin{bmatrix} c_{\mathcal{P}} & 0 \\ 0 & c_{\mathcal{N}} \end{bmatrix} \tag{27}$$

with $c_{\mathcal{P}} = \prod_{n=0}^{N-1} \lambda_{\Xi_n}^{\mathcal{P}} \simeq e^{\Delta\sum_{n=0}^{N-1}\lambda_n^{\mathcal{P}}}$, $c_{\mathcal{N}} = \prod_{n=0}^{N-1} \lambda_{\Xi_n}^{\mathcal{N}} \simeq e^{\Delta\sum_{n=0}^{N-1}\lambda_n^{\mathcal{N}}}$ [$c_{\mathcal{P},\mathcal{N}}$ are essentially the discrete dynamical

phase factors as defined in Eq. (22b) for the $\mathcal{P},\mathcal{N}$ modes]. Since inequality $\mathrm{Re}(\lambda_n^{\mathcal{P}}) > \mathrm{Re}(\lambda_n^{\mathcal{N}})$ largely applies along $\mathcal{C}^{\boldsymbol{\mathcal{R}}}$ ($\Delta > 0$), it becomes directly evident that $|c^{\mathcal{N}}/c^{\mathcal{P}}| << 1$ under adiabatic ($N \to \infty$) and non-Hermitian conditions [$\mathrm{Re}(\lambda_n^{\mathcal{P}})\mathrm{Re}(\lambda_n^{\mathcal{N}}) \neq 0$ in general along trajectory $\mathcal{C}^{\boldsymbol{\mathcal{R}}}$]. Hence, we can omit $c_{\mathcal{N}}$ and take into account primarily factor $c_{\mathcal{P}}$ in Eq. (27). Two different cases must be considered here:

(1) *Symmetric state conversion for closed paths not containing any EPs*. A representative example is shown in the last column of Fig. 7. The evolution of the eigespectra is exhibited in Figs. 7(d) and 7(l). Since no exceptional points are enclosed within $\mathcal{C}^{\boldsymbol{\mathcal{R}}}$, it will be true for the initial and final states that $\lambda_N^{\mathcal{P}} = \lambda_0^{\mathcal{P}}$, $\lambda_0^{\mathcal{N}} = \lambda_0^{\mathcal{N}}$, and accordingly $|v_{N-1}^{\mathcal{P},R}\rangle \simeq |v_N^{\mathcal{P},R}\rangle = |v_0^{\mathcal{P},R}\rangle$, $|v_{N-1}^{\mathcal{N},R}\rangle \simeq |v_N^{\mathcal{N},R}\rangle = |v_0^{\mathcal{N},R}\rangle$ with analogous relations applying for the left eigenvectors. (This is analytically shown in [26], in terms of a Taylor series expansion around a nondegenerate spectrum point.) After employing Eqs. (25)–(27) and the biorthonormality conditions, the total transfer matrix Z will assume the form

$$Z \simeq c_{\mathcal{P}} \begin{bmatrix} v_{0,x}^{\mathcal{P},R}\left(v_{0,x}^{\mathcal{P},L}\right)^* & v_{0,x}^{\mathcal{P},R}\left(v_{0,y}^{\mathcal{P},L}\right)^* \\ v_{0,y}^{\mathcal{P},R}\left(v_{0,x}^{\mathcal{P},L}\right)^* & v_{0,y}^{\mathcal{P},R}\left(v_{0,y}^{\mathcal{P},L}\right)^* \end{bmatrix}. \tag{28}$$

It can be deduced now that $\zeta^{21}/\zeta^{11} \simeq \zeta^{22}/\zeta^{12} \simeq v_{0,y}^{\mathcal{P},R}/v_{0,x}^{\mathcal{P},R} = v_{N,y}^{\mathcal{P},R}/v_{N,x}^{\mathcal{P},R}$, where ζ^{jk} are the elements of matrix Z. This relation becomes directly reflected to the components of the resulting state vector, i.e., $|u_N\rangle = Z|u_0\rangle \Rightarrow b_N/a_N \simeq v_{N,y}^{\mathcal{P},R}/v_{N,x}^{\mathcal{P},R}$ with $|u_N\rangle = [a_N\ b_N]^{\mathcal{T}}$. In other words, the state vector will asymptotically convert to the instantaneous dominant ($\mathcal{P}$) mode at the end of the cyclic process irrespective of the initial conditions [see Figs. 7(h) and 7(p), along with the description in the caption of Fig. 7]. After tracking the $\mathcal{P}$ mode (red) branch in the corresponding eigenspectra evolution diagrams [see Figs. 7(d) and 7(l)], it becomes evident that its ending point is the same irrespective of the encircling direction (CW or CCW) in parameter space [of course, the starting and ending points also coalesce under both CW and CCW conditions (the same applies for the $\mathcal{N}$ mode branch), as no eigenvalue/eigenvector swap happens after a full parameter cycle]. This is indicative of a symmetric mode switching behavior and is closely associated with the trivial spectrum topology in the vicinity of nondegenerate points [see Riemann sheet structure along with the trajectory followed by eigenvalue $\lambda_n^{\mathcal{P}}$ in Figs. 8(e) and 8(j)].

(2) *Asymmetric state conversion for paths encircling EPs*. This case scenario corresponds to the first column of Fig. 7. A unique feature of such trajectories, is the exchange of eigenvalues and eigenmodes after a complete EP encirclement (this is analytically shown in [26], in terms of a Puiseux series expansion around an EP), i.e., $\lambda_N^{\mathcal{P}} = \lambda_0^{\mathcal{N}}$, $\lambda_N^{\mathcal{N}} = \lambda_0^{\mathcal{P}}$ [see also Figs. 7(a), 7(i), 8(b), and 8(g)], $|v_{N-1}^{\mathcal{P},R}\rangle \simeq |v_N^{\mathcal{P},R}\rangle = -|v_0^{\mathcal{N},R}\rangle$, $|v_{N-1}^{\mathcal{N},R}\rangle \simeq |v_N^{\mathcal{N},R}\rangle = |v_0^{\mathcal{P},R}\rangle$ (analogous relations apply for the left eigenvectors). This implies for the total transfer matrix Z that

$$Z \simeq -c_{\mathcal{P}} \begin{bmatrix} v_{0,x}^{\mathcal{N},R}\left(v_{0,x}^{\mathcal{P},L}\right)^* & v_{0,x}^{\mathcal{N},R}\left(v_{0,y}^{\mathcal{P},L}\right)^* \\ v_{0,y}^{\mathcal{N},R}\left(v_{0,x}^{\mathcal{P},L}\right)^* & v_{0,y}^{\mathcal{N},R}\left(v_{0,y}^{\mathcal{P},L}\right)^* \end{bmatrix}. \tag{29}$$

Consequently, it will be true that $\zeta^{21}/\zeta^{11} \simeq \zeta^{22}/\zeta^{12} \simeq v_{0,y}^{\mathcal{N},R}/v_{0,x}^{\mathcal{N},R} = v_{N,y}^{\mathcal{P},R}/v_{N,x}^{\mathcal{P},R}$, i.e., the state vector will adiabatically convert to the instantaneous $\mathcal{P}$ mode after a complete cyclic evolution. This mode switching property is independently verified by the numerical results of Figs. 7(e) and 7(m) (see also caption description). Following the rationale in (ii), we can now track the $\mathcal{P}$ mode in the eigenspectrum domain [see Figs. 7(a) and 7(i)], which in turn reveals that the ending point of the respective (red) branch depends on the encircling direction in $\boldsymbol{\mathcal{R}}$ space. This clearly implies an asymmetric state conversion process, which can be also attributed to the peculiar topology of the eigenspectrum in the vicinity of EPs [see Figs. 8(b) and 8(g)].

Both scenarios (i) and (ii) indicate that the $\mathcal{P}$ mode will dictate the state vector dynamics in slowly varying and cyclic non-Hermitian environments, when no discontinuities are present in the evolution of eigenvalues $\lambda_n^{\mathcal{P}}$, $\lambda_n^{\mathcal{N}}$. This is in agreement with (a) the analytical predictions of Sec. III B (related to standard adiabatic theory), according to which a Hamiltonian system is expected to convert to its dominant eigenstate in the adiabatic limit, as long as such eigenstate remains dominant along the entire loop $\mathcal{C}^{\boldsymbol{\mathcal{R}}}$ (see respective numerical results in first and last columns of Fig. 6), (b) the analytical and numerical calculations in Sec. II C (see first and fourth rows of Fig. 2), where the values for the ratio of the state vector components at the end of the cycling period T ($r_N = b_N/a_N$) indicate conversion to the instantaneous $\mathcal{P}$ mode (see also detailed description in the captions of Figs. 2 and 7). Of course, our findings here are general and not path dependent [see for instance Fig. 9 in the case of elliptical trajectories $\mathcal{C}^{\boldsymbol{\mathcal{R}}}$: symmetric (third row of Fig. 9) or asymmetric (first row of Fig. 9) mode switching occurs depending on whether a nondegenerate or a degenerate point is encircled in $\boldsymbol{\mathcal{R}}$ space].

2. *Presence of abrupt transitions/discontinuities during the evolution of $\lambda_n^{\mathcal{P}}$ and $\lambda_n^{\mathcal{N}}$ in the complex domain*

A completely different scenario arises for the trajectories shown in the insets of Figs. 7(b) [or 7(j)] and 7(c) [or 7(k)] (second and third columns of Fig. 7). Now, abrupt "jumps" take place as eigenvalues $\lambda_n^{\mathcal{P}}$ and $\lambda_n^{\mathcal{N}}$ evolve within the complex space [see main panels of Figs. 7(b), 7(c), 7(j), and 7(k)]. Moreover, the $(\tilde{\pm})$ and $\mathcal{P},\mathcal{N}$ dynamical descriptions will differ (see corresponding simulation results—second and third columns—of Figs. 6 and 7 along with the more detailed examination of Sec. VII within SM [76]) and this can be attributed to the fact that modes $(\tilde{+})$ and $(\tilde{-})$ become interchangeably dominant as time progresses [see Figs. 6(b), 6(c), 6(j), and 6(k)]. As a result, the conclusions of Sec. III B can no longer apply in the present case. In this vein, we shall emphasize in the following analysis solely on the behavior of the $\mathcal{P},\mathcal{N}$ modes of the non-Hermitian structure (this is the preferable mode representation when non-Hermitian conditions are considered), while also exhibiting the deficiencies of standard quantum adiabatic theory.

Without loss of generality, we will assume that there is a single time instant ($t_{\overline{n_o}} = \overline{n_o}\Delta$, $\overline{n_o} \in \mathbb{N} \wedge 0 \leqslant \overline{n_o} < N$), where a sharp discontinuity is noticed in the evolution of

eigenvalues $\lambda_n^{\mathcal{P}}$ and $\lambda_n^{\mathcal{N}}$ [for instance $\overline{n_o} = 3N/4$, $N/2$, $N/4$, $N/2$ in Figs. 7(b), 7(c), 7(j), and 7(k), accordingly]. We shall now consider separately the dynamics of the system for $n \leqslant \overline{n_o}$ (parametric path $\mathcal{C}_\alpha^{\boldsymbol{\mathcal{R}}}$) and $n > \overline{n_o}$ (parametric path $\mathcal{C}_\beta^{\boldsymbol{\mathcal{R}}}$). In that manner, the total transfer matrix around the closed trajectory $\mathcal{C}^{\boldsymbol{\mathcal{R}}} = \mathcal{C}_\beta^{\boldsymbol{\mathcal{R}}} \cup \mathcal{C}_\alpha^{\boldsymbol{\mathcal{R}}}$ (evolution takes place in the direction $\mathcal{C}_\alpha^{\boldsymbol{\mathcal{R}}} \to \mathcal{C}_\beta^{\boldsymbol{\mathcal{R}}}$) can be expressed as

$$\begin{aligned} Z &= V_{N-1}^R \mathcal{F}^{(\beta)} \big[\big(V_{\overline{n_o}+1}^L\big)^\dagger V_{\overline{n_o}}^R \big] \mathcal{F}^{(\alpha)} \big(V_0^L\big)^\dagger \\ &= V_{N-1}^R \mathcal{F} \big(V_0^L\big)^\dagger, \end{aligned} \tag{30}$$

with $\mathcal{F} = \mathcal{F}^{(\beta)}[(V_{\overline{n_o}+1}^L)^\dagger V_{\overline{n_o}}^R]\mathcal{F}^{(\alpha)}$ and quantities $\mathcal{F}^{(\alpha)} = D_{\Xi_{\overline{n_o}}} \prod_{n=0}^{\overline{n_o}-1} (V_{n+1}^L)^\dagger V_n^R D_{\Xi_n}$, $\mathcal{F}^{(\beta)} = D_{\Xi_{N-1}} \prod_{n=\overline{n_o}+1}^{N-2} (V_{n+1}^L)^\dagger V_n^R D_{\Xi_n}$ being related to subpaths $\mathcal{C}_\alpha^{\boldsymbol{\mathcal{R}}}$, $\mathcal{C}_\beta^{\boldsymbol{\mathcal{R}}}$, respectively. Matrix products $(V_{n+1}^L)^\dagger V_n^R$ will assume the following form (see Appendix H):

$$\big(V_{n+1}^L\big)^\dagger V_n^R = \begin{cases} \begin{bmatrix} p_n^{11} & \Delta p_n^{12} \\ \Delta p_n^{21} & p_n^{22} \end{bmatrix}, & n \neq \overline{n_o}, \\ \begin{bmatrix} \Delta p_{\overline{n_o}}^{21} & p_{\overline{n_o}}^{22} \\ p_{\overline{n_o}}^{11} & \Delta p_{\overline{n_o}}^{12} \end{bmatrix}, & n = \overline{n_o}, \end{cases} \tag{31}$$

where $p_n^{jk} = p_n^{jk}(\Delta)$ with $j, k = 1, 2$ and $p_n^{11}(\Delta = 0) = p_n^{22}(\Delta = 0) = p_{\overline{n_o}}^{11}(\Delta = 0) = p_{\overline{n_o}}^{22}(\Delta = 0) = 1$. As $\Delta \to 0$, $(V_{n+1}^L)^\dagger V_n^R$ becomes approximately equal to either the unity matrix for $n \neq \overline{n_o}$, or to a hollow matrix with off-diagonal elements equal to unity for $n = \overline{n_o}$. This in turn signifies the presence of the spectrum discontinuity at $n = \overline{n_o}$. The matrix expressions for $\mathcal{F}^{(\alpha)}$, $\mathcal{F}^{(\beta)}$ can be subsequently retrieved as (see Appendix H)

$$\mathcal{F}^{(l)} = \begin{bmatrix} c_{\mathcal{P}}^{(l)} f_1^{(l)} + \Delta\lambda_{\Xi_{n_e^{(l)}}}^{\mathcal{P}} r_{11}^{(l)} & \Delta\lambda_{\Xi_{n_e^{(l)}}}^{\mathcal{P}} r_{12}^{(l)} \\ \Delta\lambda_{\Xi_{n_e^{(l)}}}^{\mathcal{N}} r_{21}^{(l)} & c_{\mathcal{N}}^{(l)} f_2^{(l)} + \Delta\lambda_{\Xi_{n_e^{(l)}}}^{\mathcal{N}} r_{22}^{(l)} \end{bmatrix}, \tag{32}$$

with index (l) referring to $\mathcal{C}_\alpha^{\boldsymbol{\mathcal{R}}}$ or $\mathcal{C}_\beta^{\boldsymbol{\mathcal{R}}}$ [$(l) = (\alpha)$ or (β)]. The different variables appearing in the above equation have been defined in Appendix H. Here, we shall emphasize only on the most important ones, which will later on help us identify the presence of the discrete dynamical and Berry phase factors in the expression for matrix $\mathcal{F}$: $c_{\mathcal{P}}^{(l)} = \prod_{n=n_o^{(l)}}^{n_e^{(l)}} \lambda_{\Xi_n}^{\mathcal{P}}$, $c_{\mathcal{N}}^{(l)} = \prod_{n=n_o^{(l)}}^{n_e^{(l)}} \lambda_{\Xi_n}^{\mathcal{N}}$, $f_1^{(l)} = \prod_{n=n_o^{(l)}}^{n_e^{(l)}-1} p_n^{11}$, $f_2^{(l)} = \prod_{n=n_o^{(l)}}^{n_e^{(l)}-1} p_n^{22}$ with $n_o^{(l)}, n_e^{(l)}$ denoting the starting and ending points of $\mathcal{C}_l^{\boldsymbol{\mathcal{R}}}$ ($\mathcal{C}_\alpha^{\boldsymbol{\mathcal{R}}}$: $n_o^{(\alpha)} = 0$ and $n_e^{(\alpha)} = \overline{n_o}$, $\mathcal{C}_\beta^{\boldsymbol{\mathcal{R}}}$: $n_o^{(\beta)} = \overline{n_o} + 1$ and $n_e^{(\beta)} = N - 1$). Moreover, as shown in Appendix H, it will be true that $f_1^{(l)}(\Delta = 0) = \prod_{n=n_o^{(l)}}^{n_e^{(l)}-1} p_n^{11}(\Delta = 0) = 1$ and $f_2^{(l)}(\Delta = 0) = \prod_{n=n_o^{(l)}}^{n_e^{(l)}-1} p_n^{22}(\Delta = 0) = 1$, i.e., at least for small values of Δ the coefficients of $c_{\mathcal{P}}^{(l)}$ and $c_{\mathcal{N}}^{(l)}$ in Eq. (32) will be nonzero.

Of essence is now to retrieve the expression for matrix $\mathcal{F}$. Consequently, based on Eqs. (30)–(32), it can be attained that

$$\mathcal{F} = \begin{bmatrix} \Delta\big(c_{\mathcal{P}} p_{21}^{\overline{n_o}} f_1^{(\beta)} f_1^{(\alpha)} + \lambda_{\Xi_{\overline{n_o}}}^{\mathcal{N}} c_{\mathcal{P}}^{(\beta)} p_{22}^{\overline{n_o}} f_1^{(\beta)} r_{21}^{(\alpha)} \\ \quad + \lambda_{\Xi_{N-1}}^{\mathcal{P}} c_{\mathcal{P}}^{(\alpha)} p_{11}^{\overline{n_o}} f_1^{(\alpha)} r_{12}^{(\beta)}\big) + \hat{\mathcal{F}}^{11} & c_{\mathcal{P}}^{(\beta)} c_{\mathcal{N}}^{(\alpha)} p_{22}^{\overline{n_o}} f_1^{(\beta)} f_2^{(\alpha)} + \Delta\big(\lambda_{\Xi_{\overline{n_o}}}^{\mathcal{N}} c_{\mathcal{P}}^{(\beta)} p_{22}^{\overline{n_o}} f_1^{(\beta)} r_{22}^{(\alpha)} \\ & \quad + \lambda_{\Xi_{N-1}}^{\mathcal{P}} c_{\mathcal{N}}^{(\alpha)} p_{22}^{\overline{n_o}} f_2^{(\alpha)} r_{11}^{(\beta)}\big) + \hat{\mathcal{F}}^{12} \\ c_{\mathcal{P}}^{(\alpha)} c_{\mathcal{N}}^{(\beta)} p_{11}^{\overline{n_o}} f_2^{(\beta)} f_1^{(\alpha)} + \Delta\big(\lambda_{\Xi_{N-1}}^{\mathcal{N}} c_{\mathcal{P}}^{(\alpha)} p_{11}^{\overline{n_o}} f_1^{(\alpha)} r_{22}^{(\beta)} & \Delta\big(c_{\mathcal{N}} p_{12}^{\overline{n_o}} f_2^{(\beta)} f_2^{(\alpha)} + \lambda_{\Xi_{\overline{n_o}}}^{\mathcal{P}} c_{\mathcal{N}}^{(\beta)} p_{11}^{\overline{n_o}} f_2^{(\beta)} r_{12}^{(\alpha)} \\ \quad + \lambda_{\Xi_{\overline{n_o}}}^{\mathcal{P}} c_{\mathcal{N}}^{(\beta)} p_{11}^{\overline{n_o}} f_2^{(\beta)} r_{11}^{(\alpha)}\big) + \hat{\mathcal{F}}^{21} & \quad + \lambda_{\Xi_{N-1}}^{\mathcal{N}} c_{\mathcal{N}}^{(\alpha)} p_{22}^{\overline{n_o}} f_2^{(\alpha)} r_{21}^{(\beta)}\big) + \hat{\mathcal{F}}^{22} \end{bmatrix}, \tag{33}$$

where $c_{\mathcal{P}} = c_{\mathcal{P}}^{(\beta)} c_{\mathcal{P}}^{(\alpha)} = \prod_{n=0}^{N-1} \lambda_{\Xi_n}^{\mathcal{P}} \overset{\Delta\to 0}{\simeq} e^{\Delta \sum_{n=0}^{N-1} \lambda_n^{\mathcal{P}}}$, $c_{\mathcal{N}} = c_{\mathcal{N}}^{(\beta)} c_{\mathcal{N}}^{(\alpha)} = \prod_{n=0}^{N-1} \lambda_{\Xi_n}^{\mathcal{N}} \overset{\Delta\to 0}{\simeq} e^{\Delta \sum_{n=0}^{N-1} \lambda_n^{\mathcal{N}}}$, and elements $\hat{\mathcal{F}}^{jk}$ ($j, k = 1, 2$) contain any second- or higher-order contributions with respect to Δ [see Eqs. (H14) in Appendix H]. It is of interest to note that factors $c_{\mathcal{P}}$ ($c_{\mathcal{N}}$) and $\Delta p_{21}^{\overline{n_o}} f_1^{(\beta)} f_1^{(\alpha)}$ ($\Delta p_{12}^{\overline{n_o}} f_2^{(\beta)} f_2^{(\alpha)}$) appearing in Eq. (33), can become directly related to the discrete complex dynamical and Berry phase factors attained by the $\mathcal{P}$ ($\mathcal{N}$) mode, according to the more generalized definitions of Eqs. (22) [see discussion immediately following Eqs. (H14) in Appendix H].

Owing to our mode convention, relation $\mathrm{Re}(\lambda_n^{\mathcal{P}}) \gtrdot \mathrm{Re}(\lambda_n^{\mathcal{N}})$ must be predominantly true along loop $\mathcal{C}^{\boldsymbol{\mathcal{R}}}$. If we now consider Δ to be a fixed and small value, then parameter N (total number of discrete points along path $\mathcal{C}^{\boldsymbol{\mathcal{R}}}$) should be exceedingly large to achieve an adiabatically small rate of encirclement $1/T$ [$= 1/(N\Delta)$]. Following such a rationale, it is shown in Appendix H that the $c_{\mathcal{P}}$-related terms will dominate in Eq. (33) ($|c_{\mathcal{P}}| \gg |c_{\mathcal{P}}^{(\alpha)}| \gg |c_{\mathcal{N}}^{(\alpha)}|$, $|c_{\mathcal{P}}| \gg |c_{\mathcal{P}}^{(\beta)}| \gg |c_{\mathcal{N}}^{(\beta)}|$) under non-Hermitian conditions [$\mathrm{Re}(\lambda_n^{\mathcal{P}})\mathrm{Re}(\lambda_n^{\mathcal{N}}) \neq 0$ in general along trajectory $\mathcal{C}^{\boldsymbol{\mathcal{R}}}$]. Given also the analytical forms of $\hat{\mathcal{F}}^{jk}$ (see Appendix H), this implies that all elements of $\mathcal{F}$ can be safely neglected except $\mathcal{F}^{11}$ and thus it will be true in the adiabatic limit $N, T \to \infty$ that

$$\mathcal{F} \propto \begin{bmatrix} c_{\mathcal{P}} & 0 \\ 0 & 0 \end{bmatrix}. \tag{34}$$

The analysis becomes now analogous to that of Sec. III C 1, since the corresponding expressions for matrix $\mathcal{F}$ [see Eq. (27) in Sec. III C 1 and Eq. (34) in Sec. III C 2] become equivalent under adiabatic conditions ($|c_{\mathcal{P}}| \gg |c_{\mathcal{N}}|$). It should be highlighted that here it was necessary to take into account the higher-order terms appearing in Eq. (33) in order to accurately account for the anomalous behavior of products $(V_{n+1}^L)^\dagger V_n^R$ occurring at $n = \overline{n_o}$, as depicted in Eq. (31). Had we not considered such terms (and accordingly element $\mathcal{F}^{11}$), matrix $\mathcal{F}$ would have obtained a significantly different form to Eq. (34) and consequently our theoretical predictions would have failed.

In this vein and similarly to Sec. III C 1, it is expected that slowly cycled states will converge to the instantaneous dominant eigenstate (or $\mathcal{P}$ mode) even at the presence of discontinuities in the evolution of the $\mathcal{P},\mathcal{N}$ mode spectra. This is clearly illustrated by the population dynamics plots in Figs. 7(f), 7(g), 7(n), and 7(o), where the nondominant ($\mathcal{N}$) mode completely subsides at the end of the cyclic process (see also accompanying description in the caption of Fig. 7). The resulting state conversion will have either a symmetric [compare Figs. 7(b) and 7(j) in second column of Fig. 7] or an asymmetric character [compare Figs. 7(c) and 7(k) in third column of Fig. 7], depending on whether the $\mathcal{P}$ mode branch will end at the same point (symmetric conversion) or not (asymmetric conversion) within the eigenspectrum domain after a full parameter cycle. All of the aforementioned results are independently verified by the theoretical and numerical analysis performed in Sec. II C, where the dynamics of the state vector components along with their ratio were examined within discrete $\mathcal{PT}$-symmetric-like settings (see second and third rows of Fig. 2, along with the descriptions in the captions of Figs. 2 and 7).

Interestingly enough, asymmetric (symmetric) mode switching can now take place even when encircling nondegenerate (exceptional) points. Such an unexpected behavior indicates how underlying spectrum discontinuities (see second and third columns of Fig. 7, along with the respective Riemann surfaces in rows three and four of Fig. 8) might affect the system dynamics and in the same time elucidates the significant role of the starting point of evolution along loop $\mathcal{C}^{\mathcal{R}}$ on the output quantum state [analogous results are also demonstrated in Figs. 9(e)–9(h) and 9(m)–9(p) in the case of elliptical parametric paths]. In this respect, conventional adiabatic theory cannot be applied in the present case, since it typically requires the absence of any discontinuity points in the spectra evolution. The complete breakdown of quantum adiabatic theory (even after its appropriate extension to the non-Hermitian case in Sec. III B) becomes directly reflected in Figs. 6(f), 6(g), 6(n), and 6(o) and their insets (see second and third columns of Fig. 6), where the non-Hermitian Hamiltonian configuration does not convert to the originally dominant eigenmode [assigned with $(\tilde{+})$ in our mode notation] even if such eigenmode gets initially excited.

Ultimately, the $\mathcal{P},\mathcal{N}$ mode representation is the preferred method to describe the dynamics of open quantum systems, as it enables us to predict the dynamics for generalized non-Hermitian Hamiltonian forms under cyclic and slowly varying conditions. Such a conclusion will still hold, independently of whether multiple encirclements along a closed parametric path $\mathcal{C}^{\mathcal{R}}$ are considered or if the dynamical spectra associated with the instantaneous dominant ($\lambda_n^{\mathcal{P}}$) and nondominant ($\lambda_n^{\mathcal{N}}$) modes exhibit several abrupt transitions within the complex domain. However, this behavior cannot be generalized to the case where the Hamiltonian arrangement operates at eigenspectrum degeneracy points. Then, a Jordan decomposition must be employed instead of the more familiar eigendecomposition method shown in Eq. (25) (matrix D_{Ξ_n} will no longer be diagonal but a 2×2 Jordan block), and consequently the subsequent analysis will be considerably altered. In practice though, exact operation at such singularity points is almost impossible, due to their inherent sensitivity [93–95].

IV. CONCLUSIONS AND OUTLOOK

In this paper, the dynamics of discrete and time-dependent two-level non-Hermitian Hamiltonians (in their most general form) were rigorously investigated under both cyclic and adiabatic conditions. A universal state conversion behavior, categorized as either symmetric or asymmetric, was numerically observed and theoretically proved for generalized trajectories $\mathcal{C}^{\mathcal{R}}$ in parameter space $\mathcal{R}$. In this regard, special emphasis was given to the topology of the encircling trajectories (along with their mappings onto the complex eigenspectrum space), after also introducing an alternative mode formalism based on the instantaneous (non)dominant eigenstates of the non-Hermitian structure. The specific example of a $\mathcal{PT}$-symmetric-like arrangement moving along elliptical and rhombic ($\mathcal{C}^{\mathcal{R}}_{\mathcal{R}h}$) parametric paths was numerically studied. The underlying dynamical equations were found be equivalent to those of a discrete harmonic oscillator with a (complex and time-dependent) damping profile dictated by the form of $\mathcal{C}^{\mathcal{R}}$. In this manner, explicit analytical solutions were retrieved in terms of the discrete Airy and parabolic cylinder functions in the case of the $\mathcal{C}^{\mathcal{R}}_{\mathcal{R}h}$ trajectories. State conversion was also theoretically demonstrated for small square loops (a special form of rhombic paths), by exploiting the rich phenomenon of Stokes asymptotics that the class of Airy functions exhibits.

Of course, the analysis presented here is far from complete, as there are still several open problems that need to be separately addressed. For instance, a natural question arises as to whether the conditions of cyclic parameter variation or of high degree of adiabaticity can be relaxed and to what extent, in order to still attain the observed mode switching behavior. On the same grounds, it becomes of essence to examine how the analysis and methodologies presented in this paper generalize to cases where nonlinear effects are considered or even when eigenspectrum degeneracy points are crossed as the Hamiltonian system evolves in parameter space. Of great interest is to also explore the adiabatic behavior of multilevel non-Hermitian quantum configurations within a 2D or even higher-dimensional $\mathcal{R}$ space. Such arrangements will exhibit higher-order exceptional points, which are expected to influence the respective mode switching performance. To this aim, experimental platforms in the form of active/passive fiber loop networks (discrete time evolution) and smoothly deformed optical waveguides (continuous time evolution) are being actively pursued within the optics community [27,28,48,49,67].

ACKNOWLEDGMENT

N.S.N. was supported by the Bodossaki Foundation. N.S.N. would like to thank Professor Nikolaos V. Kantartzis for immensely useful comments and discussions.

APPENDIX A: CONTINUOUS AND DISCRETE TIME DOMAIN DESCRIPTIONS OF THE QUANTUM HAMILTONIAN MODEL

The standard continuous time Schrödinger equation takes the (normalized) form

$$i\frac{\partial|u(t)\rangle}{\partial t} = H(t)|u(t)\rangle, \tag{A1}$$

where t is the normalized time parameter (the actual time coordinate is represented by $\hbar t$), $H(t)$ is the quantum mechanical Hamiltonian and $|u(t)\rangle = [a(t)\ b(t)]^{\mathcal{T}}$ is the system's state vector. The discrete formulation of Eq. (A1) becomes simply

$$|u_{n+1}\rangle = (I - i\Delta H_n)|u_n\rangle, \tag{A2}$$

where $n \in \mathbb{N}$, Δ is of course the discrete time step ($\delta t_n = t_{n+1} - t_n = \Delta$), $|u_n\rangle = [a_n\ b_n]^{\mathcal{T}}$, $q_n = q(t_n = n\Delta)$ with $q(t)$ being an arbitrary time-dependent quantity, and I is the identity matrix. The above expression becomes equivalent to Eq. (1) of Sec. II A ($|u_{n+1}\rangle = \Xi_n|u_n\rangle$) if we set $\Xi_n = I + \Delta M_n = I - i\Delta H_n$ [matrices Ξ_n (evolution/propagator matrix), M_n, H_n were all defined Sec. II A]. It should be highlighted that Eq. (A2) was obtained from Eq. (A1) after replacing the partial derivative ∂ with the forward difference operator δ defined as $\delta q_n = q_{n+1} - q_n$.

As a next step in the analysis, the difference equations that a_n, b_n satisfy shall be retrieved. Equation (A2) can be rewritten as

$$a_{n+1} = \xi_n^{11} a_n + \xi_n^{12} b_n, \tag{A3a}$$

$$b_{n+1} = \xi_n^{21} a_n + \xi_n^{22} b_n. \tag{A3b}$$

By setting $n \to n+1$ in Eq. (A3a) and after employing the expressions for a_{n+1} and b_{n+1} from the above formulas, it is obtained that

$$a_{n+2} = \left(\xi_{n+1}^{11}\xi_n^{11} + \xi_{n+1}^{12}\xi_n^{21}\right)a_n + \left(\xi_{n+1}^{11}\xi_n^{12} + \xi_{n+1}^{12}\xi_n^{22}\right)b_n. \tag{A4}$$

We can now solve Eq. (A3a) with respect to b_n and after substituting in Eq. (A4), a second-order linear difference equation is attained for a_n,

$$a_{n+2} - \frac{\xi_n^{12}\xi_{n+1}^{11} + \xi_{n+1}^{12}\xi_n^{22}}{\xi_n^{12}} a_{n+1} + \frac{\left(\xi_n^{11}\xi_n^{22} - \xi_n^{12}\xi_n^{21}\right)\xi_{n+1}^{12}}{\xi_n^{12}} a_n = 0, \tag{A5}$$

which accepts two linearly independent solutions $a_{n,1}$ and $a_{n,2}$ with a nonzero Casoratian $C(a_{n,1},\ a_{n,2})$ of the form [77,78]

$$C(a_{n,1},\ a_{n,2}) = \det\left(\begin{bmatrix} a_{n,1} & a_{n,2} \\ a_{n+1,1} & a_{n+1,2} \end{bmatrix}\right). \tag{A6}$$

Subsequently, we can derive the dynamics underpinning the evolution of the ratio of the state vector components ($r_n = b_n/a_n$). After substituting $r_n^a = a_{n+1}/a_n$, we can rewrite Eqs. (A3a) and (A3b) in the following form:

$$r_n^a = \xi_n^{11} + \xi_n^{12} r_n, \tag{A7a}$$

$$r_n^a \cdot r_{n+1} = \xi_n^{21} + \xi_n^{22} r_n, \tag{A7b}$$

which in turn lead to the following recursive nonlinear equation of the general Riccati type:

$$r_{n+1} = \frac{\xi_n^{21} + \xi_n^{22} r_n}{\xi_n^{11} + \xi_n^{12} r_n}. \tag{A8}$$

Without loss of generality, we have assumed in Eqs. (A7) and (A8) that $a_n \neq 0$. If $a_n = 0$, then we could have simply considered the evolution of $1/r_n = a_n/b_n$, without this altering the main conclusions of our analysis ($a_n = b_n = 0$ becomes a trivial case, since then $a_j \equiv b_j \equiv 0$ for $j \geqslant n \wedge j \in \mathbb{N}$). At this point, we shall also state the following relation, which will prove especially useful for determining the asymptotic dynamics of ratio r_n (see Appendix E and Sec. V within SM [76]),

$$\xi_n^{11} + \xi_n^{12} r_n = 1 + \Delta \frac{\delta a_n/\delta t_n}{a_n}. \tag{A9}$$

The above formula has been attained after reformulating Eq. (A7a) according to the first-order difference relation $a_{n+1} = a_n + \Delta\delta a_n/\delta t_n$. We shall now apply analogous but higher-order Newton series expansions (see Appendix D) to Eqs. (A5) and (A8). In this regard, based on expressions $\xi_n^{jj} = 1 + \Delta m_n^{jj}$, $\xi_n^{jk} = \Delta m_n^{jk}$ ($j, k = 1, 2 \wedge j \neq k$) and the discrete expansions $q_{n+1} = q_n + \Delta\delta q_n/\delta t_n$, $q_{n+2} = q_n + 2\Delta\delta q_n/\delta t_n + \Delta^2\delta^2 q_n/\delta t_n^2$ ($\delta t_n = \Delta$, $\delta t_n^2 = \Delta^2$, while q_n stands for an arbitrary discrete time sequence), it can be found that

$$\frac{\delta^2 a_n}{\delta t_n^2} - \left[\mathrm{tr}(M_n) + \frac{\delta m_n^{12}}{\delta t_n}\Big/ m_n^{12}\right]\frac{\delta a_n}{\delta t_n} + \left[\det(M_n) + m_n^{11}\frac{\delta m_n^{12}}{\delta t_n}\Big/ m_n^{12} - \frac{\delta m_n^{11}}{\delta t_n}\right]a_n + O(\Delta) = 0, \tag{A10a}$$

$$\frac{\delta r_n}{\delta t_n} + m_n^{12} r_n^2 + \left(m_n^{11} - m_n^{22}\right)r_n - m_n^{21} + O(\Delta) = 0. \tag{A10b}$$

In the above expression, $\mathrm{tr}(M_n)$ and $\det(M_n)$ denote the trace and determinant of the time-dependent matrix M_n, respectively, while $O(\Delta)$ stands for the big-O notation signifying in that manner terms of the order of Δ or higher ($\Delta^2,\ \Delta^3, \ldots$). In the continuous time limit $\Delta \to 0$ [$O(\Delta) \to 0$, $\delta \to d$, $t_n \to t$, $q_n \to q(t)$ with q representing an arbitrary time-dependent quantity], it can be directly attained that

$$\frac{d^2 a(t)}{dt^2} - \left\{\mathrm{tr}[M(t)] + \frac{dm^{12}(t)}{dt}\Big/ m^{12}(t)\right\}\frac{da(t)}{dt} + \left\{\det[M(t)] + m^{11}(t)\frac{dm^{12}(t)}{dt}\Big/ m^{12}(t) - \frac{dm^{11}(t)}{dt}\right\}a(t) = 0, \tag{A11a}$$

$$\frac{dr(t)}{dt} + m^{12}(t) r^2(t) + [m^{11}(t) - m^{22}(t)]r(t) - m^{21}(t) = 0, \tag{A11b}$$

which indeed are the differential equations that $a(t)$ and $r(t)$ satisfy as can be immediately shown from Eq. (A1) given that $M(t) = -iH(t)$. The dynamics of b_n and $b(t)$ can be easily retrieved from Eqs. (A10a) and (A11a) after replacing $a_n \to b_n$, $a(t) \to b(t)$, and also exchanging superscripts 1 and 2 in the elements of matrices M_n and $M(t)$ [such a permutation will of course not affect the trace and determinant of matrices M_n and $M(t)$]. Along these lines, it will be true for the Casoratian in Eq. (A6) that ($a_{n+1,1} = a_{n,1} + \Delta\delta a_{n,1}/\delta t_n$, $a_{n+1,2} = a_{n,2} + \Delta\delta a_{n,2}/\delta t_n$)

$$C(a_{n,1},\ a_{n,2}) = \Delta\left(a_{n,1}\frac{\delta a_{n,2}}{\delta t_n} - a_{n,2}\frac{\delta a_{n,1}}{\delta t_n}\right), \tag{A12}$$

where the expression inside the parenthesis attains now the familiar Wronskian form (in the $\Delta \to 0$ limit) found in continuous dynamical systems.

Of interest is now to investigate the form of Eqs. (A11) for the traceless and symmetric non-Hermitian model introduced

in Sec. II B. Already the respective discrete evolution equations for a_n, b_n, r_n have been provided in Sec. II B. Here, we shall also provide their continuous time counterparts after substituting $m^{11}(t) = -m^{22}(t) = f(t) = g(t) - i\sigma(t)$, $m^{12}(t) = m^{21}(t) = i\kappa$ [$g(t)$ and $\sigma(t)$ are the time-dependent continuous time gain/loss and detuning coefficients, accordingly, while κ is the constant coupling factor] in Eqs. (A11). Consequently, we obtain that

$$\frac{d^2a(t)}{dt^2} + \left\{\kappa^2 - f^2(t) - \frac{df(t)}{dt}\right\}a(t) = 0, \quad \text{(A13a)}$$

$$\frac{dr(t)}{dt} + i\kappa r^2(t) + 2f(t)r(t) - i\kappa = 0, \quad \text{(A13b)}$$

where Eq. (A13b) can be recognized as a typical nonlinear Ricatti differential equation. The dynamics that describes the evolution of $b(t)$ can be found after simply replacing $a(t) \to b(t)$ and $f(t) \to -f(t)$ in Eq. (A13a).

At this point, we shall turn our attention to Sec. II D and more specifically on how the second-order difference equation that the transformed component $\widetilde{a}_n$ satisfies [see Eq. (15b)] can be attained. In this respect, the following properties of the forward difference operator δ shall be employed (w_n, q_n, represent two arbitrary discrete time sequences)

$$\delta(w_nq_n) = \delta(q_nw_n) = w_{n+1}\delta q_n + q_n\delta w_n, \quad \text{(A14a)}$$

$$\delta^2q_n = \delta(\delta q_n) = q_{n+2} + q_n - 2q_{n+1}. \quad \text{(A14b)}$$

After applying operator δ to Eq. (14) of Sec. II D and based on the above identities, it becomes true that

$$\delta^2\widetilde{a}_n = \Omega^{12}_{n+1}\delta\widetilde{b}_n + \delta\Omega^{12}_n\widetilde{b}_n = \Omega^{12}_{n+1}\Omega^{21}_n\widetilde{a}_n + \frac{\delta\Omega^{12}_n}{\Omega^{12}_n}\delta\widetilde{a}_n. \quad \text{(A15)}$$

Given expressions $\Omega^{12}_n = \xi^{12}_n(\prod_{j=0}^{n}\xi^{11}_j)^{-1}\prod_{j=0}^{n-1}\xi^{22}_j$ and $\Omega^{21}_n = \xi^{21}_n(\prod_{j=0}^{n}\xi^{22}_j)^{-1}\prod_{j=0}^{n-1}\xi^{11}_j$ (see Sec. II D), we can obtain the following relation:

$$\delta^2\widetilde{a}_n + \frac{\xi^{12}_n\xi^{11}_{n+1} - \xi^{12}_{n+1}\xi^{22}_n}{\xi^{12}_n\xi^{11}_{n+1}}\delta\widetilde{a}_n - \frac{\xi^{12}_{n+1}\xi^{21}_n}{\xi^{11}_n\xi^{11}_{n+1}}\widetilde{a}_n = 0, \quad \text{(A16)}$$

which, according to Eq. (A14b) and after setting $p^{\delta\widetilde{a}}_{n,1} = (\xi^{12}_n\xi^{11}_{n+1} - \xi^{12}_{n+1}\xi^{22}_n)/(\xi^{12}_n\xi^{11}_{n+1})$ and $p^{\delta\widetilde{a}}_{n,0} = -\xi^{12}_{n+1}\xi^{21}_n/(\xi^{11}_n\xi^{11}_{n+1})$, can also read as

$$\widetilde{a}_{n+2} + \big(-2 + p^{\delta\widetilde{a}}_{n,1}\big)\widetilde{a}_{n+1} + \big(1 - p^{\delta\widetilde{a}}_{n,1} + p^{\delta\widetilde{a}}_{n,0}\big)\widetilde{a}_n = 0. \quad \text{(A17)}$$

Equations (A16) and (A17) essentially confirm Eqs. (15) of the main text.

Subsequently, we will emphasize on the discrete transformation employed in Sec. II D [see Eq. (13)] and on how it translates in continuous time dynamical systems. Such a parameter reformulation aims at recasting a Hamiltonian into a hollow matrix form, which in turn sheds light on certain dynamical traits of the original quantum mechanical arrangement. A similar rationale can be applied in continuous configurations after applying a transformation of the form

$$a(t) = e^{\int_0^t m^{11}(t')dt'}\widetilde{a}(t), \; b(t) = e^{\int_0^t m^{22}(t')dt'}\widetilde{b}(t), \quad \text{(A18)}$$

in Eq. (A1) [the choice of the lower limit in the above integral, implies that $a(0) = \widetilde{a}(0)$ and $b(0) = \widetilde{b}(0)$, but we can choose any lower limit that facilitates our analysis]. In that manner, the system dynamics will be equivalently described by $i\partial|\widetilde{u}(t)\rangle/\partial t = \widetilde{H}(t)|\widetilde{u}(t)\rangle$, where $|\widetilde{u}(t)\rangle = [\widetilde{a}(t) \;\; \widetilde{b}(t)]^{\mathcal{T}}$ and the transformed matrix $\widetilde{M}(t) = -i\widetilde{H}(t)$ will be given by

$$\widetilde{M} = \begin{bmatrix} 0 & m^{12}(t)e^{\int_0^t[m^{22}(t')-m^{11}(t')]dt'} \\ m^{21}(t)e^{\int_0^t[m^{11}(t')-m^{22}(t')]dt'} & 0 \end{bmatrix}. \quad \text{(A19)}$$

We are particularly interested on the evolution properties of $\widetilde{a}(t)$, which can be straightforwardly retrieved via Eq. (A11a) after substituting $a(t) \to \widetilde{a}(t)$ and $M(t) \to \widetilde{M}(t)$,

$$\frac{d^2\widetilde{a}(t)}{dt^2} - \left\{m^{22}(t) - m^{11}(t) + \frac{dm^{12}(t)}{dt}\Big/m^{12}(t)\right\}\frac{d\widetilde{a}(t)}{dt} - m^{12}(t)m^{21}(t)\widetilde{a}(t) = 0. \quad \text{(A20)}$$

For the special case of a traceless and symmetric non-Hermitian Hamiltonian [$m^{11}(t) = -m^{22}(t) = f(t)$, $m^{12}(t) = m^{21}(t) = i\kappa$], Eq. (A20) becomes

$$\frac{d^2\widetilde{a}(t)}{dt^2} + 2f(t)\frac{d\widetilde{a}(t)}{dt} + \kappa^2\widetilde{a}(t) = 0, \quad \text{(A21)}$$

which is exactly equivalent to Eq. (17) appearing in the main text. The correspondence of Eqs. (15) and (16) (see Sec. II D) to Eqs. (A20) and (A21) in the limit $\Delta \to 0$, accordingly, becomes directly evident after employing again the appropriate discrete Newton series expansions along with the property $1/[1 - \Delta F(\Delta)] \overset{\Delta\to 0}{\simeq} 1 + \Delta F(\Delta) + \Delta^2F^2(\Delta)$, where $F(\Delta)$ denotes an analytic function at $\Delta = 0$. Of significance is to also show the limiting behavior of the discrete transformation depicted in Eq. (13) of Sec. II D,

$$q_n = \prod_{j=0}^{n-1}\xi^{kk}_j\widetilde{q}_n = \prod_{j=0}^{n-1}\big(1 + \Delta\cdot m^{kk}_j\big)\widetilde{q}_n \overset{\Delta\to 0}{\simeq} \prod_{j=0}^{n-1}e^{\Delta\cdot m^{kk}_j}\widetilde{q}_n = e^{\Delta\cdot\sum_{j=0}^{n-1}m^{kk}_j}\widetilde{q}_n \overset{\Delta\to 0}{\simeq} e^{\int_0^{t=n\Delta}m^{kk}(t')dt'}\widetilde{q}_n, \quad \text{(A22)}$$

where q_n (or $\widetilde{q}_n$) represents either of the state vector components a_n and b_n (or $\widetilde{a}_n$ and $\widetilde{b}_n$) and $k = 1$ (when $q = a$) or $k = 2$ (when $q = b$). In the derivation of the above expression, the Riemann sum was used to convert the summation of m^{kk}_j to the respective integral. As expected, Eq. (A22) is in complete accordance with its continuous time counterpart represented by Eq. (A18).

In order to complete our analysis here, we shall also provide the definition of δ^{-1}, i.e., the inverse operator to δ. In this regard, after setting $\delta^{-1}q_n = w_n$ (q_n is an arbitrary discrete sequence) and given that $\delta^{-1}(\delta q_n) = \delta(\delta^{-1}q_n) = q_n$, we have simply $\sum_{j=0}^{n-1}q_j = \sum_{j=0}^{n-1}\delta(\delta^{-1}q_j) = \sum_{j=0}^{n-1}\delta w_j = w_n - w_0 = \delta^{-1}q_n - w_0$ or equivalently $\delta^{-1}q_n = w_0 + \sum_{j=0}^{n-1}q_j$ (w_0 is simply determined by the initial/boundary problem conditions and it is similar to the constant of integration when evaluating indefinite integrals in standard integral calculus). In other words, δ^{-1} describes the finite summation operation, as opposed to δ, which corresponds to operation of differencing.

To summarize, a direct equivalence exists between operators δ (difference operator) and δ^{-1} (summation operator) in the discrete domain with operators d (differentiation operator) and $\int$ (integration operator approximated via Riemann sums in the limit of infinitesimal intervals Δ) in the continuous domain, respectively.

APPENDIX B: EIGENSPECTRA AND SYMMETRY PROPERTIES OF DISCRETE HAMILTONIAN SYSTEMS

1. Parity inversion, time reversal, reciprocity, and energy conservation conditions

An important aspect in Hermitian quantum mechanics is the conservation of the scalar product $\langle u_n||u_n\rangle$ as time $t_n = n\Delta$ progresses ($n \in \mathbb{N}$), where $|u_n\rangle$ denotes the quantum state vector and Δ the discrete time step. This is naturally expected, as $\langle u_n||u_n\rangle$ represents the total probability of finding the quantum particle/system in any of the possible eigenstates after a potential measurement, which in turn should be equal to unity. A necessary condition for this to happen is that $\langle u_{n+1}||u_{n+1}\rangle = \langle u_n|\Xi_n^\dagger \Xi_n|u_n\rangle = \langle u_n||u_n\rangle \Leftrightarrow \Xi_n^\dagger \Xi_n = I$ [$|u_{n+1}\rangle = \Xi_n|u_n\rangle$ as indicated by Eqs. (1), (A3), and (A2) of Sec. II A and Appendix A, with $\Xi_n = I + \Delta M_n = I - i\Delta H_n$], which also implies that $\langle u'_{n+1}||u_{n+1}\rangle = \langle u'_n||u_n\rangle$ for any pair of quantum state vectors $|u_n\rangle$, $|u'_n\rangle$ (of course $\langle u'_{n+j}||u_{n+j}\rangle = \langle u'_n||u_n\rangle$ with $j \in \mathbb{N}$ will also hold, since $\Xi_n^\dagger \Xi_n = I$ should apply for all values of n). According to Wigner's theorem [96], this implies that the propagator matrix Ξ_n must be either unitary or antiunitary. Nevertheless, since $\Xi_n(\Delta) = I - i\Delta H_n$ (see Sec. II A and Appendix A) and thus $\Xi_n(\Delta = 0) = I$, it comes that Ξ_n must be unitary so as it can be continuously connected to the identity transformation, which itself is unitary. This now implies the Hermiticity of the Hamiltonian H_n as indicated by the chain of relations $\Xi_n^\dagger \Xi_n = (I + i\Delta H_n^\dagger)(I - i\Delta H_n) \simeq I + i\Delta(H_n^\dagger - H_n) = I \Leftrightarrow H_n^\dagger = H_n$, where small time steps Δ were assumed. Therefore, in non-Hermitian settings ($H_n^\dagger \neq H_n$) the inner product $\langle u'_n||u_n\rangle$ will not be conserved, which in turn has led to the development of pseudo-Hermitian theories [97,98] relying on alternative definitions of the scalar product between two quantum states. Here of course, we utilize the standard definition of the inner product, according to which $\langle u'_n||u_n\rangle = a'^*_n a_n + b'^*_n b_n$ with $|u_n\rangle = [a_n \ b_n]^\mathcal{T}$ and $|u'_n\rangle = [a'_n \ b'_n]^\mathcal{T}$.

Of interest is now to investigate the behavior of the inner product $\langle Q_n\rangle = \langle u_n|Q_n|u_n\rangle$, where Q_n represents an arbitrary matrix/operator (if $Q_n = I$ for all values of n, then we just get the inner product $\langle u_n||u_n\rangle$). In standard calculations, Q_n typically describes a potential observable and thus must correspond to a Hermitian operator so as the respective eigenvalues (or outcomes of measurements) are guaranteed to always be real. For instance, if we substitute Q_n with the Hamiltonian H_n, then $\langle H_n\rangle$ stands for the average energy at each time instant t_n. Consequently, it will apply that

$$\langle Q_{n+1}\rangle = \langle u_{n+1}|Q_{n+1}|u_{n+1}\rangle = \langle u_n|\Xi_n^\dagger Q_{n+1}\Xi_n|u_n\rangle, \tag{B1}$$

or in other words quantity $\langle Q_{n+1}\rangle$ is conserved (with time) iff $\forall n$ it is true that

$$\Xi_n^\dagger Q_{n+1}\Xi_n = Q_n \Leftrightarrow$$
$$\frac{\delta Q_n}{\delta t_n} + i(H_n^\dagger Q_n - Q_n H_n) = 0. \tag{B2}$$

In the above formula, δ stands for the forward difference operator (see Appendix A), while we have also used relationships $\Xi_n = 1 - i\Delta H_n$, $Q_{n+1} = Q_n + \Delta\delta Q_n/\delta t_n$, $\delta t_n = \Delta$ and have omitted any second- (or higher-)order contributions with respect to Δ. For Hermitian systems ($H_n^\dagger = H_n$), Eq. (B2) becomes

$$\frac{\delta Q_n}{\delta t_n} + i[H_n,\ Q_n] = 0, \tag{B3}$$

with $[H_n,\ Q_n] = H_n Q_n - Q_n H_n$ denoting the commutator of operators H_n, Q_n. It becomes evident now that energy conservation applies for Hermitian configurations iff $\delta H_n/\delta t_n = 0$ ($[H_n,\ H_n] = 0$) or equivalently iff H_n is constant (this corresponds to the case of a closed/isolated system). On the other hand, regarding non-Hermitian environments the energy conservation condition [see Eq. (B2)] can never be satisfied in the time-independent case ($\delta H_n/\delta t_n = 0$ and $H_n^\dagger H_n - H_n H_n \neq 0$ since $H_n^\dagger \neq H_n$) and cannot be guaranteed in time-dependent settings. It should be noted that for nonconserved quantities, their variation with time can be found as

$$\frac{\delta\langle Q_n\rangle}{\delta t_n} = \frac{\langle u_n|\Xi_n^\dagger Q_{n+1}\Xi_n|u_n\rangle - \langle u_n|Q_n|u_n\rangle}{\delta t_n}$$
$$= \langle u_n|\frac{\delta Q_n}{\delta t_n} + i(H_n^\dagger Q_n - Q_n H_n)|u_n\rangle, \tag{B4}$$

where operator Q_n is related to the quantity of interest and Δ assumes sufficiently small values. Equation (B4) is nothing but a generalization of Ehrenfest's theorem in the discrete time domain for an arbitrary quantum operator Q_n.

Another important aspect within any physical theory is that of symmetries describing the underlying physical/dynamical laws. In this regard, a potential symmetry W_n in quantum mechanics should map a solution $|u_n\rangle$ of the Schrödinger equation to another solution $W_n|u_n\rangle$ of the same equation. This should be also the case when we consider the respective discrete dynamics as provided in Eq. (1) of Sec. II A [or equivalently in Eq. (A2) of Appendix A]. Consequently, it should be true that

$$(W_{n+1}|u_{n+1}\rangle) = \Xi_n(W_n|u_n\rangle) \Leftrightarrow$$
$$W_{n+1}\Xi_n|u_n\rangle = \Xi_n W_n|u_n\rangle \Leftrightarrow$$
$$\Xi_n^{-1} W_{n+1}\Xi_n = W_n \Leftrightarrow$$
$$\frac{\delta W_n}{\delta t_n} + i[H_n,\ W_n] = 0, \tag{B5}$$

where we have used that $\Xi_n = I - i\Delta H_n$, $\Xi_n^{-1} = I + i\Delta H_n$, $W_{n+1} = W_n + \Delta\delta W_n/\delta t_n$ assuming small values for Δ. In conventional Hermitian quantum mechanics, the application of a map W_n should preserve the absolute value of the scalar product between any pair of states before and after applying the transformation. (As aforementioned, this is because the inner product contains basic information about the probabilities of measurements.) According to Wigner's theorem this implies that W_n might be either a linear unitary operator or an antilinear antiunitary operator, satisfying the property $W_n^\dagger W_n = I$. We can subsequently consider a smoothly defined unitary transformation $W_n(\epsilon)$, with ϵ taking on a continuous range of real values centered at zero and $\epsilon = 0$ denoting that no change is applied on the system, i.e., $W_n(\epsilon = 0) = I$

(this in turn disallows W_n from being antiunitary, as it must be continuously connected to the unitary identity matrix I). An infinitesimal version of such a mapping (described by small values of ϵ) can be written as $W_n(\epsilon) = I - i\epsilon Q_n$ after omitting any ϵ^2 or higher-order terms. This in turn implies that $W_n^\dagger W_n = I \Leftrightarrow Q_n^\dagger = Q_n$ (see respective calculation at the beginning of the present Appendix involving matrices $\Xi_n = I - i\Delta H_n$ and H_n). In this regard, Q_n is referred to as the *generator of the transformation* W_n and if W_n satisfies Eq. (B5) (i.e., describes a symmetry of the Hamiltonian system), then it can be easily shown that Q_n will also satisfy the same equation owing to the linear relationship between W_n and Q_n. For Hermitian conditions ($\Xi_n^\dagger = \Xi_n^{-1}$, $H_n^\dagger = H_n$), this implies that Q_n represents a conserved quantity according to Eq. (B3). This reflects the main conclusion of Noether's theorem, which here is applied to extended to the time-dependent case and states that: if an observable Q_n is the generator of a symmetry transformation W_n [Eq. (B5)] then it corresponds to a conserved quantity [Eq. (B3)], and conversely if a conserved (and observable) quantity Q_n corresponds to a symmetry map W_n. For instance, if a Hermitian Hamiltonian is characterized by a space/time translation symmetry or rotational invariance [for time-independent maps $\delta W_n/\delta t_n = 0 \Leftrightarrow W_n = W$, simply this implies that W should commute with the Hamiltonian H_n according to Eq. (B5)], then the corresponding generators-observables, i.e., linear momentum, energy/Hamiltonian, and angular momentum should be conserved and vice versa. This direct link between symmetry transformations and conserved quantities is broken in non-Hermitian arrangements, since now Eqs. (B2) and (B5) are not directly associated to each other ($\Xi_n^\dagger \neq \Xi_n^{-1}$, $H_n^\dagger \neq H_n$).

Of all symmetries, we shall emphasize here in the case of time translation invariance, which is directly related to the propagator/evolution operator Ξ_n since according to Eqs. (1) and (A3) of Sec. II A it applies that $|u_{n+l}\rangle = \Xi_{n+l-1}\cdots\Xi_n|u_n\rangle = \prod_{\nu=n}^{n+l-1}\Xi_\nu|u_n\rangle$ with $n,\ l,\ \nu \in \mathbb{N}$ and $l \geqslant 1$ [an ordered matrix product is used here as defined in Eq. (E3) of Sec. II C]. The relation $\Xi_n = I - i\Delta H_n$ (see Sec. II A or Appendix A) where Δ typically assumes small values, implies that the generator of time translations is the Hamiltonian itself. It can be inferred now based on Eq. (B5) that symmetry under translation by a single time unit Δ ($W_n \to \Xi_n$) implies that $\delta\Xi_n/\delta t_n = 0$ ($[H_n,\ \Xi_n] = 0$) or equivalently that the evolution and Hamiltonian matrices are constant with time ($\Xi_n = \Xi,\ H_n = H$). Under such time-independent conditions, it can be further deduced that the system dynamics will be invariant under translations of an arbitrary number of time units [if for instance we assume a shift by $n' \in \mathbb{N}$ units, then $W_n \to \Xi^{n'} = (I - i\Delta H)^{n'}$ and Eq. (B5) will be satisfied since $\delta\Xi^{n'}/\delta t_n = 0$ and $H,\ \Xi^{n'}$ commute to each other; $n,\ n'$ are two independent discrete quantities]. We could have reached to analogous conclusions had we considered the physical interpretation of time translation symmetry, which can be summarized as follows: If we allow the Hamiltonian arrangement to evolve for a particular interval of time, then the same final state must be obtained irrespective of when such evolution initiated assuming the same initial state. Mathematically, this can be expressed for a single time step via equations $|u_{n_1+1}\rangle = \Xi_{n_1}|u_{n_1}\rangle$ and $|u_{n_2+1}\rangle = \Xi_{n_2}|u_{n_2}\rangle$ ($n_1,\ n_2 \in \mathbb{N},\ n_1 \neq n_2$,), where we need to find the conditions under which if $|u_{n_2}\rangle = |u_{n_1}\rangle = |u_o\rangle$ then $|u_{n_2+1}\rangle = |u_{n_1+1}\rangle$ independently of the values of $n_1,\ n_2$ or the initial state $|u_o\rangle$. This can take place if and only if $\Xi_{n_2} = \Xi_{n_1}$ and since this must be true for all values of $n_1,\ n_2$, it becomes evident that Ξ_n (and H_n) must be constant and independent from n ($\Xi_n = \Xi,\ H_n = H$). Time invariance clearly applies now if we consider evolution for multiple time steps given that $|u_{n+l}\rangle = \Xi^l|u_n\rangle$, with Ξ^l depending only on the difference between the initial ($n\Delta$) and final time instants $[(n+l)\Delta]$. It is noteworthy to mention that the time independence of the evolution ($\Xi = [\xi^{jk}],\ j,\ k = 1,\ 2$) and Hamiltonian ($H = [h^{jk}],\ j,\ k = 1,\ 2$) matrix elements was also expected from the calculus of divided/finite differences, where a set of linear difference equations is time invariant iff all the respective coefficients are constant [in our case, these coefficients are described by elements ξ^{jk} or equivalently by h^{jk} or $m^{jk} = -ih^{jk}$ as seen in Eqs. (1), (A3), and (A2); matrix $M = -iH$ with elements m^{jk} has been defined in both Sec. II A and Appendix A]. It should be also highlighted here that while time-independent Hermitian arrangements arrangements respect both time translation symmetry and energy conservation, the same does not apply for time-independent non-Hermitian structures, which still are time invariant but energy will not be a constant of motion any more [compare and contrast Eqs. (B3), (B5) for the former case and Eqs. (B2), (B5) for the latter case, after setting $Q_n \to H$ and $W_n \to \Xi = I - i\Delta H$]. This in turn indicates the validity of Noether's theorem when considering Hermitian Hamiltonian dynamics, but also shows how it falls apart under non-Hermitian evolution conditions.

In the majority of the discussion so far, we have investigated the behavior of transformations, which apply continuous changes on the quantum mechanical arrangement and under which conditions they constitute symmetries of the quantum Hamiltonian arrangement. Of essence is to also study symmetries, which are discrete in nature, along with their implications on the Hamiltonian matrix. In this regard, we focus on the parity ($\mathcal{P}$) and time-reversal ($\mathcal{T}$) operators [96,99,100], since also our interest lies on retrieving the generalized expression of $\mathcal{PT}$-symmetric Hamiltonians. As a first step, we need to define such operators so as they satisfy the properties of the parity and time-reversal transformations. More specifically, $\mathcal{T}$ should represent an (antilinear) antiunitary operator ($\mathcal{T}^\dagger\mathcal{T} = \mathcal{T}\mathcal{T}^\dagger = I$, $\mathcal{T}z\mathcal{T}^{-1} = z^*$, where z is an arbitrary complex number and z^* its complex conjugate) and consequently it can be represented as $\mathcal{T} = UK\tau$ where U is a (linear) unitary matrix, K is the operation of complex conjugation (represented by the superscript $*$), and τ indicates the operation $n \to \mathcal{N} - n$ [$\tau : t_n = n\Delta \to t_{\mathcal{N}-n} = (\mathcal{N} - n)\Delta$, with $n,\ \mathcal{N}$ being both integers - if $\mathcal{N} = 0$ then we have the conventional definition of reflection around the origin $t_0 = 0$]. A defining property of the time-reversal operator is that when applied twice it is expected to restore the original state of the system, i.e., $\mathcal{T}^2 = \eta I$ (in Hermitian systems where the inner product $\langle u_n||u_n\rangle$ is conserved and set equal to unity, it comes that physically equivalent states differ only by a phase factor, i.e., $\eta = e^{i\phi}$). The reality of η can be shown as follows:

$$\mathcal{T}^2 = \eta I \Leftrightarrow \mathcal{T}\mathcal{T}^2\mathcal{T}^{-1} = \mathcal{T}\eta I\mathcal{T}^{-1} \Leftrightarrow$$
$$\mathcal{T}^2 = \eta^* I \Leftrightarrow \eta = \eta^*. \tag{B6}$$

Moreover, the following chain of relations will also apply [$\mathcal{T}^2 = (UK)^2\tau^2 = (UK)^2$, $\tau^2 = I$ and τ commutes with both U, K since they are time independent]

$$\mathcal{T}^2 = UKUK = U(KUK^{-1}) = UU^* = \eta I \Leftrightarrow$$
$$UU^* = \eta UU^\dagger \Leftrightarrow U^* = \eta U^\dagger \Leftrightarrow U = \eta U^{\mathcal{T}}, \tag{B7}$$

where we used relations $K^{-1} = K$ ($K^2 = I$ since $K^2 z = Kz^* = z$) and $KU = U^*K$ ($\Leftrightarrow KUK^{-1} = U^*$) with U being a unitary matrix ($U^\dagger U = UU^\dagger = I$). Based on Eq. (B7), it comes that $U = \eta U^{\mathcal{T}} \Leftrightarrow U^{\mathcal{T}} = \eta U$, which in turn implies that $\eta^2 = 1$ or $\eta = \pm 1$. In other words, $\mathcal{T}^2 = \pm I$ with $\mathcal{T}^2 = +I$ (this applies for bosonic/integer spin arrangements) and $\mathcal{T}^2 = -I$ (this applies for fermionic/half-integer spin configurations). Here, we use $\mathcal{T}^2 = I$ and more specifically $\mathcal{T} = K\tau$ ($K^2 = \tau^2 = I$ and K, τ commute), i.e., the time-reversal operator shall correspond to the simultaneous action of complex conjugation and reflection of the time coordinates. This is typically the convention used in analogous quantum mechanical [101,102] and classical optical setups [27,28]. (Continuous photonic systems satisfying the paraxiality condition/slowly varying amplitude approximation can be equivalently described by a spinless Schrödinger equation [103], and for such spinless-like configurations the expression $T = K\tau$ is a kinematically admissible form for the time-reversal operator [99]. Discrete optical arrangements, analogous to the ones described in [67] and Sec. IV within SM [76], can satisfy a discrete analog of the spinless Schrödinger equation and thus again $\mathcal{T} = K\tau$ is an appropriate choice.) Subsequently (after also defining the form of the parity operator), we shall show that conditions $\mathcal{T}^2 = I$ and $[\mathcal{P}, \mathcal{T}] = 0$ (operators $\mathcal{P}$, $\mathcal{T}$ should commute since they must act independently to each other) are so strong that even if we employ the generalized formula $\mathcal{T} = UK\tau$, expression $\mathcal{T} = K\tau$ (i.e., $U = I$) will again be obtained without loss of any generality. Finally, assigning $\mathcal{T} = K\tau$ can be independently justified, if we take into account that in the present paper we are particularly interested in the polarization dynamics of optical beams propagating within discrete photonic fiber networks (see also Sec. IV within SM [76]). In this case, the evolution is still described by the recursive relation $|u_{n+1}\rangle = \Xi_n |u_n\rangle$, but the state vector $|u_n\rangle$ corresponds to the electric field polarization at a particular frequency of operation. For a polychromatic beam, the electric field vector can be represented as a superposition of its different Fourier components as follows:

$$\boldsymbol{E}(\boldsymbol{\rho}, t) = \int_{-\infty}^{+\infty} \boldsymbol{E}(\boldsymbol{\rho}, \omega) e^{i\omega t} \frac{d\omega}{2\pi}$$
$$= \int_{-\infty}^{+\infty} \frac{\boldsymbol{E}(\boldsymbol{\rho}, \omega) e^{i\omega t} + \boldsymbol{E}(\boldsymbol{\rho}, -\omega) e^{-i\omega t}}{2} \frac{d\omega}{2\pi}, \tag{B8}$$

where ω signifies the angular frequency, $\boldsymbol{\rho}$ denotes the radial vector vector in the two-dimensional cross section of the optical fiber (quantities in bold refer here to vectors), and we have also employed identity $\int_{-\infty}^{+\infty} \boldsymbol{E}(\boldsymbol{\rho}, \omega) e^{i\omega t} d\omega = \int_{-\infty}^{+\infty} \boldsymbol{E}(\boldsymbol{\rho}, -\omega) e^{-i\omega t} d\omega$. Applying the time-reversal transformation on field $\boldsymbol{E}(\boldsymbol{\rho}, t)$ does not change its sign [$\boldsymbol{E}(\boldsymbol{\rho}, t) \rightarrow \boldsymbol{E}(\boldsymbol{\rho}, -t)$; this can be easily seen from the fact that the force experienced by a particle with charge q can be expressed as $\boldsymbol{F} = q\boldsymbol{E}$ and of course forces transform evenly with $\mathcal{T}$]. It is evident that if $\boldsymbol{E}(\boldsymbol{\rho}, t)$ is Fourier transformed as $\boldsymbol{E}(\boldsymbol{\rho}, \omega)$, then $\boldsymbol{E}(\boldsymbol{\rho}, -t)$ is Fourier transformed as $\boldsymbol{E}(\boldsymbol{\rho}, -\omega)$. Nonetheless, we have to keep in mind that the electric field corresponds to a real and measurable quantity, which in turn implies based on Eq. (B8) that $\boldsymbol{E}(\boldsymbol{\rho}, -\omega) = \boldsymbol{E}^*(\boldsymbol{\rho}, \omega)$. Consequently, it can be deduced for real fields that if $\boldsymbol{E}(\boldsymbol{\rho}, t) \rightarrow \boldsymbol{E}(\boldsymbol{\rho}, -t)$ then $\boldsymbol{E}(\boldsymbol{\rho}, \omega) \rightarrow \boldsymbol{E}(\boldsymbol{\rho}, -\omega) = \boldsymbol{E}^*(\boldsymbol{\rho}, \omega)$, which illustrates that the Fourier components must be complex conjugated owing to the action of operator $\mathcal{T}$ [103–107] (it is the Fourier components that appear in the polarization state vector). Of interest is to mention that magnetic fields $\boldsymbol{B}$ are odd with respect to $\mathcal{T}$ [$\boldsymbol{B}(\boldsymbol{\rho}, t) \rightarrow -\boldsymbol{B}(\boldsymbol{\rho}, -t)$; this can be directly seen from the expression of the Lorentz force $\boldsymbol{F} = q\boldsymbol{v} \times \boldsymbol{B}$ and clearly velocities $\boldsymbol{v}$ transform in an odd fashion with $\mathcal{T}$] and given that they also represent real quantities, it becomes clear that if $\boldsymbol{B}(\boldsymbol{\rho}, t) \rightarrow -\boldsymbol{B}(\boldsymbol{\rho}, -t)$ then $\boldsymbol{B}(\boldsymbol{\rho}, \omega) \rightarrow -\boldsymbol{B}(\boldsymbol{\rho}, -\omega) = -\boldsymbol{B}^*(\boldsymbol{\rho}, \omega)$. The validity of the aforementioned transformations under the action of operator $\mathcal{T}$ [$t \rightarrow -t$, $\boldsymbol{E}(\boldsymbol{\rho}, t) \rightarrow \boldsymbol{E}(\boldsymbol{\rho}, -t)$, $\boldsymbol{H}(\boldsymbol{\rho}, t) \rightarrow -\boldsymbol{H}(\boldsymbol{\rho}, -t)$] is also guaranteed, since they lead to the time-reversal invariance of Maxwell's field equations [106,108].

In order now to determine if a Hamiltonian configuration is time-reversal invariant (i.e., symmetric under the action of operator $\mathcal{T}$), we need to answer the question as to whether the associated state vector can retrace its path in time (apart from a multiplication factor/geometrical phase, which in any case cannot be measured). Along these lines and in order to facilitate our study of the time-reversal properties of the Hamiltonian H_n, we shall introduce an *auxiliary Hamiltonian field* $\overline{H}_n$, which can be defined in either of the following ways (depending each time on our choice):

(1) We set $\overline{H}_n = H_n$ for all possible values of n.

(2) We set $\overline{H}_n = H_n$ for $n \leqslant \lceil \mathcal{N}/2 - 1 \rceil$ ($\lceil . \rceil$ denotes the ceiling function), and $\overline{H}_n = H_{\mathcal{N}-n-1}$ otherwise (in the present definition, any external fields/sources are set to be symmetrically distributed around time $t_{\mathcal{N}}/2$ in the auxiliary field, i.e., $\overline{H}_{\mathcal{N}-n-1} = \overline{H}_n$).

In what follows, whenever the time-reversal operator is involved in studying particular symmetries, we shall always resort to this auxiliary Hamiltonian description and subsequently retrieve the respective conditions on the actual Hamiltonian H_n. Since in the present analysis we are particularly interested in the dynamics of discrete and cyclic time-dependent Hamiltonians for a single period of encirclement $T = t_N = N\Delta$ within the associated parameter space $\boldsymbol{\mathcal{R}}$, we can simply set $\mathcal{N} = 2N$. Moreover, we choose that $\overline{H}_n = H_n$ for $n \leqslant N - 1$ and $\overline{H}_n = H_{2N-n-1}$ for $n \geqslant N$ [here, we employ definition (ii) for the auxiliary field $\overline{H}_n$, as any actual external effects are assumed to cease when the encirclement in parameter space is complete (i.e., at time instant t_N)]. Such an effective temporal extension of the external fields to times beyond t_N (via $\overline{H}_n$) is depicted by the dotted orange and black lines in Fig. 10, and will in essence allow us to investigate the time-reversal features of H_n around instant $t_{\mathcal{N}}/2 = t_N$ (the solid orange lines in Fig. 10 reflect the actual external influences described by the original Hamiltonian H_n). In the same figure, the evolution matrix $\overline{\Xi}_n$ is denoted as $\overline{\Xi}_{n+1,n}$ in order to clearly indicate that when applied to the state vector $|\overline{u}_n\rangle$ it translates it by a single unit of time to

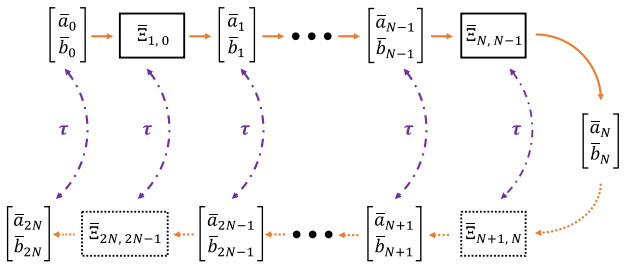

FIG. 10. Discrete time evolution of the quantum state vector $|\overline{u}_n\rangle = [\overline{a}_n\ \overline{b}_n]^{\mathcal{T}}$, whose value at each time step $[t_{n+1} = (n+1)\Delta]$ is determined by the previous time step $[t_n = n\Delta]$ via the relation $|\overline{u}_{n+1}\rangle = \overline{\Xi}_{n+1,n}|\overline{u}_n\rangle$. The auxiliary Hamiltonian $\overline{H}_n$ is defined as $\overline{H}_n = H_n$, $\overline{\Xi}_{n+1,n} = \Xi_{n+1,n} = I - i\Delta\overline{H}_n = I - i\Delta H_n$ for $n \leqslant N-1$ (in this regard, $|\overline{u}_n\rangle \equiv |u_n\rangle$ for $n \leqslant N$, where state vector $|u_n\rangle$ obeys the evolution equation $|u_{n+1}\rangle = \Xi_{n+1,n}|u_n\rangle$ associated with the original Hamiltonian representation H_n) and $\overline{H}_n = H_{2N-n-1}$, $\overline{\Xi}_{n+1,n} = \Xi_{2N-n,2N-n-1} = I - i\Delta\overline{H}_n = I - i\Delta H_{2N-n-1}$ for $n \geqslant N$, while operator τ reflects the discrete time coordinates according to $t_n = n\Delta \to t_{2N-n} = (2N-n)\Delta$ (see purple dash-dotted lines in the figure above - such a definition of τ will allow us to examine the time-reversal properties of $\overline{H}_n$ or equivalently of H_n around time instant t_N). Solid orange lines denote the actual evolution of the state vector during a full cycle within the Hamiltonian's parameter space $\boldsymbol{\mathcal{R}}$ ($|\overline{u}_n\rangle \equiv |u_n\rangle$ for $t_n \leqslant t_N$ or $n \leqslant N$), while dotted orange lines denote an effective temporal extension of the external field/source effects to times beyond t_N via the auxiliary field $\overline{H}_n$.

$|\overline{u}_{n+1}\rangle$ ($|\overline{u}_{n+1}\rangle = \overline{\Xi}_{n+1,n}|\overline{u}_n\rangle$ with $\overline{\Xi}_{n+1,n} = I - i\Delta\overline{H}_n$ as discussed in Sec. II A and Appendix A—the barred quantity $|\overline{u}_n\rangle$ describes the state vector associated with system $\overline{H}_n$, while $|u_n\rangle$ represents of course the state vector associated with the original system H_n: $\overline{H}_n = H_n$ for $n \leqslant \lceil \mathcal{N}/2 - 1 \rceil = N-1$ and thus $|\overline{u}_n\rangle \equiv |u_n\rangle$ for $n \leqslant N$).

To better comprehend the action of the time-reversal operator, we shall apply it in the ordinary discrete evolution equation $|\overline{u}_{n+1}\rangle = \overline{\Xi}_{n+1,n}|\overline{u}_n\rangle$ describing the auxiliary Hamiltonian dynamics. In this manner, it can be obtained that ($\mathcal{T} = K\tau$)

$$\begin{bmatrix} \overline{a}^*_{2N-n-1} \\ \overline{b}^*_{2N-n-1} \end{bmatrix} = \overline{\Xi}^*_{2N-n-1,2N-n} \begin{bmatrix} \overline{a}^*_{2N-n} \\ \overline{b}^*_{2N-n} \end{bmatrix} \Leftrightarrow$$
$$\begin{bmatrix} \overline{a}_{2N-n} \\ \overline{b}_{2N-n} \end{bmatrix} = \overline{\Xi}_{2N-n,2N-n-1} \begin{bmatrix} \overline{a}_{2N-n-1} \\ \overline{b}_{2N-n-1} \end{bmatrix}, \tag{B9}$$

where we have defined $|\overline{u}_n\rangle = [\overline{a}_n\ \overline{b}_n]^{\mathcal{T}}$ and $\overline{\Xi}_{n,n+1} = \overline{\Xi}^{-1}_{n+1,n}$ ($= I + i\Delta\overline{H}_n$ for sufficiently small values of the discrete time step Δ) so as $|\overline{u}_{n+1}\rangle = \overline{\Xi}_{n+1,n}|\overline{u}_n\rangle \Leftrightarrow |\overline{u}_n\rangle = \overline{\Xi}^{-1}_{n+1,n}|\overline{u}_{n+1}\rangle = \overline{\Xi}_{n,n+1}|\overline{u}_{n+1}\rangle$ [Eq. (B9) is an illustration of the equivalence $|\overline{u}_{n+1}\rangle = \overline{\Xi}_n|\overline{u}_n\rangle \Leftrightarrow \mathcal{T}|\overline{u}_{n+1}\rangle = (\mathcal{T}\overline{\Xi}_n\mathcal{T}^{-1})\mathcal{T}|\overline{u}_n\rangle$, where the latter relation is nothing but a time reversed version of the former]. Equation (B9) of course always applies as clearly revealed after setting $n \to 2N-n-1$ into the recursive formula $|\overline{u}_{n+1}\rangle = \overline{\Xi}_{n+1,n}|\overline{u}_n\rangle$ (see also Fig. 10, where a schematic illustration of the state vector evolution is provided). Time-reversal symmetry/invariance (TRS) now implies that $|\overline{u}_{n+1}\rangle = \overline{\Xi}_{n+1,n}|\overline{u}_n\rangle \Leftrightarrow \mathcal{T}|\overline{u}_{n+1}\rangle = \overline{\Xi}_{n+1,n}\mathcal{T}|\overline{u}_n\rangle$, or equivalently ($\mathcal{T} = K\tau$)

$$\begin{bmatrix} \overline{a}^*_{2N-n-1} \\ \overline{b}^*_{2N-n-1} \end{bmatrix} = \overline{\Xi}_{n+1,n} \begin{bmatrix} \overline{a}^*_{2N-n} \\ \overline{b}^*_{2N-n} \end{bmatrix} \Leftrightarrow$$
$$\begin{bmatrix} \overline{a}_{2N-n} \\ \overline{b}_{2N-n} \end{bmatrix} = \overline{\Xi}^*_{n,n+1} \begin{bmatrix} \overline{a}_{2N-n-1} \\ \overline{b}_{2N-n-1} \end{bmatrix}. \tag{B10}$$

Given Eqs. (B9) and (B10), it can be directly deduced that $\overline{\Xi}^*_{n,n+1} = \overline{\Xi}_{2N-n,2N-n-1} \Leftrightarrow I - i\Delta\overline{H}^*_n = I - i\Delta\overline{H}_{2N-n-1} \Leftrightarrow \overline{H}^*_n = \overline{H}_{2N-n-1} \Leftrightarrow H^*_n = H_n$. (We have used here relation $\overline{H}_n = H_{2N-n-1}$ for $n \geqslant N$, as also described in the caption of Fig. 10.) Hence, TRS demands the Hamiltonian H_n to be real for all possible values of n. This conclusion is of course in agreement with Eq. (B5), which suggests that for operator $\mathcal{T}$ to describe a symmetry of the system it must commute with the Hamiltonian $\overline{H}_n$ [for discrete symmetries, the term $\delta W_n/\delta t_n$ is absent in Eq. (B5)], i.e., $[\mathcal{T}, \overline{H}_n] = 0 \Leftrightarrow \mathcal{T}\overline{H}_n\mathcal{T}^{-1} = \overline{H}_n \Leftrightarrow \overline{H}^*_{2N-n} \simeq \overline{H}^*_{2N-n-1} = \overline{H}_n \Leftrightarrow H^*_n = H_n$ (here, we have used the fact that $\overline{H}_{2N-n} \simeq \overline{H}_{2N-n-1}$ assuming small time steps). Moreover, it will hold that $\mathcal{T}\overline{\Xi}_{n+1,n}\mathcal{T}^{-1} = \overline{\Xi}^*_{2N-n-1,2N-n} = (\overline{\Xi}^{-1}_{2N-n,2N-n-1})^* = I - i\Delta\overline{H}_{2N-n-1} = I - i\Delta\overline{H}_n = \overline{\Xi}_{n+1,n}$. [This can also be seen from the fact that $\mathcal{T}|\overline{u}_{n+1}\rangle = \overline{\Xi}_{n+1,n}\mathcal{T}|\overline{u}_n\rangle \Leftrightarrow |\overline{u}_{n+1}\rangle = \mathcal{T}^{-1}\overline{\Xi}_{n+1,n}\mathcal{T}|\overline{u}_n\rangle = \mathcal{T}\overline{\Xi}_{n+1,n}\mathcal{T}^{-1}|\overline{u}_n\rangle$ ($\mathcal{T}^2 = I \Leftrightarrow \mathcal{T}^{-1} = \mathcal{T}$), and since $|\overline{u}_{n+1}\rangle = \overline{\Xi}_{n+1,n}|\overline{u}_n\rangle$ it can be deduced that $\mathcal{T}\overline{\Xi}_{n+1,n}\mathcal{T}^{-1} = \overline{\Xi}_{n+1,n}$.] Consequently, time-reversal symmetry implies that not only the Hamiltonian but also the evolution operator must be invariant under the action of $\mathcal{T}$. Of interest is also to highlight here that, had we not originally set $\overline{H}_n = H_{2N-n-1}$ and instead had applied $\overline{H}_n = H_n = 0$ for $n \geqslant N$ (all actual external effects—encapsulated in H_n—cease at time t_N, i.e., after a complete parametric encirclement in space $\boldsymbol{\mathcal{R}}$), then TRS would require that $\overline{H}^*_n = \overline{H}_{2N-n-1} = 0$ for all values of n, which must be rejected. In other words, when the actual Hamiltonian arrangement (H_n) performs a single encirclement in parameter space and operator τ reflects the system around time instant t_N ($\mathcal{N} = 2N$), it only makes sense to study TRS after assuming the presence of fictitious external perturbations through the auxiliary Hamiltonian acting at times beyond the period of encirclement $T = t_N$ and satisfying relation $\overline{H}_n = H_{2N-n-1}$ ($t_n \geqslant t_N$ or $n \geqslant N$). In general, TRS (described equivalently by formulas $\mathcal{T}\overline{H}_n\mathcal{T}^{-1} = \overline{H}_n$ and $\mathcal{T}\overline{\Xi}_{n+1,n}\mathcal{T}^{-1} = \overline{\Xi}_{n+1,n}$) is summarized into either condition $H^*_n = H_{\mathcal{N}-n} \simeq H_{\mathcal{N}-n-1}$ [external influences are left intact and thus $\overline{H}_n = H_n$ for all values of n; see previously for definition (i) of field $\overline{H}_n$] or condition $H^*_n = H_n$ [external influences—including both actual ($\overline{H}_n = H_n$ for $n \leqslant \lceil \mathcal{N}/2 - 1 \rceil$) and fictitious ($\overline{H}_n = H_{\mathcal{N}-n-1}$ for $n > \lceil \mathcal{N}/2 - 1 \rceil$)—are set to be symmetrically distributed around time $t_{\mathcal{N}/2}$, i.e., $\overline{H}_{\mathcal{N}-n-1} = \overline{H}_n$, as discussed previously in definition (ii) of field $\overline{H}_n$], given that operator τ reflects the discrete time coordinates according to $t_n = n\Delta \to t_{\mathcal{N}-n} = (\mathcal{N}-n)\Delta$. For instance, if $\mathcal{N}$ was set equal to N (i.e., reflection took place around time $t_{\mathcal{N}}/2 = t_N/2 = N\Delta/2$) then the aforementioned conditions would read for the auxiliary Hamiltonian field as

$\overline{H}_n^* = \overline{H}_{N-n} \simeq \overline{H}_{N-n-1}$, while for the original Hamiltonian system H_n would imply that either $H_n^* = H_{N-n} \simeq H_{N-n-1}$ [definition (i) for $\overline{H}_n$] or $H_n^* = H_n$ [definition (ii) for $\overline{H}_n$]. *Here (and in what follows), we use definition (ii) for the auxiliary Hamiltonian* as it consistently leads to the same TRS condition for H_n irrespective of our choice of $\mathcal{N}$, i.e., it demands the reality of the Hamiltonian matrix ($H_n^* = H_n$) so as the quantum state can retrace its path in time. (In the following analysis we shall employ $\mathcal{N} = 2N$, only for the purpose of illustrating the mathematical relations that $\overline{H}_n$ should satisfy for any symmetries involving operator $\mathcal{T}$.)

A concept very closely related to TRS is that of reciprocity (in Sec. IV within SM [76] we will show that time-reversal invariant linear lossless systems must also be reciprocal), which can be loosely encapsulated into the expression "If I can see you, you can see me". The strict definition of reciprocal systems demands the respective Green's function to be symmetric (i.e., does not change) if the coordinates of the source and detector/observer are interchanged [107,109–112]. As illustrated in [107,109,112], such a statement is depicted in relation $\overline{H}_n^{qw} = \langle q|\overline{H}_n|w\rangle = \langle \mathcal{T}w|\overline{H}_n|\mathcal{T}q\rangle = \overline{H}_n^{\underline{wq}}$ (underlined subscripts are associated with the representation of $\overline{H}_n$ in terms of the time reversed states) with $\overline{H}_n$ standing for the auxiliary Hamiltonian and $|w\rangle$, $|q\rangle$ denoting two state vectors of the respective Hilbert space of states. (For a more detailed discussion related to the interpretation of the aforementioned condition in terms of the scattering features and state transition probabilities pertaining to a generalized quantum setting, the reader can refer to [107,109–112].) It should be noted that the key point essentially associating reciprocity with the time-reversal operator is the scalar product swapping identity $\langle q|\mathcal{T}|w\rangle = \langle w||q\rangle$ that $\mathcal{T}$ satisfies owing to its antiunitary nature. In this vein, it should hold that $\langle q|\overline{H}_n|w\rangle = \langle \mathcal{T}\overline{H}_n w||\mathcal{T}q\rangle = \langle \mathcal{T}\overline{H}_n w||\mathcal{T}q\rangle = \langle (\mathcal{T}\overline{H}_n\mathcal{T}^\dagger)\mathcal{T}w||\mathcal{T}q\rangle = \langle \mathcal{T}w|\mathcal{T}\overline{H}_n\mathcal{T}^\dagger|\mathcal{T}q\rangle$, which in turn implies for reciprocal quantum arrangements that $\mathcal{T}\overline{H}_n\mathcal{T}^\dagger = \overline{H}_n$ or equivalently $\overline{H}_{2N-n}^{\mathcal{T}} \simeq \overline{H}_{2N-n-1}^{\mathcal{T}} = \overline{H}_n$ (small values of Δ are typically assumed) given that $\mathcal{T} = K\tau$ and $\tau : n \to 2N - n$ [of course operator $\mathcal{T}\overline{H}_n\mathcal{T}^\dagger$ is linear since $\mathcal{T}\overline{H}_n\mathcal{T}^\dagger z = \mathcal{T}\overline{H}_n\mathcal{T}z = \mathcal{T}\overline{H}_n z^*\mathcal{T} = \mathcal{T}z^*\overline{H}_n\mathcal{T} = z\mathcal{T}\overline{H}_n\mathcal{T}$ ($\overline{H}_n z = z\overline{H}_n$ since $\overline{H}_n$ is linear, and $\mathcal{T} = \mathcal{T}^\dagger$ since $\mathcal{T}^2 = \mathcal{T}\mathcal{T}^\dagger = \mathcal{T}^\dagger\mathcal{T} = I$) with z being an arbitrary scalar complex variable, and thus $\langle (\mathcal{T}\overline{H}_n\mathcal{T}^\dagger)\mathcal{T}w||\mathcal{T}q\rangle = \langle \mathcal{T}w|(\mathcal{T}\overline{H}_n\mathcal{T}^\dagger)^\dagger|\mathcal{T}q\rangle = \langle \mathcal{T}w|\mathcal{T}\overline{H}_n\mathcal{T}^\dagger|\mathcal{T}q\rangle$]. This implies that $H_n^{\mathcal{T}} = H_n$ according to definition (ii) for $\overline{H}_n$ [had we employed definition (i), we would have obtained an alternative version of the reciprocity relation: $H_n^{\mathcal{T}} = H_{2N-n-1}$], i.e., H_n should be symmetric, which in turn is expected had we studied the underlying discrete Schrödinger-like evolution equations from the viewpoint of standard linear systems/network theory [113]. (It should be highlighted that in the more general scenario when $\mathcal{T} = UK\tau$ with $U \neq I$, analogous reciprocity conditions have been retrieved in [107,109,112].) It becomes clear now that if $Z_f = \Xi_{n+l,\,n+l-1}\cdots\Xi_{n+1,\,n}$ and $Z_b = \Xi_{n+1,\,n}\cdots\Xi_{n+l,\,n+l-1}$ ($n,\, l \in \mathbb{N}$ and $l \geqslant 1$) represent the forward and backward transfer matrices over l discrete time steps, then reciprocity ($H_n^{\mathcal{T}} = H_n \Leftrightarrow \Xi_{n+1,\,n}^{\mathcal{T}} = \Xi_{n+1,\,n}$ given that $\Xi_{n+1,\,n} = I - i\Delta H_n$) demands that $Z_f^{\mathcal{T}} = Z_b$. (In standard photonics textbooks, this is coined as the *de Hoop reciprocity relation* and is used to describe discrete optical settings, where the emphasis is on studying the evolution of the polarization state of light [103,104,114]; in Sec. IV within SM [76], we apply such concepts with the aid of Jones algebra in the specific case of discrete fiber loop platforms.)

Having defined operator $\mathcal{T}$ and the conditions for which a quantum configuration is time-reversal invariant and reciprocal, we shall proceed in retrieving the 2×2 matrix representation of the linear and unitary parity transformation $\mathcal{P}$ ($\mathcal{P}^\dagger\mathcal{P} = \mathcal{P}\mathcal{P}^\dagger = I$), given that our focus in the present paper lies on two-level quantum Hamiltonian structures. We expect that operators $\mathcal{P}$ and $\mathcal{T}$ should act independently from each other, i.e., they should commute, $[\mathcal{P},\, \mathcal{T}] = 0$. This in turn implies that $\mathcal{P}$ must be a real matrix, since $\mathcal{P} = \mathcal{T}\mathcal{P}\mathcal{T}^{-1} = K\mathcal{P}K^{-1} = \mathcal{P}^*$. As a discrete reflection transformation, the parity operator should satisfy the involuntary property $\mathcal{P}^2 = I$ (in general $\mathcal{P}^2 = \eta I$, but we can simply substitute $\mathcal{P} \to \sqrt{\eta}\mathcal{P}$ and equivalently attain that $\mathcal{P}^2 = I$). Along these lines, the respective eigenvalues satisfy the relation $\lambda_{\mathcal{P}}^2 = 1 \Leftrightarrow \lambda_{\mathcal{P}} = \pm 1$. If both eigenvalues were $+1$ or -1, this the trivial case of the parity inversion being an identity transformation, which should be abandoned. Hence, it can only be that the matrix representation of parity inversion has one eigenvalue equal to $+1$ and another equal to -1, which in turn implies that $\det(\mathcal{P}) = -1$, $\mathrm{tr}(\mathcal{P}) = 0$. Moreover, given that $\mathcal{P}^2 = \mathcal{P}^\dagger\mathcal{P} = \mathcal{P}\mathcal{P}^\dagger = I$, it can be directly deduced that $\mathcal{P} = \mathcal{P}^\dagger = (\mathcal{P}^*)^{\mathcal{T}} = \mathcal{P}^{\mathcal{T}}$, i.e., the parity operator should eventually correspond to a real involuntary symmetric matrix, $\mathcal{P} = \mathcal{P}^* = \mathcal{P}^{-1} = \mathcal{P}^{\mathcal{T}}$.

Based on the aforementioned properties, we can find a general expression for $\mathcal{P}$ by writing it as a linear superposition of the identity (I) and the Pauli matrices (σ_1, σ_2, σ_3) as $\mathcal{P} = \alpha_0 I + \sum_{j=1}^{3}\alpha_j\sigma_j$ with α_j being real numbers for $j = 0,\, 1,\, 2,\, 3$ (matrices I and σ_j form an orthogonal basis for the Hilbert space of all 2×2 Hermitian matrices for $\alpha_j \in \mathbb{R}$). Given that $\mathcal{P}$ is symmetric, it comes that $\alpha_2 = 0$ ($\sigma_2^{\mathcal{T}} = -\sigma_2$). Moreover, it can easily be found that $\mathrm{tr}(\mathcal{P}) = 2\alpha_0$ and since $\mathcal{P}$ must be traceless, it can be deduced that $\alpha_0 = 0$. The expression for $\mathcal{P}^2$ will now be given by

$$\mathcal{P}^2 = \alpha_1^2\sigma_1^2 + \alpha_3^2\sigma_3^2 + \alpha_1\alpha_3\{\sigma_1,\, \sigma_3\} = \left(\alpha_1^2 + \alpha_3^2\right)I, \quad \text{(B11)}$$

where $\{\sigma_j,\, \sigma_k\} = \sigma_j\sigma_k + \sigma_k\sigma_j$ is the anticommutator between operators σ_j, σ_k and we have used that $\sigma_j^2 = I$ and $\{\sigma_j,\, \sigma_k\} = 0$ for $j \neq k$. Since $\mathcal{P}^2 = I$, it can be inferred from Eq. (B11) that $\alpha_1^2 + \alpha_3^2 = 1$ [this is equivalent to the condition $\det(\mathcal{P}) = -1$], which accepts as solutions $\alpha_1 = \sin\theta$, $\alpha_3 = \cos\theta$ with $\theta \in (-\pi,\, \pi]$. (The general form of $\mathcal{P}$ has been also retrieved in [115] by exploiting the fact that all 2×2 matrix implementations of the parity operator must be connected via a similarity transformation, as they all share the same eigenvalues, 1 and –1.)

In the present analysis, we select $\mathcal{P} = \sigma_1$ (i.e., we set $\theta = \pi/2$ in the expressions for α_1, α_3), which is the same as the convention used in [101,102] (quantum mechanical setups) and [27,28] (photonic setups). In order to clarify such a choice, we will subsequently emphasize on the effect of the parity operator on the dynamical equations describing both continuous and discrete implementations of two-mode

photonic platforms. In the former case, we can consider a system of two coupled single-mode waveguides. Paraxial approximation conditions (this implies that the wave equation can be approximated by the Schrödinger equation, with time t being replaced by the propagation direction z and the quantum mechanical potential corresponding to the refractive index profile) along with coupled mode theory treatments (see [103]) allow us to describe the underlying dynamics in terms of an effective 2×2 Hamiltonian $H(z) = [h^{jk}(z)]$ ($j, k = 1, 2$) as $i\partial|u(z)\rangle/\partial z = H(z)|u(z)\rangle$, with z signifying the direction of propagation and the components of the state vector $|u(z)\rangle = [a(z)\ b(z)]^{\mathcal{T}}$ denoting the complex field amplitudes of the unperturbed eigenmodes associated with each waveguide site [the overall field will be expressed as a superposition of such modes weighted by $a(z)$ and $b(z)$]. The diagonal entries of $H(z)$ are determined by the material properties and dimensions of each of the guiding elements [in essence, they correspond to the effective indices $n_{\text{eff}}^{1,2}$ of the unperturbed modes—the detuning $\Re(n_{\text{eff}}^1 - n_{\text{eff}}^2)$ and differential gain/loss $\Im(n_{\text{eff}}^1 - n_{\text{eff}}^2)$ between such modes can be progressively changed along direction z by altering the pumping conditions and the waveguide width, correspondingly], while the off-diagonal entries depend mainly on the distance between the waveguides (and describe the coupling strength between the unperturbed eigenmodes in the coupled optical system). In such settings, parity inversion implies a reflection of the spatial coordinates around the origin in the plane transverse to the direction of propagation (i.e., the xy plane here), or equivalently an interchange between the waveguide subsystems and thus a subsequent flip of of the overall field distribution. This is clearly illustrated by the following relations ($\mathcal{P} = \mathcal{P}^{-1} = \sigma_1$),

$$\mathcal{P}|u(z)\rangle = \begin{bmatrix} 0 & 1 \\ 1 & 0 \end{bmatrix}\begin{bmatrix} a(z) \\ b(z) \end{bmatrix} = \begin{bmatrix} b(z) \\ a(z) \end{bmatrix}, \tag{B12a}$$

$$\mathcal{P}H(z)\mathcal{P}^{-1} = \begin{bmatrix} 0 & 1 \\ 1 & 0 \end{bmatrix}\begin{bmatrix} h^{11}(z) & h^{12}(z) \\ h^{21}(z) & h^{22}(z) \end{bmatrix}\begin{bmatrix} 0 & 1 \\ 1 & 0 \end{bmatrix} = \begin{bmatrix} h^{22}(z) & h^{21}(z) \\ h^{12}(z) & h^{11}(z) \end{bmatrix}, \tag{B12b}$$

where field amplitudes $a(z)$, $b(z)$ become flipped and an exchange of both diagonal $[h^{11}(z) \leftrightarrow h^{22}(z)]$ and off-diagonal $[h^{12}(z) \leftrightarrow h^{21}(z)]$ elements of matrix $H(z)$ is noticed under the action of the $\mathcal{P}$ operator. Consequently, our choice for the matrix representation of $\mathcal{P}$ as the first Pauli matrix becomes justified and as we will subsequently see, it leads to the standard form of $\mathcal{PT}$-symmetric Hamiltonian matrices employed in the field of non-Hermitian optics [27,28].

Alternatively to the dual-waveguide system, we can also consider a single-waveguide channel supporting only its fundamental transverse electric (TE) and magnetic (TM) modes [38]. Paraxial conditions and coupled mode theory analysis reveals again that the evolution dynamics will be dictated by the 2×2 system of equations $i\partial|u(z)\rangle/\partial z = H(z)|u(z)\rangle$, but now the state vector $|u(z)\rangle$ will actually represent the polarization state (TE and TM modes are linearly polarized in orthogonal directions). The coupling between the TE and TM modes can be provided by slanting the waveguide sidewalls, while a variable differential gain/loss and detuning/birefringence can be attained along the propagation direction by changing the pumping conditions and waveguide width, respectively. In such an experimental scenario, we can still define the parity operator as $\mathcal{P} = \sigma_1$ and in turn Eqs. (B12) will imply an exchange of the $E_x(z) = a(z)$ and $E_y(z) = b(z)$ field components, while the overall structure will be reflected with respect to the 45° angular direction in the xy plane (propagation direction is along the z axis).

So far, we have discussed about continuous two-level optical arrangements to illuminate the effect of parity inversion, but our emphasis in the present paper is on discrete photonic systems. More specifically, by employing a fiber loop network it becomes possible to emulate the discrete dynamics $i\delta|u_n\rangle/\delta t_n = H_n|u_n\rangle \Leftrightarrow |u_{n+1}\rangle = \Xi_{n+1,n}|u_n\rangle = \Xi_n|u_n\rangle$ ($\Xi_{n+1,n} = \Xi_n = I - i\Delta H_n$, with $n \in \mathbb{N}$ and $\delta t_n = \Delta$ describing the incremental time step) as illustrated in [67] (for an almost $\mathcal{PT}$-symmetric configuration) and in Sec. IV within SM [76] (for a generalized binary Hamiltonian H_n). In this regard, state vector $|u_n\rangle = [a_n\ b_n]^{\mathcal{T}}$ will once again represent the polarization state, while the (discrete) time variable t_n becomes reinstated in the place of the (continuous) space coordinate z as in typical Schrödinger equation descriptions. Equations (B12) will still apply here, after replacing the spatial variable z with the discrete temporal coordinate $t_n = n\Delta$. The diagonal and off-diagonal elements of the Hamiltonian H_n will be interchanged $[h_n^{11} \leftrightarrow h_n^{22},\ h_n^{12} \leftrightarrow h_n^{21}]$ after the action of operator $\mathcal{P} = \sigma_1$, which experimentally implies that the associated optical devices should be modulated in such a manner so as the effect on the x and y polarizations ($E_n^x = a_n$, $E_n^y = b_n$) becomes flipped. (This is of course equivalent to a reflection of the overall arrangement with respect to the 45° angular direction in the transverse xy plane—propagation direction now is along the optical fiber axis.) Here, all optical parameters including coupling strength, gain/loss, and detuning between polarization modes E_n^x and E_n^y, can be precisely synthesized by employing appropriate (electrically driven) polarization controllers, along with electro-optic amplitude and phase modulators. This leads to a sufficiently greater degree of flexibility as compared to the aforementioned waveguide configurations (the discrete Hamiltonian system can in essence follow arbitrary cyclic or noncyclic trajectories within the parameter space), while also alleviating the need for any complex fabrication processes.

Having described viable optical implementations of two-dimensional complex Hamiltonian matrices along with the physical interpretation and matrix representation of the parity operator, we proceed by providing the necessary conditions for $\mathcal{PT}$ symmetry to occur. In order to better comprehend the action of the combined parity-time ($\mathcal{PT}$) operator, we apply it to the state vector evolution equation [we reinstate here the barred quantities and the auxiliary Hamiltonian $\overline{H}_n$ to account for the operation of $\mathcal{T} = K\tau$, as analyzed previously in the present Appendix, K: complex conjugation operator, $\tau : t_n = n\Delta \rightarrow t_{\mathcal{N}-n} = (\mathcal{N} - n)\Delta$ or $n \rightarrow \mathcal{N} - n$]. In this regard, we have that $\mathcal{PT}|\overline{u}_{n+1}\rangle = [\mathcal{PT}\overline{\Xi}_{n+1,n}(\mathcal{PT})^{-1}]\mathcal{PT}|\overline{u}_n\rangle \Leftrightarrow \mathcal{PT}|\overline{u}_{n+1}\rangle = [\mathcal{P}(\mathcal{T}\overline{\Xi}_{n+1,n}\mathcal{T}^{-1})\mathcal{P}^{-1}]\mathcal{PT}|\overline{u}_n\rangle \Leftrightarrow \mathcal{PT}|\overline{u}_{n+1}\rangle = [\mathcal{P}\,\overline{\Xi}^*_{2N-n-1,2N-n}\mathcal{P}^{-1}]\mathcal{PT}|\overline{u}_n\rangle$, which for

two-mode systems reads as ($\overline{\Xi}_{n+1,\,n} = I - i\Delta\overline{H}_n$ and $\overline{\Xi}_{n,\,n+1} = \overline{\Xi}^{-1}_{n+1,\,n} = I + i\Delta\overline{H}_n$ for small values of Δ)

$$\begin{bmatrix} \overline{b}^{*}_{2N-n-1} \\ \overline{a}^{*}_{2N-n-1} \end{bmatrix} = \begin{bmatrix} 1 - i\Delta\big(\overline{h}^{22}_{2N-n-1}\big)^{*} & -i\Delta\big(\overline{h}^{21}_{2N-n-1}\big)^{*} \\ -i\Delta\big(\overline{h}^{12}_{2N-n-1}\big)^{*} & 1 - i\Delta\big(\overline{h}^{11}_{2N-n-1}\big)^{*} \end{bmatrix} \begin{bmatrix} \overline{b}^{*}_{2N-n} \\ \overline{a}^{*}_{2N-n} \end{bmatrix}$$
$$\Leftrightarrow \begin{bmatrix} \overline{b}_{2N-n} \\ \overline{a}_{2N-n} \end{bmatrix} = \begin{bmatrix} 1 - i\Delta\overline{h}^{22}_{2N-n-1} & -i\Delta\overline{h}^{21}_{2N-n-1} \\ -i\Delta\overline{h}^{12}_{2N-n-1} & 1 - i\Delta\overline{h}^{11}_{2N-n-1} \end{bmatrix} \begin{bmatrix} \overline{b}_{2N-n-1} \\ \overline{a}_{2N-n-1} \end{bmatrix} \tag{B13}$$

after also employing Eqs. (B12) for the parity operator. The above expression is simply an illustration of relation $|\overline{u}_{2N-n}\rangle = \overline{\Xi}_{2N-n,\,2N-n-1}|\overline{u}_{2N-n-1}\rangle = (1 - i\Delta\overline{H}_{2N-n-1})|\overline{u}_{2N-n-1}\rangle$ (for a schematic depiction of the operation of $\overline{H}_n$ see also Fig. 10), with the components of the state vector and the (off-)diagonal elements of the evolution matrix being interchanged as expected owing to the action of $\mathcal{P}$. Parity-time symmetry implies now that $|\overline{u}_{n+1}\rangle = \overline{\Xi}_{n+1,\,n}|\overline{u}_n\rangle \Leftrightarrow \mathcal{PT}|\overline{u}_{n+1}\rangle = \overline{\Xi}_{n+1,\,n}\mathcal{PT}|\overline{u}_n\rangle$, or equivalently that $\mathcal{PT}\,\overline{\Xi}_{n+1,\,n}(\mathcal{PT})^{-1} = (\mathcal{PT})^{-1}\overline{\Xi}_{n+1,\,n}\mathcal{PT} = \mathcal{PT}\,\overline{\Xi}_{n+1,\,n}\mathcal{PT} = \overline{\Xi}_{n+1,\,n} \Leftrightarrow \mathcal{PT}\,\overline{\Xi}_{n+1,\,n} = \overline{\Xi}_{n+1,\,n}\mathcal{PT} \Leftrightarrow [\mathcal{PT},\,\overline{\Xi}_{n+1,\,n}] = 0$ (here, we have used identities $\mathcal{P}^2 = \mathcal{T}^2 = I$). Along these lines, it can be also obtained that $\overline{\Xi}_{n+1,\,n} = \mathcal{PT}\,\overline{\Xi}_{n+1,\,n}(\mathcal{PT})^{-1} = \mathcal{P}(\mathcal{T}\,\overline{\Xi}_{n+1,\,n}\mathcal{T}^{-1})\mathcal{P}^{-1} = \mathcal{P}\,\overline{\Xi}^{*}_{2N-n-1,\,2N-n}\mathcal{P}^{-1} = \mathcal{P}\,(I - i\Delta\overline{H}^{*}_{2N-n-1})\mathcal{P}^{-1} \Leftrightarrow \overline{H}_n = \mathcal{P}\overline{H}^{*}_{2N-n-1}\mathcal{P}^{-1}$, which for sufficiently small time steps leads to $\overline{H}_n = \mathcal{PT}\overline{H}_n(\mathcal{PT})^{-1} \Leftrightarrow [\mathcal{PT},\,\overline{H}_n] = 0$. [This clearly confirms Eq. (B5) after substituting $W_n \to \mathcal{PT}$ and keeping in mind that term $\delta W_n/\delta t_n$ is omitted, when referring to a specific discrete symmetry.] Based on the previous chain of relations, it will apply that $\overline{H}^{*}_n = \mathcal{P}\overline{H}_{2N-n-1}\mathcal{P}^{-1}$ ($\mathcal{P}^{*} = \mathcal{P}$), from where the $\mathcal{PT}$-symmetry conditions pertaining to the auxiliary ($\overline{H}_n$) and original Hamiltonian (H_n) representations can be directly attained: $(\overline{h}^{11}_n)^{*} = \overline{h}^{22}_{2N-n-1}$, $(\overline{h}^{12}_n)^{*} = \overline{h}^{21}_{2N-n-1}$ and $(h^{11}_n)^{*} = h^{22}_n$, $(h^{12}_n)^{*} = h^{21}_n$ [$\overline{H}_n = H_n$ for $n \leqslant N-1$ and $\overline{H}_n = H_{2N-n-1}$ for $n \geqslant N$, according to definition (ii) of the auxiliary field as provided previously in the present Appendix]. For arbitrary values of $\mathcal{N}$ in the definition of operator τ ($\tau : n \to \mathcal{N} - n$), the aforementioned conditions will read as $(\overline{h}^{11}_n)^{*} = \overline{h}^{22}_{\mathcal{N}-n-1}$, $(\overline{h}^{12}_n)^{*} = \overline{h}^{21}_{\mathcal{N}-n-1}$ and $(h^{11}_n)^{*} = h^{22}_n$, $(h^{12}_n)^{*} = h^{21}_n$. [Had we alternatively employed definition (i) for $\overline{H}_n$ (i.e., $\overline{H}_n = H_n$ for all values of n), then $\mathcal{PT}$-symmetry relations would remain unchanged for $\overline{H}_n$ and for H_n would of course read as $(h^{11}_n)^{*} = h^{22}_{\mathcal{N}-n-1}$, $(h^{12}_n)^{*} = h^{21}_{\mathcal{N}-n-1}$ and consequently depend on the choice of $\mathcal{N}$.] Along these lines, the traceless non-Hermitian model introduced in Sec. II B ($h^{11}_n = -h^{22}_n = if_n = ig_n + \sigma_n$ and $h^{12}_n = h^{21}_n = -\kappa$; g_n, σ_n, κ are real-valued parameters and represent the optical gain/loss, detuning, and coupling strength) can become $\mathcal{PT}$ symmetric as long as $(h^{11}_n)^{*} = h^{22}_n \Leftrightarrow \Re(h^{11}_n) = 0 \Leftrightarrow \sigma_n = 0$ [i.e., absence of any detuning between the optical modes—relation $(h^{12}_n)^{*} = h^{21}_n = -\kappa$ is clearly satisfied and thus imposes no further constraints], which in turn leads to the conventional form of 2×2 parity-time-symmetric Hamiltonian matrices used in non-Hermitian photonics [27,28]. It should be highlighted at this point that if a quantum arrangement respects the combined $\mathcal{PT}$ symmetry, this does by no means imply that the respective Hamiltonian will be $\mathcal{P}$ symmetric [in this case, if $|u_{n+1}\rangle = \Xi_{n+1,\,n}|u_n\rangle$ then it must also apply that $\mathcal{P}|u_{n+1}\rangle = \Xi_{n+1,\,n}\mathcal{P}|u_n\rangle$, i.e., $\mathcal{P}$ must commute with both $\Xi_{n+1,\,n}$, H_n - see also Eq. (B5) - and thus $H_n = \mathcal{P}H_n\mathcal{P}^{-1}$ or equivalently $h^{11}_n = h^{22}_n$, $h^{12}_n = h^{21}_n$ according to Eqs. (B12)] or $\mathcal{T}$ symmetric [$\overline{H}^{*}_n = \overline{H}_{\mathcal{N}-n-1}$ and $H^{*}_n = H_n$ according to definition (ii) of $\overline{H}_n$]. On the other hand, if the system is $\mathcal{PT}$ symmetric and either $\mathcal{P}$ symmetric or $\mathcal{T}$ symmetric, then it must be invariant under the individual action of both operators $\mathcal{P}$ and $\mathcal{T}$.

Having investigated the essence of both parity and time-reversal discrete symmetries, along with their implications in quantum settings and experimentally viable photonic platforms, we can now examine as to whether operator $\mathcal{T}$ can attain a more generalized form according to its definition $\mathcal{T} = UK\tau$ with $U \neq I$ representing a unitary transformation. To simplify our analysis, we shall bring our attention to time-independent Hamiltonians H ($H_n = H$, with H being constant as n varies) and as such operator τ—causing the reflection of the time coordinates here as $n \to 2N - n$ (or more generally as $n \to \mathcal{N} - n$)—can be omitted in the representation of $\mathcal{T}$. Given now the properties of the time-reversal operator, matrix U should satisfy both conditions $UU^{*} = U^{*}U = I$ ($\mathcal{T}^2 = UKUK = UU^{*} = I$ since $KUK^{-1} = U^{*}$ and $K^{-1} = K$, as has been previously shown) and $[\mathcal{P},\,U] = 0$ ($[\mathcal{P},\,\mathcal{T}] = 0 \Leftrightarrow \mathcal{P}UK = UK\mathcal{P} \Leftrightarrow \mathcal{P}U = UK\mathcal{P}K = U\mathcal{P}^{*} = U\mathcal{P} \Leftrightarrow [\mathcal{P},\,U] = 0$ after exploiting both facts that $K^2 = I$ and $\mathcal{P}$ is a real matrix). After setting some straightforward algebra, it can be shown that U can be expressed as follows with a freedom of a phase factor ($\mathcal{P} = \sigma_1$),

$$U = \begin{bmatrix} i(-1)^{\nu}\cos\theta' & \sin\theta' \\ \sin\theta' & i(-1)^{\nu}\cos\theta' \end{bmatrix}, \tag{B14}$$

with ν being an integer and $\theta' \in (-\pi,\,\pi]$. We can select ν to be even and thus the diagonal elements of U will be equal to $i\cos\theta$ (matrices U corresponding to ν being even and ν being odd are complex conjugates of each other; hence it is sufficient to study only one of the two cases). Moreover, we assume that $\sin\theta' \neq 0$ (i.e., $\theta' \neq \pm\pi/2$ so as U remains different from the identity transformation or from multiples of it by a phase factor) and $\cos\theta' \neq 0$ (i.e., $\theta' \neq 0,\,\pi$ so as $U \neq \mathcal{P} = \sigma_1$; if $U = \sigma_1$ then $\mathcal{PT} = \sigma_1^2 K = K$, i.e., the $\mathcal{PT}$ operator entails only the action of complex conjugation and thus this scenario should be rejected). In order to obtain a better insight on the physical meaning of the unitary operator U as depicted in Eq. (B14), we can retrieve the form that the

Hamiltonian H should have in order to be symmetric under the action of U. This of course entails that U and H should commute ($[U,\ H]=0$), which in turn leads to the following two independent equations ($H=[h^{jk}],\ j,\ k=1,\ 2$):

$$\sin\theta'(h^{22}-h^{11})-i\cos\theta'(h^{21}-h^{12})=0, \tag{B15a}$$

$$\sin\theta'(h^{21}-h^{12})-i\cos\theta'(h^{22}-h^{11})=0. \tag{B15b}$$

The aforementioned formulas demand that $h^{11}=h^{22}$ and $h^{12}=h^{21}$, because otherwise we would have attained that $i\cos\theta'/\sin\theta'=-i\sin\theta'/\cos\theta' \Leftrightarrow \cos^2\theta'+\sin^2\theta'=0$, which cannot hold. Of interest is to note that exactly the same conditions are imposed on the Hamiltonian matrix elements, when the associated quantum arrangement is $\mathcal{P}$ symmetric or even $\mathcal{P}U$ symmetric. It is expected therefore for operators $\mathcal{P}$, U, and $\mathcal{P}U$, to have an analogous underlying physical significance (but clearly not the same, since U, $\mathcal{P}U$ are complex while $\mathcal{P}$ is real). Capitalizing now on such observation, we can further speculate that operators $\mathcal{T}=UK$ and $\mathcal{PT}=\mathcal{P}UK$ will have a similar effect when acted upon the Hamiltonian. Indeed, matrix $\mathcal{P}U$ acquires the following form [we set ν to be even in Eq. (B14)]

$$\mathcal{P}U=\begin{bmatrix}\sin\theta' & i\cos\theta'\\ i\cos\theta' & \sin\theta'\end{bmatrix}, \tag{B16}$$

which can be attained from Eq. (B14) after setting $\theta'\to\pi/2+\theta'$ and multiplying by the phase factor $e^{i\pi/2}$. In other words, the parity-time operator belongs in the general family of time-reversal operators, as defined in Eq. (B14). This in turn should be rejected, since the action of the $\mathcal{PT}$ operator should be distinctly different (from a mathematical and a physical standpoint) as compared to the action of $\mathcal{T}$ (conditions for $\mathcal{PT}$ symmetry should also differ from conditions for $\mathcal{T}$ symmetry, unless the system is both $\mathcal{P}$ and $\mathcal{T}$ symmetric). Consequently, we have to retract our original hypothesis that $U\neq I$ and instead set $U=I$, which identifies $\mathcal{T}$ with the complex conjugation operation used in the current analysis (of course in the time-dependent case, the action of τ must also be included in the definition of $\mathcal{T}$). It should also be noted that $\mathcal{T}=K$ is the minimal (i.e., simplest possible) representation of the time-reversal operator that satisfies both constraints $\mathcal{T}^2=I,[\mathcal{P},\ \mathcal{T}]=0$, and as such it is much more preferable that any more complex definitions of $\mathcal{T}$.

In summary, in the present Appendix we have thoroughly analyzed the notions of transformations (both continuous and discrete) and associated symmetries pertaining to generalized and two-level Hamiltonian arrangements, under the prism of standard quantum mechanical theory. In the SM [76], an alternative view of such concepts is presented in terms of Jones calculus [103,104,114], where the state vector $|u_n\rangle$ represents the polarization state of light (Jones vector) and the evolution operator Ξ_n will correspond to the transfer (or Jones) matrix describing a single or an array of linear optical elements [we will apply this to the specific case of a discrete fiber loop network, where we will show how it is possible to experimentally attain a generalized two-level Hamiltonian system as shown in Eq. (1) of Sec. II A]. In this vein, mathematical conditions for parity/time/parity-time reversal symmetry, reciprocity, and energy conservation will be found to be the same either if we view the underlying dynamics from a quantum mechanics (operator theory, Appendix B 1) or from a classical optics/electromagnetics (Jones algebra, Sec. IV within SM [76]) perspective, since in both cases the associated state vector will be described by the same discrete dynamical equation, see Eqs. (1), (A3), and (A2) of Sec. II A and Appendix A].

2. Clockwise and counterclockwise parametric evolution: A special symmetry for trajectories symmetric with respect to the g_n axis

Here, we are interested in the case of traceless and symmetric non-Hermitian Hamiltonians discussed in Sec. II B and characterized by the real-valued parameters g_n, σ_n, κ, which denote the gain/loss, detuning, and coupling strength factors, respectively. In this regard, we can consider two distinct closed trajectories $\mathcal{C}^{\mathcal{R}}$ and $\overline{\mathcal{C}^{\mathcal{R}}}$ in parameter space $\mathcal{R}=(g_n,\ \sigma_n)$, which are mirror symmetric with respect to the horizontal or g_n axis, as illustrated in Fig. 11(a). Both curves consist of the same number of discrete points (N) and are encircled with the same rate $1/T=1/(N\Delta)$. Then it will be true that $\overline{g}_n^{\circlearrowleft}=g_n^{\circlearrowright}$ and $\overline{\sigma}_n^{\circlearrowleft}=-\sigma_n^{\circlearrowright}$ or in other words $\overline{f}_n^{\circlearrowleft}=(f_n^{\circlearrowright})^*$, where symbols $\circlearrowleft$ and $\circlearrowright$ denote CCW and CW encirclements, accordingly ($f_n=g_n-i\sigma_n$, $\overline{f}_n=\overline{g}_n-i\overline{\sigma}_n$, in our analysis here, unbarred and barred quantities will correspond to paths $\mathcal{C}^{\mathcal{R}}$ and $\overline{\mathcal{C}^{\mathcal{R}}}$, respectively). The following chain of relations will now apply:

$$\begin{bmatrix}a_{n+1}\\ b_{n+1}\end{bmatrix}=\begin{bmatrix}1+\Delta f_n^{\circlearrowleft} & i\Delta\kappa\\ i\Delta\kappa & 1-\Delta f_n^{\circlearrowleft}\end{bmatrix}\begin{bmatrix}a_n\\ b_n\end{bmatrix}\Leftrightarrow$$

$$\begin{bmatrix}a_{n+1}^*\\ b_{n+1}^*\end{bmatrix}=\begin{bmatrix}1+\Delta\left(f_n^{\circlearrowleft}\right)^* & -i\Delta\kappa\\ -i\Delta\kappa & 1-\Delta\left(f_n^{\circlearrowleft}\right)^*\end{bmatrix}\begin{bmatrix}a_n^*\\ b_n^*\end{bmatrix}\Leftrightarrow$$

$$\begin{bmatrix}a_{n+1}^*\\ -b_{n+1}^*\end{bmatrix}=\begin{bmatrix}1+\Delta\overline{f}_n^{\circlearrowleft} & i\Delta\kappa\\ i\Delta\kappa & 1-\Delta\overline{f}_n^{\circlearrowleft}\end{bmatrix}\begin{bmatrix}a_n^*\\ -b_n^*\end{bmatrix}, \tag{B17}$$

where the first and last lines correspond to the CW and CCW state vector dynamics along loops $\mathcal{C}^{\mathcal{R}}$ and $\overline{\mathcal{C}^{\mathcal{R}}}$, respectively, according to Eq. (7) of Sec. II B. It becomes clear here that if after a full cycle, the Hamiltonian system adiabatically converts to state vector$[a_N\ b_N]^{\mathcal{T}}$ in the former case, then in the latter case conversion to state vector $[a_N^*\ -b_N^*]^{\mathcal{T}}$ will be observed after a complete encirclement. This directly implies for the respective state vector component ratios that $\overline{r}_N^{\circlearrowleft}=-b_N^*/a_N^*=-(r_N^{\circlearrowright})^*$. The aforementioned relationships of course apply assuming that the starting points of evolution for curves $\mathcal{C}^{\mathcal{R}}$, $\overline{\mathcal{C}^{\mathcal{R}}}$ are symmetric with respect to the g_n axis. On the other hand, the starting conditions for the state vector (i.e., values of a_0, b_0) will not alter our conclusions here, since they do not affect the adiabatic behavior of the examined quantum arrangements (see Secs. II C and III C). If parametric trajectory $\mathcal{C}^{\mathcal{R}}$ is itself mirror symmetric to the horizontal axis (i.e., $\mathcal{C}^{\mathcal{R}}\equiv\overline{\mathcal{C}^{\mathcal{R}}}$), then an analogous symmetry relation to Eq. (B17) will apply for CW and CCW encirclements [see Fig. 11(b)]. If we additionally assume that the starting/ending point of evolution lies on the g_n axis ($\sigma_N=\sigma_0=0$) and that slowly varying conditions apply so as the quantum state is fully described by a single instantaneous eigenvector after a

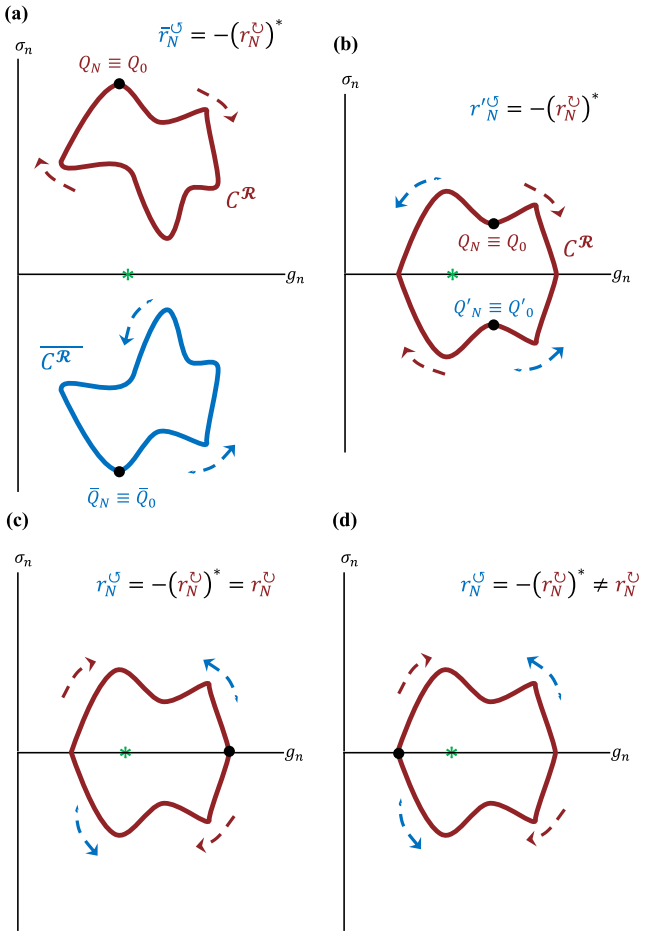

FIG. 11. Adiabatic parametric evolution ($N \to \infty$) along mirror symmetric and closed curves (with respect to the g_n axis) $\mathcal{C}^{\mathcal{R}}$ and $\overline{\mathcal{C}^{\mathcal{R}}}$ associated with the symmetric and traceless non-Hermitian model of Sec. II B, when $\mathcal{C}^{\mathcal{R}} \neq \overline{\mathcal{C}^{\mathcal{R}}}$ (a) and when $\mathcal{C}^{\mathcal{R}} \equiv \overline{\mathcal{C}^{\mathcal{R}}}$ [(b)–(d)]. Starting/ending points of evolution are designated with a filled black circle, while the green asterisk denotes the location of the exceptional point $(g_n, \sigma_n) = (\kappa, 0)$. Factors r_N, r'_N, $\bar{r}_N$ represent the ratio of the state vector components after a full cycle along paths $\mathcal{C}^{\mathcal{R}}$ (starting point $Q_N \equiv Q_0$), $\mathcal{C}^{\mathcal{R}}$ (starting point $Q'_N \equiv Q'_0$), and $\overline{\mathcal{C}^{\mathcal{R}}}$ (starting point $\bar{Q}_N \equiv \bar{Q}_0$) either for CW ($\circlearrowright$) or CCW ($\circlearrowleft$) evolutions [the direction of encirclement is each time annotated with dark red (CW) and blue (CCW) dashed lines]. The symmetry relations $\bar{r}_N^{\circlearrowleft} = -(r_N^{\circlearrowright})^*$ [(a)] and $r'^{\circlearrowleft}_N = -(r_N^{\circlearrowright})^*$ (b) based on Eq. (B17) are depicted, which also lead to symmetric [(c) $r_N^{\circlearrowleft} = r_N^{\circlearrowright}$] or asymmetric [(d) $r_N^{\circlearrowleft} \neq r_N^{\circlearrowright}$] state conversion when the starting/ending point lies on the g_n axis to the right or to the left of the exceptional point, correspondingly. In all cases, curves are discretely defined but they appear as continuous for better representation purposes since $N \to \infty$.

full cycle (see Secs. II C and III C), then such a quantum state conversion is symmetric iff $r_N^{\circlearrowleft}$ becomes purely imaginary [$r_N^{\circlearrowleft} = r_N^{\circlearrowright} \Leftrightarrow (r_N^{\circlearrowright})^* + r_N^{\circlearrowright} = 0$, see Fig. 11(c)] and asymmetric in any other case [$r_N^{\circlearrowleft} \neq r_N^{\circlearrowright}$, see Fig. 11(d)].

Since the adiabatic dynamics of the non-Hermitian configurations under study are essentially dictated by their instantaneous eigenstates assuming cyclic parametric conditions (for analytic proofs, see Secs. II C and III C along with Sec. V within SM [76] and Appendix H), of essence is to retrieve the respective eigenvalues and eigenvectors in order to determine also the expected form of r_N as $N \to \infty$. This will allow us to deduce certain useful conclusions based also on the relations that r_N satisfies for the case of the traceless and symmetric non-Hermitian Hamiltonian model of Sec. II B. In this regard, we start with the generalized two-mode non-Hermitian model given in Eq. (1) of Sec. II A. We will emphasize on the eigenvalues of matrix M_n, whose form is given as

$$M_n = \begin{bmatrix} m_n^{11} & m_n^{12} \\ m_n^{21} & m_n^{22} \end{bmatrix}, \tag{B18}$$

and consequently the corresponding characteristic eigenvalue equation will read as

$$\lambda_n^2 - \left(m_n^{11} + m_n^{22}\right) + m_n^{11} m_n^{22} - m_n^{12} m_n^{21} = 0. \tag{B19}$$

The solutions will be given as

$$\lambda_n^{\pm} = \frac{m_n^{11} + m_n^{22} \pm \sqrt{\mathcal{D}_n}}{2}, \tag{B20}$$

with quantity $\mathcal{D}_n$ taking the form

$$\begin{aligned} \mathcal{D}_n &= \left(m_n^{11} + m_n^{22}\right)^2 - 4\left(m_n^{11} m_n^{22} - m_n^{12} m_n^{21}\right) \\ &= \left(m_n^{22} - m_n^{11}\right)^2 + 4 m_n^{12} m_n^{21} \\ &= 4 m_n^{12} m_n^{21} \left[1 - \left(-i \frac{m_n^{22} - m_n^{11}}{2\sqrt{m_n^{12} m_n^{21}}}\right)^2\right] \\ &= 4 m_n^{12} m_n^{21} \cos^2\theta_n, \end{aligned} \tag{B21}$$

and complex angle θ_n being defined by equations $\sin\theta_n = -i(m_n^{22} - m_n^{11})/(2\sqrt{m_n^{12} m_n^{21}})$ and $\cos\theta_n = \sqrt{1 - \sin^2\theta_n}$ [in order to attain a single solution, we assume that $-\pi < \Re(\theta_n) \leqslant \pi$]. For the calculation of the square roots, the principal roots are assumed as defined in Sec. II within SM [76]. Of course the eigenvalues of the propagator/evolution matrix Ξ_n and Hamiltonian H_n can be found from relations $\lambda_{\Xi_n}^{\pm} = 1 - i\Delta\lambda_{H_n}^{\pm} = 1 + \Delta\lambda_n^{\pm}$ given that $\Xi_n = I - i\Delta H_n = I + \Delta M_n$ (see Sec. II A). Based now on equation $(\lambda_n^{\pm} I - M_n)|v_n^{\pm}\rangle = [0\ 0]^{\mathcal{T}}$, the (right) eigenvectors $|v_n^{\pm}\rangle = [v_{n,x}^{\pm}\ v_{n,y}^{\pm}]^{\mathcal{T}}$ will satisfy the following formula:

$$\begin{aligned} \frac{v_{n,y}^{\pm}}{v_{n,x}^{\pm}} &= \frac{m_n^{22} - m_n^{11} \pm \sqrt{\mathcal{D}_n}}{2 m_n^{12}} = \sqrt{\frac{m_n^{21}}{m_n^{12}}}(\pm\cos\theta_n + i\sin\theta_n) \\ &= \pm\sqrt{\frac{m_n^{21}}{m_n^{12}}} e^{\pm i\theta_n}. \end{aligned} \tag{B22}$$

It should be noted that an eigenvalue degeneracy will take place if $\mathcal{D}_n = 0$ or equivalently if $\cos\theta_n = 0$ according to Eq. (B21). Assuming that this situation occurs for some $n = n_{EP}$, then it must be true that either $\theta_{n_{EP}} = \pi/2$ [i.e., $-i(m_{n_{EP}}^{22} - m_{n_{EP}}^{11})/(2\sqrt{m_{n_{EP}}^{12} m_{n_{EP}}^{21}}) = 1$] or $\theta_{n_{EP}} = -\pi/2$ [i.e., $-i(m_{n_{EP}}^{22} - m_{n_{EP}}^{11})/(2\sqrt{m_{n_{EP}}^{12} m_{n_{EP}}^{21}}) = -1$]. Moreover, according to Eqs. (B20) and (B22) it must apply that $\lambda_{n_{EP}}^{\pm} = (m_{n_{EP}}^{11} + m_{n_{EP}}^{22})/2$ and $v_{n_{EP},y}^{\pm}/v_{n_{EP},x}^{\pm} = (m_{n_{EP}}^{22} - m_{n_{EP}}^{11})/(2m_{n_{EP}}^{12})$.

In the special case of the traceless non-Hermitian configuration introduced in Sec. II B ($m_n^{11} = -m_n^{22} = f_n = g_n - i\sigma_n$, $m_n^{12} = m_n^{21} = i\kappa$, with g_n, σ_n, κ being all real valued

as initially mentioned in the present Appendix), it becomes evident that $\lambda_n^{\pm} = \pm i\kappa\cos\theta_n = \pm i\sqrt{\kappa^2 - f_n^2}$ and and $v_{n,y}^{\pm}/v_{n,x}^{\pm} = \pm e^{\pm i\theta_n} = \pm\sqrt{1 - f_n^2/\kappa^2} + if_n/\kappa$ (eigenspectrum degeneracies take place at $f_n = \pm\kappa$, but they will not be considered here since we have assumed in our main text analysis that no such singularity points are crossed during the evolution of the non-Hermitian Hamiltonian; see also corresponding comments in the beginning of Sec. III C). Returning now to the adiabatic behavior of ratio r_N for evolution along cyclic trajectories $\mathcal{C}^{\mathcal{R}}$, $\overline{\mathcal{C}^{\mathcal{R}}}$, we need to discern the following three cases (for simplicity we assume that the gain parameter belongs in the interval $[0\ +\infty)$):

(1) *Detuning parameter σ_N obtains a nonzero value after a complete cycle in parameter space ($\sigma_N = \sigma_0 \neq 0$).* This scenario corresponds to Fig. 11(a) if $\mathcal{C}^{\mathcal{R}} \neq \overline{\mathcal{C}^{\mathcal{R}}}$, and to Fig. 11(b) if $\mathcal{C}^{\mathcal{R}} \equiv \overline{\mathcal{C}^{\mathcal{R}}}$. Without loss of generality, we shall analyze the former case. Then, it will be true that

$$-\left(\frac{v_{N,y}^{\pm}}{v_{N,x}^{\pm}}\right)^* = \left(\mp\sqrt{1 - \frac{f_N^2}{\kappa^2}}\right)^* - i\frac{f_N^*}{\kappa} = \mp\sqrt{1 - \frac{(f_N^*)^2}{\kappa^2}} - i\frac{f_N^*}{\kappa} = \frac{\overline{v}_{N,y}^{\mp}}{\overline{v}_{N,x}^{\mp}}, \tag{B23}$$

where quantities with and without a bar refer to mirror-symmetric paths (with respect to the horizontal g_n axis) $\mathcal{C}^{\mathcal{R}}$, $\overline{\mathcal{C}^{\mathcal{R}}}$, respectively, and we also used the identity $\sqrt{z}^* = \sqrt{z^*}$, which applies for all complex numbers z except from the negative real numbers (e.g., $(\sqrt{-1})^* = -i \neq \sqrt{(-1)^*} = \sqrt{-1} = i$, this stems from the definition of the principal roots as explained in Sec. II within SM [76]). A clear consistency now exists between Eqs. (B17) and (B23), since relation $\overline{r}_N^{\circlearrowleft} = -(r_N^{\circlearrowleft})^*$ [or equivalently $\overline{r}_N^{\circlearrowleft} = -(r_N^{\circlearrowleft})^*$] is directly reflected in the ratio of the instantaneous eigenvector components at the end of the cyclic evolution along $\mathcal{C}^{\mathcal{R}}$ and $\overline{\mathcal{C}^{\mathcal{R}}}$. In this vein, it is expected that if the quantum state vector converts to eigenvector $|v_N^{\pm}\rangle$ after slowly cycling path $\mathcal{C}^{\mathcal{R}}$, then for an opposite direction of encirclement along $\overline{\mathcal{C}^{\mathcal{R}}}$ it will asymptotically convert to $|\overline{v}_N^{\mp}\rangle$. Moreover, for both cases the resulting eigenstates will correspond to eigenvalues λ_N with real parts being both positive or negative and this can be seen from the fact that $\Re(\lambda_N^{\pm})\Re(\overline{\lambda}_N^{\mp}) = \sqrt{\kappa^2 - f_N^2}(\sqrt{\kappa^2 - f_N^2})^* = \sqrt{\kappa^2 - f_N^2}\sqrt{\kappa^2 - (f_N^*)^2} = |\sqrt{\kappa^2 - f_N^2}|^2$ (|.| denotes the magnitude/absolute value of the associated complex argument). As illustrated in analogous case scenarios depicted in Fig. 2 (second and fourth rows), Fig. 6 (second and fourth columns), Fig. 7 (second and fourth columns), and Fig. 9 (last two rows) of the main text, state conversion takes place to the instantaneous dominant eigenmode, which in turn is related to the eigenvalue λ_N with the positive real part. This will be true irrespective of the starting point (g_0, σ_0) along trajectories $\mathcal{C}^{\mathcal{R}}$, $\overline{\mathcal{C}^{\mathcal{R}}}$.

(2) *Detuning and gain parameters satisfy conditions $\sigma_N = \sigma_0 = 0$ and $g_N = g_0 > \kappa$.* Such a scenario is reflected in Fig. 11(c) ($\mathcal{C}^{\mathcal{R}} \equiv \overline{\mathcal{C}^{\mathcal{R}}}$) with the starting/ending point of parametric evolution lying on the right of the spectrum degeneracy located at $(g_n, \sigma_n) = (\kappa, 0)$. Now it will be true that $f_N = g_N > \kappa$ and consequently $\lambda_N^{\pm} = \mp\sqrt{f_N^2 - \kappa^2}$ will be real. Furthermore, the following will apply

$$-\left(\frac{v_{N,y}^{\pm}}{v_{N,x}^{\pm}}\right)^* = -\left(\pm i\sqrt{\frac{f_N^2}{\kappa^2} - 1} + i\frac{f_N}{\kappa}\right)^* = \pm i\sqrt{\frac{f_N^2}{\kappa^2} - 1} + i\frac{f_N}{\kappa} = \frac{v_{N,y}^{\pm}}{v_{N,x}^{\pm}}. \tag{B24}$$

This confirms again Eq. (B17) and now it is expected to attain conversion to the same eigenstate $|v_N^+\rangle$ ($\lambda_N^+ < 0$) or $|v_N^-\rangle$ ($\lambda_N^- > 0$) for both directions of encirclement. Such a symmetric mode switching behavior is also revealed in Figs. 9(e)–9(h) within the main text. In all respective simulation scenarios, the adiabatic dynamics of the traceless non-Hermitian configuration is well described by eigenvector $|v_N^-\rangle$ assuming cyclic conditions.

(3) *Detuning and gain parameters satisfy conditions $\sigma_N = \sigma_0 = 0$ and $g_N = g_0 < \kappa$.* This scenario is depicted in Fig. 11(d) ($\mathcal{C}^{\mathcal{R}} \equiv \overline{\mathcal{C}^{\mathcal{R}}}$) with the starting/ending point of parametric evolution lying on the left of the exceptional point degeneracy $g_n = \kappa$. Here, eigenvalues $\lambda_N^{\pm} = \pm i\sqrt{\kappa^2 - f_N^2}$ will be imaginary since $f_N = g_N < \kappa$. Consequently, it will be true that

$$-\left(\frac{v_{N,y}^{\pm}}{v_{N,x}^{\pm}}\right)^* = -\left(\pm\sqrt{1 - \frac{f_N^2}{\kappa^2}} + i\frac{f_N^*}{\kappa}\right)^* = \mp\sqrt{1 - \frac{f_N^2}{\kappa^2}} + i\frac{f_N}{\kappa} = \frac{v_{N,y}^{\mp}}{v_{N,x}^{\mp}}, \tag{B25}$$

which is consistent with Eq. (B17) and indicates an asymmetric mode switching behavior (i.e., if the quantum Hamiltonian structure converts to eigenmode $|v_n^{\pm}\rangle$ for CW evolution, then it will convert to mode $|\overline{v}_n^{\mp}\rangle$ for CCW evolution). This is clearly verified by the respective numerical results of Figs. 2 (first and third rows), 6 (first and third columns), 7 (first and third columns), and 9 (first row).

All of the examined scenarios reveal for the special case of the non-Hermitian model analyzed in Sec. II B, that the behavior of the respective eigenvalues and eigenvectors is consistent with the symmetry relation $\overline{r}_N^{\circlearrowleft} = -(r_N^{\circlearrowleft})^*$ as described by Eq. (B17) [any alternative possibilities can be essentially ascribed to one of the cases (i)–(iii), since what is of essence in the adiabatic limit is the location of the starting/ending point along the cyclic parametric curve]. This is of course assuming that slowly varying states within non-Hermitian arrangements asymptotically convert to the instantaneous eigenmodes at the end of a full cycle in parameter space; this is separately proven in Sec. V within SM [76] (by studying the asymptotic behavior of a particular class of analytical solutions describing the dynamics of the traceless and symmetric non-Hermitian model of Sec. II B) and Sec. III C (for generalized Hamiltonian models and parametric trajectories - see also Appendix H). It should be highlighted that Eq. (B17) applies also in the nonadiabatic limit and consequently it allows us to draw useful conclusions as to the evolution dynamics underpinning Eqs. (7) and (10) of Sec. II B.

APPENDIX C: DEFINITION OF THE $\mathcal{G}$ TRANSFORM AND ITS ASSOCIATED PROPERTIES

In this paper, a generalized version of the Möbius transformation, where the associated coefficients are assumed to be time dependent, has been introduced [see Eq. (6)] and subsequently employed to study the evolution of the ratio r_n of the state vector components (see Sec. II C). The term $\mathcal{G}$ *transform* has been coined for that purpose and the respective defining formula given by

$$\mathcal{G}_{Q_n}(z) = \frac{q_n^{21} + q_n^{22} z}{q_n^{11} + q_n^{12} z}, \tag{C1}$$

where q_n^{jk} $(j,\, k = 1,\, 2)$ are the elements of the time-dependent matrix Q_n (q_n^{jk} and z belong in the complex domain, while index n signifies the dependence on time). Based on the above definition, it is easy to see when applying the operation of function composition that

$$\begin{aligned}\left(\mathcal{G}_{W_n} \circ \mathcal{G}_{Q_n}\right)(z) &= \mathcal{G}_{W_n}\left(\mathcal{G}_{Q_n}(z)\right) \\ &= \frac{w_n^{21} q_n^{11} + w_n^{22} q_n^{21} + \left(w_n^{21} q_n^{12} + w_n^{22} q_n^{22}\right) z}{w_n^{11} q_n^{11} + w_n^{12} q_n^{21} + \left(w_n^{11} q_n^{12} + w_n^{12} q_n^{22}\right) z},\end{aligned} \tag{C2}$$

which directly implies that $\mathcal{G}_{W_n} \circ \mathcal{G}_{Q_n} = \mathcal{G}_{W_n Q_n}$. This property can be straightforwardly extended to $\bigcirc_{j=1,\,2,\,3,\ldots} \mathcal{G}_{Q_n^{(l)}} = \cdots \circ \mathcal{G}_{Q_n^{(3)}} \circ \mathcal{G}_{Q_n^{(2)}} \circ \mathcal{G}_{Q_n^{(1)}} = \mathcal{G}_{\cdots Q_n^{(3)} Q_n^{(2)} Q_n^{(1)}} = \mathcal{G}_{\prod_{j=1,\,2,\,3,\ldots} Q_n^{(j)}}$ [matrices $Q_n^{(j)}$ are arbitrary time-dependent matrices where j is a positive integer, while we also assume ordered matrix multiplications and function compositions as described in Eqs. (E3) and (E7) of the main text], while if we set $W_n = Q_n^{-1}$ (assuming that matrix Q_n is invertible) then it comes that $\mathcal{G}_{Q_n^{-1} Q_n} = \mathcal{G}_{Q_n Q_n^{-1}} = \mathcal{G}_I \Leftrightarrow \mathcal{G}_{Q_n} \circ \mathcal{G}_{Q_n^{-1}} = \mathcal{G}_I \Leftrightarrow \mathcal{G}_{Q_n}^{-1} = \mathcal{G}_{Q_n^{-1}}$ [$Q_n^{-1} Q_n = Q_n Q_n^{-1} = I$, where I is the 2×2 identity matrix, $\mathcal{G}_I$ is simply the identity function/map $\mathcal{G}_I(z) = z$, and $\mathcal{G}_{Q_n}^{-1}$ represents the inversion function to $\mathcal{G}_{Q_n}$]. It should be emphasized, of course, that generally $\mathcal{G}_{W_n} \circ \mathcal{G}_{Q_n} = \mathcal{G}_{W_n Q_n} \neq \mathcal{G}_{Q_n} \circ \mathcal{G}_{W_n} = \mathcal{G}_{Q_n W_n}$ and this can be also seen from the noncommutativity of matrix multiplication.

A special family of points exists for the $\mathcal{G}$ transform, which satisfy equation $\mathcal{G}_{Q_n}(z) = z$ and thus can be retrieved as

$$z_{Q_n}^{1,2} = \frac{q_n^{22} - q_n^{11} \pm \sqrt{\left(q_n^{22} - q_n^{11}\right)^2 + 4 q_n^{21} q_n^{12}}}{2 q_n^{12}}. \tag{C3}$$

As opposed to the standard Möbius transformation, such points are no longer fixed/constant but instead become time dependent. Along these lines, the following relation can be attained

$$\frac{\mathcal{G}_{Q_n}(z) - z_{Q_n}^2}{\mathcal{G}_{Q_n}(z) - z_{Q_n}^1} = \frac{\lambda_{Q_n}^1}{\lambda_{Q_n}^2} \frac{z - z_{Q_n}^2}{z - z_{Q_n}^1}, \tag{C4}$$

where $\lambda_{Q_n}^{1,2} = q_n^{12} z_{Q_n}^{1,2} + q_n^{11} = [q_n^{22} + q_n^{11} \pm \sqrt{(q_n^{22} - q_n^{11})^2 + 4 q_n^{21} q_n^{12}}]/2$ are the instantaneous eigenvalues of matrix Q_n. In general, $\lambda_{Q_n}^1 / \lambda_{Q_n}^2$ is a complex number with magnitude different to unity and as such the transformation described by Eq. (C1) can be characterized as loxodromic. (If $\lambda_{Q_n}^1 / \lambda_{Q_n}^2$ has magnitude equal to one then the transformation is classified as elliptic/circular, while if the respective phase is zero or an integer multiple of 2π then it belongs in the class of hyperbolic/parabolic transforms.) We can now perform the substitutions $Q_n \to \Xi_n$, $z \to r_n$, $z_{Q_n}^{1,2} \to r_{\tilde{\Xi}_n}^{\tilde{\pm}}$, $\lambda_{Q_n}^{1,2} \to \lambda_{\tilde{\Xi}_n}^{\tilde{\pm}}$ in Eq. (C4) [see also analysis in Secs. II C and III B, where notation $(\tilde{\pm})$ was used to signify a smooth evolution of the involved quantities] and subsequently attain after an iterative application of $\mathcal{G}_{\Xi_n}$ $[r_{n+1} = \mathcal{G}_{\Xi_n}(r_n),\, n \in \mathbb{N} \wedge 0 \leqslant n \leqslant N]$ in the limit of small discrete time steps Δ ($r_{\tilde{\Xi}_{n+1}}^{\tilde{\pm}} \simeq r_{\tilde{\Xi}_n}^{\tilde{\pm}}$ and $\lambda_{\tilde{\Xi}_n}^{\tilde{\pm}} = 1 + \Delta \lambda_n^{\tilde{\pm}} \simeq e^{\Delta \lambda_n^{\tilde{\pm}}}$, where $\lambda_n^{\tilde{\pm}}$ are the instantaneous eigenvalues of matrix M_n as defined in Sec. II A) that

$$\begin{aligned}&\prod_{n=0}^{N-1} \frac{r_{n+1} - r_{\tilde{\Xi}_n}^{\tilde{-}}}{r_{n+1} - r_{\tilde{\Xi}_n}^{\tilde{+}}} = \prod_{n=0}^{N-1} \frac{\lambda_{\tilde{\Xi}_n}^{\tilde{+}}}{\lambda_{\tilde{\Xi}_n}^{\tilde{-}}} \frac{r_n - r_{\tilde{\Xi}_n}^{\tilde{-}}}{r_n - r_{\tilde{\Xi}_n}^{\tilde{+}}} \Rightarrow \\ &\frac{r_N - r_{\tilde{\Xi}_N}^{\tilde{-}}}{r_N - r_{\tilde{\Xi}_N}^{\tilde{+}}} \simeq \prod_{n=0}^{N-1} \frac{\lambda_{\tilde{\Xi}_n}^{\tilde{+}}}{\lambda_{\tilde{\Xi}_n}^{\tilde{-}}} \frac{r_0 - r_{\tilde{\Xi}_0}^{\tilde{-}}}{r_0 - r_{\tilde{\Xi}_0}^{\tilde{+}}} \Rightarrow \\ &\left|\frac{r_N - r_{\tilde{\Xi}_N}^{\tilde{-}}}{r_N - r_{\tilde{\Xi}_N}^{\tilde{+}}}\right| \simeq \prod_{n=0}^{N-1} e^{\Delta \mathrm{Re}(\tilde{\lambda_n^+} - \tilde{\lambda_n^-})} \left|\frac{r_0 - r_{\tilde{\Xi}_0}^{\tilde{-}}}{r_0 - r_{\tilde{\Xi}_0}^{\tilde{+}}}\right|,\end{aligned} \tag{C5}$$

where $r_0 = b_0/a_0$ is the initial value of the ratio of the state vector components and $|.|$ stands for the complex absolute value function. If we assume now that relation $\mathrm{Re}(\tilde{\lambda_n^+}) > \mathrm{Re}(\tilde{\lambda_n^-})$ becomes predominantly true [except maybe at a limited number of points where $\mathrm{Re}(\tilde{\lambda_n^+}) = \mathrm{Re}(\tilde{\lambda_n^-})$], then Eq. (C5) suggests that $r_N \to r_{\tilde{\Xi}_N}^{\tilde{+}}$ as $N \to \infty$ [if $r_0 = r_{\tilde{\Xi}_0}^{\tilde{-}}$ this behavior still persists but we need to resort to the more detailed analysis of Secs. III B and III C 1] or equivalently that $r_{\tilde{\Xi}_N}^{\tilde{+}}$ is an attractive point and $r_{\tilde{\Xi}_N}^{\tilde{-}}$ is a repulsive point (this property also justifies the characterization of the transformation as loxodromic). This confirms our theoretical (Sec. III B) and numerical (Fig. 6) conclusions in the main text, where we saw that if mode $(\tilde{+})$ remains dominant for any time instant, then it will also dictate the resulting dynamics under adiabatic/slowly varying conditions ($N \to \infty$). On the other hand, in Hermitian systems it must be true that $\mathrm{Re}(\tilde{\lambda_n^+}) = \mathrm{Re}(\tilde{\lambda_n^-}) = 0$ and points $r_{\tilde{\Xi}_N}^{\tilde{\pm}}$ are neither attractive nor repulsive but indifferent—the respective transformation can be now classified as elliptic. Finally, we should note another interesting property of the $\mathcal{G}$ transform (inherited by the ordinary Möbius transformation), according to which cross-ratios remain invariant under such transformations

$$\frac{\left[\mathcal{G}_{Q_n}(z) - \mathcal{G}_{Q_n}(w)\right]\left[\mathcal{G}_{Q_n}(z') - \mathcal{G}_{Q_n}(w')\right]}{\left[\mathcal{G}_{Q_n}(z') - \mathcal{G}_{Q_n}(w)\right]\left[\mathcal{G}_{Q_n}(z) - \mathcal{G}_{Q_n}(w')\right]} = \frac{(z - w)(z' - w')}{(z' - w)(z - w')}, \tag{C6}$$

where $z,\, z',\, w,\, w'$ are complex quantities.

APPENDIX D: CALCULUS OF DIVIDED DIFFERENCES AND THE DISCRETE NEWTON SERIES EXPANSION

Frequently in our analysis we have used the Newton series expansion for discrete sequences, which as we will see here is nothing but the discrete equivalent of the familiar Taylor expansion appearing in differential calculus. In order to demonstrate this, we shall firstly introduce the *Newton polynomial*, which is an interpolation polynomial for an arbitrary set of data points $(x_0,\ y_0), \ldots, (x_n,\ y_n)$ with no two x_j being the same ($j,\ n \in \mathbb{N},\ 0 \leqslant j \leqslant n$). Such a polynomial is a linear combination of the *Newton basis polynomials* $P_j(x) = \prod_{k=0}^{j-1}(x - x_k)$ $[P_0(x) = 1]$ and takes the form

$$P(x) = \sum_{j=0}^{n} o_j P_j(x) = \sum_{j=0}^{n} o_j \prod_{k=0}^{j-1}(x - x_k), \tag{D1}$$

where the coefficients are defined as $o_j = [y_0, \ldots, y_j]$ and $[y_0, \ldots, y_j]$ is the notation for the *forward divided differences*, i.e.,

$$[y_\nu] = y_\nu, \tag{D2}$$

for $0 \leqslant \nu \leqslant n$ and

$$[y_\nu, \ldots, y_{\nu+l}] = \frac{[y_{\nu+1}, \ldots, y_{\nu+l}] - [y_\nu, \ldots, y_{\nu+l-1}]}{x_{\nu+l} - x_\nu}, \tag{D3}$$

for $0 \leqslant \nu \leqslant n - l$ and $1 \leqslant l \leqslant n$ $(\nu,\ l \in \mathbb{N})$. Based on the above definition, it can be deduced that $[y_{\nu+l}, \ldots, y_\nu] = [y_\nu, \ldots, y_{\nu+l}]$, i.e., the divided difference of a number of terms will remain invariant if we reverse their order. This can be easily shown via the method of induction, which we shall frequently use in the present Appendix to prove a number of propositions. More specifically, if $l = 1$ we have that $[y_{\nu+1}, y_\nu] = (y_\nu - y_{\nu+1})/(x_\nu - x_{\nu+1}) = (y_{\nu+1} - y_\nu)/(x_{\nu+1} - x_\nu) = [y_\nu, y_{\nu+1}]$. Assuming that $[y_{\nu+l-1}, \ldots, y_\nu] = [y_\nu, \ldots, y_{\nu+l-1}]$ is true, then it will hold that $[y_{\nu+l}, \ldots, y_\nu] = ([y_{\nu+l-1}, \ldots, y_\nu] - [y_{\nu+l}, \ldots, y_{\nu+1}])/(x_\nu - x_{\nu+l}) = ([y_{\nu+1}, \ldots, y_{\nu+l}] - [y_\nu, \ldots, y_{\nu+l-1}])/(x_{\nu+l} - x_\nu) = [y_\nu, \ldots, y_{\nu+l}]$ and this completes our proof.

In order now to show that Eq. (D1) is indeed an interpolation polynomial for the given set of data points, we shall prove via the method of induction that

$$[y_0, \ldots, y_n]P_n(x_n) = y_n - W(x_n) = P(x_n) - W(x_n), \tag{D4}$$

where $W(x)$ is the unique polynomial of degree $n - 1$ $(n \geqslant 1)$ passing through points $(x_0,\ y_0), \ldots, (x_{n-1},\ y_{n-1})$ and $P(x)$ is the unique polynomial of degree j passing through points $(x_0,\ y_0), \ldots, (x_n,\ y_n)$. For $n = 1$, polynomial $W(x)$ is of zero degree satisfying relation passing through point $W(x_0) = y_0$, which directly implies that $W(x) = y_0$. Consequently, the left-hand side of Eq. (D4) becomes $[y_0, y_1]P_1(x_1) = [y_0, y_1](x_1 - x_0) = y_1 - W(x_1)$, which confirms the aforementioned equation. Assuming now that Eq. (D4) holds true for $n \to n - 1 \geqslant 1$, then the following will apply:

$$\begin{aligned}
[y_0, \ldots, y_n]P_n(x_n) &= \frac{[y_1, \ldots, y_n] - [y_0, \ldots, y_{n-1}]}{x_n - x_0} \prod_{k=0}^{n-1}(x_n - x_k) \\
&= [y_1, \ldots, y_n] \prod_{k=1}^{n-1}(x_n - x_k) - [y_0, \ldots, y_{n-1}] \prod_{k=1}^{n-1}(x_n - x_k) = y_n \\
&\quad - Q(x_n) - [y_0, \ldots, y_{n-1}] \prod_{k=1}^{n-1}(x_n - x_k) = y_n - \left\{ Q(x_n) + [y_0, \ldots, y_{n-1}] \prod_{k=1}^{n-1}(x_n - x_k) \right\},
\end{aligned} \tag{D5}$$

where $Q(x)$ is the unique interpolation polynomial of degree $n - 2$ going through points $(x_1,\ y_1), \ldots, (x_{n-1},\ y_{n-1})$. [In the derivation of the above expression, we have exploited Eq. (D4), which according to our induction hypothesis applies for $n \to n - 1$.] After setting $W(x) = Q(x) + [y_0, \ldots, y_{n-1}] \prod_{k=1}^{n-1}(x - x_k)$, it becomes easy to see that $W(x_k) = y_k$ for $1 \leqslant k \leqslant n - 1$ while it will be also true that $W(x_0) = Q(x_0) + [y_0, \ldots, y_{n-1}] \prod_{k=1}^{n-1}(x_0 - x_k) = Q(x_0) + [y_{n-1}, \ldots, y_0] \prod_{k=1}^{n-1}(x_0 - x_k) = y_0$. In that manner, $W(x)$ becomes the unique polynomial passing through points $(x_0,\ y_0), \ldots, (x_{n-1},\ y_{n-1})$ and given Eq. (D5), Eq. (D4) becomes immediately confirmed. Of interest is to see now, after rewriting Eq. (D4) as $P(x_n) = W(x_n) + [y_0, \ldots, y_n]P_n(x_n) = W(x_n) + o_n P_n(x_n)$, that if polynomial $W(x)$ goes through points $(x_0,\ y_0), \ldots, (x_{n-1},\ y_{n-1})$ then polynomial $P(x) = W(x) + o_n P_n(x)$ will also go through all the aforementioned points but will also cross point (x_n, y_n). This is a straightforward way to add points in an existing interpolating polynomial curve and also clearly indicates the validity of the Newton interpolation formula illustrated in Eq. (D1). It should be also highlighted that the *uniqueness of polynomial* $P(x)$ of degree n defined in Eq. (D1) is guaranteed by the fact that it should satisfy $n + 1$ distinct equations $[P(x_j) = y_j$ for $0 \leqslant j \leqslant n$, which leads to $n + 1$ equations with $n + 1$ unknown polynomial coefficients; a similar rationale also applies for polynomials $W(x)$ and $Q(x)$ of degrees $n - 1$ and $n - 2$ defined in Eqs. (D4) and (D5), respectively].

The discrete Newton series expansion can now be attained from Eq. (D1), after assuming equidistant data points $(x_{\nu+1} - x_\nu = \Delta$ with $\nu \in [0, n - 1])$ and considering the relation between the forward difference operator δ $(\delta q_\nu = q_{\nu+1} - q_\nu$ for an arbitrary discrete sequence $q_\nu)$ and the forward divided differences

$$[y_0, \ldots, y_n] = \frac{1}{n!} \frac{\delta^n y_0}{\delta x_0^n}. \tag{D6}$$

In the above expression $n! = 1 \cdot 2 \cdots n$ represents of course the factorial $(0! = 1)$, $\delta x_0^n = \Delta^n$, and δ^n refers to the

higher-order forward difference operator recursively defined as

$$\delta^0 y_\nu = y_\nu,\ \delta^1 y_\nu = y_{\nu+1} - y_\nu, \tag{D7a}$$

$$\delta^l y_\nu = \delta(\delta^{l-1} y_\nu), \tag{D7b}$$

with $0 \leqslant \nu \leqslant n-l,\ 2 \leqslant l \leqslant n$, and $\nu,\ l \in \mathbb{N}$. Equation (D6) can be shown again based on the method of induction as follows: (i) for $n = 0$, we have that $\delta^0 y_0/(0!\delta x_0^0) = y_0 = [y_0]$ and (ii) assuming that Eq. (D6) holds for $n \to n-1 \geqslant 0$, then we sequentially have that

$$[y_0, \ldots, y_n] = \frac{[y_1, \ldots, y_n] - [y_0, \ldots, y_{n-1}]}{x_n - x_0} = \frac{\frac{1}{(n-1)!}\frac{\delta^{n-1} y_1}{\delta x_1^{n-1}} - \frac{1}{(n-1)!}\frac{\delta^{n-1} y_0}{\delta x_0^{n-1}}}{n\Delta}$$

$$= \frac{\delta^{n-1}(y_1 - y_0)}{n!\Delta^n} = \frac{1}{n!}\frac{\delta^n y_0}{\delta x_0^n}, \tag{D8}$$

where we have exploited the linearity of operator δ, along with relations $\delta x_1^{n-1} = \delta x_0^{n-1} = \Delta^{n-1}$ and $\delta^{n-1}(y_1 - y_0) = \delta^{n-1}(\delta y_0) = \delta^n y_0$. This completes the proof of Eq. (D6). Along these lines, of interest is also to prove the following relation pertaining to the higher-order difference operator:

$$\delta^n y_0 = \sum_{j=0}^{n} \binom{n}{j} (-1)^{n-j} y_j, \tag{D9}$$

where $\binom{n}{j} = \frac{n!}{j!(n-j)!}$ $(n \geqslant j)$ is the binomial coefficient. After following similar steps as for the proof of Eq. (D6), we have that: (i) for $n = 0$, both the left- and right-hand sides of Eq. (D9) become equal to y_0, (ii) assuming that Eq. (D9) is true for $n \to n-1 \geqslant 0$, it can be attained that

$$\delta^n y_0 = \delta(\delta^{n-1} y_0) = \sum_{j=0}^{n-1} \binom{n-1}{j} (-1)^{n-1-j} \delta y_j = \sum_{j=0}^{n-1} \binom{n-1}{j} (-1)^{n-1-j} (y_{j+1} - y_j) = \sum_{j=1}^{n-1} \left[\binom{n-1}{j} + \binom{n-1}{j-1} \right] (-1)^{n-j} y_j$$

$$+ (-1)^n y_0 + y_n = \sum_{j=1}^{n-1} \binom{n}{j} (-1)^{n-j} y_j + (-1)^n y_0 + y_n = \sum_{j=0}^{n} \binom{n}{j} (-1)^{n-j} y_j. \tag{D10}$$

In the derivation of the above expression, we have exploited an important property of binomial coefficients: $\binom{n}{j} = \binom{n-1}{j} + \binom{n-1}{j-1}$. Statements (i) and (ii) along with Eq. (D10) complete the proof by induction of Eq. (D9). Based now on Eqs. (D1) and (D6), we can retrieve the *finite Newton series* as

$$P(x) = \sum_{j=0}^{n} \frac{1}{j!} \frac{\delta^j y_0}{\delta x_0^j} \prod_{k=0}^{j-1} (x - x_0 - k\Delta), \tag{D11}$$

where if we set $x = x_n = n\Delta$ $[P(x_n) = y_n]$ we obtain that

$$y_n = \sum_{j=0}^{n} \binom{n}{j} \Delta^j \frac{\delta^j y_0}{\delta x_0^j}. \tag{D12}$$

The above expression together with Eq. (D9) state the full relationship between y_j and the respective higher-order differences. Indicatively, we substitute $n = 1,\ 2,\ 3$ in Eq. (D12) to obtain the respective Newton series expansions: $y_1 = y_0 + \Delta\delta y_0/\delta x_0$, $y_2 = y_0 + 2\Delta\delta y_0/\delta x_0 + \Delta^2\delta^2 y_0/\delta x_0^2$, $y_3 = y_0 + 3\Delta\delta y_0/\delta x_0 + 3\Delta^2\delta^2 y_0/\delta x_0^2 + \Delta^3\delta^3 y_0/\delta x_0^3$. The summation illustrated in Eq. (D12) can be also extended to contain an infinite amount of terms, if $P(x)$ is replaced by a generalized analytic function $F(x)$. In that manner, the *infinite Newton series* can be attained

$$F(x) = \lim_{n\to\infty} \sum_{j=0}^{n} \frac{1}{j!} \frac{\delta^j F(x_0)}{\delta x_0^j} \prod_{k=0}^{j-1} (x - x_0 - k\Delta)$$

$$= \sum_{j=0}^{\infty} \frac{1}{j!} \frac{\delta^j F(x_0)}{\delta x_0^j} \prod_{k=0}^{j-1} (x - x_0 - k\Delta) \tag{D13}$$

and applies for a wide range (but not the entirety) of analytic functions $F(x)$. (See [116,117] for a detailed discussion on functions, which do not accept expansions of the aforementioned form.) If we allow now $\delta x_0 = \Delta \to 0$ and $k\Delta \to 0$ [if k approaches infinity, then we can simply set $\Delta = 1/n^l$ $(l > 1)$ in the limit shown in Eq. (D13) and thus acquire $\lim_{n\to\infty} n\Delta = \lim_{n\to\infty} n^{1-l} = 0$ or equivalently $\lim_{n\to\infty} k\Delta = 0$ since $n \geqslant k$], then Eq. (D13) takes the familiar form of a *Taylor series expansion* [$F(x)$ is assumed to be infinitely differentiable at x_0],

$$F(x) = \sum_{j=0}^{\infty} \frac{1}{j!} \frac{d^j F(x_0)}{dx^j} (x - x_0)^j, \tag{D14}$$

where the difference operator δ has been replaced by the differential operator d. Such a substitution $(\delta \to d)$ can take place given that $(\delta x_0 = \Delta)$

$$\lim_{\Delta\to 0} \frac{\delta F(x_0)}{\delta x_0} = \lim_{\Delta\to 0} \frac{F(x_0 + \Delta) - F(x)}{\Delta} = \frac{dF(x_0)}{dx}, \tag{D15}$$

which can be easily extended to higher-order differences and derivatives. The equivalence of Eqs. (D13) and (D14) for infinitesimally small discrete steps Δ indicates that the Newton expansion is nothing but the discrete analog of the continuous Taylor series. A Taylor series expansion reveals the behavior of a function, based on its y value and its derivatives at a particular x value. On the other hand, a Newton series expansion demonstrates the traits of a function in terms of divided differences (instead of the instantaneous rates of change).

Of interest is to note that Eq. (D14) could have been retrieved directly from Eq. (D1) by taking into advantage the *mean value theorem for (forward) divided differences*

$$[F(x_0), \ldots, F(x_n)] = \frac{1}{n!} \frac{d^n F(\rho)}{dx^n}, \tag{D16}$$

where $\min(x_0,\ldots,x_n) < \rho < \max(x_0,\ldots,x_n)$ [functions min(.) and max(.) denote of course the minimum and maximum of their arguments, respectively]. In the limit of an infinite number of nodes ($n \to \infty$), which all coincide ($x_j \to x_0$, $\forall j \in [0, n]$), the Newton interpolation formula of Eq. (D1) will take the form of a Taylor series after exploiting identity $\lim_{x_j \to x_0, \forall j\in[0,n]}[F(x_0),\ldots,F(x_n)] = \lim_{x_j \to x_0, \forall j\in[0,n]} 1/n!\, d^nF(\rho)/dx^j = 1/n!\, d^nF(x_0)/dx^j$ and replacing polynomial $P(x)$ with the generalized analytic function $F(x)$. Proving Eq. (D16) becomes straightforward after setting $G(x) = F(x) - P(x)$, where $P(x)$ is the Newton interpolation polynomial for $F(x)$ at points $(x_0, y_0),\ldots,(x_n, y_n)$ [see Eq. (D1)]. Since function $G(x)$ has $n+1$ roots and assuming $F(x)$ [and thus $G(x)$] is n-times differentiable, we can apply Rolle's theorem sequentially to $dG(x)/dx$, $d^2G(x)/dx^2$, and so on till $d^{n-1}G(x)/dx^{n-1}$. Consequently, we find that $d^nG(x)/dx^n$ has a root at $\rho \in (\min(x_0,\ldots,x_n), \max(x_0,\ldots,x_n))$, i.e., $d^nF(\rho)/dx^n - d^nP(\rho)/dx^n = 0 \Leftrightarrow [y_0,\ldots,y_n] = 1/n!\, d^nF(\rho)/dx^n$ (the largest-order term of $P(x)$ is $[y_0,\ldots,y_n]x^n$) and this completes the proof of Eq. (D16). Finally, it should be highlighted that the mean value theorem for divided differences—as expressed through Eq. (D16)—is actually an extension of the ordinary mean value theorem of differential calculus to higher-order derivatives, with the latter stemming from the former if we set $n = 1$ in Eq. (D16).

APPENDIX E: RETRIEVING THE ANALYTICAL DYNAMICS OF THE TRACELESS AND SYMMETRIC NON-HERMITIAN HAMILTONIAN MODEL ALONG THE ENTIRE PATH $\mathcal{C}^{\mathcal{R}}_{\mathcal{R}\hbar}$

In Sec. II C, we provided closed-form expressions for the dynamics associated with the $\mathcal{PT}$-symmetric-like model of Sec. II B as it evolves along a particular segment $\ell_j^{\mathcal{R}}$ ($j = 1, 2, 3, 4$) of the parametric path $\mathcal{C}^{\mathcal{R}}_{\mathcal{R}\hbar}$ (a detailed derivation of such expressions was presented in Sec. II within SM [76]). More specifically, the state vector evolution was found to be dictated in the limit of small time steps by discrete Weber or Airy functions, depending on the magnitude of the modulating parameters ϵ_g, ϵ_σ. If we turn our attention to the state vector component a_n [see Eqs. (11) and (12) of Sec. II C], then we can write $a_n = c_1^a a_{n,1} + c_2^a a_{n,2}$ with $a_{n,1}$, $a_{n,2}$ denoting the discrete Weber/Airy functions of the first and second kind, respectively; of course, variables $c_{1,2}^a$, $a_{n,1}$, $a_{n,2}$ will depend on the segment $\ell_j^{\mathcal{R}}$ that we refer to, but for now we shall omit the additional index (j) to simplify our notation. By substituting the aforementioned expression for a_n to Eq. (7) (see Sec. II B), the matrix relation $[a_n\ b_n]^{\mathcal{T}} = \hat{Z}_n\,[c_1^a\ c_2^a]^{\mathcal{T}}$ can be attained with $\hat{Z}_n$ defined as

$$\hat{Z}_n = \begin{bmatrix} a_{n,1} & a_{n,2} \\ \dfrac{1}{i\kappa}\dfrac{\delta a_{n,1}}{\delta t_n} - \dfrac{f_n a_{n,1}}{i\kappa} & \dfrac{1}{i\kappa}\dfrac{\delta a_{n,2}}{\delta t_n} - \dfrac{f_n a_{n,2}}{i\kappa} \end{bmatrix}. \tag{E1}$$

Constants c_1^a, c_2^a can be directly determined from the initial conditions a_{n_o}, b_{n_o} ($n \geqslant n_o$); the integer parameter n_o essentially signifies here the starting point of $\ell_j^{\mathcal{R}}$. As a result, state vectors $|u_n\rangle$ and $|u_{n_o}\rangle$ will be connected via the following equality

$$|u_n\rangle = \hat{Z}_n \hat{Z}_{n_o}^{-1} |u_{n_o}\rangle = Z_{n,n_o} |u_{n_o}\rangle. \tag{E2}$$

The well-definedness of the above equation is guaranteed, since matrix $\hat{Z}_{n_o}$ is invertible [for $n \geqslant n_o$ it will apply that $\det(\hat{Z}_n) = C(a_{n,1}, a_{n,2})/(i\kappa) \neq 0$, where det(.) denotes the determinant of a matrix and $C(.,.)$ the Casoratian of two discrete sequences]. It should be also noted that Z_{n,n_o} is in general not a time invariant quantity ($Z_{n,n_o} \neq Z_{n-n_o}$), which is an immediate consequence of the time dependence of the Hamiltonian matrix (for more details, see also Appendix B 1). The full evolution dynamics of state vector $|u_n\rangle$ (as the Hamiltonian system cycles around the complete rhombic path $\mathcal{C}^{\mathcal{R}}_{\mathcal{R}\hbar}$ in parameter space) can be now directly attained, after inserting superscripts (j) in Eq. (E2) in order to identify each subpath $\ell_j^{\mathcal{R}}$. Subsequently, it will be true that

$$\begin{aligned} |u_N\rangle &= Z^{(4)}_{n_e,n_o} Z^{(3)}_{n_e,n_o} Z^{(2)}_{n_e,n_o} Z^{(1)}_{n_e,n_o} |u_0\rangle \\ &= \prod_{j=1}^{4} Z^{(j)}_{n_e,n_o} |u_0\rangle = Z_{\mathcal{R}\hbar} |u_0\rangle, \end{aligned} \tag{E3}$$

where $n_o = (j-1)N/4$ and $n_e = jN/4$ designate the starting and ending points of each linear segment $\ell_j^{\mathcal{R}}$, correspondingly, and N represents the total number of discrete points along $\mathcal{C}^{\mathcal{R}}_{\mathcal{R}\hbar}$. In Eq. (E3), an *ordered matrix product* was used in order to signify that segments $\ell_j^{\mathcal{R}}$ are traversed in the order $\ell_1^{\mathcal{R}} \to \ell_2^{\mathcal{R}} \to \ell_3^{\mathcal{R}} \to \ell_4^{\mathcal{R}}$. This is true independently of the direction of encirclement, owing to the convention used in the definition of such subpaths (see for instance Fig. 1 and Fig. S1 within SM [76]). Equation (E3) provides a closed-form expression for the state vector after a cycling period T ($=N\Delta$), given that the analytical forms of $a_{n,1}$ and $a_{n,2}$ are already known (here, they represent either Weber or Airy functions).

As a next step in our analysis, we will study the dynamics that govern the ratio factor r_n ($= b_n/a_n$), as the Hamiltonian system evolves around the closed loop $\mathcal{C}^{\mathcal{R}}_{\mathcal{R}\hbar}$. In this regard, we shall exploit Eq. (A9) of Appendix A, which can be rewritten as follows given the form of the evolution matrix elements [$\xi_n^{11} = 1 + \Delta f_n$, $\xi_n^{22} = 1 - \Delta f_n$, $\xi_n^{12} = \xi_n^{21} = i\Delta\kappa$; see definition of Ξ_n at the beginning of Sec. II A and Eq. (7) of Sec. II B] and the expression $a_n = c_1^a a_{n,1} + c_2^a a_{n,2}$ ($c^a = c_2^a/c_1^a$),

$$r_n = \mathcal{G}_{\hat{Z}_n}(c^a) = \frac{\hat{\xi}_n^{21} + \hat{\xi}_n^{22} c^a}{\hat{\xi}_n^{11} + \hat{\xi}_n^{12} c^a}. \tag{E4}$$

In the above equation, it is assumed that $n \geqslant n_o$ (n_o: starting point along segment $\ell_j^{\mathcal{R}}$), $c_1^a \neq 0$ (otherwise the inverse ratio c_1^a/c_2^a could have been considered; c_1^a, c_2^a being zero simultaneously leads to the trivial case of $a_n \equiv 0$ for $n \geqslant n_o$), while $\hat{\xi}_n^{jk}$ ($j, k = 1, 2$) represent the elements of matrix $\hat{Z}_n$. The constant parameter c^a can be determined based on the initial condition r_{n_o} as follows:

$$c^a = \mathcal{G}^{-1}_{\hat{Z}_{n_o}}(r_{n_o}) = \mathcal{G}_{\hat{Z}^{-1}_{n_o}}(r_{n_o}) = \frac{-\hat{\xi}_{n_o}^{21} + \hat{\xi}_{n_o}^{11} r_{n_o}}{\hat{\xi}_{n_o}^{22} - \hat{\xi}_{n_o}^{12} r_{n_o}}, \tag{E5}$$

where the inverse of matrix $\hat{Z}_{n_o}$ is well defined since $\det(\hat{Z}_{n_o}) \neq 0$ and $\mathcal{G}^{-1}_{\hat{Z}_{n_o}} = \mathcal{G}_{\hat{Z}^{-1}_{n_o}}$ as shown in Appendix C. Based

now on Eqs. (E4) and (E5), the relation between r_n and r_{n_o} can be obtained as

$$r_n = \left(\mathcal{G}_{\hat{Z}_n} \circ \mathcal{G}_{\hat{Z}_{n_o}^{-1}}\right)(r_{n_o}) = \mathcal{G}_{Z_{n,n_o}}(r_{n_o}) = \frac{\hat{\xi}_n^{21}\hat{\xi}_{n_o}^{22} - \hat{\xi}_n^{22}\hat{\xi}_{n_o}^{21} + \left(\hat{\xi}_n^{22}\hat{\xi}_{n_o}^{11} - \hat{\xi}_n^{21}\hat{\xi}_{n_o}^{12}\right) r_{n_o}}{\hat{\xi}_n^{11}\hat{\xi}_{n_o}^{22} - \hat{\xi}_n^{12}\hat{\xi}_{n_o}^{21} + \left(\hat{\xi}_n^{12}\hat{\xi}_{n_o}^{11} - \hat{\xi}_n^{11}\hat{\xi}_{n_o}^{12}\right) r_{n_o}}, \tag{E6}$$

after also taking into account an important property related to the iterative operation of $\mathcal{G}$ transforms (see Appendix C): $\mathcal{G}_{\hat{Z}_n} \circ \mathcal{G}_{\hat{Z}_{n_o}^{-1}} = \mathcal{G}_{\hat{Z}_n \hat{Z}_{n_o}^{-1}} = \mathcal{G}_{Z_{n,n_o}}$ [symbol $\circ$ denotes the operation of function composition, while $Z_{n,n_o} = \hat{Z}_n \hat{Z}_{n_o}^{-1}$ according to Eq. (E2)]. So far, we have analyzed how parameter r_n evolves along a specific linear segment $\ell_j^{\mathcal{R}}$. For the complete rhombic path $C_{\mathcal{R}\hbar}^{\mathcal{R}}$, it will be true that

$$r_N = \left(\mathcal{G}_{Z_{n_e,n_o}^{(4)}} \circ \mathcal{G}_{Z_{n_e,n_o}^{(3)}} \circ \mathcal{G}_{Z_{n_e,n_o}^{(2)}} \circ \mathcal{G}_{Z_{n_e,n_o}^{(1)}}\right)(r_0) = \left(\bigcirc_{j=1}^{4} \mathcal{G}_{Z_{n_e,n_o}^{(j)}}\right)(r_0) = \mathcal{G}_{Z_{\mathcal{R}\hbar}}(r_0), \tag{E7}$$

where notation $\bigcirc_{j=1}^{4}$ signifies an *ordered function composition* and is completely analogous to the ordered matrix product $Z_{\mathcal{R}\hbar} = \prod_{j=1}^{4} Z_{n_e,n_o}^{(j)}$ used in Eq. (E3). (It should be noted that both operations of matrix multiplication and function composition are not commutative and this necessitates the use of ordered matrix products and ordered function compositions.) Equations (E1)–(E7) are overall applicable for the general family of rhombic trajectories $\mathcal{C}_{\mathcal{R}\hbar}^{\mathcal{R}}$, irrespective of their dimensions (ϵ_g, ϵ_σ) or location of their centers (g_C, σ_C). Moreover, Eqs. (E4)–(E7) [which are equivalent to Eqs. (E1)–(E3)] grant us direct access to the dynamics of r_n without the need of attaining the evolution equations for either of the state vector components a_n, b_n. In this vein, we can also exploit the properties of nonlinear Ricatti difference equations and $\mathcal{G}$ transforms in order to attain a more effective and elegant description for the dynamical behavior that r_n exhibits.

Of interest now is to examine the adiabatic dynamics (T, $N \to \infty$) for the traceless and symmetric Hamiltonian system under study, as it evolves along the parametric path $\mathcal{C}_{\mathcal{R}\hbar}^{\mathcal{R}}$. Here, we shall provide a heuristic derivation of the mode switching effect described in Sec. II C, under the assumption of small dimensions for loop $\mathcal{C}_{\mathcal{R}\hbar}^{\mathcal{R}}$ (the reader should refer to Sec. V within SM [76] for a fully rigorous proof). In this case, it will apply that $a_n = c_1^a \mathrm{Ai}(\chi_n) + c_2^a \mathrm{Bi}(\chi_n)$ and thus factor r_n will satisfy the following relation along each linear subsegment $\ell_j^{\mathcal{R}}$ [see Eq. (A9)],

$$r_n = -i\frac{1}{\kappa a_n}\frac{\delta a_n}{\delta t_n} + i\frac{f_n}{\kappa} = -i\frac{1}{\kappa}\frac{\delta\chi_n}{\delta t_n}\frac{c_1^a\,\delta\mathrm{Ai}(\chi_n)/\delta\chi_n + c_2^a\,\delta\mathrm{Bi}(\chi_n)/\delta\chi_n}{c_1^a\,\mathrm{Ai}(\chi_n) + c_2^a\,\mathrm{Bi}(\chi_n)} + i\frac{f_n}{\kappa}. \tag{E8}$$

In the asymptotic limit $T \to \infty$, it will be true that

$$\lim_{T\to\infty} \eta_{f,1} = \lim_{T\to\infty} 4(\pm\epsilon_g \pm i\epsilon_\sigma)/T = 0, \tag{E9a}$$

$$\lim_{T\to\infty} |\chi_n| \simeq \lim_{T\to\infty} \left|f_n^2 - \kappa^2 + \eta_{f,1}\right| \Big/ |2\eta_{f,1}\eta_{f,0}|^{2/3} = \infty, \tag{E9b}$$

given that parameters $\epsilon_{g,\sigma}$, f_n, κ, $\eta_{f,0}$ attain finite values and $f_n \neq \kappa$ assuming that no exceptional points are crossed (for the expressions of $\eta_{f,1}$, $\eta_{f,0}$ see Sec. I within SM [76]). Now, we can employ the Airy asymptotic expansions valid for large magnitudes of the respective arguments (see [118–120] and Sec. II within SM [76]). After considering only the prevalent terms (i.e., terms related to either $e^{2\chi_n^{3/2}/3}$ or $e^{-2\chi_n^{3/2}/3}$, depending on the sign of the real part of $\chi_n^{3/2}$), it can be shown that both relations $\mathrm{Ai}(\chi_n)/\mathrm{Bi}(\chi_n) \simeq [\delta\mathrm{Ai}(\chi_n)/\delta\chi_n]/[\delta\mathrm{Bi}(\chi_n)/\delta\chi_n]$ and $[\delta\mathrm{Bi}(\chi_n)/\delta\chi_n]/\mathrm{Bi}(\chi_n) \simeq \pm\chi_n^{1/2}$ will apply as $|\chi_n| \to \infty$. Equation (E8) will now read as

$$\lim_{T\to\infty} r_n = \lim_{T\to\infty}\left\{-i\frac{1}{\kappa}\frac{\delta\chi_n}{\delta t_n}\frac{\delta\mathrm{Bi}(\chi_n)/\delta\chi_n}{\mathrm{Bi}(\chi_n)} + i\frac{f_n}{\kappa}\right\} = \lim_{T\to\infty}\left\{\mp i\frac{(2\eta_{f,1}\eta_{f,0})^{1/3}\,\chi_n^{1/2}}{\kappa} + i\frac{f_n}{\kappa}\right\} = \begin{cases} \mp\sqrt{1-\dfrac{f_n^2}{\kappa^2}} + i\dfrac{f_n}{\kappa} = \mp e^{\mp i\theta_n}, \\ \pm\sqrt{1-\dfrac{f_n^2}{\kappa^2}} + i\dfrac{f_n}{\kappa} = \pm e^{\pm i\theta_n}, \end{cases} \tag{E10}$$

where angle θ_n has been defined in Sec. II B and we have taken into account that $\chi_n = (2\eta_{f,1}\eta_{f,0}t_n + \eta_{f,0}^2 - \kappa^2 + \eta_{f,1})/(2\eta_{f,1}\eta_{f,0})^{2/3} \simeq (f_n^2 - \kappa^2 + \eta_{f,1})/(2\eta_{f,1}\eta_{f,0})^{2/3}$ (the approximate relation stems from the fact that small magnitudes ϵ_g, ϵ_σ are assumed; see also discussion at the beginning of Sec. V within SM [76]). The two separate branches appearing in the last line of Eq. (E10) are attributed to the evaluation of factors $(2\eta_{f,1}\eta_{f,0})^{1/3}$ and $\chi_n^{1/2}$ (see also definition for principal roots of complex numbers in Sec. II within SM [76]). According to Sec. II B, it will be true that $v_{n,y}^{\pm}/v_{n,x}^{\pm} = \pm e^{\pm i\theta_n}$, which in turn implies that in the asymptotic limit state vector $|u_n\rangle$ will inevitably convert to either of the instantaneous eigenvectors $|v_n^{\pm}\rangle$.

Of course, the above derivation of adiabatic mode switching considers only the dominant terms in the asymptotic expansions of Airy functions. Yet by doing so, we can obtain that $C[\mathrm{Ai}(\chi_n), \mathrm{Bi}(\chi_n)] = 0$, which is not true based on the properties of Airy functions ($C[\mathrm{Ai}(\chi_n), \mathrm{Bi}(\chi_n)] \overset{\delta\chi_n\to 0}{=\!=} \delta\chi_n/\pi \overset{\Delta\to 0}{=} \Delta(2\eta_{f,1}\eta_{f,0})^{1/3}/\pi \neq 0$, as shown in Sec. II within SM [76]). Moreover, if parameter $\chi_n^{3/2}$ becomes a purely imaginary number, no terms will dominate within the associated Airy series expansions. Hence, it becomes of essence to consider both factors $e^{2\chi_n^{3/2}/3}$ and $e^{-2\chi_n^{3/2}/3}$, so that we can also accurately account for the effect of the Stokes phenomenon on the dynamics of both state vector $|u_n\rangle$ and ratio r_n. Along these lines, special care should be taken in the actual values attained by constants c_1^a and c_2^a along the different linear segments $\ell_j^{\mathcal{R}}$ [see Eq. (E5)], as they might lead to singularities in Eqs. (E4), (E6), and (E7). All such issues are being accounted for in Sec. V within SM [76], where a comprehensive proof of state conversion is presented for traceless and symmetric non-Hermitian Hamiltonian settings traversing square parametric trajectories. By taking into account the cyclic evolution conditions, symmetric and asymmetric mode switching was demonstrated depending on the region of operation within the space of parameters and the initial values of gain and

detuning. In Appendix B 2 it is also shown how such a switching effect is consistent with a dynamical property unique to the $\mathcal{PT}$-symmetric-like configuration of Sec. II B, which correlates CW and CCW cyclically evolving states along pairs of (or individual) trajectories symmetric to the g_n axis in $\mathcal{R}$ space.

APPENDIX F: DISCRETE BERRY PHASE, BIORTHONORMALITY CONDITIONS, AND THE CONTINUOUS TIME LIMIT OF THE DISCRETE MODE POPULATION EQUATIONS

In Sec. III, the adiabatic behavior of generalized non-Hermitian and discrete arrangements was rigorously analyzed by decomposing the respective state vector according to a *biorthonormnal basis*. The biorthogonality condition $\langle v_n^{\hat{\pm},L}||v_n^{\hat{\mp},R}\rangle = 0$ is guaranteed for a non-Hermitian quantum system [90], yet the additional condition $\langle v_n^{\hat{\pm},L}||v_n^{\hat{\pm},R}\rangle = 1$ needs special attention [here we use notation $(\hat{\pm})$; see Sec. III A to represent any possible mode designation used in the present paper; see Fig. 4 of main text for different mode notation definitions]. Assuming that the left and right eigenvectors are evaluated as $\langle v_n^{\hat{\pm},L}|$ and $|v_n^{\hat{\pm},R}\rangle$, then we employ the following transformation:

$$\langle v_n^{\hat{\pm},L}| = \frac{\langle v_n^{\hat{\pm},L}|}{\sqrt{\langle v_n^{\hat{\pm},L}||v_n^{\hat{\pm},R}\rangle}}, \quad |v_n^{\hat{\pm},R}\rangle = \frac{|v_n^{\hat{\pm},R}\rangle}{\sqrt{\langle v_n^{\hat{\pm},L}||v_n^{\hat{\pm},R}\rangle}} \tag{F1}$$

which clearly now satisfies relation $\langle v_n^{\hat{\pm},L}||v_n^{\hat{\pm},R}\rangle = 1$. Under conditions of Hermiticity [$H_n^\dagger = H_n$ and $(\lambda_{H_n}^{\hat{\pm}})^* = \lambda_{H_n}^{\hat{\pm}}$ or equivalently $M_n^\dagger = -M_n$ and $(\lambda_n^{\hat{\pm}})^* = -\lambda_n^{\hat{\pm}}$ given that $M_n = -iH_n$, where $\lambda_{H_n}^{\hat{\pm}}$ and $\lambda_n^{\hat{\pm}}$ are the eigenvalues of matrices H_n and M_n, respectively], it will be true that $\langle v_n^{\hat{\pm},L}|H_n = \lambda_{H_n}^{\hat{\pm}}\langle v_n^{\hat{\pm},L}| \overset{H_n^\dagger = H_n}{\Longleftrightarrow} H_n|v_n^{\hat{\pm},L}\rangle = \lambda_{H_n}^{\hat{\pm}}|v_n^{\hat{\pm},L}\rangle$, which directly implies that $|v_n^{\hat{\pm},L}\rangle = |v_n^{\hat{\pm},R}\rangle = |v_n^{\hat{\pm}}\rangle$ or equivalently that the left ($\langle v_n^{\hat{\pm},L}|$) and right ($|v_n^{\hat{\pm},R}\rangle$) eigenvectors are conjugate transposes of each other (of course M_n and H_n share the same left and right eigenvectors since they are linearly related). In this case, the normalization condition shown in Eq. (F1) will take the familiar form $|v_n^{\hat{\pm}}\rangle = |v_n^{\hat{\pm}}\rangle/\sqrt{\langle v_n^{\hat{\pm}}||v_n^{\hat{\pm}}\rangle}$ with eigenvectors $|v_n^{\hat{\pm}}\rangle$ forming now an orthonormal basis ($\langle v_n^{\hat{\pm}}||v_n^{\hat{\pm}}\rangle = 1$, $\langle v_n^{\hat{\pm}}||v_n^{\hat{\mp}}\rangle = 0$).

It should be highlighted that the normalization as dictated by Eq. (F1) cannot be applied at degeneracy (or exceptional) points, since it will hold that $\langle v_{n_{EP}}^L||v_{n_{EP}}^R\rangle = 0$ with $\langle v_{n_{EP}}^{\hat{\pm},L}| = \langle v_{n_{EP}}^L|$, $|v_{n_{EP}}^{\hat{\pm},R}\rangle = |v_{n_{EP}}^R\rangle$, and $n = n_{EP}$ is where the degeneracy occurs. Indeed after solving the left eigenvalue problem $\langle v_n^{\hat{\pm},L}|M_n = \lambda_n^{\hat{\pm}}\langle v_n^{\hat{\pm},L}|$, it can be found that $(v_{n,y}^{\hat{\pm},L}/v_{n,x}^{\hat{\pm},L})^* = 2m_n^{12}/(m_n^{11} - m_n^{22} \pm \sqrt{\mathcal{D}_n})$ [owing to our mode notation convention, here $(\hat{\pm})$ can be arbitrarily assigned to signs $\pm$ as opposed to $(\pm)$ used in Sec. II A and Appendix B 2 where $(+)$ corresponds to sign $+$ and $(-)$ corresponds to sign $-$] where $\langle v_n^{\hat{\pm},L}| = [v_{n,x}^{\hat{\pm},L}\ v_{n,y}^{\hat{\pm},L}]^*$ and the expression for $\mathcal{D}_n$ is given by Eq. (B21). [The eigenvalues remain the same as with the respective right eigenvalue problem treated in Appendix B 2, i.e., they can be obtained as solutions to the quadratic equation $\det(\lambda_n^{\hat{\pm}}I - M_n) = 0$.] After setting $\mathcal{D}_n = 0$ (condition for eigenvalue and eigenvector degeneracy), it becomes true that $(v_{n_{EP},y}^L/v_{n_{EP},x}^L)^* = 2m_n^{12}/(m_n^{11} - m_n^{22})$, while in Appendix B 2 it was found that $v_{n_{EP},y}^R/v_{n_{EP},x}^R = (m_n^{22} - m_n^{11})/(2m_n^{12})$. Consequently, we attain that $\langle v_{n_{EP}}^L||v_{n_{EP}}^R\rangle = 0$, i.e., at the exceptional point degeneracy there exists a unique left and a unique right eigenvector, which are orthogonal to each other. Such a situation never arose in the analysis performed in the main text, since our original assumption was that no spectrum degeneracies are crossed during the time evolution of the quantum Hamiltonian arrangement [see also comments at the beginning of Sec. III C pertaining to the eigendecomposition of the system's evolution matrix Ξ_n depicted in Eq. (25) of the same section]; practically of course, operation at such singularity points points is almost impossible due to their inherent sensitivity [93–95].

As a next step in our analysis, we can retrieve the mode population dynamics in its continuous time manifestation and subsequently compare it with its discrete counterpart depicted in Eq. (21) of Sec. III A. In that regard, the state vector $|u(t)\rangle$ is decomposed as follows:

$$|u(t)\rangle = c^{\tilde{+}}(t)e^{\int_0^t \lambda^{\tilde{+}}(t')dt'}|v^{\tilde{+},R}(t)\rangle + c^{\tilde{-}}(t)e^{\int_0^t \lambda^{\tilde{-}}(t')dt'}|v^{\tilde{-},R}(t)\rangle, \tag{F2}$$

where $\lambda^{\tilde{\pm}}(t)$ and $|v^{\tilde{\pm},R}(t)\rangle$ represent the instantaneous eigenvalues and right eigenvectors of matrix $M(t)$ [$= -iH(t)$ as defined in Sec. II A], and also mode notation $(\tilde{\pm})$ is employed to signify continuous time evolution of the involved variables (in Sec. III B, the same notation was used for discrete variables to highlight the absence of any discontinuities in the evolution of the Hamiltonian eigenspectra). Of course for a time-independent Hamiltonian [$H(t) = H_o$, $M(t) = M_o$], Eq. (F2) takes a very familiar form as $e^{\int_0^t \lambda^{\tilde{\pm}}(t')dt'} = e^{\lambda_o^{\tilde{\pm}}t} = e^{-i\lambda_{H_o}^{\tilde{\pm}}t}$ ($\lambda_o^{\tilde{\pm}} = -i\lambda_{H_o}^{\tilde{\pm}}$, where $\lambda_o^{\tilde{\pm}}$ and $\lambda_{H_o}^{\tilde{\pm}}$ are the eigenvalues of M_o and H_o, respectively; in typical terminology $\lambda_{H_o}^{\tilde{\pm}}$ stand for the eigenenergies of the quantum Hamiltonian system). Equation (F2) can be directly substituted in the Schrödinger equation illustrated in Eq. (A1) [which is equivalent to $\partial|u(t)\rangle/\partial t = M(t)|u(t)\rangle$] and keeping in mind that $M(t)|v^{\tilde{\pm},R}(t)\rangle = \lambda^{\tilde{\pm}}(t)|v^{\tilde{\pm},R}(t)\rangle$, the following formula can be obtained:

$$\frac{dc^{\tilde{+}}(t)}{dt}e^{\int_0^t \lambda^{\tilde{+}}(t')dt'}\left|v^{\tilde{+},R}(t)\right\rangle + \frac{dc^{\tilde{-}}(t)}{dt}e^{\int_0^t \lambda^{\tilde{-}}(t')dt'}\left|v^{\tilde{-},R}(t)\right\rangle = -c^{\tilde{+}}(t)e^{\int_0^t \lambda^{\tilde{+}}(t')dt'}\left|\frac{dv^{\tilde{+},R}(t)}{dt}\right\rangle - c^{\tilde{-}}(t)e^{\int_0^t \lambda^{\tilde{-}}(t')dt'}\left|\frac{dv^{\tilde{-},R}(t)}{dt}\right\rangle. \tag{F3}$$

After multiplying the above expression with $e^{-\int_0^t \tilde{\lambda}^{\tilde{\pm}}(t')dt'}\langle v^{\tilde{\pm},L}(t)|$ and taking into account the biorthonormality conditions $\langle v^{\tilde{\pm},L}(t)||v^{\tilde{\pm},R}(t)\rangle = 1$ and $\langle v^{\tilde{\mp},L}(t)||v^{\tilde{\pm},R}(t)\rangle = 0$ ($\langle v^{\tilde{\pm},L}(t)|$ represent the left eigenvectors of the continuous Hamiltonian system), it can be attained that

$$i\frac{dc^{\tilde{\pm}}(t)}{dt} = -c^{\tilde{\pm}}(t)\langle v^{\tilde{\pm},L}(t)|\left|i\frac{dv^{\tilde{\pm},R}(t)}{dt}\right\rangle - c^{\tilde{\mp}}(t)e^{\int_0^t(\tilde{\lambda}^{\tilde{\mp}}(t')-\tilde{\lambda}^{\tilde{\pm}}(t'))dt'}\langle v^{\tilde{\pm},L}(t)|\left|i\frac{dv^{\tilde{\mp},R}(t)}{dt}\right\rangle. \tag{F4}$$

The above formula is nothing but the continuous time counterpart of Eq. (21) given that at the limit $\Delta \to 0$ it will be true that $\prod_{j=0}^n(1+\Delta\tilde{\lambda}_j^{\tilde{\mp}})(1+\Delta\tilde{\lambda}_j^{\tilde{\pm}})^{-1} \simeq e^{\Delta\sum_{j=0}^n(\tilde{\lambda}_j^{\tilde{\mp}}-\tilde{\lambda}_j^{\tilde{\pm}})} \simeq e^{\int_0^t(\tilde{\lambda}^{\tilde{\mp}}(t')-\tilde{\lambda}^{\tilde{\pm}}(t'))dt'}$, where we also used the standard definition of Riemann sums. In other words, Eq. (21) of the main text generalizes Eq. (F4) to the discrete domain and in that manner allows for the presence of any abrupt discontinuities in the evolution of the system's eigenenergies/eigenvalues. The right-hand side of Eq. (F4) can be viewed as the overall contribution of an adiabatic and a nonadiabatic term [analogous terms were also recognized in Eq. (20) of Sec. III A, where the discrete evolution of the population dynamics was analyzed]. The generalized form of the *continuous time complex Berry phase* for non-Hermitian arrangements (see also [51–55]) becomes immediately recognizable as $\gamma^{\tilde{\pm}} = \int_0^T\langle v^{\tilde{\pm},L}(t)||i\,dv^{\tilde{\pm},R}(t)/dt\rangle dt = \oint_{\mathcal{C}^{\boldsymbol{\mathcal{R}}}}\langle v^{\tilde{\pm},L}(\boldsymbol{\mathcal{R}})||i\,\nabla_{\boldsymbol{\mathcal{R}}}v^{\tilde{\pm},R}(\boldsymbol{\mathcal{R}})\rangle d\boldsymbol{\mathcal{R}}$, where $T = N\Delta$ ($N \in \mathbb{N}$) is the period of evolution around the cyclic/closed path $\mathcal{C}^{\boldsymbol{\mathcal{R}}}$ in parameter space $\boldsymbol{\mathcal{R}}$. [The biorthonormality conditions $\langle v^{\tilde{\pm},L}(t)||v^{\tilde{\pm},R}(t)\rangle = 1$, $\langle v^{\tilde{\pm},L}(t)||v^{\tilde{\mp},R}(t)\rangle = 0$ are assumed.] This also reveals the geometric nature of Berry's phase, since it depends on the characteristics of the parametric trajectory $\mathcal{C}^{\boldsymbol{\mathcal{R}}}$, rather than the rate of encirclement. On the other hand, the *continuous dynamical phase factor* $e^{i\tau^{\tilde{\pm}}}$ [$= e^{\int_0^T\tilde{\lambda}^{\tilde{\pm}}(t)dt}$ for a single encirclement around $\mathcal{C}^{\boldsymbol{\mathcal{R}}}$] will evidently depend on how fast or slow the Hamiltonian varies with time. Under Hermitian conditions [$|v^{\tilde{\pm},L}(t)\rangle = |v^{\tilde{\pm},R}(t)\rangle = |v^{\tilde{\pm}}(t)\rangle$], the continuous Berry phase becomes purely real as the following chain of relations reveals (orthonormal conditions are assumed): $\langle v^{\tilde{\pm}}(t)||v^{\tilde{\pm}}(t)\rangle = 1 \Rightarrow d\langle v^{\tilde{\pm}}(t)||v^{\tilde{\pm}}(t)\rangle/dt = 0 \Leftrightarrow \langle dv^{\tilde{\pm}}(t)/dt||v^{\tilde{\pm}}(t)\rangle + \langle v^{\tilde{\pm}}(t)||dv^{\tilde{\pm}}(t)/dt\rangle = 0 \Leftrightarrow \mathrm{Im}(\gamma^{\tilde{\pm}}) = \int_0^T \mathrm{Im}[\langle v^{\tilde{\pm}}(t)||i\,dv^{\tilde{\pm}}(t)/dt\rangle]dt = 0$. Moreover, quantity $\gamma^{\tilde{\pm}}$ will then attain its standard form applicable to Hermitian settings [1–6] and the same will be true for the mode population dynamics depicted in Eq. (F4). [The dynamical phase over a period T retains the same expression $\tau^{\tilde{\pm}} = -i\int_0^T\tilde{\lambda}^{\tilde{\pm}}(t)dt$ for all continuous physical systems.]

Returning now to our discrete formulation, it becomes evident for discrete time Hermitian arrangements, whose Hamiltonian eigenspectra do not manifest any discontinuities [implying that mode notation ($\tilde{\pm}$) is in order here] that the respective discretely defined Berry phase $\gamma^{\tilde{\pm}} = \sum_{n=0}^{N-1}\gamma_{n+1,n}^{\tilde{\pm}}$ [see Eq. (22a) of Sec. III A and replace ($\hat{\pm}$) with ($\tilde{\pm}$)] will be predominantly real for sufficiently small time steps. (This can be inferred from the fact that in the limit $\Delta \to 0$ the discrete and continuous time versions of $\gamma^{\tilde{\pm}}$ become identical, as will be illustrated at the end of the present paragraph, and thus they will exhibit a similar behavior for small values of Δ.) Along these lines, only the real part of $\gamma^{\tilde{\pm}}$ in Eq. (22a) is of relevant interest, and the discrete Berry phase can then be equivalently expressed as $\mathrm{Im}(\sum_{n=0}^{N-1}\ln\langle v_{n+1}^{\tilde{\pm}}||v_n^{\tilde{\pm}}\rangle)$. Analogous results would have been attained, if the discrete contributions $\gamma_{n+1,n}^{\tilde{\pm}}$ were redefined according to $\gamma_{n+1,n}^{\tilde{\pm}} = -i\ln(\langle v_{n+1}^{\tilde{\pm}}||v_n^{\tilde{\pm}}\rangle/|\langle v_{n+1}^{\tilde{\pm}}||v_n^{\tilde{\pm}}\rangle|)$ [$= \mathrm{Im}(\ln\langle v_{n+1}^{\tilde{\pm}}||v_n^{\tilde{\pm}}\rangle)$]. Of course, in the general non-Hermitian case we expect a complex Berry phase, which implies that both the magnitude and phase of $\langle v_{n+1}^{\tilde{\pm},L}||v_n^{\tilde{\pm},R}\rangle$ ought to be considered. In this vein, the definition $\gamma_{n+1,n}^{\tilde{\pm}} = -i\ln\langle v_{n+1}^{\tilde{\pm},L}||v_n^{\tilde{\pm},R}\rangle$ becomes more appropriate (this applies for all mode notations used in this paper), with $\mathrm{Re}(\gamma_{n+1,n}^{\tilde{\pm}})$ denoting a discrete real phase accumulation (similar to conventional Hermitian systems) and $\mathrm{Im}(\gamma_{n+1,n}^{\tilde{\pm}})$ signifying a geometric multiplier both of which are gained by slowly cycled quantum states when the adiabatic approximation is valid [see Eqs. (23) and (24), along with discussion in Sec. III B and Appendix G]. Moreover, it should be noted that in the continuous time limit $\Delta \to 0$, it will hold that $\gamma_{n+1,n}^{\tilde{\pm}} = -i\ln\langle v_{n+1}^{\tilde{\pm},L}||v_n^{\tilde{\pm},R}\rangle = -i\ln[1-\Delta\langle v_{n+1}^{\tilde{\pm},L}||\delta v_n^{\tilde{\pm},R}/\delta t_n\rangle] \simeq \Delta\langle v_{n+1}^{\tilde{\pm},L}||i\,\delta v_n^{\tilde{\pm},R}/\delta t_n\rangle$. The resulting Berry phase expression turns out to be $\gamma^{\tilde{\pm}} \simeq \Delta\sum_{n=0}^{N-1}\langle v_{n+1}^{\tilde{\pm},L}||i\,\delta v_n^{\tilde{\pm},R}/\delta t_n\rangle \simeq \int_0^T\langle v^{\tilde{\pm},L}(t)||i\,dv^{\tilde{\pm},R}(t)/dt\rangle dt = \oint_{\mathcal{C}^{\boldsymbol{\mathcal{R}}}}\langle v^{\tilde{\pm},L}(\boldsymbol{\mathcal{R}})||i\,\nabla_{\boldsymbol{\mathcal{R}}}v^{\tilde{\pm},R}(\boldsymbol{\mathcal{R}})\rangle d\boldsymbol{\mathcal{R}}$, which is in perfect agreement with the respective formula developed in the previous paragraph for continuous quantum mechanical systems. (This proof also holds for the Hermitian case, with the only difference being that the left and right eigenvectors will then be conjugate transposes of each other at each time step.)

APPENDIX G: ADIABATIC APPROXIMATION IN DISCRETE QUANTUM HAMILTONIAN SETTINGS

In Sec. III B, particular emphasis was given on the state vector dynamics, when only the adiabatic terms in Eqs. (20) and (21) are considered. Here, we shall provide an extensive mathematical study as to when such an approximation (known as *adiabatic approximation*) becomes valid in discrete quantum systems, which will in turn lead us to Eq. (24) of Sec. III B [the notation ($\tilde{\pm}$) will be adopted in the present analysis in accordance to Sec. III B]. In this respect, the behavior of the nonadiabatic/cross-modulation term [this refers to the coefficient of the complex amplitude $c_n^{\tilde{\mp}}$ in Eq. (20), i.e., $\prod_{j=0}^n(1+\Delta\tilde{\lambda}_j^{\tilde{\mp}})$

$(1+\Delta\tilde{\lambda}_j^{\tilde{\pm}})^{-1}\langle v_{n+1}^{\tilde{\pm},L}||v_n^{\tilde{\mp},R}\rangle \simeq e^{\Delta\sum_{j=0}^{n}(\tilde{\lambda}_j^{\tilde{\mp}}-\tilde{\lambda}_j^{\tilde{\pm}})}\langle v_{n+1}^{\tilde{\pm},L}||v_n^{\tilde{\mp},R}\rangle \overset{\lambda_n=-i\lambda_{H_n}}{=} e^{-i\Delta\sum_{j=0}^{n}(\tilde{\lambda}_{H_j}^{\tilde{\mp}}-\tilde{\lambda}_{H_j}^{\tilde{\pm}})}\langle v_{n+1}^{\tilde{\pm},L}||v_n^{\tilde{\mp},R}\rangle]$ will be examined for both Hermitian and non-Hermitian arrangements in the limit of small time steps:

(1) λ_j *purely imaginary and* λ_{H_j} *purely real (Hermitian case)*. The cross-modulation term contains an exponential contribution, which has a harmonic time dependency. The faster this factor oscillates, the more the nonadiabatic contribution will become suppressed. This condition can be mathematically expressed as $|\tilde{\lambda}_j^{\tilde{\mp}}-\tilde{\lambda}_j^{\tilde{\pm}}| \gg |\langle v_{j+1}^{\tilde{\pm}}||v_j^{\tilde{\mp}}\rangle/\Delta|$ for all possible integer values of j ($|v_j^{\tilde{\pm},R}\rangle = |v_j^{\tilde{\pm},L}\rangle = |v_j^{\tilde{\pm}}\rangle$). After using the orthonormality relation $\langle v_{j+1}^{\tilde{\pm}}||v_{j+1}^{\tilde{\mp}}\rangle = 0$, the aforementioned constraint can also read as ($\delta t_j = \Delta$): $|\tilde{\lambda}_j^{\tilde{\mp}}-\tilde{\lambda}_j^{\tilde{\pm}}| \gg |\langle v_{j+1}^{\tilde{\pm}}||\delta v_j^{\tilde{\mp}}/\delta t_j\rangle| \propto 1/T \Rightarrow T \gg 1/|\tilde{\lambda}_j^{\tilde{\mp}}-\tilde{\lambda}_j^{\tilde{\pm}}|$ with $T = N\Delta$ being the period of cyclic evolution around $\mathcal{C}^{\mathcal{R}}$. (The larger T is, the slower $|v_j\rangle$ will change with time or equivalently $|\delta v_j^{\tilde{\mp}}/\delta t_j\rangle \propto 1/T$.) This implies that the system parameters must vary very slowly in time with respect to the typical quantum mechanical oscillating frequencies (slow driving conditions), and consequently no transitions can be excited between any energy levels.

(2) λ_j *and* λ_{H_j} *defined over the complex plane (non-Hermitian case)*. The cross-modulation term will now develop an exponential factor with magnitude different from unity [$\mathrm{Re}(\tilde{\lambda}_j^{\tilde{\mp}}-\tilde{\lambda}_j^{\tilde{\pm}}) \neq 0$]. In this case, the nonadiabatic contribution in Eq. (20) [or Eq. (21)] can be safely neglected, only if the population dynamics of the *dominant mode* are considered [mode $(\tilde{\pm})$ becomes dominant iff $\mathrm{Re}(\Delta\tilde{\lambda}_j^{\tilde{\pm}}) \geqslant \mathrm{Re}(\Delta\tilde{\lambda}_j^{\tilde{\mp}}) \overset{\Delta>0}{\Rightarrow} \mathrm{Re}(\tilde{\lambda}_j^{\tilde{\pm}}) \geqslant \mathrm{Re}(\tilde{\lambda}_j^{\tilde{\mp}})$ along trajectory $\mathcal{C}^{\mathcal{R}}$, with the equality not holding simultaneously for all operation points]. For instance, if we assume that eigenmode $(\tilde{+})$ plays the dominant role, then the respective nonadiabatic coefficient is expected to rapidly decay to zero for large evolution times as long as $|\tilde{\lambda}_j^{\tilde{-}}-\tilde{\lambda}_j^{\tilde{+}}| \gg |\langle v_{j+1}^{\tilde{+},L}||v_j^{\tilde{-},R}\rangle/\Delta|$. Indeed, the latter condition requires that either $\mathrm{Re}[\Delta(\tilde{\lambda}_j^{\tilde{+}}-\tilde{\lambda}_j^{\tilde{-}})] \gg |\langle v_{j+1}^{\tilde{+},L}||v_j^{\tilde{-},R}\rangle|$ [in this case, the exponential factor $e^{\Delta(\tilde{\lambda}_j^{\tilde{-}}-\tilde{\lambda}_j^{\tilde{+}})}$ will clearly dominate over $\langle v_{j+1}^{\tilde{+},L}||v_j^{\tilde{-},R}\rangle$] or $|\mathrm{Im}[\Delta(\tilde{\lambda}_j^{\tilde{+}}-\tilde{\lambda}_j^{\tilde{-}})]| \gg |\langle v_{j+1}^{\tilde{+},L}||v_j^{\tilde{-},R}\rangle|$ [this implies the fast oscillation frequency of $e^{\Delta(\tilde{\lambda}_j^{\tilde{-}}-\tilde{\lambda}_j^{\tilde{+}})}$ and thus the applicability of the analysis in (a)], which in turn leads irrevocably to $e^{\Delta\sum_{j=0}^{n}(\tilde{\lambda}_j^{\tilde{-}}-\tilde{\lambda}_j^{\tilde{+}})}\langle v_{n+1}^{\tilde{+},L}||v_n^{\tilde{-},R}\rangle \to 0$. A similar rationale will also hold, if eigenstate $(\tilde{-})$ becomes dominant along $\mathcal{C}^{\mathcal{R}}$.

Therefore, we can conclude that for a generalized quantum Hamiltonian system, *the condition for adiabatic evolution* can always be expressed as

$$\left|\tilde{\lambda}_n^{\tilde{\mp}}-\tilde{\lambda}_n^{\tilde{\pm}}\right| \gg \left|\frac{\langle v_{n+1}^{\tilde{\pm},L}||v_n^{\tilde{\mp},R}\rangle}{\delta t_n}\right| = \left|\langle v_{n+1}^{\tilde{\pm},L}|\left|i\frac{\delta v_n^{\tilde{\mp},R}}{\delta t_n}\right\rangle\right|, \tag{G1}$$

and must be true for every point along the discrete trajectory $\mathcal{C}^{\mathcal{R}}$. (The biorthonormality relation $\langle v_{n+1}^{\tilde{\pm},L}||v_{n+1}^{\tilde{\mp},R}\rangle = 0$ has been used in the above relation.) It should be noted that the limitations of the adiabatic condition, as depicted in Eq. (G1) [or Eq. (24) in the main text], have been discussed in Sec. III B in the context of both eigenspectrum degeneracy points ($\tilde{\lambda}_n^{+} = \tilde{\lambda}_n^{-}$) and of modes, which do not retain their dominant role under non-Hermitian evolution.

Finally, we shall prove an important formula relating the time variation of the eigenvectors with the time variation of the system matrix M_n (see Sec. II A for definition of M_n). A similar relationship will also apply for the Hamiltonian matrix H_n, since $M_n = -iH_n$, which in turn implies that (i) $\tilde{\lambda}_n^{\tilde{\mp}} = -i\tilde{\lambda}_{H_n}^{\tilde{\mp}}$, and (ii) M_n and H_n share the same left and right eigenvectors. Along these lines, the following chain of relations will apply

$$\begin{aligned} M_n\left|v_n^{\tilde{\mp},R}\right\rangle = \tilde{\lambda}_n^{\tilde{\mp}}\left|v_n^{\tilde{\mp},R}\right\rangle &\Rightarrow \delta\left(M_n\left|v_n^{\tilde{\mp},R}\right\rangle\right) = \delta\left(\tilde{\lambda}_n^{\tilde{\mp}}\left|v_n^{\tilde{\mp},R}\right\rangle\right) \\ &\overset{\Delta\to 0}{\Longrightarrow} M_{n+1}\left|\delta v_n^{\tilde{\mp},R}\right\rangle + \delta M_n\left|v_{n+1}^{\tilde{\mp},R}\right\rangle = \tilde{\lambda}_{n+1}^{\tilde{\mp}}\left|\delta v_n^{\tilde{\mp},R}\right\rangle \\ &\quad + \delta\tilde{\lambda}_n^{\tilde{\mp}}\left|v_{n+1}^{\tilde{\mp},R}\right\rangle, \end{aligned} \tag{G2}$$

where we have exploited relation $\delta(w_n q_n) = w_{n+1}\delta q_n + \delta w_n q_{n+1} - \delta w_n \delta q_n \overset{\Delta\to 0}{=\!=} w_{n+1}\delta q_n + \delta w_n q_{n+1}$ ($w_n\, q_n$ represent arbitrary discrete time variables) and at the limit $\Delta \to 0$ we have omitted any second-order (Δ^2) contributions. After multiplying (from the left) both the left- and right-hand sides of Eq. (G2) with $\langle v_{n+1}^{\tilde{\pm},L}|$ and based on relations $\langle v_{n+1}^{\tilde{\pm},L}|M_n = \tilde{\lambda}_{n+1}^{\tilde{\pm}}\langle v_{n+1}^{\tilde{\pm},L}|$ and $\langle v_{n+1}^{\tilde{\pm},L}||v_{n+1}^{\tilde{\mp},R}\rangle = 0$, it can be deduced that ($\delta t_n = \Delta$),

$$\begin{aligned} &\tilde{\lambda}_{n+1}^{\tilde{\pm}}\left\langle v_{n+1}^{\tilde{\pm},L}\middle|\middle|\delta v_n^{\tilde{\mp},R}\right\rangle + \left\langle v_{n+1}^{\tilde{\pm},L}\middle|\delta M_n\middle|v_{n+1}^{\tilde{\mp},R}\right\rangle = \tilde{\lambda}_{n+1}^{\tilde{\mp}}\left\langle v_{n+1}^{\tilde{\pm},L}\middle|\middle|\delta v_n^{\tilde{\mp},R}\right\rangle \\ &\overset{\Delta\to 0}{\Longleftrightarrow} \left\langle v_{n+1}^{\tilde{\pm},L}\middle|\middle|i\frac{\delta v_n^{\tilde{\mp},R}}{\delta t_n}\right\rangle = \frac{\left\langle v_{n+1}^{\tilde{\pm},L}\middle|i\frac{\delta M_n}{\delta t_n}\middle|v_{n+1}^{\tilde{\mp},R}\right\rangle}{\tilde{\lambda}_n^{\tilde{\mp}}-\tilde{\lambda}_n^{\tilde{\pm}}}. \end{aligned} \tag{G3}$$

Equations (G1) and (G3) complete now the proof of Eq. (24) [the approximate sign appearing in Eq. (24) is attributed to the fact that the discrete step Δ is small but not infinitesimal in the main text analysis] and with that our discussion on the adiabatic condition/approximation in the present Appendix.

APPENDIX H: STATE VECTOR DYNAMICS EXPRESSED IN TERMS OF THE $\mathcal{P}, \mathcal{N}$ MODES

As a first step in our analysis, we shall show how the mathematical framework provided in Sec. III A [see Eqs. (18)–(21)] to describe the state vector dynamics [which in Sec. III B was applied to the specific case of the $(\tilde{\pm})$ mode representation] is essentially equivalent to that of Sec. III C [see Eqs. (25) and (26)], with the latter being simply a matrix reformulation of the former. We shall use here the (generic) notation $(\hat{\pm})$, which as described in Sec. III A of the main text may represent any of the mode notations $(\pm)$, $(\tilde{\pm})$, and $\mathcal{P}, \mathcal{N}$

used in the present paper (see Fig. 4 for their definition and respective eigenspectra plots). In this regard, it will be true for the quantum mechanical state vector that $|u_{n+1}\rangle = \Xi_n|u_n\rangle = V_n^{\hat{\pm},R} D_{\Xi_n}^{\hat{\pm}} (V_n^{\hat{\pm},L})^{\dagger}|u_n\rangle$ based on the definition of the evolution matrix Ξ_n in Sec. II A [see Eq. (1)] and its eigendecomposition according to $\Xi_n = V_n^{\hat{\pm},R} D_{\Xi_n}^{\hat{\pm}} (V_n^{\hat{\pm},L})^{\dagger}$, where $V_n^{\hat{\pm},R} = [|v_n^{\hat{+},R}\rangle \ |v_n^{\hat{-},R}\rangle]$ (i.e., matrix $V_n^{\hat{\pm},R}$ contains in its columns the right eigenvectors of Ξ_n), $V_n^{\hat{\pm},L} = [|v_n^{\hat{+},L}\rangle \ |v_n^{\hat{-},L}\rangle]$ [i.e., matrix $(V_n^{\hat{\pm},L})^{\dagger}$ contains in its rows the left eigenvectors of Ξ_n], and $D_{\Xi_n}^{\hat{\pm}}$ is a diagonal matrix with elements the eigenvalues $\lambda_{\Xi_n}^{\hat{\pm}}$ of Ξ_n. [In Eq. (25) of Sec. III C an analogous decomposition is performed but in terms of the $\mathcal{P},\mathcal{N}$ modes, i.e., matrices V_n^R, D_{Ξ_n}, V_n^L in Sec. III C refer specifically to the $\mathcal{P},\mathcal{N}$ mode decomposition, while here matrices $V_n^{\hat{\pm},R}, D_{\Xi_n}^{\hat{\pm}}, V_n^{\hat{\pm},L}$ refer to the decomposition according to the generic mode formalism ($\hat{\pm}$).] Consequently, the following relation will also apply

$$\begin{aligned}\big(V_{n+1}^{\hat{\pm},L}\big)^{\dagger}|u_{n+1}\rangle &= \big(V_{n+1}^{\hat{\pm},L}\big)^{\dagger} V_n^{\hat{\pm},R} D_{\Xi_n}^{\hat{\pm}} \big(V_n^{\hat{\pm},L}\big)^{\dagger}|u_n\rangle \\ &= \mathcal{L}_n^{\hat{\pm}} \big(V_n^{\hat{\pm},L}\big)^{\dagger}|u_n\rangle, \end{aligned} \tag{H1}$$

where $\mathcal{L}_n^{\hat{\pm}} = (V_{n+1}^{\hat{\pm},L})^{\dagger} V_n^{\hat{\pm},R} D_{\Xi_n}^{\hat{\pm}}$ takes the matrix form

$$\mathcal{L}_n^{\hat{\pm}} = \begin{bmatrix} \lambda_{\Xi_n}^{\hat{+}} \langle v_{n+1}^{\hat{+},L} || v_n^{\hat{+},R}\rangle & \lambda_{\Xi_n}^{\hat{-}} \langle v_{n+1}^{\hat{+},L} || v_n^{\hat{-},R}\rangle \\ \lambda_{\Xi_n}^{\hat{+}} \langle v_{n+1}^{\hat{-},L} || v_n^{\hat{+},R}\rangle & \lambda_{\Xi_n}^{\hat{-}} \langle v_{n+1}^{\hat{-},L} || v_n^{\hat{-},R}\rangle \end{bmatrix}. \tag{H2}$$

On the other hand, according to Eq. (18) of Sec. III A, state vector $|u_n\rangle$ can be expressed as follows:

$$|u_n\rangle = c_n^{\hat{+}} \prod_{j=0}^{n-1} \lambda_{\Xi_j}^{\hat{+}} |v_n^{\hat{\pm},R}\rangle + c_n^{\hat{-}} \prod_{j=0}^{n-1} \lambda_{\Xi_j}^{\hat{-}} |v_n^{\hat{-},R}\rangle. \tag{H3}$$

This implies for the product $(V_n^{\hat{\pm},L})^{\dagger}|u_n\rangle$ that

$$\begin{bmatrix} c_n^{\hat{+}} \prod_{j=0}^{n-1} \lambda_{\Xi_j}^{\hat{+}} \langle v_n^{\hat{+},L} || v_n^{\hat{+},R}\rangle + c_n^{\hat{-}} \prod_{j=0}^{n-1} \lambda_{\Xi_j}^{\hat{-}} \langle v_n^{\hat{+},L} || v_n^{\hat{-},R}\rangle \\ c_n^{\hat{+}} \prod_{j=0}^{n-1} \lambda_{\Xi_j}^{\hat{+}} \langle v_n^{\hat{-},L} || v_n^{\hat{+},R}\rangle + c_n^{\hat{-}} \prod_{j=0}^{n-1} \lambda_{\Xi_j}^{\hat{-}} \langle v_n^{\hat{-},L} || v_n^{\hat{-},R}\rangle \end{bmatrix},$$

which after assuming biorthonormality conditions [$\langle v_n^{\hat{\pm},L}| |v_n^{\hat{\pm},R}\rangle = 1$, $\langle v_n^{\hat{\pm},L}||v_n^{\hat{\mp},R}\rangle = 0$ or equivalently $(V_n^{\hat{\pm},L})^{\dagger} V_n^{\hat{\pm},R} = (V_n^{\hat{\pm},R})^{\dagger} V_n^{\hat{\pm},L} = I$; see also Appendix F] takes the form

$$\big(V_n^{\hat{\pm},L}\big)^{\dagger}|u_n\rangle = \begin{bmatrix} c_n^{\hat{+}} \prod_{j=0}^{n-1} \lambda_{\Xi_j}^{\hat{+}} \\ c_n^{\hat{-}} \prod_{j=0}^{n-1} \lambda_{\Xi_j}^{\hat{-}} \end{bmatrix}. \tag{H4}$$

Based now on Eqs. (H1), (H2), and (H4), it becomes apparent that ($\Xi_n = I + \Delta M_n$ and thus $\lambda_{\Xi_n}^{\hat{\pm}} = 1 + \Delta\lambda_n^{\hat{\pm}}$, where $\lambda_n^{\hat{\pm}}$ are the eigenvalues of the quantum system's matrix M_n as defined in Sec. II A)

$$c_{n+1}^{\hat{\pm}} = c_n^{\hat{\pm}} \langle v_{n+1}^{\hat{\pm},L} || v_n^{\hat{\pm},R}\rangle + c_n^{\hat{\mp}} \prod_{j=0}^{n} \frac{1 + \Delta\lambda_j^{\hat{\mp}}}{1 + \Delta\lambda_j^{\hat{\pm}}} \langle v_{n+1}^{\hat{\pm},L} || v_n^{\hat{\mp},R}\rangle, \tag{H5}$$

which confirms Eq. (20) [or equivalently Eq. (21)] of Sec. III A and indicates that the mathematical descriptions provided in Secs. III A and III C regarding the state vector dynamics are in essence equivalent [the only difference is that the former section refers to the generic mode notation ($\hat{\pm}$), while in the latter the specific case of the $\mathcal{P},\mathcal{N}$ eigenmodes is examined]. In the latter section, the matrix formalism [i.e., Eqs. (25) and (26)] is preferred since it leads to a more direct and neat proof of the state conversion taking place in sufficiently slowly varying, cyclic, and discrete non-Hermitian environments. Of course we assume that no eigenspectrum degeneracies are crossed, otherwise the eigendecomposition of the evolution matrix as $\Xi_n = V_n^{\hat{\pm},R} D_{\Xi_n}^{\hat{\pm}} (V_n^{\hat{\pm},L})^{\dagger}$ with $D_{\Xi_n}^{\hat{\pm}}$ being diagonal would not apply, and as a result our analysis would need to be modified accordingly [in this case Ξ_n should be decomposed in terms of its Jordan canonical form and the respective Jordan chain of generalized (and linearly independent) eigenvectors]. Along these lines, the expansion for the state vector as demonstrated in Eq. (H3) [or Eq. (18) in the main text] would also not be feasible, since at the exceptional degeneracy points (which characterize non-Hermitian structures) the eigenvectors will coalesce (see Appendices B 2 and F) and thus will not span the complex Hilbert space formed by the state vectors of the quantum Hamiltonian system.

At this point, we will provide supplementary proofs regarding the analytical derivation of state conversion demonstrated in Sec. III C 2, where the case of $\mathcal{P},\mathcal{N}$ modes exhibiting discontinuous eigenspectra evolution was studied. The introduction of the instantaneous dominant ($\mathcal{P}$) and nondominant ($\mathcal{N}$) modes (which is justified only for non-Hermitian Hamiltonian arrangements as explained in the beginning of Sec. III C), was necessary in order to obtain a simplified form for matrix $\mathcal{F}$ [see Eq. (34)] originally defined in Eq. (26) [see also equivalent expression for $\mathcal{F}$ in Eq. (30) used in the derivation of Sec. III C 2, when an eigenspectrum discontinuity point exists]. In this vein, we will initially emphasize on the form of the products $(V_{n+1}^L)^{\dagger} V_n^R$ as illustrated in Eq. (31), by also taking advantage of the formalism introduced so far. More specifically, it will be true that

$$\begin{aligned}\big(V_{n+1}^L\big)^{\dagger} V_n^R &= \begin{bmatrix} \langle v_{n+1}^{\mathcal{P},L}| \\ \langle v_{n+1}^{\mathcal{N},L}| \end{bmatrix} \big[|v_n^{\mathcal{P},R}\rangle \quad |v_n^{\mathcal{N},R}\rangle\big] \\ &= \begin{bmatrix} \langle v_{n+1}^{\mathcal{P},L} || v_n^{\mathcal{P},R}\rangle & \langle v_{n+1}^{\mathcal{P},L} || v_n^{\mathcal{N},R}\rangle \\ \langle v_{n+1}^{\mathcal{N},L} || v_n^{\mathcal{P},R}\rangle & \langle v_{n+1}^{\mathcal{N},L} || v_n^{\mathcal{N},R}\rangle \end{bmatrix}, \end{aligned} \tag{H6}$$

where here of course (and for the remaining analysis of Appendix H) we use exclusively the $\mathcal{P},\mathcal{N}$ mode notation. If we assume now that only a single eigenvalue "jump" happens at $n = \overline{n_o}$ (i.e., from $n = \overline{n_o}$ to $n = \overline{n_o} + 1$) within the $\mathcal{P},\mathcal{N}$ complex eigenspectrum domain, then for $n \in [0, \overline{n_o}) \cup [\overline{n_o}, N)$—$N \in \mathbb{N}$ corresponds to a complete cyclic evolution in parameter space as also schematically

shown in Fig. 5(a) of the main text—it is easy to see that $\langle v_{n+1}^{\mathcal{P},L}||v_n^{\mathcal{P},R}\rangle \xrightarrow{\Delta\to 0} \langle v_n^{\mathcal{P},L}||v_n^{\mathcal{P},R}\rangle = 1$ and $\langle v_{n+1}^{\mathcal{P},L}||v_n^{\mathcal{N},R}\rangle \xrightarrow{\Delta\to 0} \langle v_n^{\mathcal{P},L}||v_n^{\mathcal{N},R}\rangle = 0$ given the biorthonormality conditions associated with the $\mathcal{P},\mathcal{N}$ modes ($\langle v_n^{\mathcal{P},L}|v_n^{\mathcal{P},R}\rangle = \langle v_n^{\mathcal{N},L}|v_n^{\mathcal{N},R}\rangle = 1$, $\langle v_n^{\mathcal{P},L}|v_n^{\mathcal{N},R}\rangle = \langle v_n^{\mathcal{N},L}|v_n^{\mathcal{P},R}\rangle = 0$ as also illustrated in the beginning of Sec. III C). In other words, for such a range of values for n we can perform the assignments $\langle v_{n+1}^{\mathcal{P},L}||v_n^{\mathcal{P},R}\rangle = p_n^{11}(\Delta)$ and $\langle v_{n+1}^{\mathcal{P},L}||v_n^{\mathcal{N},R}\rangle = \Delta p_n^{12}(\Delta)$, with functions $p_n^{11}(\Delta)$, $p_n^{12}(\Delta)$ being both analytical in the neighborhood of $\Delta = 0$ and $p_n^{11}(\Delta = 0) = 1$. In a completely analogous manner, assignments $\langle v_{n+1}^{\mathcal{N},L}||v_n^{\mathcal{P},R}\rangle = \Delta p_n^{21}(\Delta)$ and $\langle v_{n+1}^{\mathcal{N},L}||v_n^{\mathcal{N},R}\rangle = p_n^{22}(\Delta)$ can be performed, with $p_n^{21}(\Delta)$, $p_n^{22}(\Delta)$ being both analytical in the neighborhood of $\Delta = 0$ and $p_n^{22}(\Delta = 0) = 1$.

The situation becomes now different for $n = \overline{n_o}$, i.e., the following will be true: $\langle v_{\overline{n_o}+1}^{\mathcal{P},L}||v_{\overline{n_o}}^{\mathcal{P},R}\rangle \xrightarrow{\Delta\to 0} \langle v_{\overline{n_o}}^{\mathcal{N},L}||v_{\overline{n_o}}^{\mathcal{P},R}\rangle = 0$, $\langle v_{\overline{n_o}+1}^{\mathcal{P},L}||v_{\overline{n_o}}^{\mathcal{N},R}\rangle \xrightarrow{\Delta\to 0} \langle v_{\overline{n_o}}^{\mathcal{N},L}||v_{\overline{n_o}}^{\mathcal{N},R}\rangle = 1$, $\langle v_{\overline{n_o}+1}^{\mathcal{N},L}||v_{\overline{n_o}}^{\mathcal{P},R}\rangle \xrightarrow{\Delta\to 0} \langle v_{\overline{n_o}}^{\mathcal{P},L}||v_{\overline{n_o}}^{\mathcal{P},R}\rangle = 1$, $\langle v_{\overline{n_o}+1}^{\mathcal{N},L}||v_{\overline{n_o}}^{\mathcal{N},R}\rangle \xrightarrow{\Delta\to 0} \langle v_{\overline{n_o}}^{\mathcal{P},L}||v_{\overline{n_o}}^{\mathcal{N},R}\rangle = 0$. (To better comprehend how the presence of discontinuities in the $\mathcal{P},\mathcal{N}$ eigenspectra evolution affects the behavior of the respective eigenvectors, refer to Fig. 4 and Sec. III C 2 within the main text.) Hence now it will apply that $\langle v_{\overline{n_o}+1}^{\mathcal{P},L}||v_{\overline{n_o}}^{\mathcal{P},R}\rangle = \Delta p_{\overline{n_o}}^{21}(\Delta)$, $\langle v_{\overline{n_o}+1}^{\mathcal{P},L}||v_{\overline{n_o}}^{\mathcal{N},R}\rangle = p_{\overline{n_o}}^{22}(\Delta)$, $\langle v_{\overline{n_o}+1}^{\mathcal{N},L}||v_{\overline{n_o}}^{\mathcal{P},R}\rangle = p_{\overline{n_o}}^{11}(\Delta)$, $\langle v_{\overline{n_o}+1}^{\mathcal{N},L}||v_{\overline{n_o}}^{\mathcal{N},R}\rangle = \Delta p_{\overline{n_o}}^{12}(\Delta)$, where functions $p_{\overline{n_o}}^{jk}(\Delta)$ with $j,k = 1,2$ are all analytical in the vicinity of $\Delta = 0$ and $p_{\overline{n_o}}^{11}(\Delta = 0) = p_{\overline{n_o}}^{22}(\Delta = 0) = 1$. This differentiation in the behavior of the matrix products $(V_{n+1}^L)^\dagger V_n^R$ for $n \in [0, \overline{n_o}) \cup [\overline{n_o}, N)$ and $n = \overline{n_o}$ can be summarized as follows:

$$\left(V_{n+1}^L\right)^\dagger V_n^R = \begin{cases} \begin{bmatrix} p_n^{11} & \Delta p_n^{12} \\ \Delta p_n^{21} & p_n^{22} \end{bmatrix}, & n \neq \overline{n_o}, \\ \begin{bmatrix} \Delta p_{\overline{n_o}}^{21} & p_{\overline{n_o}}^{22} \\ p_{\overline{n_o}}^{11} & \Delta p_{\overline{n_o}}^{12} \end{bmatrix}, & n = \overline{n_o}. \end{cases} \tag{H7}$$

As a next step in our analysis, we shall show how the expression for matrix $\mathcal{F}^{(l)}$ presented in Eq. (32) of Sec. III C 2 is retrieved and also provide some additional details as to the different coefficients appearing in such formula. Superscript (l) can be either (α) or (β) depending on whether it refers to the parametric trajectory just before (i.e., path $\mathcal{C}_\alpha^{\mathcal{R}}$) or just after (i.e., path $\mathcal{C}_\beta^{\mathcal{R}}$) the spectrum discontinuity. Paths $\mathcal{C}_\alpha^{\mathcal{R}}$ and $\mathcal{C}_\beta^{\mathcal{R}}$ are each free of any underlying eigenvalue "jumps", according also to our assumption of the presence of only a single $\mathcal{P},\mathcal{N}$ eigenspectrum discontinuity as the discrete Hamiltonian arrangement cyclically evolves along the closed (and discretely defined) path $\mathcal{C}^{\mathcal{R}} = \mathcal{C}_\beta^{\mathcal{R}} \cup \mathcal{C}_\alpha^{\mathcal{R}}$ (direction of encirclement $\mathcal{C}_\alpha^{\mathcal{R}} \to \mathcal{C}_\beta^{\mathcal{R}}$). In order to facilitate our proof of Eq. (32) by the method of induction, we shall use here a slightly different notation than Sec. III C 2, i.e., $\mathcal{F}^{(l)} \to \mathcal{F}^{n_e,n_o}$, $c_{\mathcal{P},\mathcal{N}}^{(l)} \to c_{\mathcal{P},\mathcal{N}}^{n_e,n_o}$, $f_j^{(l)} \to f_j^{n_e,n_o}$, $r_{jk}^{(l)} \to r_{jk}^{n_e,n_o}$ $(c_\nu^{(l)} \to c_\nu^{n_e,n_o}$, $h_{\nu,jk}^{(l)} \to h_{\nu,jk}^{n_e,n_o})$ with $j,k = 1,2$ and n_o, n_e denoting the starting and ending points ($n_e \geqslant n_o \wedge n_o$, $n_e \in \mathbb{N}$) of the discrete path to which $\mathcal{F}^{(l)}$ corresponds to; in our case, such path is either $\mathcal{C}_\alpha^{\mathcal{R}}$ ($n_o = 0$, $n_e = \overline{n_o}$) or $\mathcal{C}_\beta^{\mathcal{R}}$ ($n_o = \overline{n_o} + 1$, $n_e = N - 1$). Since evolution along either $\mathcal{C}_\alpha^{\mathcal{R}}$ or $\mathcal{C}_\beta^{\mathcal{R}}$ is characterized by the absence of any spectrum discontinuities, the following definitions will be employed in the upcoming derivation: $\langle v_{n+1}^{\mathcal{P},L}||v_n^{\mathcal{P},R}\rangle = p_n^{11}(\Delta)$, $\langle v_{n+1}^{\mathcal{P},L}||v_n^{\mathcal{N},R}\rangle = \Delta p_n^{12}(\Delta)$, $\langle v_{n+1}^{\mathcal{N},L}||v_n^{\mathcal{P},R}\rangle = \Delta p_n^{21}(\Delta)$, $\langle v_{n+1}^{\mathcal{N},L}||v_n^{\mathcal{P},R}\rangle = p_n^{22}(\Delta)$ where $n \in [n_o, n_e)$. Equation (32) will now assume the subsequent form

$$\mathcal{F}^{n_e,n_o} = \begin{bmatrix} c_{\mathcal{P}}^{n_e,n_o} f_1^{n_e,n_o} + \Delta\lambda_{\Xi_{n_e}}^{\mathcal{P}} r_{11}^{n_e,n_o} & \Delta\lambda_{\Xi_{n_e}}^{\mathcal{P}} r_{12}^{n_e,n_o} \\ \Delta\lambda_{\Xi_{n_e}}^{\mathcal{N}} r_{21}^{n_e,n_o} & c_{\mathcal{N}}^{n_e,n_o} f_2^{n_e,n_o} + \Delta\lambda_{\Xi_{n_e}}^{\mathcal{N}} r_{22}^{n_e,n_o} \end{bmatrix}, \tag{H8}$$

where all quantities refer of course to the $\mathcal{P},\mathcal{N}$ modes. The various discrete variables appearing in the aforementioned equation are defined as $c_{\mathcal{P}}^{n_e,n_o} = \prod_{n=n_o}^{n_e} \lambda_{\Xi_n}^{\mathcal{P}}$, $c_{\mathcal{N}}^{n_e,n_o} = \prod_{n=n_o}^{n_e} \lambda_{\Xi_n}^{\mathcal{N}}$, $f_1^{n_e,n_o} = \prod_{n=n_o}^{n_e-1} p_n^{11}$, $f_2^{n_e,n_o} = \prod_{n=n_o}^{n_e-1} p_n^{22}$, $r_{jk}^{n_e,n_o} = \sum_{\nu=1}^{2^{n_e-n_o}} c_\nu^{n_e,n_o} h_{\nu,jk}^{n_e,n_o}$ $(j,k = 1,2)$ with $c_\nu^{n_e,n_o} = c_{s_\nu^{n_e,n_o}} = \prod_{n=n_o}^{n_e-1} \lambda_{\Xi_n}^{s_n^\nu}$ and $\boldsymbol{s}_\nu^{n_e,n_o} \in \{(s_{n_e-1}^\nu, \ldots, s_{n_o}^\nu) | s_n^\nu = \mathcal{P} \text{ or } \mathcal{N},\ n \in \mathbb{N} \wedge n \in [n_o, n_e), \nu \in \mathbb{Z}^+ \wedge \nu \in [1, 2^{n_e-n_o}]\}$. If $n_e = n_o$, then we set $r_{jk}^{n_o,n_o} \equiv 0$ and $f_j^{n_o,n_o} \equiv 1$ for all possible values of j, k. It is of interest at this point to highlight the close relevance between coefficients $c_{\mathcal{P}}^{n_e,n_o}$, $c_{\mathcal{N}}^{n_e,n_o}$ and the discrete dynamical phase factors pertaining to the (non)dominant eigenmodes of the non-Hermitian quantum Hamiltonian, according to the more generalized definition of Eq. (22b) in Sec. III A [of course, the generic mode designation $(\hat{\pm})$ needs to be substituted with the $\mathcal{P},\mathcal{N}$ mode notation in Eq. (22b)]. On the other hand, terms $f_1^{n_e,n_o}$, $f_2^{n_e,n_o}$ can be directly associated with the discrete Berry phase factors pertaining to the $\mathcal{P},\mathcal{N}$ eigenmodes, according to the generalized definition of Eq. (22a).

In our analysis, the convention $s_n^1 = \mathcal{P}$, $s_n^2 = \mathcal{N}$ for $0 \leqslant n < N - 1$ shall be employed (i.e., $c_1^{n_e,n_o} = \prod_{n=n_o}^{n_e-1} \lambda_{\Xi_n}^{\mathcal{P}}$, $c_2^{n_e,n_o} = \prod_{n=n_o}^{n_e-1} \lambda_{\Xi_n}^{\mathcal{N}}$), which allows us to set $h_{1,11}^{n_e,n_o} = h_{2,22}^{n_e,n_o} = 0$. This becomes apparent after considering the diagonal entries of matrix $\mathcal{F}^{n_e,n_o}$: $\Delta\lambda_{\Xi_{n_e}}^{\mathcal{P}} r_{11}^{n_e,n_o} = \Delta\lambda_{\Xi_{n_e}}^{\mathcal{P}} \sum_\nu c_\nu^{n_e,n_o} h_{\nu,11}^{n_e,n_o} \xrightarrow{\nu=1} \Delta\lambda_{\Xi_{n_e}}^{\mathcal{P}} c_1^{n_e,n_o} h_{1,11}^{n_e,n_o} = \Delta \prod_{n=n_o}^{n_e} \lambda_{\Xi_n}^{\mathcal{P}} h_{1,11}^{n_e,n_o} = c_{\mathcal{P}}^{n_e,n_o} \Delta h_{1,11}^{n_e,n_o}$ and similarly $\Delta\lambda_{\Xi_{n_e}}^{\mathcal{N}} r_{22}^{n_e,n_o} = \Delta\lambda_{\Xi_{n_e}}^{\mathcal{N}} \sum_\nu c_\nu^{n_e,n_o} h_{\nu,22}^{n_e,n_o} \xrightarrow{\nu=2} \Delta\lambda_{\Xi_{n_e}}^{\mathcal{N}} c_2^{n_e,n_o} h_{2,22}^{n_e,n_o} = \Delta \prod_{n=n_o}^{n_e} \lambda_{\Xi_n}^{\mathcal{N}} h_{2,22}^{n_e,n_o} = c_{\mathcal{N}}^{n_e,n_o} \Delta h_{2,22}^{n_e,n_o}$. Yet, analogous terms of the form $c_{\mathcal{P}}^{n_e,n_o} f_1^{n_e,n_o}$ [$f_1^{n_e,n_o} = f_1^{n_e,n_o}(\Delta)$] and $c_{\mathcal{N}}^{n_e,n_o} f_2^{n_e,n_o}$ [$f_2^{n_e,n_o} = f_2^{n_e,n_o}(\Delta)$] have already been accounted for in Eq. (H8), which implies that both coefficients $h_{1,11}^{n_e,n_o}$, $h_{2,22}^{n_e,n_o}$ can be safely set to zero. In what follows, it will be also shown via the method of induction that $h_{1,12}^{n_e,n_o} = h_{1,22}^{n_e,n_o} = h_{2,11}^{n_e,n_o} = h_{2,21}^{n_e,n_o} = 0$. (This equivalently implies that the products $c_1^{n_e,n_o} = \prod_{n=n_o}^{n_e-1} \lambda_{\Xi_n}^{\mathcal{P}}$ and $c_2^{n_e,n_o} = \prod_{n=n_o}^{n_e-1} \lambda_{\Xi_n}^{\mathcal{N}}$ do not appear in the expressions of $r_{12}^{n_e,n_o}$, $r_{22}^{n_e,n_o}$ and $r_{11}^{n_e,n_o}$, $r_{21}^{n_e,n_o}$, respectively.)

The original definition of submatrix $\mathcal{F}^{n_e,n_o}$ stems from Eq. (30) of Sec. III C 2, which translates here as $\mathcal{F}^{n_e,n_o} = D_{\Xi_{n_e}} \prod_{n=n_o}^{n_e-1} (V_{n+1}^L)^\dagger V_n^R D_{\Xi_n} = D_{\Xi_{n_e}} \prod_{n=n_o}^{n_e-1} \mathcal{L}_n$ [$\mathcal{L}_n$ can be found from Eq. (H2) after replacing $(\hat{+}) \to \mathcal{P}$ and $(\hat{-}) \to \mathcal{N}$]. Hence the overall matrix $\mathcal{F}$ along the entire parametric loop $\mathcal{C}^{\mathcal{R}} = \mathcal{C}_\beta^{\mathcal{R}} \cup \mathcal{C}_\alpha^{\mathcal{R}}$ $(\mathcal{C}_\alpha^{\mathcal{R}} \to \mathcal{C}_\beta^{\mathcal{R}})$ will be given by

$\mathcal{F} = \mathcal{F}^{N-1,\overline{n_o}+1}[(V^L_{\overline{n_o}+1})^\dagger V^R_{\overline{n_o}}]\mathcal{F}^{\overline{n_o},0}$, where $\mathcal{F}^{\overline{n_o},0} = \mathcal{F}^{(\alpha)}$ and $\mathcal{F}^{N-1,\overline{n_o}+1} = \mathcal{F}^{(\beta)}$ according to the notation of Sec. III C 2 [see also Eq. (30)]. Based on the definition of $\mathcal{F}^{n_e,n_o}$, the recursive formula $\mathcal{F}^{n_e,n_o} = D_{\Xi_{n_e}}(V^L_{n_e})^\dagger V^R_{n_e-1}\mathcal{F}^{n_e-1,n_o}$ will also apply and shall prove essential in the following derivation.

We start our proof by induction for $n_e = n_o + 1$ [case $n_e = n_o$ corresponds to the trivial form $\mathcal{F}^{n_o,n_o} = D_{\Xi_{n_o}}$, which is indeed verified by Eq. (H8) given that $c^{n_o,n_o}_{\mathcal{P},\mathcal{N}} = \lambda^{\mathcal{P},\mathcal{N}}_{\Xi_{n_o}}$ and $r^{n_o,n_o}_{jk} = 0$, $f^{n_o,n_o}_j = 1$ for $j, k = 1, 2$]. It will be true then that $\mathcal{F}^{n_e,n_o} = D_{\Xi_{n_o+1}}\mathcal{L}_{n_o}$, which in turn leads to the expression

$$\mathcal{F}^{n_o+1,n_o} = \begin{bmatrix} \lambda^{\mathcal{P}}_{\Xi_{n_o+1}}\lambda^{\mathcal{P}}_{\Xi_{n_o}}p^{11}_{n_o} & \Delta\lambda^{\mathcal{P}}_{\Xi_{n_o+1}}\lambda^{\mathcal{N}}_{\Xi_{n_o}}p^{12}_{n_o} \\ \Delta\lambda^{\mathcal{N}}_{\Xi_{n_o+1}}\lambda^{\mathcal{P}}_{\Xi_{n_o}}p^{21}_{n_o} & \lambda^{\mathcal{N}}_{\Xi_{n_o+1}}\lambda^{\mathcal{N}}_{\Xi_{n_o}}p^{22}_{n_o} \end{bmatrix}. \tag{H9}$$

After comparing the aforementioned equation with Eq. (H8), it becomes apparent that $c^{n_o+1,n_o}_{\mathcal{P}} = \lambda^{\mathcal{P}}_{\Xi_{n_o+1}}\lambda^{\mathcal{P}}_{\Xi_{n_o}}$, $c^{n_o+1,n_o}_{\mathcal{N}} = \lambda^{\mathcal{N}}_{\Xi_{n_o+1}}\lambda^{\mathcal{N}}_{\Xi_{n_o}}$, $f^{n_o+1,n_o}_1 = p^{11}_{n_o}$, $f^{n_o+1,n_o}_2 = p^{22}_{n_o}$, while $r^{n_o+1,n_o}_{11} = r^{n_o+1,n_o}_{12} = r^{n_o+1,n_o}_{22} = 0$ and $r^{n_o+1,n_o}_{12} = \lambda^{\mathcal{N}}_{\Xi_{n_o}}p^{12}_{n_o}$, $r^{n_o+1,n_o}_{21} = \lambda^{\mathcal{P}}_{\Xi_{n_o}}p^{21}_{n_o}$. In this case, parameter $\nu = 1, 2$ and based on the aforementioned values of r^{n_o+1,n_o}_{jk}, it comes that $h^{n_o+1,n_o}_{1,11} = h^{n_o+1,n_o}_{1,12} = h^{n_o+1,n_o}_{1,22} = h^{n_o+1,n_o}_{2,11} = h^{n_o+1,n_o}_{2,21} = h^{n_o+1,n_o}_{2,22} = 0$ and also $h^{n_o+1,n_o}_{1,21} = p^{21}_{n_o}$, $h^{n_o+1,n_o}_{2,12} = p^{12}_{n_o}$ (of course $c^{n_o+1,n_o}_1 = \lambda^{\mathcal{P}}_{\Xi_{n_o}}$, $c^{n_o+1,n_o}_2 = \lambda^{\mathcal{N}}_{\Xi_{n_o}}$). In order to obtain an even better understanding of the form of the different discrete functions appearing in Eq. (H8), we also provide the form of matrix $\mathcal{F}^{n_o+2,n_o} = D_{\Xi_{n_0+2}}\mathcal{L}_{n_o+1}\mathcal{L}_{n_o}$ and this turns out to be

$$\mathcal{F}^{n_o+2,n_o} = \begin{bmatrix} \lambda^{\mathcal{P}}_{\Xi_{n_o+2}}\lambda^{\mathcal{P}}_{\Xi_{n_o+1}}\lambda^{\mathcal{P}}_{\Xi_{n_o}}\left(p^{11}_{n_o+1}p^{11}_{n_o}\right) & \Delta\lambda^{\mathcal{P}}_{\Xi_{n_o+2}}\left[\lambda^{\mathcal{P}}_{\Xi_{n_o+1}}\lambda^{\mathcal{N}}_{\Xi_{n_o}}\left(p^{11}_{n_o+1}p^{12}_{n_o}\right)\right. \\ \quad + \Delta\lambda^{\mathcal{P}}_{\Xi_{n_o+2}}\left[\lambda^{\mathcal{N}}_{\Xi_{n_o+1}}\lambda^{\mathcal{P}}_{\Xi_{n_o}}\left(\Delta p^{12}_{n_o+1}p^{21}_{n_o}\right)\right] & \quad \left. + \lambda^{\mathcal{N}}_{\Xi_{n_o+1}}\lambda^{\mathcal{N}}_{\Xi_{n_o}}\left(p^{12}_{n_o+1}p^{22}_{n_o}\right)\right] \\ \quad \Delta\lambda^{\mathcal{N}}_{\Xi_{n_o+2}}\left[\lambda^{\mathcal{P}}_{\Xi_{n_o+1}}\lambda^{\mathcal{P}}_{\Xi_{n_o}}\left(p^{21}_{n_o+1}p^{11}_{n_o}\right)\right. & \lambda^{\mathcal{N}}_{\Xi_{n_o+2}}\lambda^{\mathcal{N}}_{\Xi_{n_o+1}}\lambda^{\mathcal{N}}_{\Xi_{n_o}}\left(p^{22}_{n_o+1}p^{22}_{n_o}\right) \\ \quad \left. + \lambda^{\mathcal{N}}_{\Xi_{n_o+1}}\lambda^{\mathcal{P}}_{\Xi_{n_o}}\left(p^{11}_{n_o+1}p^{21}_{n_o}\right)\right] & \quad + \Delta\lambda^{\mathcal{N}}_{\Xi_{n_o+2}}\left[\lambda^{\mathcal{P}}_{\Xi_{n_o+1}}\lambda^{\mathcal{N}}_{\Xi_{n_o}}\left(\Delta p^{21}_{n_o+1}p^{12}_{n_o}\right)\right] \end{bmatrix}. \tag{H10}$$

The following quantities can now be identified: $c^{n_o+2,n_o}_{\mathcal{P}} = \lambda^{\mathcal{P}}_{\Xi_{n_o+2}}\lambda^{\mathcal{P}}_{\Xi_{n_o+1}}\lambda^{\mathcal{P}}_{\Xi_{n_o}}$, $c^{n_o+2,n_o}_{\mathcal{N}} = \lambda^{\mathcal{N}}_{\Xi_{n_o+2}}\lambda^{\mathcal{N}}_{\Xi_{n_o+1}}\lambda^{\mathcal{N}}_{\Xi_{n_o}}$, $f^{n_o+2,n_o}_1 = p^{11}_{n_o+1}p^{11}_{n_o}$, $f^{n_o+2,n_o}_2 = p^{22}_{n_o+1}p^{22}_{n_o}$. Regarding factors r^{n_o+2,n_o}_{jk}, it will be true according to Eq. (H10) that $r^{n_o+2,n_o}_{11} = \lambda^{\mathcal{N}}_{\Xi_{n_o+1}}\lambda^{\mathcal{P}}_{\Xi_{n_o}}(\Delta p^{12}_{n_o+1}p^{21}_{n_o})$, $r^{n_o+2,n_o}_{12} = \lambda^{\mathcal{P}}_{\Xi_{n_o+1}}\lambda^{\mathcal{N}}_{\Xi_{n_o}}(p^{11}_{n_o+1}p^{12}_{n_o}) + \lambda^{\mathcal{N}}_{\Xi_{n_o+1}}\lambda^{\mathcal{N}}_{\Xi_{n_o}}(p^{12}_{n_o+1}p^{22}_{n_o})$, $r^{n_o+2,n_o}_{21} = \lambda^{\mathcal{P}}_{\Xi_{n_o+1}}\lambda^{\mathcal{P}}_{\Xi_{n_o}}(p^{21}_{n_o+1}p^{11}_{n_o}) + \lambda^{\mathcal{N}}_{\Xi_{n_o+1}}\lambda^{\mathcal{P}}_{\Xi_{n_o}}(p^{11}_{n_o+1}p^{21}_{n_o})$, $r^{n_o+2,n_o}_{22} = \lambda^{\mathcal{P}}_{\Xi_{n_o+1}}\lambda^{\mathcal{N}}_{\Xi_{n_o}}(\Delta p^{21}_{n_o+1}p^{12}_{n_o})$. In other words, discrete variables r^{n_o+2,n_o}_{jk} are nothing but weighted sums [the weights— i.e., functions $h^{n_o+2,n_o}_{\nu,jk}$—are related to products of inner products between the left and right eigenvectors at successive discrete time instants t_n and t_{n+1} (p^{jk}_n), where $n = n_o, n_o + 1$ here] of eigenvalue products ($c^{n_o+2,n_o}_\nu = \lambda^{\mathcal{P}}_{\Xi_{n_o+1}}\lambda^{\mathcal{P}}_{\Xi_{n_o}}$, $\lambda^{\mathcal{P}}_{\Xi_{n_o+1}}\lambda^{\mathcal{N}}_{\Xi_{n_o}}$, $\lambda^{\mathcal{N}}_{\Xi_{n_o+1}}\lambda^{\mathcal{P}}_{\Xi_{n_o}}$, $\lambda^{\mathcal{N}}_{\Xi_{n_o+1}}\lambda^{\mathcal{N}}_{\Xi_{n_o}}$, i.e., $\nu \in [1, 4]$). Moreover, it is verified again that $h^{n_o+2,n_o}_{1,11} = h^{n_o+2,n_o}_{1,12} = h^{n_o+2,n_o}_{1,22} = h^{n_o+2,n_o}_{2,11} = h^{n_o+2,n_o}_{2,21} = h^{n_o+2,n_o}_{2,22} = 0$.

So far we have shown the validity of Eq. (H8) for $n_e = n_o$, $n_o + 1$, $n_o + 2$. In order to complete our proof by induction, we shall assume now that the aforementioned equation holds for $n_e \to n_e - 1 \geqslant n_o$. Along these lines, it will be also assumed that $c^{n_e-1,n_o}_{\mathcal{P},\mathcal{N}} = \prod_{n=n_o}^{n_e-1}\lambda^{\mathcal{P},\mathcal{N}}_{\Xi_n}$, $f^{n_e-1,n_o}_1 = \prod_{n=n_o}^{n_e-2}p^{11}_n$, $f^{n_e-1,n_o}_2 = \prod_{n=n_o}^{n_e-2}p^{22}_n$, $r^{n_e-1,n_o}_{jk} = \sum_{\nu'=1}^{2^{n_e-1-n_o}}c^{n_e-1,n_o}_{\nu'}h^{n_e-1,n_o}_{\nu',jk}$, with $h^{n_e-1,n_o}_{1,11} = h^{n_e-1,n_o}_{1,12} = h^{n_e-1,n_o}_{1,22} = h^{n_e,n_o}_{2,11} = h^{n_e-1,n_o}_{2,21} = h^{n_e-1,n_o}_{2,22} = 0$ and $c^{n_e-1,n_o}_{\nu'}$ representing eigenvalue products ($\nu' \in [1, 2^{n_e-1-n_o}]$). Given then the recursive relation $\mathcal{F}^{n_e,n_o} = D_{\Xi_{n_e}}(V^L_{n_e})^\dagger V^R_{n_e-1}\mathcal{F}^{n_e-1,n_o}$ [see Eqs. (H6) and (H8), after setting $n_e \to n_e - 1$],

$$\mathcal{F}^{n_e,n_o} = \begin{bmatrix} \lambda^{\mathcal{P}}_{\Xi_{n_e}}c^{n_e-1,n_o}_{\mathcal{P}}p^{11}_{n_e-1}f^{n_e-1,n_o}_1 + \Delta\lambda^{\mathcal{P}}_{\Xi_{n_e}}\left(\lambda^{\mathcal{P}}_{\Xi_{n_e-1}}p^{11}_{n_e-1}r^{n_e-1,n_o}_{11}\right. & \Delta\lambda^{\mathcal{P}}_{\Xi_{n_e}}\left(\lambda^{\mathcal{P}}_{\Xi_{n_e-1}}p^{11}_{n_e-1}r^{n_e-1,n_o}_{12} + \Delta c^{n_e-1,n_o}_{\mathcal{N}}p^{12}_{n_e-1}f^{n_e-1,n_o}_2\right. \\ \quad \left. + \Delta\lambda^{\mathcal{N}}_{\Xi_{n_e-1}}p^{12}_{n_e-1}r^{n_e-1,n_o}_{21}\right) & \quad \left. + \Delta\lambda^{\mathcal{N}}_{\Xi_{n_e-1}}p^{12}_{n_e-1}r^{n_e-1,n_o}_{22}\right) \\ \Delta\lambda^{\mathcal{N}}_{\Xi_{n_e}}\left(\lambda^{\mathcal{N}}_{\Xi_{n_e-1}}p^{22}_{n_e-1}r^{n_e-1,n_o}_{21} + \Delta c^{n_e-1,n_o}_{\mathcal{P}}p^{21}_{n_e-1}f^{n_e-1,n_o}_1\right. & \lambda^{\mathcal{N}}_{\Xi_{n_e}}c^{n_e-1,n_o}_{\mathcal{N}}p^{22}_{n_e-1}f^{n_e-1,n_o}_2 + \Delta\lambda^{\mathcal{N}}_{\Xi_{n_e}}\left(\lambda^{\mathcal{N}}_{\Xi_{n_e-1}}p^{22}_{n_e-1}r^{n_e-1,n_o}_{22}\right. \\ \quad \left. + \Delta\lambda^{\mathcal{P}}_{\Xi_{n_e-1}}p^{21}_{n_e-1}r^{n_e-1,n_o}_{11}\right) & \quad \left. + \Delta\lambda^{\mathcal{P}}_{\Xi_{n_e-1}}p^{21}_{n_e-1}r^{n_e-1,n_o}_{12}\right) \end{bmatrix}, \tag{H11}$$

which indeed takes the form of Eq. (H8) after performing substitutions

$$c^{n_e,n_o}_{\mathcal{P}} = \lambda^{\mathcal{P}}_{\Xi_{n_e}}c^{n_e-1,n_o}_{\mathcal{P}} = \prod_{n=n_o}^{n_e}\lambda^{\mathcal{P}}_{\Xi_n}, \tag{H12a}$$

$$c^{n_e,n_o}_{\mathcal{N}} = \lambda^{\mathcal{N}}_{\Xi_{n_e}}c^{n_e-1,n_o}_{\mathcal{N}} = \prod_{n=n_o}^{n_e}\lambda^{\mathcal{N}}_{\Xi_n}, \tag{H12b}$$

$$f^{n_e,n_o}_1 = p^{11}_{n_e-1}f^{n_e-1,n_o}_1 = \prod_{n=n_o}^{n_e-1}p^{11}_n, \tag{H12c}$$

$$f^{n_e,n_o}_2 = p^{22}_{n_e-1}f^{n_e-1,n_o}_2 = \prod_{n=n_o}^{n_e-1}p^{22}_n, \tag{H12d}$$

while for factors $r_{jk}^{n_e,n_o}$ it will be true that

$$r_{11}^{n_e,n_o} = \lambda_{\Xi_{n_e-1}}^{\mathcal{P}} p_{n_e-1}^{11} r_{11}^{n_e-1,n_o} + \Delta\lambda_{\Xi_{n_e-1}}^{\mathcal{N}} p_{n_e-1}^{12} r_{21}^{n_e-1,n_o}, \tag{H13a}$$

$$r_{12}^{n_e,n_o} = \lambda_{\Xi_{n_e-1}}^{\mathcal{P}} p_{n_e-1}^{11} r_{12}^{n_e-1,n_o} + \Delta c_{\mathcal{N}}^{n_e-1,n_o} p_{n_e-1}^{12} f_2^{n_e-1,n_o} + \Delta\lambda_{\Xi_{n_e-1}}^{\mathcal{N}} p_{n_e-1}^{12} r_{22}^{n_e-1,n_o}, \tag{H13b}$$

$$r_{21}^{n_e,n_o} = \lambda_{\Xi_{n_e-1}}^{\mathcal{N}} p_{n_e-1}^{22} r_{21}^{n_e-1,n_o} + \Delta c_{\mathcal{P}}^{n_e-1,n_o} p_{n_e-1}^{21} f_1^{n_e-1,n_o} + \Delta\lambda_{\Xi_{n_e-1}}^{\mathcal{P}} p_{n_e-1}^{21} r_{11}^{n_e-1,n_o}, \tag{H13c}$$

$$r_{22}^{n_e,n_o} = \lambda_{\Xi_{n_e-1}}^{\mathcal{N}} p_{n_e-1}^{22} r_{22}^{n_e-1,n_o} + \Delta\lambda_{\Xi_{n_e-1}}^{\mathcal{P}} p_{n_e-1}^{21} r_{12}^{n_e-1,n_o}. \tag{H13d}$$

It becomes apparent now from the above formulas that $c_\nu^{n_e,n_o} = \lambda_{\Xi_{n_e-1}}^{\mathcal{P}} c_{\nu'}^{n_e-1,n_o}$ or $c_\nu^{n_e,n_o} = \lambda_{\Xi_{n_e-1}}^{\mathcal{N}} c_{\nu'}^{n_e-1,n_o}$, which implies that there will be in total $2^{n_e-n_o}$ possible eigenvalue products $c_\nu^{n_e,n_o}$ (since there are $2^{n_e-1-n_o}$ products $c_{\nu'}^{n_e-1,n_o}$) and thus $\nu \in [1,\ 2^{n_e-n_o}]$. Accordingly, there will be $2^{n_e-n_o}$ different "weight" functions $h_{\nu,jk}^{n_e,n_o}$—one for each eigenvalue product $c_\nu^{n_e,n_o}$—within the general form of $r_{jk}^{n_e,n_o}$, which is given as $r_{jk}^{n_e,n_o} = \sum_{\nu=1}^{2^{n_e-n_o}} c_\nu^{n_e,n_o} h_{\nu,jk}^{n_e,n_o}$. [This expression can be found based on Eqs. (H13a)–(H13d) given also that $r_{jk}^{n_e-1,n_o} = \sum_{\nu'=1}^{2^{n_e-1-n_o}} c_{\nu'}^{n_e-1,n_o} h_{\nu',jk}^{n_e-1,n_o}$.] Moreover, based on Eq. (H13a) it will hold that $h_{1,11}^{n_e,n_o} = p_{n_e-1}^{11} h_{1,11}^{n_e-1,n_o}$ and since $h_{1,11}^{n_e-1,n_o} = 0$, it also comes that $h_{1,11}^{n_e,n_o} = 0$. Similarly, it will be true according to Eq. (H13a) that $h_{2,11}^{n_e,n_o} = p_{n_e-1}^{12} h_{2,21}^{n_e-1,n_o}$ and hence $h_{2,11}^{n_e,n_o} = 0$ (since $h_{2,21}^{n_e-1,n_o} = 0$). In a completely analogous manner, it can be shown that $h_{1,12}^{n_e,n_o} = h_{1,22}^{n_e,n_o} = h_{2,21}^{n_e,n_o} = h_{2,22}^{n_e,n_o} = 0$ by exploiting Eqs. (H13b)–(H13d). This completes the proof by induction of Eq. (H8) and of the form of the discrete quantities appearing in the same equation.

The evaluation of the total matrix $\mathcal{F} = \mathcal{F}^{N-1,\overline{n_o}+1}[(V_{\overline{n_o}+1}^L)^\dagger V_{\overline{n_o}}^R]\mathcal{F}^{\overline{n_o},0}$ [$\mathcal{F}^{\overline{n_o},0} \to \mathcal{F}^{(\alpha)}$ and $\mathcal{F}^{N-1,\overline{n_o}+1} \to \mathcal{F}^{(\beta)}$ according to the notation of Sec. III C 2; see also Eq. (30) in the main text] becomes now straightforward after employing Eq. (H8) along with the form of the matrix product $(V_{\overline{no}+1}^L)^\dagger V_{\overline{n_o}}^R$ [see Eqs. (H6) and (H7)]. This leads to Eq. (33) of the main text, where elements $\hat{\mathcal{F}}^{jk}$ are given as follows in the notation of Sec. III C 2:

$$\begin{aligned}\hat{\mathcal{F}}^{11} = {} & \Delta^2\big(\lambda_{\Xi_{N-1}}^{\mathcal{P}} c_{\mathcal{P}}^{(\alpha)} p_{21}^{\overline{n_o}} f_1^{(\alpha)} r_{11}^{(\beta)} + \lambda_{\Xi_{\overline{n_o}}}^{\mathcal{P}} c_{\mathcal{P}}^{(\beta)} p_{21}^{\overline{n_o}} f_1^{(\beta)} r_{11}^{(\alpha)} + \lambda_{\Xi_{N-1}}^{\mathcal{P}} \lambda_{\Xi_{\overline{n_o}}}^{\mathcal{P}} p_{11}^{\overline{n_o}} r_{12}^{(\beta)} r_{11}^{(\alpha)} + \lambda_{\Xi_{N-1}}^{\mathcal{P}} \lambda_{\Xi_{\overline{n_o}}}^{\mathcal{N}} p_{22}^{\overline{n_o}} r_{11}^{(\beta)} r_{21}^{(\alpha)}\big) \\ & + \Delta^3\big(\lambda_{\Xi_{N-1}}^{\mathcal{P}} \lambda_{\Xi_{\overline{n_o}}}^{\mathcal{P}} p_{21}^{\overline{n_o}} r_{11}^{(\beta)} r_{11}^{(\alpha)} + \lambda_{\Xi_{N-1}}^{\mathcal{P}} \lambda_{\Xi_{\overline{n_o}}}^{\mathcal{N}} p_{12}^{\overline{n_o}} r_{12}^{(\beta)} r_{21}^{(\alpha)}\big),\end{aligned} \tag{H14a}$$

$$\begin{aligned}\hat{\mathcal{F}}^{12} = {} & \Delta^2\big(\lambda_{\Xi_{\overline{n_o}}}^{\mathcal{P}} c_{\mathcal{P}}^{(\beta)} p_{21}^{\overline{n_o}} f_1^{(\beta)} r_{12}^{(\alpha)} + \lambda_{\Xi_{N-1}}^{\mathcal{P}} c_{\mathcal{N}}^{(\alpha)} p_{12}^{\overline{n_o}} f_2^{(\alpha)} r_{12}^{(\beta)} + \lambda_{\Xi_{N-1}}^{\mathcal{P}} \lambda_{\Xi_{\overline{n_o}}}^{\mathcal{P}} p_{11}^{\overline{n_o}} r_{12}^{(\beta)} r_{12}^{(\alpha)} + \lambda_{\Xi_{N-1}}^{\mathcal{P}} \lambda_{\Xi_{\overline{n_o}}}^{\mathcal{N}} p_{22}^{\overline{n_o}} r_{11}^{(\beta)} r_{22}^{(\alpha)}\big) \\ & + \Delta^3\big(\lambda_{\Xi_{N-1}}^{\mathcal{P}} \lambda_{\Xi_{\overline{n_o}}}^{\mathcal{P}} p_{21}^{\overline{n_o}} r_{11}^{(\beta)} r_{12}^{(\alpha)} + \lambda_{\Xi_{N-1}}^{\mathcal{P}} \lambda_{\Xi_{\overline{n_o}}}^{\mathcal{N}} p_{12}^{\overline{n_o}} r_{12}^{(\beta)} r_{22}^{(\alpha)}\big),\end{aligned} \tag{H14b}$$

$$\begin{aligned}\hat{\mathcal{F}}^{21} = {} & \Delta^2\big(\lambda_{\Xi_{N-1}}^{\mathcal{N}} c_{\mathcal{P}}^{(\alpha)} p_{21}^{\overline{n_o}} f_1^{(\alpha)} r_{21}^{(\beta)} + \lambda_{\Xi_{\overline{n_o}}}^{\mathcal{N}} c_{\mathcal{N}}^{(\beta)} p_{12}^{\overline{n_o}} f_2^{(\beta)} r_{21}^{(\alpha)} + \lambda_{\Xi_{\overline{n_o}}}^{\mathcal{P}} \lambda_{\Xi_{N-1}}^{\mathcal{N}} p_{11}^{\overline{n_o}} r_{22}^{(\beta)} r_{11}^{(\alpha)} + \lambda_{\Xi_{N-1}}^{\mathcal{N}} \lambda_{\Xi_{\overline{n_o}}}^{\mathcal{N}} p_{22}^{\overline{n_o}} r_{21}^{(\beta)} r_{21}^{(\alpha)}\big) \\ & + \Delta^3\big(\lambda_{\Xi_{\overline{n_o}}}^{\mathcal{P}} \lambda_{\Xi_{N-1}}^{\mathcal{N}} p_{21}^{\overline{n_o}} r_{21}^{(\beta)} r_{11}^{(\alpha)} + \lambda_{\Xi_{N-1}}^{\mathcal{N}} \lambda_{\Xi_{\overline{n_o}}}^{\mathcal{N}} p_{12}^{\overline{n_o}} r_{22}^{(\beta)} r_{21}^{(\alpha)}\big),\end{aligned} \tag{H14c}$$

$$\begin{aligned}\hat{\mathcal{F}}^{22} = {} & \Delta^2\big(\lambda_{\Xi_{N-1}}^{\mathcal{N}} c_{\mathcal{N}}^{(\alpha)} p_{12}^{\overline{n_o}} f_2^{(\alpha)} r_{22}^{(\beta)} + \lambda_{\Xi_{\overline{n_o}}}^{\mathcal{N}} c_{\mathcal{N}}^{(\beta)} p_{12}^{\overline{n_o}} f_2^{(\beta)} r_{22}^{(\alpha)} + \lambda_{\Xi_{\overline{n_o}}}^{\mathcal{P}} \lambda_{\Xi_{N-1}}^{\mathcal{N}} p_{11}^{\overline{n_o}} r_{22}^{(\beta)} r_{12}^{(\alpha)} + \lambda_{\Xi_{N-1}}^{\mathcal{N}} \lambda_{\Xi_{\overline{n_o}}}^{\mathcal{N}} p_{22}^{\overline{n_o}} r_{21}^{(\beta)} r_{22}^{(\alpha)}\big) \\ & + \Delta^3\big(\lambda_{\Xi_{\overline{n_o}}}^{\mathcal{P}} \lambda_{\Xi_{N-1}}^{\mathcal{N}} p_{21}^{\overline{n_o}} r_{21}^{(\beta)} r_{12}^{(\alpha)} + \lambda_{\Xi_{N-1}}^{\mathcal{N}} \lambda_{\Xi_{\overline{n_o}}}^{\mathcal{N}} p_{12}^{\overline{n_o}} r_{22}^{(\beta)} r_{22}^{(\alpha)}\big).\end{aligned} \tag{H14d}$$

Of particular interest are the diagonal entries $c_{\mathcal{P}}(\Delta p_{21}^{\overline{n_o}} f_1^{(\beta)} f_1^{(\alpha)})$ and $c_{\mathcal{N}}(\Delta p_{12}^{\overline{n_o}} f_2^{(\beta)} f_2^{(\alpha)})$ appearing in the matrix expression for $\mathcal{F}$ in Eq. (33). Clearly $c_{\mathcal{P},\mathcal{N}} = c_{\mathcal{P},\mathcal{N}}^{(\beta)} c_{\mathcal{P},\mathcal{N}}^{(\alpha)} = c_{\mathcal{P},\mathcal{N}}^{N-1,\overline{n_o}+1} c_{\mathcal{P},\mathcal{N}}^{\overline{n_o},0} = \prod_{n=0}^{N-1} \lambda_{\Xi_n}^{\mathcal{P},\mathcal{N}}$ [see also Eqs. (H12a) and (H12b)] represent the discrete dynamical phase factors associated with the $\mathcal{P},\mathcal{N}$ modes, which are acquired by the Hamiltonian arrangement during its parametric evolution along closed loop $\mathcal{C}^{\mathcal{R}}$ [see respective definition in Eq. (22b) of Sec. III A after replacing the generic mode annotation $(\hat{\pm})$ with the $\mathcal{P},\mathcal{N}$ mode representation, i.e., $(\hat{+}) \to \mathcal{P}$ and $(\hat{-}) \to \mathcal{N}$]. On the other hand, it will be true that $\Delta p_{21}^{\overline{n_o}} f_1^{(\beta)} f_1^{(\alpha)} = \Delta p_{21}^{\overline{n_o}} f_1^{N-1,\overline{n_o}+1} f_1^{\overline{n_o},0} = \prod_{n=0}^{N-1} \langle v_{n+1}^{\mathcal{P}} || v_n^{\mathcal{P}} \rangle$ and $\Delta p_{12}^{\overline{n_o}} f_2^{(\beta)} f_2^{(\alpha)} = \Delta p_{12}^{\overline{n_o}} f_2^{N-1,\overline{n_o}+1} f_2^{\overline{n_o},0} = \prod_{n=0}^{N-1} \langle v_{n+1}^{\mathcal{N}} || v_n^{\mathcal{N}} \rangle$ according to Eqs. (H6), (H7), (H12c), and (H12d). In other words, quantities $\Delta p_{21}^{\overline{n_o}} f_1^{(\beta)} f_1^{(\alpha)}$, $\Delta p_{12}^{\overline{n_o}} f_2^{(\beta)} f_2^{(\alpha)}$ become clearly associated to the discrete Berry phase factors related to the $\mathcal{P},\mathcal{N}$ modes and are acquired by the quantum system after a complete evolution around the cyclic path $\mathcal{C}^{\mathcal{R}}$ [see respective definition in Eq. (22a) of Sec. III A after replacing $(\hat{+}) \to \mathcal{P}$ and $(\hat{-}) \to \mathcal{N}$]. It should be also noted here that relations $f_{1,2}^{(\alpha)}(\Delta = 0) = f_{1,2}^{\overline{n_o},0}(\Delta = 0) = 1$ and $f_{1,2}^{(\beta)}(\Delta = 0) = f_{1,2}^{N-1,\overline{n_o}+1}(\Delta = 0) = 1$ will apply as can be seen from Eqs. (H12c) and (H12d) given that $p_n^{11}(\Delta = 0) = p_n^{22}(\Delta = 0) = 1$.

Finally, we need to show the dominance of the $c_{\mathcal{P}}$-related terms in the expression of matrix $\mathcal{F}$ provided in Eq. (33) in the adiabatic limit ($N \to \infty$ and $T = N\Delta \to \infty$, where T is the cycling period around parametric loop $\mathcal{C}^{\mathcal{R}}$). We will demonstrate this by indicatively comparing terms $\Delta c_{\mathcal{P}} p_{21}^{\overline{n_o}} f_1^{(\beta)} f_1^{(\alpha)}$ and $c_{\mathcal{P}}^{(\alpha)} c_{\mathcal{N}}^{(\beta)} p_{11}^{\overline{n_o}} f_2^{(\beta)} f_1^{(\alpha)}$ appearing in the first column of $\mathcal{F}$. Along these lines, it will hold that

$$\left|\frac{\Delta c_{\mathcal{P}} p_{21}^{\overline{n_o}} f_1^{(\beta)} f_1^{(\alpha)}}{c_{\mathcal{P}}^{(\alpha)} c_{\mathcal{N}}^{(\beta)} p_{11}^{\overline{n_o}} f_2^{(\beta)} f_1^{(\alpha)}}\right| = \left|\Delta \frac{c_{\mathcal{P}}^{(\beta)}}{c_{\mathcal{N}}^{(\beta)}} \frac{p_{21}^{\overline{n_o}} f_1^{(\beta)}}{p_{11}^{\overline{n_o}} f_2^{(\beta)}}\right| \simeq \left|\Delta \frac{p_{21}^{\overline{n_o}} f_1^{(\beta)}}{p_{11}^{\overline{n_o}} f_2^{(\beta)}}\right| \cdot e^{\sum_{n=\overline{n_o}+1}^{N-1} \mathrm{Re}\left(\Delta\lambda_n^{\mathcal{P}} - \Delta\lambda_n^{\mathcal{N}}\right)}, \tag{H15}$$

where we utilized relations $c_{\mathcal{P}} = c_{\mathcal{P}}^{(\beta)} c_{\mathcal{P}}^{(\alpha)}$ and $c_{\mathcal{P},\mathcal{N}}^{(\beta)} = c_{\mathcal{P},\mathcal{N}}^{N-1,\overline{n_o}+1} = \prod_{\overline{n_o}+1}^{N-1} \lambda_{\Xi_n}^{\mathcal{P},\mathcal{N}} = \prod_{\overline{n_o}+1}^{N-1} (1 + \Delta\lambda_n^{\mathcal{P},\mathcal{N}}) \simeq e^{\sum_{n=\overline{n_o}+1}^{N-1} \Delta\lambda_n^{\mathcal{P},\mathcal{N}}}$ [see also Eqs. (H12a) and (H12b)] and assumed small values for the discrete time step Δ ($\lambda_{\Xi_n}^{\mathcal{P},\mathcal{N}}$, $\lambda_n^{\mathcal{P},\mathcal{N}}$ represent of course the eigenvalues in the $\mathcal{P},\mathcal{N}$ basis representation corresponding to matrices Ξ_n and M_n as defined in Sec. II A, $\Xi_n = I + \Delta M_n$). For the majority of non-Hermitian settings [$\mathrm{Re}(\Delta\lambda_n^{\mathcal{P}})\mathrm{Re}(\Delta\lambda_n^{\mathcal{N}}) \neq 0$] it is predominantly true that $\mathrm{Re}(\Delta\lambda_n^{\mathcal{P}}) > \mathrm{Re}(\Delta\lambda_n^{\mathcal{N}})$, except for very special cases where $\mathrm{Re}(\Delta\lambda_n^{\mathcal{P}}) \equiv \mathrm{Re}(\Delta\lambda_n^{\mathcal{N}})$ for all possible values of n and which do not exhibit any dominant or nondominant modes. (For more details on the description of the $\mathcal{P},\mathcal{N}$ mode representation, refer to Fig. 4 and Sec. III C.) Here we are interested in the former case and consequently it is expected that the summation term $\sum_{n=\overline{n_o}+1}^{N-1} \mathrm{Re}(\lambda_n^{\mathcal{P}} - \lambda_n^{\mathcal{N}})$ to be of the order of N and as such the exponential factor appearing in Eq. (H15) will be of the order $e^{N|\Delta|}$. Assuming now that Δ has a small but fixed value, then similarly ratio $|\Delta p_{21}^{\overline{n_o}} f_1^{(\beta)} / p_{11}^{\overline{n_o}} f_2^{(\beta)}|$ will attain a small value [$p_{11}^{\overline{n_o}}(\Delta = 0) = f_{1,2}^{(\beta)}(\Delta = 0) = 1$ and $p_{21}^{\overline{n_o}}(\Delta)$ is also finitely defined in the vicinity of $\Delta = 0$]. Yet as parameter N gets increased to achieve adiabatic evolution conditions, there will be inevitably a point after which $e^{N|\Delta|}$ will overcome the effect of the aforementioned ratio and this will eventually lead to the dominance of $\Delta c_{\mathcal{P}} p_{21}^{\overline{n_o}} f_1^{(\beta)} f_1^{(\alpha)}$ over $c_{\mathcal{P}}^{(\alpha)} c_{\mathcal{N}}^{(\beta)} p_{11}^{\overline{n_o}} f_2^{(\beta)} f_1^{(\alpha)}$ in Eq. (H15). In a similar manner, it can be shown that $\Delta c_{\mathcal{P}} p_{21}^{\overline{n_o}} f_1^{(\beta)} f_1^{(\alpha)}$ will dominate over all terms appearing in the expression for matrix $\mathcal{F}$ [Eq. (33)], which in turn implies that $\mathcal{F}$ will obtain the form shown in Eq. (34) and thus the quantum state vector will convert to the instantaneous dominant ($\mathcal{P}$) mode under sufficiently slow driving conditions (see Sec. III C 2). It should be highlighted of course that here (and in Sec. III C 2) we have assumed the presence of a single discontinuity in the $\mathcal{P},\mathcal{N}$ mode eigenspectra (i.e., in the evolution of eigenvalues $\lambda_{\Xi_n}^{\mathcal{P},\mathcal{N}}$ or equivalently $\lambda_n^{\mathcal{P},\mathcal{N}}$). Analogous results (i.e., form of $\mathcal{F}$ in the adiabatic limit and state conversion to the instantaneous $\mathcal{P}$ mode) can nevertheless be attained even if more discontinuities of this nature arise, as long as the $\mathcal{P},\mathcal{N}$ mode formalism is employed to study the dynamics of slowly cycled states. [Equation (H8) will still apply, yet Eq. (H7) must be modified and parametric trajectory $\mathcal{C}^{\mathcal{R}}$ should be divided in an appropriate number of subpaths to reflect the number of spectrum discontinuities; matrix $\mathcal{F}$ can then be found based on the values of products $(V_{n+1}^L)^\dagger V_n^R$ at such anomalous points along with the expression for $\mathcal{F}^{n_e,n_o}$ in Eq. (H8).] If no such abrupt spectrum behavior exists, then the theoretical investigation performed in Sec. III C 1 would simply apply.

[1] M. Born and V. Fock, Beweis des Adiabatensatzes, Z. Phys. **51**, 165 (1928).

[2] T. Kato, On the adiabatic theorem of quantum mechanics, J. Phys. Soc. Jpn. **5**, 435 (1950).

[3] D. J. Griffiths and D. F. Schroeter, *Introduction to Quantum Mechanics* (Cambridge University Press, Cambridge, England, 2018)

[4] M. V. Berry, Quantal phase factors accompanying adiabatic changes, Proc. R. Soc. A **392**, 45 (1984).

[5] B. Simon, Holonomy, the Quantum Adiabatic Theorem, and Berry's Phase, Phys. Rev. Lett. **51**, 2167 (1983).

[6] B. R. Holstein, The adiabatic theorem and Berry's phase, Am. J. Phys. **57**, 1079 (1989).

[7] Y. Aharonov and D. Bohm, Significance of electromagnetic potentials in the quantum theory, Phys. Rev. **115**, 485 (1959).

[8] Y. Aharonov and D. Bohm, Further considerations on electromagnetic potentials in the quantum theory, Phys. Rev. **123**, 1511 (1961).

[9] Y. Aharonov and A. Casher, Topological Quantum Effects for Neutral Particles, Phys. Rev. Lett. **53**, 319 (1984).

[10] S. Weigert, Topological quenching of the tunnel splitting for a particle in a double-well potential on a planar loop, Phys. Rev. A **50**, 4572 (1994).

[11] H. C. Longuet-Higgins, U. Öpik, M. H. L. Pryce, and R. Sack, Studies of the Jahn-Teller effect.II. The dynamical problem, Proc. R. Soc. A **244**, 1 (1958).

[12] K. v. Klitzing, G. Dorda, and M. Pepper, New Method for High-Accuracy Determination of the Fine-Structure Constant Based on Quantized Hall Resistance, Phys. Rev. Lett. **45**, 494 (1980).

[13] D. J. Thouless, M. Kohmoto, M. P. Nightingale, and M. den Nijs, Quantized Hall Conductance in a Two-Dimensional Periodic Potential, Phys. Rev. Lett. **49**, 405 (1982).

[14] C. L. Kane and E. J. Mele, Quantum Spin Hall Effect in Graphene, Phys. Rev. Lett. **95**, 226801 (2005).

[15] C. L. Kane and E. J. Mele, Z2 Topological Order and the Quantum Spin Hall Effect, Phys. Rev. Lett. **95**, 146802 (2005).

[16] M. Z. Hasan and C. L. Kane, Colloquium: Topological insulators, Rev. Mod. Phys. **82**, 3045 (2010).

[17] F. D. M. Haldane and S. Raghu, Possible Realization of Directional Optical Waveguides in Photonic Crystals with Broken Time-Reversal Symmetry, Phys. Rev. Lett. **100**, 013904 (2008).

[18] M. Hafezi, E. A. Demler, M. D. Lukin, and J. M. Taylor, Robust optical delay lines with topological protection, Nat. Phys. **7**, 907 (2011).

[19] M. C. Rechtsman, J. M. Zeuner, Y. Plotnik, Y. Lumer, D. Podolsky, F. Dreisow, S. Nolte, M. Segev, and A. Szameit, Photonic Floquet topological insulators, Nature (London) **496**, 196 (2013).

[20] M. Hafezi, S. Mittal, J. Fan, A. Migdall, and J. Taylor, Imaging topological edge states in silicon photonics, Nat. Photon. **7**, 1001 (2013).

[21] C. He, X.-C. Sun, X.-P. Liu, M.-H. Lu, Y. Chen, L. Feng, and Y.-F. Chen, Photonic topological insulator with broken time-reversal symmetry, Proc. Natl. Acad. Sci. USA **113**, 4924 (2016).

[22] M. A. Bandres, S. Wittek, G. Harari, M. Parto, J. Ren, M. Segev, D. N. Christodoulides, and M. Khajavikhan, Topological insulator laser: Experiments, Science **359**, eaar4005 (2018).

[23] F. N. Ünal, A. Eckardt, and R.-J. Slager, Hopf characterization of two-dimensional Floquet topological insulators, Phys. Rev. Res. **1**, 022003(R) (2019).

[24] Y. Chen, F. Meng, Y. Kivshar, B. Jia, and X. Huang, Inverse design of higher-order photonic topological insulators, Phys. Rev. Res. **2**, 023115 (2020).

[25] S. Xia, D. Kaltsas, D. Song, I. Komis, J. Xu, A. Szameit, H. Buljan, K. G. Makris, and Z. Chen, Nonlinear tuning of PT symmetry and non-Hermitian topological states, Science **372**, 72 (2021).

[26] N. Moiseyev, *Non-Hermitian Quantum Mechanics* (Cambridge University Press, Cambridge, England, 2011)

[27] R. El-Ganainy, K. G. Makris, M. Khajavikhan, Z. H. Musslimani, S. Rotter, and D. N. Christodoulides, Non-Hermitian physics and PT symmetry, Nat. Phys. **14**, 11 (2018).

[28] Ş. K. Özdemir, S. Rotter, F. Nori, and L. Yang, Parity–time symmetry and exceptional points in photonics, Nat. Mater. **18**, 783 (2019).

[29] G. Nenciu and G. Rasche, On the adiabatic theorem for nonself-adjoint Hamiltonians, J. Phys. A: Math. Gen. **25**, 5741 (1992).

[30] A. Fleischer and N. Moiseyev, Adiabatic theorem for non-Hermitian time-dependent open systems, Phys. Rev. A **72**, 032103 (2005).

[31] T. Kato, *Perturbation Theory for Linear Operators* (Springer, Berlin, 1966).

[32] H. Cartarius, J. Main, and G. Wunner, Exceptional Points in Atomic Spectra, Phys. Rev. Lett. **99**, 173003 (2007).

[33] M. V. Berry and R. Uzdin, Slow non-Hermitian cycling: exact solutions and the Stokes phenomenon, J. Phys. A: Math. Theor. **44**, 435303 (2011).

[34] R. Uzdin, A. Mailybaev, and N. Moiseyev, On the observability and asymmetry of adiabatic state flips generated by exceptional points, J. Phys. A: Math. Theor. **44**, 435302 (2011).

[35] I. Gilary and N. Moiseyev, Asymmetric effect of slowly varying chirped laser pulses on the adiabatic state exchange of a molecule, J. Phys. B: At. Mol. Opt. Phys. **45**, 051002 (2012).

[36] T. J. Milburn, J. Doppler, C. A. Holmes, S. Portolan, S. Rotter, and P. Rabl, General description of quasiadiabatic dynamical phenomena near exceptional points, Phys. Rev. A **92**, 052124 (2015).

[37] H. Menke, M. Klett, H. Cartarius, J. Main, and G. Wunner, State flip at exceptional points in atomic spectra, Phys. Rev. A **93**, 013401 (2016).

[38] A. U. Hassan, B. Zhen, M. Soljačić, M. Khajavikhan, and D. N. Christodoulides, Dynamically Encircling Exceptional Points: Exact Evolution and Polarization State Conversion, Phys. Rev. Lett. **118**, 093002 (2017).

[39] A. U. Hassan, G. L. Galmiche, G. Harari, P. LiKamWa, M. Khajavikhan, M. Segev, and D. N. Christodoulides, Chiral state conversion without encircling an exceptional point, Phys. Rev. A **96**, 052129 (2017).

[40] X.-L. Zhang, S. Wang, B. Hou, and C. T. Chan, Dynamically Encircling Exceptional Points: *In situ* Control of Encircling Loops and the Role of the Starting Point, Phys. Rev. X **8**, 021066 (2018).

[41] X.-L. Zhang and C. T. Chan, Dynamically encircling exceptional points in a three-mode waveguide system, Commun. Phys. **2**, 1 (2019).

[42] M.-A. Miri and A. Alù, Exceptional points in optics and photonics, Science **363**, eaar7709 (2019).

[43] J. Höller, N. Read, and J. G. E. Harris, Non-Hermitian adiabatic transport in spaces of exceptional points, Phys. Rev. A **102**, 032216 (2020).

[44] C. F. Fong, Y. Ota, Y. Arakawa, S. Iwamoto, and Y. K. Kato, Chiral modes near exceptional points in symmetry broken H1 photonic crystal cavities, Phys. Rev. Res. **3**, 043096 (2021).

[45] H. Hu, S. Sun, and S. Chen, Knot topology of exceptional point and non-Hermitian no-go theorem, Phys. Rev. Res. **4**, L022064 (2022).

[46] J. Doppler, A. A. Mailybaev, J. Böhm, U. Kuhl, A. Girschik, F. Libisch, T. J. Milburn, P. Rabl, N. Moiseyev, and S. Rotter, Dynamically encircling an exceptional point for asymmetric mode switching, Nature (London) **537**, 76 (2016).

[47] H. Xu, D. Mason, L. Jiang, and J. Harris, Topological energy transfer in an optomechanical system with exceptional points, Nature (London) **537**, 80 (2016).

[48] J. W. Yoon, Y. Choi, C. Hahn, G. Kim, S. H. Song, K.-Y. Yang, J. Y. Lee, Y. Kim, C. S. Lee, J. K. Shin, H.-S. Lee, and P. Berini, Time-asymmetric loop around an exceptional point over the full optical communications band, Nature (London) **562**, 86 (2018).

[49] Q. Liu, J. Liu, D. Zhao, and B. Wang, On-chip experiment for chiral mode transfer without enclosing an exceptional point, Phys. Rev. A **103**, 023531 (2021).

[50] W. Liu, Y. Wu, C.-K. Duan, X. Rong, and J. Du, Dynamically Encircling an Exceptional Point in a Real Quantum System, Phys. Rev. Lett. **126**, 170506 (2021).

[51] J. Garrison and E. M. Wright, Complex geometrical phases for dissipative systems, Phys. Lett. A **128**, 177 (1988).

[52] A. A. Mailybaev, O. N. Kirillov, and A. P. Seyranian, Geometric phase around exceptional points, Phys. Rev. A **72**, 014104 (2005).

[53] A. I. Nesterov and F. A. De La Cruz, Complex magnetic monopoles, geometric phases and quantum evolution in the vicinity of diabolic and exceptional points, J. Phys. A: Math. Theor. **41**, 485304 (2008).

[54] S.-D. Liang and G.-Y. Huang, Topological invariance and global Berry phase in non-Hermitian systems, Phys. Rev. A **87**, 012118 (2013).

[55] R. Hayward and F. Biancalana, Complex Berry phase dynamics in PT-symmetric coupled waveguides, Phys. Rev. A **98**, 053833 (2018).

[56] Z. Gong, Y. Ashida, K. Kawabata, K. Takasan, S. Higashikawa, and M. Ueda, Topological Phases of Non-Hermitian Systems, Phys. Rev. X **8**, 031079 (2018).

[57] K. Kawabata and M. Sato, Real spectra in non-Hermitian topological insulators, Phys. Rev. Res. **2**, 033391 (2020).

[58] A. Dranov, J. Kellendonk, and R. Seiler, Discrete time adiabatic theorems for quantum mechanical systems, J. Math. Phys. **39**, 1340 (1998).

[59] A. Tanaka, Adiabatic theorem for discrete time evolution, J. Phys. Soc. Jpn. **80**, 125002 (2011).

[60] M. V. Berry, N. L. Balazs, M. Tabor, and A. Voros, Quantum maps, Ann. Phys. (NY) **122**, 26 (1979).

[61] M. A. Nielsen and I. L. Chuang, *Quantum Computation and Quantum Information* (Cambridge University Press, Cambridge, UK, 2010).

[62] T. Hogg, Adiabatic quantum computing for random satisfiability problems, Phys. Rev. A **67**, 022314 (2003).
[63] P. Cabauy and P. Benioff, Cyclic networks of quantum gates, Phys. Rev. A **68**, 032315 (2003).
[64] A. Tanaka and M. Miyamoto, Quasienergy Anholonomy and its Application to Adiabatic Quantum State Manipulation, Phys. Rev. Lett. **98**, 160407 (2007).
[65] A. Regensburger, C. Bersch, M.-A. Miri, G. Onishchukov, D. N. Christodoulides, and U. Peschel, Parity–time synthetic photonic lattices, Nature (London) **488**, 167 (2012).
[66] M.-A. Miri, A. Regensburger, U. Peschel, and D. N. Christodoulides, Optical mesh lattices with PT symmetry, Phys. Rev. A **86**, 023807 (2012).
[67] H. Nasari, G. Lopez-Galmiche, H. E. Lopez-Aviles, A. Schumer, A. U. Hassan, Q. Zhong, S. Rotter, P. LiKamWa, D. N. Christodoulides, and M. Khajavikhan, Observation of chiral state transfer without encircling an exceptional point, Nature (London) **605**, 256 (2022).
[68] L. Barker, C. Candan, T. Hakioglu, M. A. Kutay, and H. M. Ozaktas, The discrete harmonic oscillator, Harper's equation, and the discrete fractional Fourier transform, J. Phys. A: Math. Gen. **33**, 2209 (2000).
[69] M. Lorente, Continuous vs. discrete models for the quantum harmonic oscillator and the hydrogen atom, Phys. Lett. A **285**, 119 (2001).
[70] J. L. Cieśliński and B. Ratkiewicz, On simulations of the classical harmonic oscillator equation by difference equations, Adv. Differ. Equ. **2006**, 040171 (2006).
[71] N. M. Atakishiyev, A. U. Klimyk, and K. B. Wolf, A discrete quantum model of the harmonic oscillator, J. Phys. A: Math. Theor. **41**, 085201 (2008).
[72] J. L. Cieśliński, On the exact discretization of the classical harmonic oscillator equation, J. Differ. Equ. Appl. **17**, 1673 (2011).
[73] V. E. Tarasov, Exact discretization of Schrödinger equation, Phys. Lett. A **380**, 68 (2016).
[74] J. Heading, *An Introduction to Phase-Integral Methods* (Methuen, London, 1962).
[75] R. B. Dingle, *Asymptotic Expansions: Their Derivation and Interpretation* (Academic Press, New York, 1973).
[76] See Supplemental Material at http://link.aps.org/supplemental/10.1103/PhysRevResearch.5.033053 for further details on the properties of the discrete Airy and parabolic cylinder functions, which describe the dynamics of a traceless and symmetric non-Hermitian model evolving along rhombic parametric paths (additional solutions were also retrieved in terms of generalized hypergeometric functions, when the parametric trajectories were allowed to have alternative geometric forms). An analytical derivation of symmetric/asymmetric mode switching is provided in the special case of rhombic loops of sufficiently small dimensions, by taking advantage of the asymptotic properties of the Airy functions (the effect of the Stokes phenomenon is also clearly illustrated). Moreover, details regarding the optical implementation of a generalized and discrete two-level Hamiltonian model are discussed (in this case the evolution of the polarization state of light and the effect of certain symmetries on the system's transfer matrices were analyzed in terms of Jones algebra), along with a more in-depth explanation of the various mode notations used in this paper. Finally, additional supplementary figures are presented to further corroborate the numerical findings depicted in Figs. 2, 6, 7, 9 of the main text.
[77] A. J. Jerri, *Linear Difference Equations with Discrete Transform Methods* (Kluwer Academic Publishers, Dordrecht, 1996).
[78] S. Elaydi, *An Introduction to Difference Equations* (Springer Verlag, New York, 2005).
[79] P. Caldirola, Forze non conservative nella meccanica quantistica, Il Nuovo Cimento (1924-1942) **18**, 393 (1941).
[80] E. Kanai, On the quantization of the dissipative systems, Prog. Theor. Phys. **3**, 440 (1948).
[81] I. A. Pedrosa, G. P. Serra, and I. Guedes, Wave functions of a time-dependent harmonic oscillator with and without a singular perturbation, Phys. Rev. A **56**, 4300 (1997).
[82] F. Hertweck and A. Schlüter, Die "adiabatische Invarianz" des magnetischen Bahnmomentes geladener Teilchen, Z. Naturforsch. A **12**, 844 (1957).
[83] L. M. Garrido, Approximate constancy of adiabatic invariants, Prog. Theor. Phys. **26**, 577 (1961).
[84] H. R. Lewis, Jr., Classical and Quantum Systems with Time-Dependent Harmonic-Oscillator-Type Hamiltonians, Phys. Rev. Lett. **18**, 510 (1967).
[85] H. R. Lewis Jr., Class of exact invariants for classical and quantum time-dependent harmonic oscillators, J. Math. Phys. **9**, 1976 (1968).
[86] T. Padmanabhan, Demystifying the constancy of the Ermakov–Lewis invariant for a time-dependent oscillator, Mod. Phys. Lett. A **33**, 1830005 (2018).
[87] A. N. Lukashkin, M. N. Walling, and I. J. Russell, Power amplification in the mammalian cochlea, Curr. Biol. **17**, 1340 (2007).
[88] K. D. Lerud, J. C. Kim, F. V. Almonte, L. H. Carney, and E. W. Large, A canonical oscillator model of cochlear dynamics, Hear. Res. **380**, 100 (2019).
[89] D. Daugherty, T. Roque-Urrea, J. Urrea-Roque, J. Troyer, S. Wirkus, and M. A. Porter, Mathematical models of bipolar disorder, Commun. Nonlinear Sci. Numer. Simul. **14**, 2897 (2009).
[90] D. C. Brody, Biorthogonal quantum mechanics, J. Phys. A: Math. Theor. **47**, 035305 (2014).
[91] Y. Aharonov and J. Anandan, Phase Change During a Cyclic Quantum Evolution, Phys. Rev. Lett. **58**, 1593 (1987).
[92] A. Garg, Berry phases near degeneracies: Beyond the simplest case, Am. J. Phys. **78**, 661 (2010).
[93] J. Wiersig, Enhancing the Sensitivity of Frequency and Energy Splitting Detection by Using Exceptional Points: Application to Microcavity Sensors for Single-Particle Detection, Phys. Rev. Lett. **112**, 203901 (2014).
[94] H. Hodaei, A. U. Hassan, S. Wittek, H. Garcia-Gracia, R. El-Ganainy, D. N. Christodoulides, and M. Khajavikhan, Enhanced sensitivity at higher-order exceptional points, Nature (London) **548**, 187 (2017).
[95] W. Chen, Ş. Kaya Özdemir, G. Zhao, J. Wiersig, and L. Yang, Exceptional points enhance sensing in an optical microcavity, Nature (London) **548**, 192 (2017).
[96] S. Weinberg, *The Quantum Theory of Fields*, Vol. I (Cambridge University Press, Cambridge, England, 1995).

[97] A. Mostafazadeh, Pseudo-Hermiticity versus PT symmetry: The necessary condition for the reality of the spectrum of a non-Hermitian Hamiltonian, J. Math. Phys. **43**, 205 (2002).

[98] A. Fring and M. H. Y. Moussa, Unitary quantum evolution for time-dependent quasi-Hermitian systems with nonobservable Hamiltonians, Phys. Rev. A **93**, 042114 (2016).

[99] R. G. Sachs, *The Physics of Time Reversal* (University of Chicago Press, Chicago, 1987).

[100] M. S. Sozzi, *Discrete Symmetries and CP Violation: From Experiment to Theory* (Oxford University Press, Oxford, UK, 2008).

[101] C. M. Bender, M. V. Berry, and A. Mandilara, Generalized PT symmetry and real spectra, J. Phys. A: Math. Gen. **35**, L467 (2002).

[102] C. M. Bender, D. C. Brody, and H. F. Jones, Complex Extension of Quantum Mechanics, Phys. Rev. Lett. **89**, 270401 (2002).

[103] A. Yariv and P. Yeh, *Photonics: Optical Electronics in Modern Communications*, 6th ed. (Oxford University Press, New York, 2007).

[104] R. J. Potton, Reciprocity in optics, Rep. Prog. Phys. **67**, 717 (2004).

[105] G. Leuchs and M. Sondermann, Time-reversal symmetry in optics, Phys. Scr. **85**, 058101 (2012).

[106] M. G. Silveirinha, Time-reversal symmetry in antenna theory, Symmetry **11**, 486 (2019).

[107] O. Sigwarth and C. Miniatura, Time reversal and reciprocity, AAPPS Bull. **32**, 23 (2022).

[108] H. B. G. Casimir, Reciprocity theorems and irreversible processes, Proc. IEEE **51**, 1570 (1963).

[109] D. E. Bilhorn, L. L. Foldy, R. M. Thaler, W. Tobocman, and V. A. Madsen, Remarks concerning reciprocity in quantum mechanics, J. Math. Phys. **5**, 435 (1964).

[110] H. Y. Xie, P. T. Leung, and D. P. Tsai, General validity of reciprocity in quantum mechanics, Phys. Rev. A **78**, 064101 (2008).

[111] P. T. Leung and K. Young, Gauge invariance and reciprocity in quantum mechanics, Phys. Rev. A **81**, 032107 (2010).

[112] L. Deák and T. Fülöp, Reciprocity in quantum, electromagnetic and other wave scattering, Ann. Phys. **327**, 1050 (2012).

[113] D. M. Pozar, *Microwave Engineering*, 4th ed. (Wiley, New York, 2011).

[114] R. C. Jones, A new calculus for the treatment of optical systems, J. Opt. Soc. Am. **31**, 488 (1941).

[115] Q.-H. Wang, 2×2 *PT*-symmetric matrices and their applications, Philos. Trans. R. Soc. A **371**, 20120045 (2013).

[116] J. M. Whittaker, *Interpolatory Function Theory* (Cambridge University Press, Cambridge, England, 1935).

[117] R. P. Boas and R. C. Buck, *Polynomial Expansions of Analytic Functions* (Academic Press, New York, 1964).

[118] M. Abramowitz and I. A. Stegun, *Handbook of Mathematical Functions with Formulas, Graphs, and Mathematical Tables* (Dover Publications, New York, 1972).

[119] *Wolfram Research, Inc., The Wolfram Functions Site*, https://functions.wolfram.com/, Champaign, Illinois (1999).

[120] F. W. J. Olver, A. B. Olde Daalhuis, D. W. Lozier, B. I. Schneider, R. F. Boisvert, C. W. Clark, B. R. Mille, B. V. Saunders, H. S. Cohl, and M. A. McClain, eds., NIST Digital Library of Mathematical Functions, https://dlmf.nist.gov/, Release 1.1.5 of 2022-03-15.